

Modal Analysis Techniques in Wide-Area Frequency Monitoring Systems

Mark Walter Baldwin

A dissertation submitted to the Faculty of Virginia Polytechnic Institute and State University in partial fulfillment of the requirements for the degree of

Doctor of Philosophy
in
Electrical Engineering

Committee Members:

Dr. Yilu Liu (Chair)

Dr. Gary S. Brown

Dr. Virgilio Centeno

Dr. Richard Conners

Dr. Carl Prather

February 29th, 2008

Blacksburg, Virginia

Keywords: disturbance identification; electromechanics; FNET; modal analysis; state-space model; wide-area monitoring

Abstract

The advent of synchronized wide-area frequency measurements obtained from frequency disturbance recorders and phasor measurement units has presented the power industry with special opportunities to study power system dynamics. I propose the use of wide-area frequency measurements in identifying system disturbances based on power system post-event modal properties.

In this work, power system dynamics are examined from an internal system energy viewpoint. Since an electric power system is composed of coupled rotating machines (large generators) which have air gap magnetic fields that are essentially static, or quasi-static, the power system may be modeled as a system with energy stored in quasi-static magnetic fields. The magnetic fields in the machines do change with time but may be modeled as static as far as wave propagation is concerned. The dynamic model that I develop treats this magnetic energy specifically as potential energy. Each rotating machine also contains an inertia due to the mass and motion of its rotor train and so each machine contains a rotational kinetic energy. Thus the internal system energy for a power system dynamic model may be considered to be contained in potential (magnetic) and kinetic (rotating mass) energies. This notion of internal energy lends itself to the use of a state-space model where each system state is associated with either a kinetic energy or a potential energy. An n -machine system would have a total of $2n$ states and would thus be a $2n$ -th order system. For many power system disturbances, I postulate that a linearized version of this model may be used to examine system natural response in terms of frequency and phasor measurements. The disturbances that I will investigate include generator and line outages. For any particular outage, the power system exhibits a very specific natural response in terms of its kinetic and potential energies. Kinetic energy in the system is directly related to each specific machine's rotational speed. I propose that the kinetic energy corresponds directly with bus frequencies through a linear transformation. Likewise magnetic field energy in each machine corresponds directly with a torque angle. The potential energy in the system thus corresponds directly with bus angles through a linear transformation.

The primary focus of this work is on frequency deviation modal

characteristics – specifically damped oscillation frequencies, mode shapes, and damping ratios. This work presents how specific disturbances on a power system will lead to specific oscillation frequencies in the deviation quantities and that these oscillation frequencies may be used to identify the disturbance. The idea of disturbance identification stems out of previous work done in locating disturbances by using a distributed parameter (DP) model of an electric power system. This DP model, which assumes a wave-like motion of frequency and phase quantities, was used to locate disturbances via a triangulation method. This present work, instead of using a DP model of the power system, assumes lumped parameters and focuses on disturbance identification strictly via modal characteristics – particularly oscillation frequency in the frequency deviations. This model is not concerned with geographic location but focuses on system topology, loading, and machine mass as lumped parameters. Advantages of disturbance identification include mainly reliability enhancements but can also be used in marketing applications.

The state-space model used to realize this theory is verified via simulation using small, "academic" systems which should prove useful in classroom settings. Additionally the model is verified on a larger test system in order prove its validity and potential usefulness on large power systems.

Acknowledgements

My first and foremost appreciation goes to the folks who administrate the Via Foundation. As a Fellow of the Harry Lynne Bradley Department of Electrical and Computer Engineering at Virginia Tech, the foundation has provided my funding, in its entirety, during my Ph.D.-student years at Virginia Tech. This funding, in terms of typical graduate student standards, is lavish. It provides Bradley Fellows with a means of focusing exclusively on research toward their Ph.D. requirements and publications. I am not able to acknowledge enough appreciation for this gift.

Next, I thank Dr. Yilu Liu, my academic advisor, for her guidance and support in both personal and academic activities. Her counsel has proven invaluable, driving me to produce innovative and progressive work that is useful in both theoretical and practical settings. Dr. Liu takes her role as advisor beyond academic issues by considering her students to be family – giving advice on basically all life issues and making sacrifices for, and providing for her students unlike any advisor that I know of.

Thanks goes to the remaining members of my advisory committee: Dr. Virgilio Centeno who through his industry and academic experience has provided me with valuable advice concerning research and industry endeavors but also in providing guidance for the teaching assignments that I was involved in as a masters student; Dr. Richard Connors who, *in his retirement*, gladly gives up his own personal time to advise me and the rest of the FNET research group; Dr. Gary Brown who, back in my days as an undergraduate student, helped to foster in me a love of the central science of all things electrical engineering – electromagnetics. The setting for this fostering - the radio waves class in spring '93; Dr. Carl Prather who's relationship with me goes back to the Fall of 1990 – he taught me the fundamentally ever-important subject of differential equations which knowledge and understanding I put to practical use in down-right rigorous fashion here in this work.

Thanks go to the power-area students that I have worked with, both members of FNET and Dr. Centeno's group in the Center for Power Engineering. A very special thanks goes to Robert M. Gardner for his help in developing a Matrix Pencil signal-processing tool for use with frequency measurements. The power of the Matrix Pencil

application has made my work shine with its ability to quantitatively assess modes of a signal and with resolution unparalleled by other signal decomposition techniques. The compatibility of the Matrix Pencil algorithm with electromechanical modal analysis is extraordinary, as seen by the results in this research.

Additional thanks goes to members of the Virginia Tech Graduate Christian Fellowship especially Ki Hwan Park, Stephen Craven, Seth Lee, Jay Mcghee, and Jordan Cofer for their support.

A special thanks goes to my mom and dad, Rose and Harry, for bringing me into this world, supporting me in every way imaginable, and raising me to have personal attributes both rough and refined that have lead me through both life and career and up to this great accomplishment of obtaining a Ph.D.

And most of all, I thank my God through Jesus Christ who sovereignly orders every event in my life in both success and failure in order to carry out his own plan. None of this work would be possible without His Word, His guidance, comfort, and discipline.

Table of Contents

Abstract	ii
Acknowledgements	iv
List of Figures	viii
List of Tables.....	xi
Chapter 1 Introduction	1
1.1 Frequency Measurement History	1
1.2 Applications Under Development.....	3
1.3 Proposed Uses of Frequency Measurements.....	4
Chapter 2 Basics of Lumped Parameter Model Frequency Characteristics	7
2.1 The Electromechanical Nature of a Single-Machine AC Electric Power System.....	11
2.2 Salient Electromechanical Features of Simple AC Systems	13
Chapter 3 Generator Outage Identification Using Modal Analysis	23
3.1 Outage Identification in a Two-Machine Infinite Bus System	23
3.2 Small-Signal State Modeling of an Electromechanical System.....	28
3.3 Eigenvalues, Eigenvectors of the Plant Matrix and Mode Excitation	31
3.4 Plant Matrix Development for an n-Machine system	34
3.5 Simulation Results for a Three-Machine System.....	37
3.5.1 Machine 1 Outage	39
3.5.2 Machine 2 Outage	44
3.5.3 Machine 3 Outage	49
3.6 Comparison of Machine 2 and Machine 3 Outage Modal Characteristics.....	55
3.7 Output matrix development for an n-Machine, m-Measurement point system	58
Chapter 4 Non - Idealized System Modeling	67
4.1 Modeling of Transmission Losses.....	69
4.2 Load Modeling	76
4.3 System Modeling in the Absence of Infinite Bus and Basic Modal Characteristics of Line Outages	83
4.3.1 Investigation of Line Outage Followed by no Reclose Action	92
4.3.2 Investigation of Line Outage Followed by Reclose Action	103
4.4 Speed Governor Modeling.....	109
4.4.1 Single-Machine Infinite Bus System	113
4.4.2 Two-Machine System	119
4.5 Modeling of Machine Damping.....	130
Chapter 5 Theory Verification Using a Non-trivial System.....	133
5.1 System Description and State Equation Development.....	134

5.2	<i>Q-point Determination Method</i>	141
5.3	<i>Modal Analyses and Comparison with Simulation Results</i>	144
5.3.1	151-152 line outage.....	144
5.3.2	201-204 line outage.....	152
5.3.3	3003-3005 line outage.....	158
5.3.4	3005-3006 line outage.....	163
5.3.5	Final Remarks and Conclusions Concerning Predicted and Simulated Results.....	168
5.4	<i>Output Matrix Development and Simulation Results</i>	173
Chapter 6	Final Remarks	181
6.1	<i>Conclusions</i>	181
6.2	<i>Contributions</i>	183
6.3	<i>Potential Future Research</i>	185
References	187
Appendix I	Proof of Equation 3.9	189
Appendix II	Sample Plant Matrix Formulation	191
Appendix III	Sample Output Matrix Formulation	194
Appendix IV	Test System Static and Dynamic Parameter Files for PSS/E	196
Appendix V	MATLAB Codes Used to Generate Plant Matrix and Output Matrix	201
	<i>Instruction Manual for MATLAB Codes</i>	201
	<i>PaRcalc.m</i>	201
	<i>SixbusLF_iter.m</i>	202
	<i>PlantMatrix.m</i>	212
	<i>OutputMatrix.m</i>	213

List of Figures

Figure 2.1: SMIB system.....	13
Figure 2.2: angle variation along line that connects source to infinite bus.....	15
Figure 2.3: single-machine infinite bus simulated system to show frequency variations along transmission line.....	17
Figure 2.4: simulation results of system in figure 2.3	18
Figure 2.5: two-machine system	19
Figure 2.6: two machines oscillating against each other	21
Figure 2.7: simulation results of system in figure 2.6	21
Figure 2.8: two machines oscillating against each other through a meshed transmission system.....	22
Figure 2.9: simulation results of system in figure 2.8	22
Figure 3.1: two-machine infinite-bus system.....	23
Figure 3.2: frequency and angle measurements for machine 1 outage.....	26
Figure 3.3: frequency and angle measurements for machine 2 outage.....	27
Figure 3.4: three-machine infinite bus system	38
Figure 3.5: frequency and phase waveforms at tie line – machine 1 outage.....	39
Figure 3.6: Magnitude Spectrum FFT of tie line frequency – machine 1 outage.....	40
Figure 3.7: frequency and phase waveforms at machine 1’s intertie point – machine 1 outage.....	41
Figure 3.8: FFT of frequency waveform at machine 1’s intertie point – machine 1 outage	41
Figure 3.9: frequency and phase waveforms at machine 2’s intertie point – machine 1 outage.....	42
Figure 3.10: FFT of frequency waveform at machine 2’s intertie point – generator 1 outage	42
Figure 3.11: frequency and phase waveforms at machine 3’s intertie point – machine 1 outage.....	43
Figure 3.12: FFT of frequency waveform at machine 3’s intertie point – machine 1 outage.....	43
Figure 3.13: frequency and phase waveforms at tie line – machine 2 outage.....	44
Figure 3.14: Magnitude Spectrum FFT of tie line frequency – machine 2 outage.....	45
Figure 3.15: frequency and phase waveforms at machine 1’s intertie point – machine 2 outage.....	46
Figure 3.16: FFT of frequency waveform at machine 1’s intertie point – machine 2 outage.....	46
Figure 3.17: frequency and phase waveforms at machine 2’s intertie point – machine 2 outage.....	47
Figure 3.18: FFT of frequency waveform at machine 2’s intertie point – machine 2 outage.....	47
Figure 3.19: frequency and phase waveforms at machine 3’s intertie point – machine 2 outage.....	48
Figure 3.20: FFT of frequency waveform at machine 3’s intertie point – machine 2 outage.....	48
Figure 3.21: frequency and phase waveforms at tie line – machine 3 outage.....	49
Figure 3.22: Magnitude Spectrum FFT of tie line frequency – machine 3 outage.....	50
Figure 3.23: frequency and phase waveforms at machine 1’s intertie point – machine 3 outage.....	50
Figure 3.24: FFT of frequency waveform at machine 1’s intertie point – machine 3 outage.....	51
Figure 3.25: frequency and phase waveforms at machine 2’s intertie point – machine 3 outage.....	51
Figure 3.26: FFT of frequency waveform at machine 2’s intertie point – machine 3 outage.....	52
Figure 3.27: frequency and phase waveforms at machine 3’s intertie point – machine 3 outage.....	52
Figure 3.28: FFT of frequency waveform at machine 3’s intertie point – machine 3 outage.....	53
Figure 3.29: Magnitude Spectrum FFT of tie line frequency – machine 3 outage, 20-second waveform	54
Figure 3.30: FFT of frequency waveform at machine 3’s intertie point – machine 3 outage, 20-second waveform	54
Figure 3.31: FFT of machine 1 per unit speed – machine 2 outage.....	56
Figure 3.32: FFT of machine 3 per unit speed – machine 2 outage.....	56
Figure 3.33: FFT of machine 1 per unit speed – machine 3 outage.....	57
Figure 3.34: FFT of machine 2 per unit speed – machine 3 outage.....	57
Figure 4.1: power-angle curve comparison between lossless and lossy systems.....	74
Figure 4.2: SMIB system.....	75
Figure 4.3: system used to present loading effects on electromechanical coupling.....	79
Figure 4.4: unregulated system without infinite bus	85
Figure 4.5: impedance diagram of system in figure 4.4 – line outage followed by no reclose action .	93
Figure 4.6: reduced impedance and admittance diagrams for system in figure 4.5	94

Figure 4.7: frequency waveforms for two-machine two line system following a line outage with no reclose.....	102
Figure 4.8: impedance diagram of system in figure 4.4 – line outage followed by reclose action.....	104
Figure 4.9: reduced impedance and admittance diagrams for system in figure 4.8	104
Figure 4.10: frequency waveforms for two-machine two line system following a line outage with successful reclose	106
Figure 4.11: frequency waveforms for two-machine two line system following a line outage with successful reclose – zoomed in on line outage before reclose.....	107
Figure 4.12: frequency waveforms for two-machine two-line system following a line outage with successful reclose – zoomed out to show system acceleration following reclose	108
Figure 4.13: function block diagrams for SMIB system	114
Figure 4.14: function block diagram for governor TGOV1	115
Figure 4.15: function block diagram of entire electromechanical system for SMIB	115
Figure 4.16: function block diagram of entire electromechanical system for SMIB decomposed into a collection of integrators and multipliers	116
Figure 4.17: regulated system in steady state.....	122
Figure 4.18: frequency following line outage; $\tau_2 = 0.05$ seconds	127
Figure 4.19: frequency following line outage; $\tau_2 = 0.3$ seconds	128
Figure 4.20: frequency following line outage; $\tau_2 = 0.5$ seconds.....	129
Figure 5.1: single-line diagram of 23-bus test system.....	136
Figure 5.2: Representation of Power System as a Six-Port Network.....	138
Figure 5.3: Iteration scheme for q-point calculation	143
Figure 5.4: 151-152 line outage: (a) machine 5 estimated vs. measured speed signal; (b) display of each oscillatory component	150
Figure 5.5: 151-152 line outage: (a) machines 1 and 2 estimated vs. measured speed signal; (b) display of each oscillatory component.....	150
Figure 5.6: 151-152 line outage: (a) machine 3 estimated vs. measured speed signal; (b) display of each oscillatory component	151
Figure 5.7: 151-152 line outage: (a) machine 4 estimated vs. measured speed signal; (b) display of each oscillatory component	151
Figure 5.8: 151-152 line outage: (a) machine 6 estimated vs. measured speed signal; (b) display of each oscillatory component	152
Figure 5.9: 201-204 line outage: (a) machines 1 and 2 estimated vs. measured speed signal; (b) display of each oscillatory component.....	155
Figure 5.10: 201-204 line outage: (a) machine 3 estimated vs. measured speed signal; (b) display of each oscillatory component	156
Figure 5.11: 201-204 line outage: (a) machine 4 estimated vs. measured speed signal; (b) display of each oscillatory component	156
Figure 5.12: 201-204 line outage: (a) machine 5 estimated vs. measured speed signal; (b) display of each oscillatory component	157
Figure 5.13: 201-204 line outage: (a) machine 6 estimated vs. measured speed signal; (b) display of each oscillatory component	157
Figure 5.14: 3003-3005 line outage: (a) machines 1 and 2 estimated vs. measured speed signal; (b) display of each oscillatory component.....	161
Figure 5.15: 3003-3005 line outage: (a) machine 3 estimated vs. measured speed signal; (b) display of each oscillatory component.....	161
Figure 5.16: 3003-3005 line outage: (a) machine 4 estimated vs. measured speed signal; (b) display of each oscillatory component.....	162
Figure 5.17: 3003-3005 line outage: (a) machine 5 estimated vs. measured speed signal; (b) display of each oscillatory component.....	162
Figure 5.18: 3003-3005 line outage: (a) machine 6 estimated vs. measured speed signal; (b) display of each oscillatory component.....	163
Figure 5.19: 3005-3006 line outage: (a) machines 1 and 2 estimated vs. measured speed signal; (b) display of each oscillatory component.....	166

Figure 5.20: 3005-3006 line outage: (a) machine 3 estimated vs. measured speed signal; (b) display of each oscillatory component..... 166

Figure 5.21: 3005-3006 line outage: (a) machine 4 estimated vs. measured speed signal; (b) display of each oscillatory component..... 167

Figure 5.22: 3005-3006 line outage: (a) machine 5 estimated vs. measured speed signal; (b) display of each oscillatory component..... 167

Figure 5.23: 3005-3006 line outage: (a) machine 6 estimated vs. measured speed signal; (b) display of each oscillatory component..... 168

Figure AIII.1: system diagram for output matrix formulation..... 195

List of Tables

Table 4.1: variation in natural frequency with X/R ratio	76
Table 4.2: mode data for unblocked two-machine two line system with line outage followed by no reclosure action. Governor time constant is varied.....	129
Table 5.1: selected line outages for the system in figure 5.1 with pre-fault power flows.....	141
Table 5.2: comparison of modal properties for 151-152 line outage, mode 1.....	147
Table 5.3: comparison of modal properties for 151-152 line outage, mode 2.....	147
Table 5.4: comparison of modal properties for 151-152 line outage, mode 4.....	147
Table 5.5: comparison of modal properties for 151-152 line outage, mode 5.....	148
Table 5.6: comparison of modal properties for 201-204 line outage, mode 1.....	153
Table 5.7: comparison of modal properties for 201-204 line outage, mode 3.....	154
Table 5.8: comparison of modal properties for 201-204 line outage, mode 4.....	154
Table 5.9: comparison of modal properties for 201-204 line outage, mode 5.....	154
Table 5.10: comparison of modal properties for 3003-3005 line outage, mode 1.....	159
Table 5.11: comparison of modal properties for 3003-3005 line outage, mode 2.....	159
Table 5.12: comparison of modal properties for 3003-3005 line outage, mode 4.....	159
Table 5.13: comparison of modal properties for 3003-3005 line outage, mode 5.....	160
Table 5.14: comparison of modal properties for 3005-3006 line outage, mode 1.....	164
Table 5.15: comparison of modal properties for 3005-3006 line outage, mode 2.....	165
Table 5.16: comparison of modal properties for 3005-3006 line outage, mode 4.....	165
Table 5.17: comparison of modal properties for 3005-3006 line outage, mode 5.....	165
Table 5.18: oscillation frequency measurements: 151-152 outage	171
Table 5.19: oscillation frequency measurements: 201-204 outage	172
Table 5.20: oscillation frequency measurements: 3003-3005 outage.....	172
Table 5.21: oscillation frequency measurements: 3005-3006 outage.....	173
Table 5.22: frequency residues: calculated vs. measured, 151-152 outage.....	178
Table 5.23: frequency residues: calculated vs. measured, 201-204 outage.....	179
Table 5.24: frequency residues: calculated vs. measured, 3003-3005 outage.....	179
Table 5.25: frequency residues: calculated vs. measured, 3005-3006 outage.....	180

Chapter 1 Introduction

The foremost issue in operating an AC power system is maintaining system frequency [1]. This is the case because time-averaged frequency can be considered uniform throughout an interconnection whereas voltage and element flows are localized quantities. Deviations from rated values of voltage and element flows, as a general rule, do not affect the overall system. Since the vast majority of all energy supplied to a power grid is supplied by synchronous generators and since synchronous generator speeds translate directly to system frequency [2], power system operation, monitoring, analysis and design might be considered a collection of machine speed problems.

1.1 Frequency Measurement History

In order to put frequency measurements and their use in power system operation and analysis into perspective it is useful to review the history of frequency measurement applications. The comparison between traditional uses and advanced uses is, for the most part, a matter of comparing measurement speeds and measurement scope (wide area vs. local). Traditional frequency measurements on an electric power system are, as a general rule, neither wide area nor high speed. For example, NERC, in the Eastern Interconnection will report frequency for each control area on a once-per-minute basis [3]. Sub-minute wide-area data on frequency is typically not available. To operators and other entities in the power industry this is satisfactory because 1) power system frequency is considered to be a uniform quantity throughout an interconnection, and so wide-area measurements have not been considered useful; and 2) traditional power system central control schemes (secondary generator control) use frequency primarily as a quasi-steady-

state feedback quantity for ACE regulation [1],[4]. ACE or area control error is part of a low speed control system (time constants may be as high as a couple of minutes [5]) that operators may not expect to benefit from high-speed measurements. Traditional *local* control schemes (primary generator control) use frequency as a feedback quantity for speed-droop regulation. This part of the control system does require sub-minute (but not sub-second) frequency data. Frequency measurements made by conventional low-accuracy transducers which take measurements at the generator terminal have been satisfactory for purposes of speed-droop regulation. And so historically there has been little or no demand for high-speed wide-area frequency measurements among power system operators. In addition to this lack of demand, time-synchronization, which is necessary for the implementation of a wide-area frequency measurement system, has previously been either unavailable or too expensive [6].

In addition to feedback for primary and secondary generation controls, frequency measurements have been used for protection of transformers and machines [7]. In these cases, sub-second frequency data is not necessary as machine and transformer capability characteristics generally allow for operation above or below rated frequency for an extended period of time – usually on the order of minutes or even indefinitely [8], [9]. A protection scheme that may be considered an exception when it comes to high-speed wide-area requirements is load shedding and restoration [7]. However, an out-of-tolerance frequency condition that does lead to either load shedding or restoration may be accomplished satisfactorily by using local measurements. An underfrequency condition will be detected earliest by frequency monitors in the vicinity of the generator trip. Load shedding, naturally, should take place as closely as possible to the disturbance.

In recent years, generation excitation systems, HVDC, and FACTS device development have brought about a demand for higher speed frequency data since all three of these systems can benefit from sub-second measurements [10], [11], [12]. The feedback measurement requirement for these applications calls for a single local frequency measurement or perhaps multiple local measurements. Wide area measurements may come into play in the future.

1.2 Applications Under Development

The advent of FNET, or Frequency Monitoring Network, has brought about opportunities to use both wide-area and high-speed measurements [6]. FNET is a collection of distribution voltage synchronized frequency monitors spread out over both the Eastern and Western Interconnections that stream high-speed frequency data to a central server which stores and processes the frequency data. The most prominent use of this system presently is in disturbance location. In order to determine an approximate geographical location of a generator outage, the FNET uses a triangulation algorithm based on wave motion principles [13], [14]. In addition to outage location, FNET can use system Frequency Response Characteristic (also called system β) to determine the magnitude of megawatt drop due to a generator outage [15]. Mode identification [16] and post mortem analysis are additional applications of FNET that are presently under development.

In addition to the FNET system, which is a collection of distribution-level monitors, there has been under development since the mid-80's the use of synchronized wide-area phasor measurements via phasor measurement units, or PMU's [17]. Presently

PMU's have the ability to monitor voltage magnitude, phase angle, frequency, and other electrical quantities and are primarily installed at transmission levels. There has been a gracious plenty of research done using phasor measurements in areas of stability, state estimation and several other areas.

Digital fault recorders have been in use since the 1970's [1] and currently provide wide-area frequency information, however these devices are not designed to operate in real-time such as the PMU's and FRU's mentioned above.

1.3 Proposed Uses of Frequency Measurements

In this work, I propose the use of wide-area, high-speed frequency measurements for disturbance identification. Identification, here, is subtly different from disturbance location mentioned above. The identification is based on a generator's location topologically in a system, rather than it's geographical location on a map. Chapter 3 will discuss this further. The algorithm is based on power system modal analysis which is basically a system natural response study. The natural response of the power system is due to the energy stored in the rotating masses and generator magnetic fields. Thus, a state-space model is established to identify operational modes following a disturbance. This use is possibly more didactic than practical, especially in larger interconnections such as those in the United States. However, this application may be useful in smaller interconnections such as the Texas interconnection and perhaps those in developing countries.

The approach that this work uses in presenting the disturbance identification technique using modal analysis proceeds through the following steps: 1) Chapter 2 gives

a presentation of lumped parameter frequency behavior basics. This is done in the context of oscillatory activity in a system. The purpose of this presentation is to prepare the reader to understand the relationships between machine speed(s) and frequency measurements taken at some remote point from the machines. When a system is subject to oscillatory activity, there are, what some may call, unconventional relationships in between the machine speeds and the frequency measurements; 2) Chapter 3 gives a presentation of generator outage identification using modal analysis on an idealized simple system. This presentation is intended to be instructional as it presents oscillatory mode behavior in terms of machine speed and frequency measurements in addition to the outage identification process. The idealized simple system is blocked (concerning governors and AVR's), lossless, has no line-charging susceptances, has zero damping, and has an infinite bus connected to the system. This chapter also includes the development of an output matrix which is intended to translate system states (machine speeds) into frequency at measurement points on the power system; 3) Chapter 4 expands the modal analysis disturbance technique into a system state model which includes several non-ideal system characteristics such as losses, damping, and the absence of an infinite bus. Additional system modal characteristics due to the absence of the infinite bus are developed, in a sense, separately from the rest of the modal characteristics of the system. This is mentioned here because the presence of an infinite bus on a system guarantees that the system average frequency will always be rated frequency – any frequency variation due to a disturbance will be temporary and always oscillatory in nature. The absence of an infinite bus does not have this characteristic of guaranteeing that all machine speeds have an average speed of rated speed. But it should be kept in

mind that the average speeds of all machines on an interconnection must necessarily be equal – otherwise the machines would not be in synchronism with each other. Loss of synchronism due to instability or any other reason is not explored in this work. In chapter 4, the modal analysis technique of outage identification will be applied to line outages. And finally 4) Chapter 5 presents a test of all of the non-idealizations on a non-trivial system, a 23-bus, 6-machine test system. This test is done as a verification of the electromechanical model that is used to perform modal analysis.

Chapter 2 Basics of Lumped Parameter Model Frequency Characteristics

In the course of developing a generator outage identification scheme, several basic frequency characteristics become evident. Most of the frequency characteristics discussed here are characteristics that deal with both the time and space relationships of frequency values in a power system that result from machine speed oscillations about a quiescent operating speed. The reason for investigating system behavior in the presence of machine speed oscillations is primarily due to the fact that oscillations, both interarea and intermachine, occur in power systems. Interarea oscillations are important to system operators primarily because 1) continuous interarea oscillations reduce line transfer capability and can decrease circuit breaker critical clearing times; 2) negatively damped oscillations are unstable; 3) severe interarea oscillations lead to voltage magnitude fluctuations at intermediate points in the transmission system; 4) interarea oscillations occur on a somewhat frequent basis. The results of chapter 3, which focuses on generator outages exclusively, indicate that a power system that is subject to a generator outage will also be subject to machine speed oscillations – both interarea and intermachine. The results also indicate that these oscillations may be quantified in terms of frequency and, at least partially, in terms of oscillation magnitude.

The need for generator outage identification or location stems from two different aspects of power system operation. The first that I mention is a *financial* aspect. Whenever a unit trip occurs, the interconnection frequency proceeds to drop. This drop in frequency forces generator secondary controls to increase power outputs. This increase in power output is required for frequency support and in the case of North American interconnections, the increase in power is required and specified by NERC.

This increase in power results in an increase of fuel use over the scheduled (contracted) power production (a condition defined as inadvertent interchange). Without knowledge of a dropped unit's location, there is no one to account to for the necessary increase in power production. A single control area's tie line information, by itself, will not identify the control area where the unit outage occurred. It is the responsibility of each control area to keep track of inadvertent interchange. It is their own resources that they must dedicate to this task. Aspect number two is *reliability*. After the occurrence of a unit trip in an adjacent area, the subsequent increase in power output from each generator creates an immediate decrease in reserve capacity. The implications of inadequate reserve capacity are somewhat obvious and outlined in [1] - the most severe consequence being total system blackout.

In order to present how frequency measurements may be used to identify a disturbance, namely a generator outage, I will first go over the electromechanical principles of a single-machine infinite-bus (SMIB) system. These principles are thoroughly developed in several texts [4], [18], [19] et al. Some of these principles will be repeated here for convenience and because of their importance and simplicity for understanding power system electromechanics in general. The theory behind the SMIB system will be used to prove that a disturbance in generator speed (and also internal voltage angle) from equilibrium will result in a "frequency signature" that is, in a sense, unique to the generator's parameter set and operating point. Simulation is used to verify the theory in a two-machine infinite-bus system. A unit trip is shown to result in a frequency signature that corresponds to the natural response of the unit that was left online after the unit trip.

The same theory is expanded to a three-machine infinite-bus system. In this case the system calls for the use of a linearized state-space model where the natural response corresponds to 1) initial conditions which lead to mode excitation; 2) state matrix eigenvectors (or mode shapes); and 3) state matrix eigenvalues. All of these components of the natural response do actually exist in the SMIB system. However the order of the governing differential equation does not necessitate the use of vector-matrix differential equations and their solution methods. There are several texts that cover state modeling theory [20], [21].

Development of an electromechanical state-space model for power systems is not new [19]. However, its use in studying frequency signatures is. Previously the state model was used to perform *stability* studies by examining state matrix eigenvalues. If the eigenvalues do not lie in the left-half of the complex plane, then the system is not stable. Little attention was paid to the actual real and imaginary parts of the eigenvalues. It was not necessary to compute eigenvectors and the effect of machine oscillations on bus frequency has not been investigated. Further, the state model was not used to identify disturbances such as generator outages. In this work, the conventional electromechanical state model is modified to perform this task. Mode shapes, which are derived from plant matrix eigenvectors can be a key component in the disturbance identification process as shown in an example in chapter 3.

Once the theory has been expanded to a three-machine infinite-bus system, it is essentially expanded to n-machine theory. In principle, the linearized vector-matrix governing equation characteristics and solution methods are the same for the three-machine system as they are for an n-machine system. Formulation of the output matrix

will be one of the novelties of this process. The purpose of the output matrix is to transform the system state variables into outputs. The outputs are “load” bus frequencies and phase angles i.e. the *measured* quantities. It is important to understand, that when dealing with a state model, the output quantities may be considered to be measurement quantities and as a general rule, the term output has nothing to do with actual energy extraction from the system being modeled. The outputs are considered information signals only – they do not represent energy injection, withdrawal, or storage. Using the calculated outputs from the model and comparing them with the actual measured values from the simulation should yield enough information to identify a specific generator outage (or a set of generators, depending on the observability of the system). For the initial idealized system in chapter three, I develop an output matrix based on linear load flow principles (DC load-flow). The linear load flow is, perhaps, a grossly oversimplified model of a power system. However, some of the simulation results for the three-machine system yield good enough accuracy to verify that the approach of using the linear load flow has some merit. The generator outage identification problem is discussed in detail in chapter 3. This present chapter will focus exclusively on developing and investigating the basic time-space relationships of frequency values in a power system subject to either intermachine or interarea oscillations. All of the models used in this work are lumped parameter models. Previously, distributed parameter models have been developed and investigated. The distributed parameter models treat energy quantities (inertia, voltage angle, power injection, power withdrawal) as distributed parameter quantities, whereas this present work treats all energy quantities as lumped. This type of model should theoretically be superior to the distributed parameter model

due to the fact that all energy quantities in a power system manifest themselves only at specific points in the system. They are not spread out over the geographic space of the power system.

2.1 The Electromechanical Nature of a Single-Machine AC Electric Power System

There are various principles that are good to examine before looking into the theory behind frequency dynamics. The first of these is how frequency is related to generator speed. Based on Faraday's law, the frequency of a generator's induced voltage is directly proportional to the generator's shaft speed. Since, for an elementary machine, the flux linkage, λ , may be expressed as

$$\lambda = SB \cos \theta \quad (2.1)$$

Where B is the uniform and constant flux density of the region where the rotating armature coil resides, θ is the armature's angular position with respect to a specific reference, and S is the area of the armature coil. With the coil rotated at a speed equal to ω , which is not necessarily a constant speed, $\theta = \omega t$ and so

$$\lambda(t) = SB \cos(\omega t) \quad (2.2)$$

Thus the voltage of the coil, v , may be expressed as

$$v(t) = \frac{d\lambda}{dt} = SB \frac{d}{dt} \cos(\omega t) = -SB\omega \sin(\omega t) \quad (2.3)$$

And so the frequency of this voltage is directly related to generator speed.

The next principle is the relationship between frequency deviation (from rated) and the change in voltage angle. If $\delta(t)$ is the angular position of the rotor with respect to a synchronously rotating reference axis, then $\delta(t)$ may be expressed as

$$\delta(t) = \int_{t_0}^t \omega_r(\tau) d\tau - \omega_s t + \delta_0 \quad (2.4)$$

where $\omega_r(\tau)$ is the angular velocity of the rotor, ω_s , a constant quantity, is the rotational speed of the synchronously rotating reference axis, and δ_0 is the initial value of the rotor angle with respect to the synchronously rotating reference axis. It's important to understand that the electrical angle of the generator's internal voltage is directly related to this angle since the pole faces of the machine, and thus the rotor's flux, cut the armature conductors in accordance with the rotor angle. This cutting action is what produces the internal voltage, and thus the internal angle. Taking the derivative with respect to time of $\delta(t)$ and using the second fundamental theorem of calculus yields

$$\frac{d\delta(t)}{dt} = \omega_r(t) - \omega_s \quad (2.5)$$

This expression is identical to machine speed deviation, $\Delta\omega$, and thus, per the conclusion from equation (2.3) above, is also identical to frequency deviation (from synchronous frequency), measured in rad/sec.

$$\frac{d\delta(t)}{dt} = \Delta\omega \quad (2.6)$$

As a side note, it is important to understand that the identity (2.6) holds only for a two-pole machine. If the machine has more than two poles then a proportionality constant needs to be included in the equation. Both of these relationships, (2.3) and (2.6), are derived in more detail in various texts [4], [18], [22].

2.2 Salient Electromechanical Features of Simple AC Systems

A couple of simple relationships that demonstrate the special distribution of frequency deviations are presented next. To show how frequency deviations are distributed throughout a system, a single-machine oscillating against an infinite bus may be used for the demonstration. The system is shown in figure 2.1.

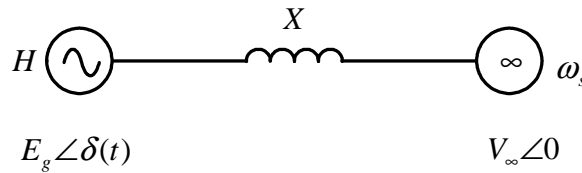


Figure 2.1: SMIB system

In the case of an infinite bus, it is important to understand that an infinite bus has a phase angle that is held stiff at zero degrees (or some other number of degrees that you may choose as a reference). Therefore the infinite bus frequency is also held stiff at rated frequency. This is part of the definition of an infinite bus. The two definitions that state that an infinite bus frequency and phase angle are held stiff are, in fact, redundant statements. If a single-machine (or a single equivalent machine) oscillates against an infinite bus, the frequency of the machine's internal voltage angle will have a deviation according to the swing equation as follows

$$\frac{2H}{\omega_s} \frac{d^2 \delta(t)}{dt^2} = P_a = P_m - P_e \quad (2.7)$$

where H is the machine's inertia constant, ω_s is the synchronous frequency in rad/sec^2 , δ is the internal voltage angle in radians, P_a is the rotor train's acceleration power, P_m is the mechanical power being injected into the rotor train, and P_e is the electrical power

being drawn from the generator's electrical terminal. All of these power quantities are expressed in per-unit. Since P_e may be expressed as follows for a lossless system

$$P_e = \frac{E_g V_\infty}{X} \sin \delta \quad (2.8)$$

where E_g is the generator's internal voltage magnitude, V_∞ is the infinite bus voltage magnitude, X is the reactance that connects the internal voltage to the infinite bus and δ is the angle difference between the generator's internal voltage and the infinite bus angle (set at zero). Since P_m is generally considered constant due to slow action on the generator governor's part, then equation (2.7) becomes

$$\frac{2H}{\omega_s} \frac{d^2 \delta(t)}{dt^2} = P_m - \frac{E_g V_\infty}{X} \sin \delta \quad (2.9)$$

This equation, when rearranged and linearized about a quiescent operating point, δ_0 , becomes

$$\frac{d^2 \Delta \delta(t)}{dt^2} + \frac{\omega_s P_{\max} \cos \delta_0}{2H} \Delta \delta(t) = 0 \quad (2.10)$$

Here P_{\max} is the maximum value of P_e on the system's power-angle curve and $\Delta \delta(t)$ is the deviation in machine angle from the quiescent point angle. The system behaves exactly like a pendulum. For a disturbance that results in an initial value of $\Delta \delta_0$ the solution to this equation is

$$\begin{aligned} \Delta \delta(t) &= \Delta \delta_0 \cos \omega_n t \text{ and} \\ \delta(t) &= \delta_0 + \Delta \delta(t) \end{aligned} \quad (2.11)$$

This is assuming that $\Delta \dot{\delta}(t_0) = 0$. Regardless of initial conditions, the *natural* frequency, ω_n , may be expressed as

$$\omega_n = \sqrt{\frac{\omega_s P_{\max} \cos \delta_0}{2H}} \tag{2.12}$$

Notice how the machine parameters affect the *natural* frequency – heavier masses (rotor trains), and higher reactances lead to lower *natural* frequencies and vice versa. Higher voltages lead to higher frequencies and vice versa. We may consider that higher *natural* frequencies correspond to tighter coupling of the machine to the infinite bus and lower *natural* frequencies correspond to looser coupling to the infinite bus. It is this *natural* frequency that is used in chapter 3 to identify a generator outage.

Assuming that the line that connects the generator terminal to the infinite bus has no voltage sag and that the internal voltage magnitude is equal to the infinite bus voltage magnitude, then the voltage angle along the line must necessarily decrease in a linear fashion (with respect to distance from the generator) from the generator’s internal voltage to the infinite bus. This notion may be understood through the triangle relationship shown in figure 2.2.

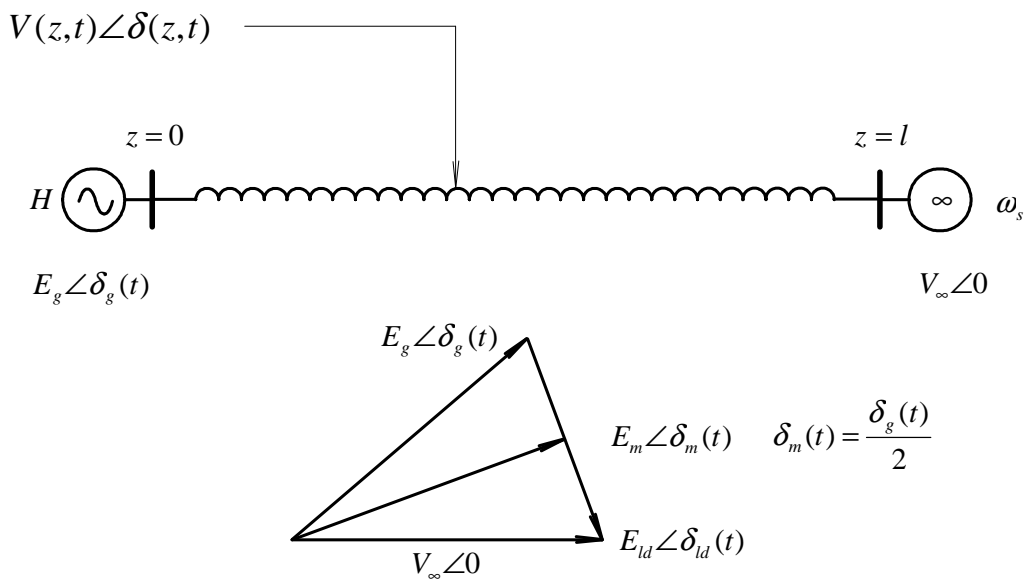


Figure 2.2: angle variation along line that connects source to infinite bus

This figure shows how Kirchoff's voltage law being used in the complex plane gives a triangle where the vector sum of the machine's internal voltage and the voltage drop along the line must be equal to the internal voltage. Assuming that the infinite bus angle is equal to zero, and following a disturbance that has an initial condition of $\Delta\delta_g(t_0) = \Delta\delta_0$, it can be seen that the angle deviation at any point varies in a linear fashion along the line.

$$\Delta\delta(z,t) = \frac{(z-l)}{l} \Delta\delta_0 \cos(\omega_n t) \quad (2.13)$$

Due to the relationship derived in (2.6), $\frac{d\delta(t)}{dt} = \Delta\omega$, the frequency deviation from rated frequency will have a maximum amplitude at the generator's internal voltage and will linearly decrease along the line until it reaches zero at the infinite bus.

$$\Delta\omega(z,t) = \frac{\partial\Delta\delta(z,t)}{\partial t} = -\frac{(z-l)}{l} \Delta\delta_0 \omega_n \sin(\omega_n t) \quad (2.14)$$

This relationship shows that the instantaneous frequency is, by no means, equal at all points in the system. And based on this equation, this conclusion may be drawn - though instantaneous frequency is in general not uniform throughout a system, the time-average frequency is uniform throughout the system. This case of a single machine oscillating against an infinite bus is not an exception. Notice that the oscillations in both angle and frequency have the same frequency, the system *natural* frequency - it is the oscillation *amplitude* that varies along the line. Expanding this notion from a single-line connection to the infinite bus to having a mesh connection to the infinite bus, one could postulate that oscillation frequencies would be constant throughout the mesh, even though the magnitude of the oscillations must necessarily be, in general, different

throughout the system – the closer the measurement is to the generator, the higher the amplitude; the closer the measurement to the infinite bus, the lower the amplitude.

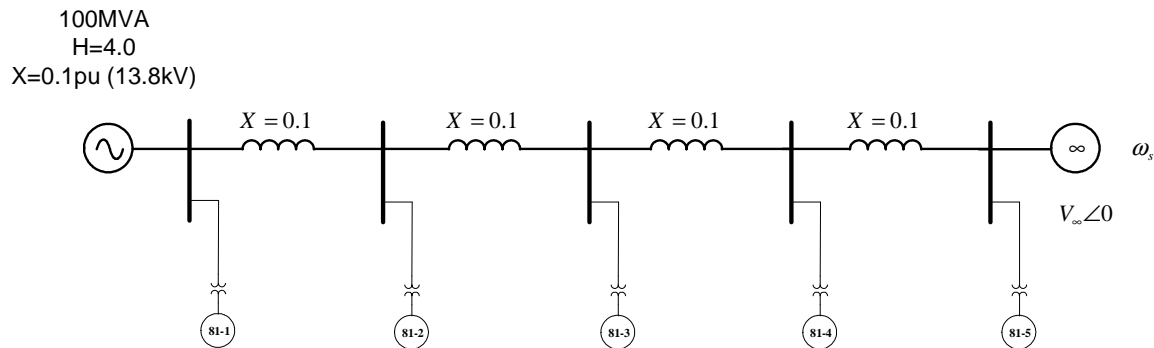


Figure 2.3: single-machine infinite bus simulated system to show frequency variations along transmission line

To verify the linear variation in frequency deviation presented by equation (2.14), the system in figure 2.3 was simulated with frequency measurements being taken at roughly 1/4 – length intervals of the transmission line. The single machine here is oscillating at its natural frequency against the infinite bus. Figure 2.4 shows the highest frequency deviation is seen to be at the generator terminals, 4 hertz. The frequency deviations decrease in a linear fashion, 3 hertz at 3/4 distance from the infinite bus, 2 hertz at half the distance, 1 hertz at 1/4 of the distance and finally dropping off to zero deviation at the infinite bus as expected.

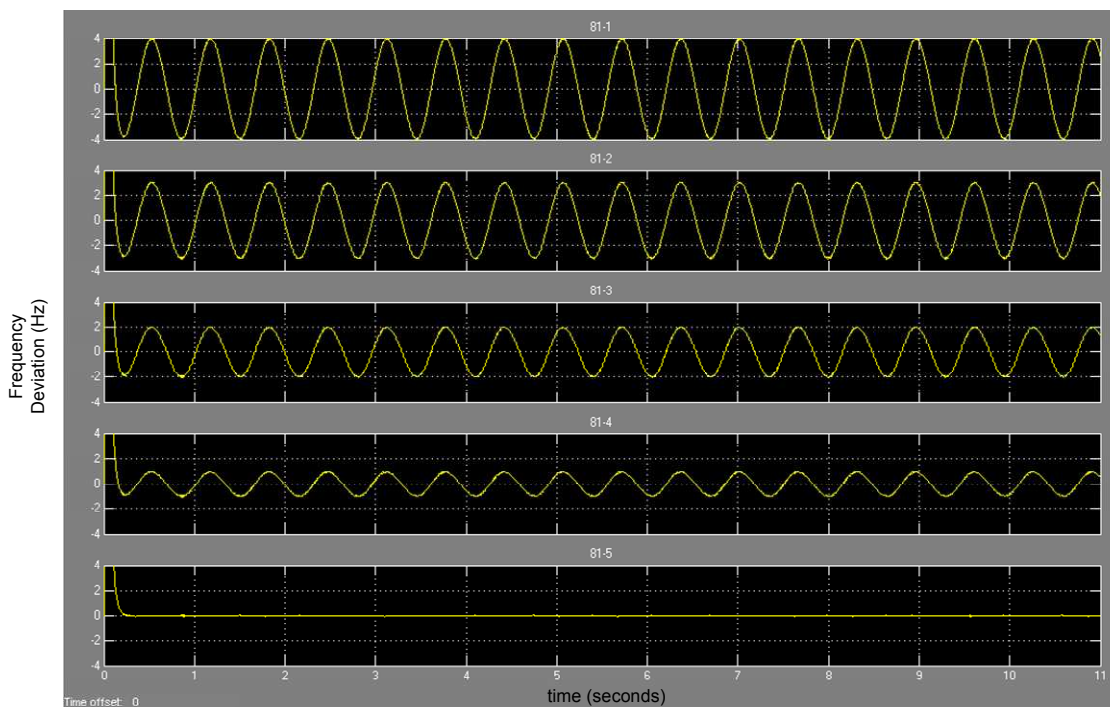


Figure 2.4: simulation results of system in figure 2.3

One final principle derived here before developing the two-machine infinite bus outage case is that of frequency deviation cancellation. Using a two-machine system shown in figure 2.5 and using the linear phase angle distribution principle presented above, it is shown below that there exists a frequency deviation cancellation on the transmission line at some point. For two identical machines oscillating against each other, their internal voltage angles may be expressed as follows

$$\delta_1(t) = \delta_{1q} + k \sin(\omega_n t) \quad \text{and} \quad \delta_2(t) = \delta_{2q} - k \sin(\omega_n t) \quad (2.15)$$

where the constant k depends on the initial conditions, δ_{1q} and δ_{2q} are the quiescent values of $\delta_1(t)$ and $\delta_2(t)$, and ω_n is the natural frequency of the two-machine combination. Here, as the case of the single-machine infinite-bus above, the angle at the midpoint is the average of the two machine angles. In this case, however, $\delta_m(t)$ turns out to be a constant value. The oscillating components cancel each other out according to

$$\delta_m(t) = \frac{\delta_1(t) + \delta_2(t)}{2} \tag{2.16}$$

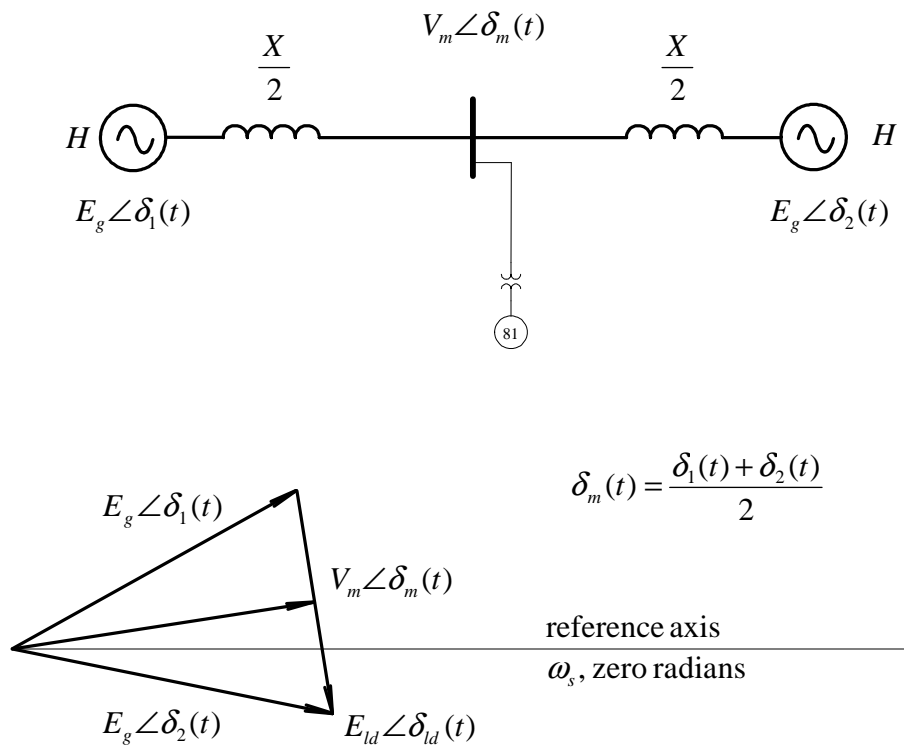


Figure 2.5: two-machine system

It's derivative must be zero and so $\Delta\omega$ at the midpoint bus is identically zero. This is true regardless of the amplitude of the two machine's oscillations. Their frequency deviation magnitudes may, in theory, be any value and the oscillation will not show in a frequency measurement at the midpoint bus.

In figure 2.5 the voltage angle along the line that connects the two machines may be expressed as

$$\delta(z,t) = [\delta_1(t) - \delta_2(t)] \frac{l-z}{l} + \delta_2(t) \tag{2.17}$$

where l is the total length of the line that connects the two sources and z is the distance from source number 1. For the case of two machines oscillating against each other, equation (2.15) may be inserted into equation (2.17) to yield

$$\delta(z,t) = [(\delta_{1q} - \delta_{2q}) + 2k \sin(\omega_n t)] \frac{l-z}{l} + \delta_{2q} - k \sin(\omega_n t) \quad (2.18)$$

The voltage angle and thus the frequency may be derived at any point on the line assuming that the impedance per unit length of the line is uniform.

$$\begin{aligned} \Delta\omega(z,t) &= \frac{\partial\delta(z,t)}{\partial t} \\ &= k\omega_n \cos(\omega_n t) \left[2\frac{l-z}{l} - 1 \right] \end{aligned} \quad (2.19)$$

This principle points to the notion of a frequency “center of mass” that exists somewhere in a transmission mesh while a pair of generators (or equivalent generators) oscillate against each other. Since a tie line (or any transmission line) may be tapped at or near its center point, this example has implications in practical situations where a frequency measurement may be taken off of the transmission line’s tap. Likewise a frequency measurement may also be taken at a mesh’s “center of mass.” Since interarea oscillations take on a similar form as the above two-machine system, the *mode* associated with an interarea oscillation, when viewed using a frequency measurement at the center of the tie line (or at a hypothetical “center of mass” in a mesh), is a *mode* that is *not observable*. This example should be useful in understanding frequency deviation distributions and may be kept in mind whenever frequency measurement unit placement is considered. A monitoring system planner may consider that important modes, if they can be determined, should not be unobservable as in this case. Observability could be achieved by unit placement away from the “center of mass.”

To verify the notion of frequency “center of mass,” the system in figure 2.6 was simulated. This system is a pair of machines that are oscillating against each other at their natural frequency. The simulation results, shown in figure 2.7, show that there is a

linear variation in frequency deviation from each machine toward the center-point of the transmission line. There is no deviation in frequency at the center point as shown by the measurement taken by device 81-3.

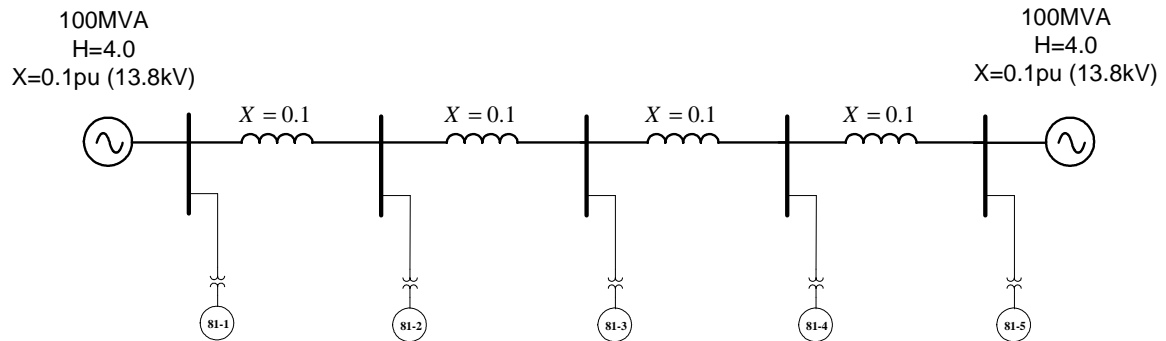


Figure 2.6: two machines oscillating against each other

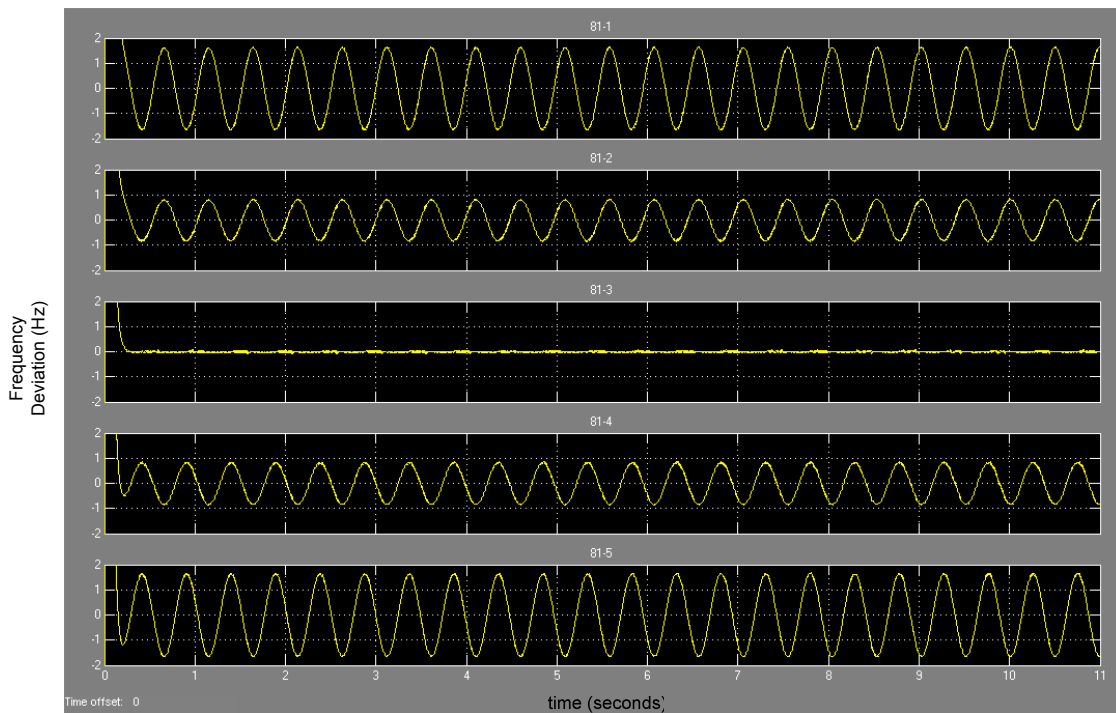


Figure 2.7: simulation results of system in figure 2.6

And the exact same results are shown in figure 2.9 for a meshed two-machine system shown in figure 2.8.

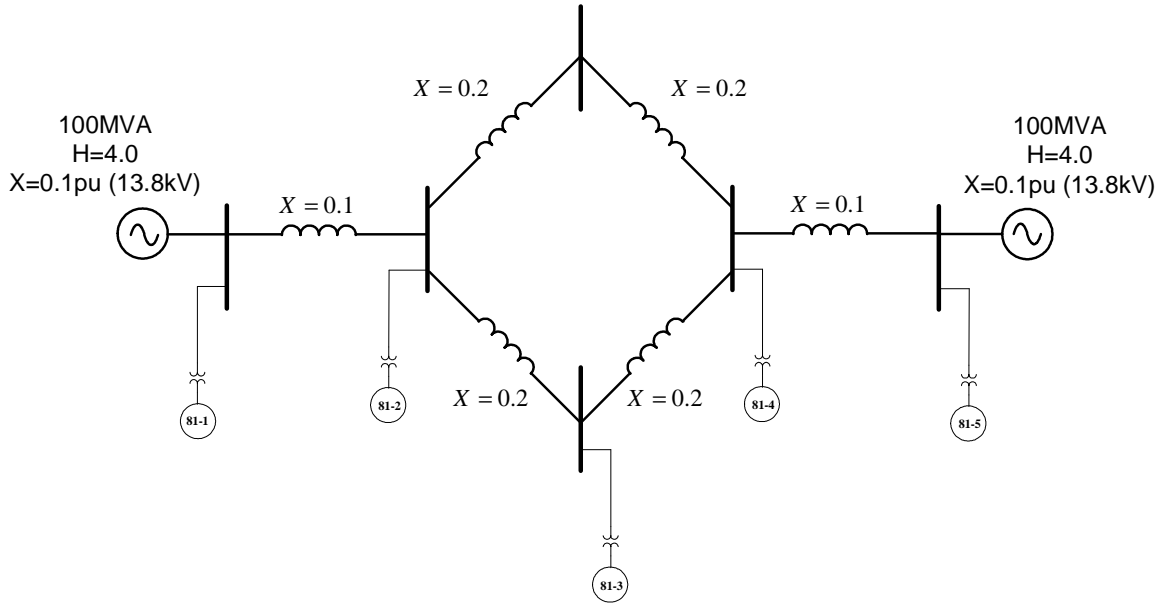


Figure 2.8: two machines oscillating against each other through a meshed transmission system

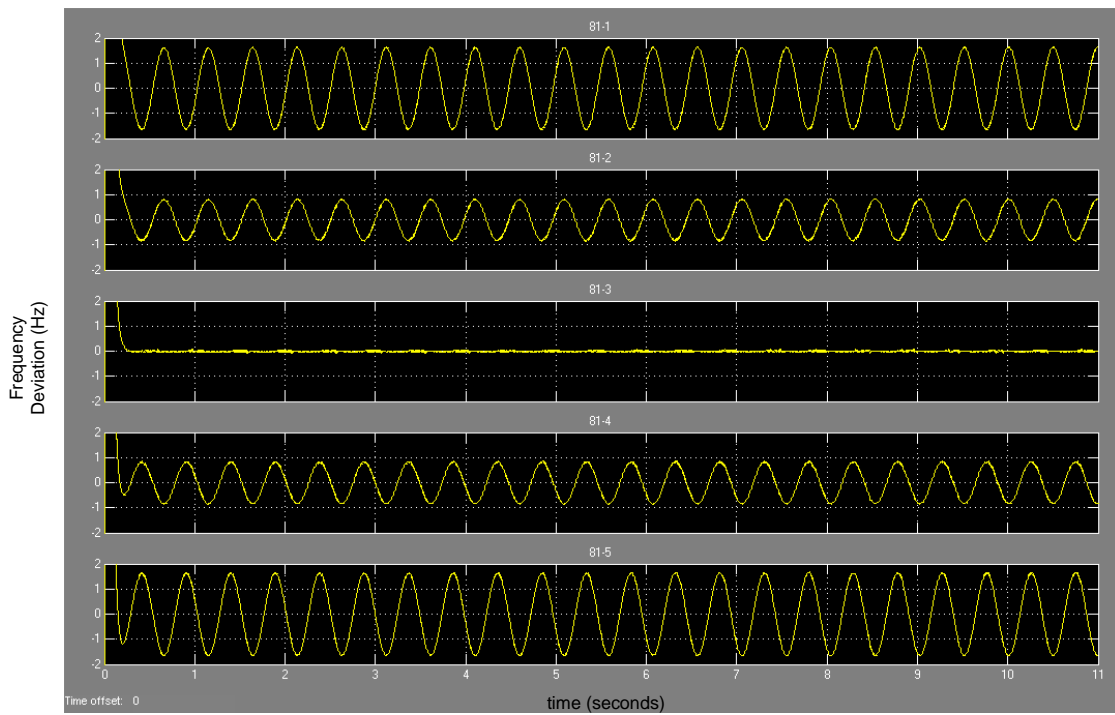


Figure 2.9: simulation results of system in figure 2.8

Chapter 3 Generator Outage Identification Using Modal Analysis

3.1 Outage Identification in a Two-Machine Infinite Bus System

In order to present the theory and process of generator outage identification based on frequency measurements, a two-machine infinite-bus system will be examined first.

The two-machine system is shown in figure 3.1.

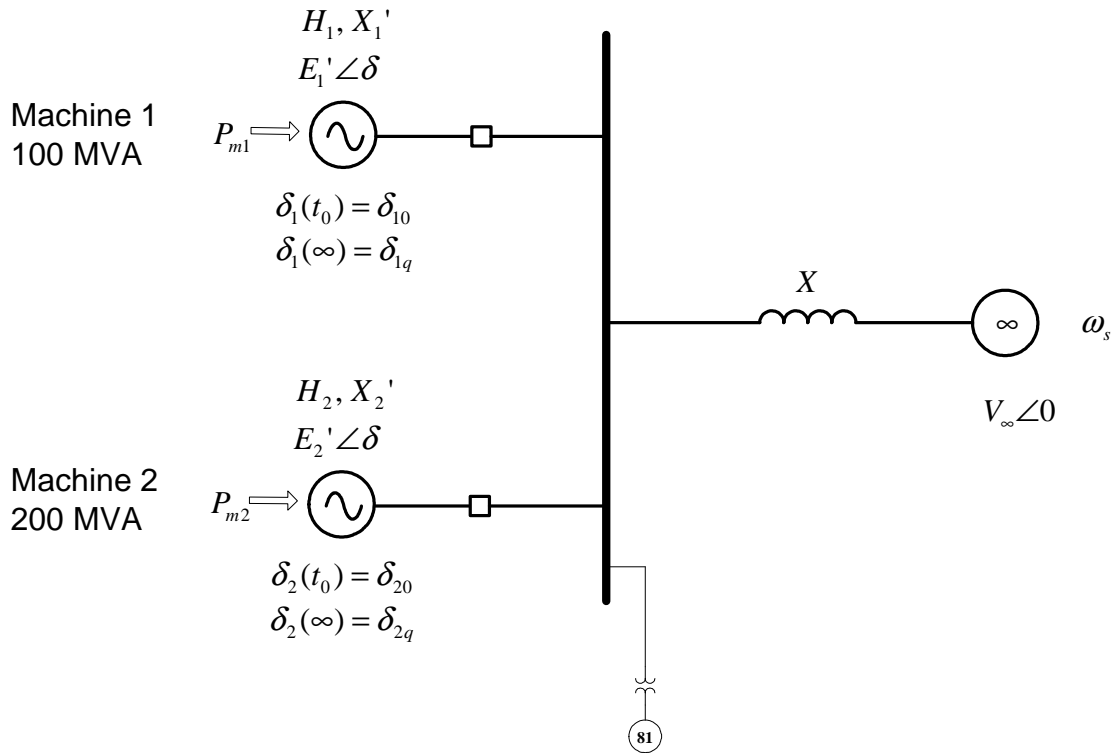


Figure 3.1: two-machine infinite-bus system

Both of the machines are injecting one-half of their rated power into an infinite bus. For this example one of the machines is rated at 100MVA, the other at 200MVA. The machine parameters on nameplate base are exactly the same. Based on the theory presented in section 2.2, each one of the machines has a specific natural frequency, ω_{n1} for machine 1 and ω_{n2} for machine 2. To be exact about the expression “natural frequency” it should formally be referred to as *undamped* natural frequency. The

relationship of equation (2.7), the swing equation for a single-machine infinite-bus system, assumes that there are no losses in the system and so damping does not exist. In an actual machine, damping coefficients between 1 and 3 are typical [19]. Damping coefficients of this order will result in damping *ratios* of much lower than 10 percent; i.e. they are classified as lightly damped oscillations. These low damping ratios result in 10 or more full oscillations before complete decay and create a minimal difference between the undamped natural frequency and the damped natural frequency. The machines in this example are unregulated, that is to say that their mechanical power injected via turbines and internal voltages remain constant after the disturbance. This is known as the classical machine model [19].

In order to solve for $\delta_i(t)$, the internal angle of the machine that is left online after the outage, the values $\delta_1(t_0)$ and $\delta_2(t_0)$ must be determined before-hand via load flow. These values need to be determined because, immediately following a generator outage, the $\delta_i(t_0)$ value of the generator that is left online will provide the oscillation excitation. This is the case because immediately following an outage, the angle of the generator that is left online must proceed to retard to a new quiescent value. In a practical situation, both values need to be determined simply because the system operator does not know which one will drop offline.

According to the mathematical model of (2.7), $\delta_i(t)$ will never reach that quiescent value but instead will oscillate around it according to the solution of linearized (2.7), which in this case will be

$$\delta_i(t) = \delta_{iq} + \Delta\delta_i(t)$$

$$\Delta\delta_i(t) = (\delta_{i0} - \delta_{iq}) \cos(\omega_{ni}t) \quad (3.1)$$

due to the initial conditions

$$\begin{aligned} \Delta\dot{\delta}_i(t_0) = \Delta\omega_i(t_0) = 0 \quad \text{and} \\ \Delta\delta_i(t_0) = \delta_{i0} - \delta_{iq} \end{aligned} \quad (3.2)$$

The first initial condition indicates that the unfaulted machine was running at synchronous speed just prior to the fault. It is certainly assumed that both machines were running at synchronous speed just prior to the fault. The quantity ω_{ni} is the natural frequency of machine i when it oscillates alone against the infinite bus with the other machine disconnected. The quantities δ_{i0} and δ_{iq} may be considered to be the pre- and post- quiescent values of $\delta_i(t)$. The detected frequency at the bus should be expected to be per (2.14) with proper adjustments made to the equation for uneven distribution of the impedance due to the internal impedance of the generator. It is the oscillation frequency that is of greatest importance here as opposed to the actual excitation magnitude, in this case $\delta_{i0} - \delta_{iq}$. The measured oscillation frequency can be compared with the two calculated natural frequencies, ω_{n1} and ω_{n2} . Whichever natural frequency is present in the frequency waveform will reveal which machine is left online, thus identifying the machine that was taken out of service. In a practical situation a Fourier analysis could be performed on the frequency waveform to verify that the only AC component of the oscillation is one of the two natural frequencies. There is the case where both machines may oscillate against the infinite bus due to special initial conditions, say a cleared short-circuit on the main bus. Under this type of condition, the system has yet another natural frequency. The nature of this additional oscillation mode actually corresponds to a single

machine oscillating against the infinite bus with aggregate impedance, inertia, and power injection and the natural frequency for this mode may be solved for in accordance with equation (2.12). The machine parameters based on nameplate MVA are as follows:

Voltage: 13.8kV Frequency: 60Hz Damping factor $K_d = 0.0$

Number of poles: 2 $X_d' = j0.3$ ohms

The impedance in front of the infinite bus, X , is 0.3 pu on a 100MVA, 13.8kV base.

Each machine is injecting a power 0.5 pu on it's own base into the infinite bus. For machine 1 oscillating alone against the infinite bus (machine 2 taken out of service), the corresponding natural frequency is 1.4112 Hz. For machine 2 oscillating alone against the infinite bus (machine 1 taken out of service), the corresponding natural frequency is 1.1185 Hz.

With machine 1 taken offline at $t = 1.0$ seconds, the frequency and phase measured by the 81 device (frequency measurement unit) are shown in figure 3.2.

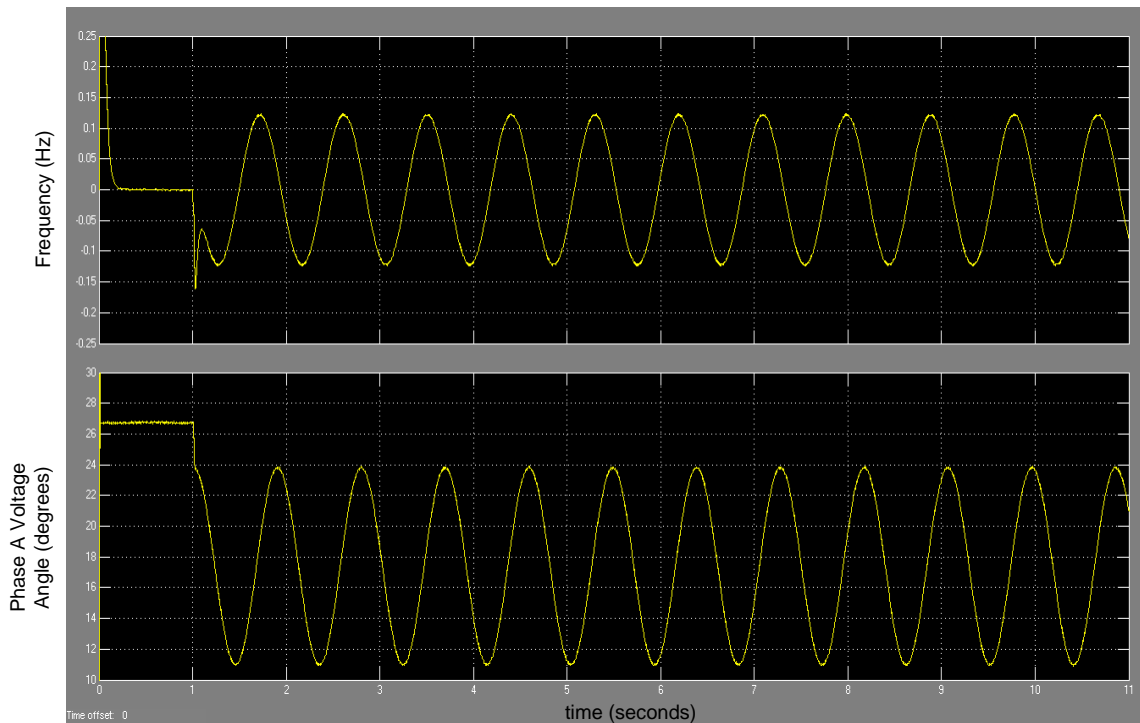


Figure 3.2: frequency and angle measurements for machine 1 outage

The oscillation frequency in both voltage angle and frequency is measured to be 1.11 Hz as expected. The initial downward spike in frequency is due to the necessary downward step in voltage angle at the instant that machine 1 is taken offline. Due to the fact that there are no mechanical losses in this system, both of the waveforms in figure 3.2 are undamped.

With machine 2 taken offline at $t = 1.0$ seconds, the frequency and phase measured by the 81 device is shown in figure 3.3.

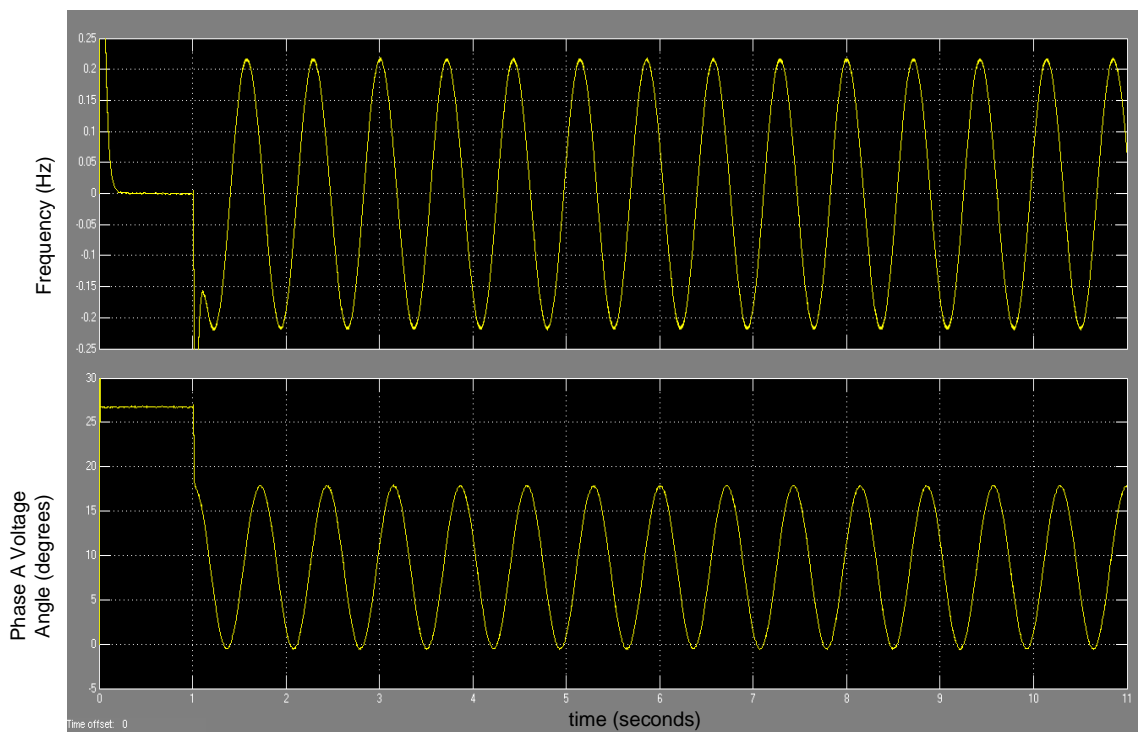


Figure 3.3: frequency and angle measurements for machine 2 outage

The oscillation frequency is 1.41 Hz as expected.

If an appropriate oscillation trigger is applied to the system before a machine outage [16], the oscillation could be detected, the waveform saved into a buffer and processed through an FFT (or some other signal decomposition processor) to determine the oscillation frequency. After comparing the oscillation frequency to the two calculated

frequencies, the machine outage could be identified. This example, though trivial compared to most power systems, demonstrates the ability to identify a generator outage based on a single frequency measurement.

3.2 *Small-Signal State Modeling of an Electromechanical System*

In the past, small-signal state models have been used to study system stability [19]. The governing equation was simply the homogeneous vector-matrix differential equation

$$\dot{\mathbf{x}}(t) = \mathbf{A}\mathbf{x}(t) \tag{3.3}$$

where $\mathbf{x}(t)$ is the system state, a vector that resides in \mathfrak{R}^n , and the plant matrix \mathbf{A} is a matrix whose elements are all real and *constant*. Because of the slow response of generator governors, their influence on the dynamic activity of the state was neglected and so their input was neglected. The resulting was a homogeneous equation. The states in these models were machine speed *differences*, and machine internal voltage angle *differences* with respect to one particular machine. This one particular machine was a reference of sorts for the small-signal model. There were two main reasons for setting up the model to study *differences* in speeds and angles as opposed to studying *absolute* speeds and angles. The first reason is that the model is simpler. An $n+1$ - machine system would have a state-space of dimension $2n$. When doing hand calculations to determine elements of the plant matrix, this reduction, for example, would result in a three-machine system that has a 4 x 4 plant matrix versus a 6 x 6 plant matrix for an absolute speed/angle model. Thus the reduction, in this case cuts the number of elements that must be calculated from 36 to 16. The second reason is that the primary objective in

stability studies is to determine whether or not the system will “stick” together following a disturbance. Machine speed and internal voltage angle differences will adequately tell whether or not a system of machines will stick together.

In the formulation of the state model for this present work, absolute quantities instead of *differences* in quantities will be used because it is assumed that the measured quantities, which constitute the system output, frequency (or perhaps phase angles) are absolute quantity and not differences in quantities. System stability is also assumed in this present work. Rigid-body modes, which occur when system frequency, and thus angles, all drift together away from a quiescent value are not revealed in the “differences” state model. The study of rigid-body modes will be conducted in a later chapter as the very important interconnection parameter of *frequency response characteristic* is a rigid-body phenomenon.

It is important to point out now that this model is a linearized model and is only good for “small” deviations from a quiescent point. The word “small” here should be qualified as follows – as the state moves through the state space, there must be approximately a linear relationship between the first derivative of each state variable and the state variables themselves. If this condition does not hold true, the model will not be accurate. Notice that the change in the state position as the state moves through the space need not necessarily be “small” compared to some reference quantity, say the “magnitude” of the quiescent point that the system is linearized about. The term “small” in this description is not relative to the size of the deviation but whether or not the deviation remains in a linear region.

For an n -machine system, the state model used in this work will take on the form

$$\frac{d}{dt} \begin{bmatrix} \Delta\delta(t) \\ \Delta\omega(t) \end{bmatrix} = \mathbf{A} \begin{bmatrix} \Delta\delta(t) \\ \Delta\omega(t) \end{bmatrix} \quad (3.4)$$

where $\Delta\delta(t)$ is an $n \times 1$ column vector of machine internal voltage angle deviations and $\Delta\omega(t)$ is an $n \times 1$ column vector of machine speed deviations. Thus the state vector

$\mathbf{x}(t) = \begin{bmatrix} \Delta\delta(t) \\ \Delta\omega(t) \end{bmatrix}$ resides in \mathfrak{R}^{2n} and the plant matrix \mathbf{A} is a $2n \times 2n$ matrix with all real

non-time varying elements. Just to look at a simple example, the one-machine system of section 2.3 above would have a state vector of two elements (each 1×1 column vectors) and thus the state vector would reside in \mathfrak{R}^2 . In formulating this state model, the elements of the plant matrix could be obtained from the governing second order differential equation, (2.10) which can be decomposed into two first order equations as follows

$$\begin{aligned} \frac{d\Delta\delta(t)}{dt} &= \Delta\omega(t) \\ \frac{d\Delta\omega(t)}{dt} &= -\frac{\omega_s S_p}{2H} \Delta\delta(t) \end{aligned} \quad (3.5)$$

Here $S_p = P_{\max} \cos \delta_0$. These equations may be arranged in the vector-matrix equation

$$\frac{d}{dt} \begin{bmatrix} \Delta\delta(t) \\ \Delta\omega(t) \end{bmatrix} = \begin{bmatrix} 0 & 1 \\ -\frac{\omega_s S_p}{2H} & 0 \end{bmatrix} \cdot \begin{bmatrix} \Delta\delta(t) \\ \Delta\omega(t) \end{bmatrix} \quad (3.6)$$

The key to generating the plant matrix is in writing out the governing differential equation for each machine and decomposing each governing equation into a pair of first order equations. There is an example of a two-machine system in the next section.

3.3 Eigenvalues, Eigenvectors of the Plant Matrix and Mode Excitation

Before proceeding to the two-machine example it is necessary to examine the eigenproperties of the plant matrix, specifically the eigenvalues, eigenvectors and their relationship to the solution of the state equation (3.4).

The state equation, (3.4), which is subjected to an initial condition $\mathbf{x}(t_0) = \mathbf{x}_0$ has the following solution

$$\mathbf{x}(t) = e^{\mathbf{A}t} \cdot \mathbf{x}_0 \quad (3.7)$$

where $e^{\mathbf{A}t}$ is the transition matrix defined by the power series representation of the exponential function [20]. If all of the eigenvalues of \mathbf{A} are distinct, and they will be for a practical system, then \mathbf{A} may be diagonalized as follows [23]

$$\mathbf{A} = \mathbf{P}\mathbf{\Lambda}\mathbf{P}^{-1} = \mathbf{\Phi} \begin{bmatrix} \lambda_1 & 0 & 0 \\ 0 & \ddots & 0 \\ 0 & 0 & \lambda_n \end{bmatrix} \mathbf{\Psi} \quad (3.8)$$

$$\text{where } \mathbf{\Phi} = [\boldsymbol{\varphi}_1 \quad \dots \quad \boldsymbol{\varphi}_n] \text{ and } \mathbf{\Psi} = [\boldsymbol{\psi}_1^t \quad \dots \quad \boldsymbol{\psi}_n^t]^t$$

where $\mathbf{\Phi}$ is an $n \times n$ matrix whose *columns*, $\boldsymbol{\varphi}_i$, are the normalized right eigenvectors of \mathbf{A} ; $\mathbf{\Psi}$ is an $n \times n$ matrix whose *rows*, $\boldsymbol{\psi}_i$, are left eigenvectors (not necessarily normalized) of \mathbf{A} ; and the λ_i 's in the diagonal matrix, $\mathbf{\Lambda}$, are the n distinct eigenvalues of \mathbf{A} .

The solution, $\mathbf{x}(t)$, may be expressed as (proof provided in Appendix I)

$$\mathbf{x}(t) = \langle \boldsymbol{\psi}_1, \mathbf{x}(t_0) \rangle \cdot \boldsymbol{\varphi}_1 \cdot e^{\lambda_1 t} + \dots + \langle \boldsymbol{\psi}_n, \mathbf{x}(t_0) \rangle \cdot \boldsymbol{\varphi}_n \cdot e^{\lambda_n t} \quad (3.9)$$

Each term in (3.9)'s summation corresponds to a *mode* of the system's natural response. A mode may be defined as follows: one of the linearly independent components of a system's natural (free, unforced) response. Each $e^{\lambda_i t}$ in the summation tells whether or not the i th mode is oscillatory or non-oscillatory. If λ_i is pure real, then the i th mode is non-oscillatory, that is to say that it is a pure decay-type mode with no oscillation. If λ_i is pure imaginary then the i th mode is an undamped sinusoid. The i th mode is pure oscillatory when λ_i is pure imaginary. And finally if λ_i is complex, then the i th mode will have a decaying (or exploding) sinusoidal character.

Each inner product term, $\langle \boldsymbol{\psi}_i, \mathbf{x}(t_0) \rangle$, in the summation is the excitation magnitude of the i th mode. It's useful to point out the fact that since the $\boldsymbol{\Phi}$ and $\boldsymbol{\Psi}$ matrices are inverses of each other that the inner product $\langle \boldsymbol{\psi}_i, \boldsymbol{\phi}_j \rangle$ is identically equal to zero for $i \neq j$ and is identically equal to 1 for $i = j$. Thus if the initial condition state vector, $\mathbf{x}(t_0)$, lies along (parallel to) the j th right eigenvector (or linear combination of a set of right eigenvectors) that none of the modes will be excited by the initial condition save the j th mode (or in the case of linear combinations of right eigenvectors only the corresponding modes will be excited). This is the case because $\mathbf{x}(t_0)$ is orthogonal to all of the left eigenvectors except for the j th eigenvector, $\langle \boldsymbol{\psi}_i, \mathbf{x}(t_0) \rangle = 0$ for $i \neq j$. This is a case of exclusive mode excitation. It can be seen by this discussion that the orientation of the initial condition vector, $\mathbf{x}(t_0)$, determines which modes will be excited and the magnitude of their excitation; and which modes will not be excited at all.

Each of the normalized right eigenvectors of \mathbf{A} , $\boldsymbol{\phi}_i$, represent the *shape* of mode i , that is to say the relative amount of activity (both magnitude and phase) of each state in

mode i , since $\boldsymbol{\phi}_i$ is normalized. Notice that, generally speaking, some of the components of any eigenvector, say the eigenvector that corresponds to the i th mode, may be equal to zero and thus the corresponding state for that eigenvector does not participate at all in the i th mode.

As a general rule, most of the eigenvalues for a practical system will be complex and for the case of a system with no damping factors, the complex eigenvalues will be pure *imaginary*. As a side note, if an infinite bus is present in the system, none of the eigenvalues will be zero as this would indicate that the system could have a rigid-body mode i.e. frequency drift from nominal value. Since all of the elements of the plant matrix \mathbf{A} are pure real, the eigenvalues that are complex will occur in conjugate pairs and so will the elements of the corresponding eigenvectors of \mathbf{A} . This will hold true so that all complex components of the state vector, $\mathbf{x}(t_0)$, will cancel. Examination of equation (3.9) reveals that for the case of all pure imaginary eigenvalues of \mathbf{A} , each state is a linear combination of undamped sinusoids of different frequencies. If the states could be measured, a decomposition of the states could reveal the type of disturbance that resulted in the states themselves i.e. the modes that the system is operating in. It is important to understand that the solution, (3.9), contains only a finite number of terms, n . This is due to the fact that the governing equation, (3.4), is a finite order ordinary differential equation as opposed to a partial differential equation (which would be used to model an infinite dimension system). There are only a finite number of eigenvalues that will solve the equation $\dot{\mathbf{x}}(t) = \mathbf{A}\mathbf{x}(t)$.

Since the states cannot be measured directly, it is necessary to translate the states into output measurements. This will be done in a following section by formulating a

companion equation to $\dot{\mathbf{x}}(t) = \mathbf{A}\mathbf{x}(t)$ which will be called an output equation, $\mathbf{y}(t) = \mathbf{C}\mathbf{x}(t)$, where $\mathbf{y}(t)$ is the output of the system and it is a vector of m measurements, specifically a vector with each component being a frequency deviation measurement; and \mathbf{C} is an $m \times n$ matrix that transforms the states into output measurements.

3.4 Plant Matrix Development for an n -Machine system

Before solving equation (3.3) using the solution form of equation (3.9), the plant matrix of the system must be developed. For the single-machine infinite-bus system, the plant matrix was formed simply by writing out the governing differential equation, equation (2.9), then linearizing (2.9) to obtain equation (2.10). The result was the vector-matrix differential equation (3.6). The same procedure may be followed to formulate the plant matrix for an n -machine system, keeping in mind that the end resulting equations must express the first derivative of each state as a linear combination of all of the states. Also, the n -machine model here will be lossless and have no loads connected to any of the buses – the system has an infinite bus that will act as a load. In other words the first derivative of the i th state, $x_i(t)$, must be expressed as

$$\frac{dx_i(t)}{dt} = \sum_{j=1}^n a_{ij} \bullet x_j(t) \quad (3.10)$$

The first step in formulating this equation may be to write out the swing equation for each of the n machines as follows:

$$\frac{2H_i}{\omega_s} \frac{d^2\delta_i(t)}{dt^2} = P_{mi} - P_{ei} = P_{mi} - \sum_{j=1}^n E_i E_j B_{ij} \sin(\delta_i - \delta_j) \quad (3.11)$$

A few features of this equation need to be pointed out. First, this equation describes the motion of the i th machine that is connected to a lossless transmission system. Second,

there is no damping in the mechanical portion of the system. Third, this is a non-linear differential equation with *constant* coefficients. All of the state derivatives are coupled to the other states via a non-linear relationship. Equation (3.11) may be linearized into the form of equation (3.3) around a quiescent operating point. That quiescent operating point must be the post-fault quiescent point. This is the case because the system will be oscillating around the post-fault q-point after a generator is taken off line as opposed to oscillating around the pre-fault q-point. Forth, the terms B_{ij} are the elements of the post fault *short circuit* admittance matrix for the lossless transmission system. This is an $(n-1) \times (n-1)$ matrix and must be the short circuit matrix since it takes into account all of the machine reactances. It is important to differentiate this matrix with a load flow admittance matrix because the load flow matrix does not contain generator internal reactances. Also this admittance matrix is a reduced form of the standard short circuit matrix which relates injected currents to applied voltages only at each generator's internal voltage. The other buses in the system, i.e. line tap points, are eliminated from the current and voltage vectors associated with the admittance matrix via some reduction technique such as a Kron reduction [18]. When a Kron reduction is performed on a matrix for a system that does have loads, all loads must be modeled as constant impedances. Due to the frequency and voltage sensitivity of many loads on a power system, this is an approximation that may not suffice. However with small signal disturbances, the approximation should be accurate enough at least in certain cases, if not most. For disturbances that result in large excursions of frequency, a non-linear analysis may need to be performed. Modal properties of the system in a non-linear region of the

state-space may or may not significantly deviate from the modal properties close in to the quiescent point.

The quiescent point around which equation (3.11) is to be linearized may be expressed as

$$x_0 = [\delta_{10} \quad \cdots \quad \delta_{n0} \quad \omega_{10} \quad \cdots \quad \omega_{n0}]^t \quad (3.12)$$

and so the linearization of equation (3.11) results in

$$\frac{2H_i}{\omega_s} \frac{d^2 \Delta \delta_i(t)}{dt^2} = - \sum_{j=1}^n E_i E_j B_{ij} \cos(\delta_{i0} - \delta_{j0}) [\Delta \delta_i(t) - \Delta \delta_j(t)] \quad (3.13)$$

since, according to equation (2.6), $\frac{d\Delta \delta_i(t)}{dt} = \Delta \omega(t)$, equation (3.13) may be expressed as

equation (3.4) repeated here

$$\frac{d}{dt} \begin{bmatrix} \Delta \delta(t) \\ \Delta \omega(t) \end{bmatrix} = \mathbf{A} \begin{bmatrix} \Delta \delta(t) \\ \Delta \omega(t) \end{bmatrix} \quad (3.4)$$

where the $n \times 1$ column vectors, $\Delta \delta(t)$ and $\Delta \omega(t)$ are expressed as vectors of the individual states

$$\begin{aligned} \Delta \delta(t) &= [\Delta \delta_1(t) \quad \cdots \quad \Delta \delta_n(t)]^t & \text{and} \\ \Delta \omega(t) &= [\Delta \omega_1(t) \quad \cdots \quad \Delta \omega_n(t)]^t \end{aligned} \quad (3.14)$$

The state vector may be solved for in closed form per equation (3.9) if the initial condition is known. In order to use this model for outage identification, a relationship between the states and the outputs (measurements) needs to be developed. This is done in a following section. However, without this relationship between states and outputs one might anticipate that if the eigenvalues of the plant matrix are known for a given generator outage, that the corresponding oscillation frequencies (or in the case of non-

oscillatory modes, the time constants and rigid-body characteristics) would manifest themselves, in some fashion, in the outputs. And thus, the potential to identify modes, at least with some degree of certainty, without an explicit relationship between states and outputs should exist. This is due to the fact that the outputs are anticipated to be linear combinations of the states as $\mathbf{y}(t) = \mathbf{C}\mathbf{x}(t)$.

3.5 Simulation Results for a Three-Machine System

In order to present this potential, the three-machine – 8 bus system shown in figure 3.4 will be analyzed for each generator outage. The system will then be simulated to compare the calculated values of oscillation frequencies versus the measured values drawn from the simulation. This is similar to what was done in section 3.1.

As stated previously, the oscillation frequencies are the imaginary components of the eigenvalues of the plant matrix. In order to formulate the plant matrix per equation (3.13), a quiescent operating point needs to be determined for each of the three generator outages. Running a load flow on the system will determine the Q-point. The B_{ij} terms in equation (3.13) may be found according to the procedure mentioned in section 3.4 and the E_i and E_j terms found from a pre-fault load flow. This is done because it is assumed that the system is unregulated. A different plant matrix must be formulated for each machine outage, as each term in equation (3.13), in general, will change with the number of units that are in service. A sample plant matrix formulation for machine 1 outage is shown in Appendix II.

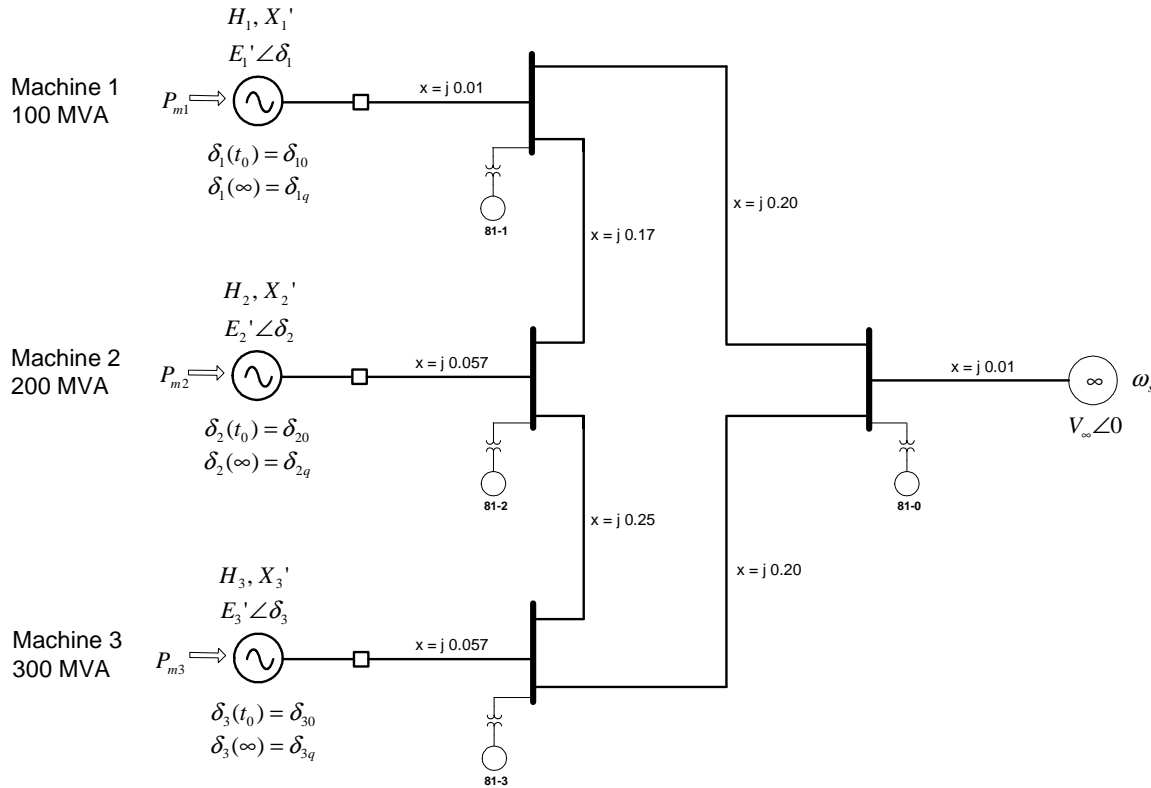


Figure 3.4: three-machine infinite bus system

Each machine in figure 3.4 has the same parameters as was used in the two-machine case in section 3.1 and each unit is operated in the pre-fault condition such that its terminal voltage is equal to rated voltage. There is a frequency measurement unit placed at each bus. The infinite bus on the right-hand side of the diagram may be viewed as a power system area itself. This system is used here to demonstrate the modal identification and thus generator outage identification but it may also be used to investigate the characteristics of interarea modes versus intermachine modes. As will be seen for the first case, machine one outage, there are a pair of operating modes which are excited by the outage. One of the modes is machine 2 and 3 both oscillating together against the infinite bus (interarea oscillation) and the other mode is machines 2 and 3 oscillating against each other (intermachine oscillation). As might be expected per

equation (2.12), the interarea oscillation has a lower frequency than the intermachine oscillation because there is more mass associated with the interarea oscillation. Other modal characteristics will be discerned below from the modal analysis and simulation results.

3.5.1 Machine 1 Outage

After machine 1 is taken offline ($t = 1.0$ second), the following frequency waveform is observed via simulation at the tie line's generator side (called 81-0 in figure 3.4).

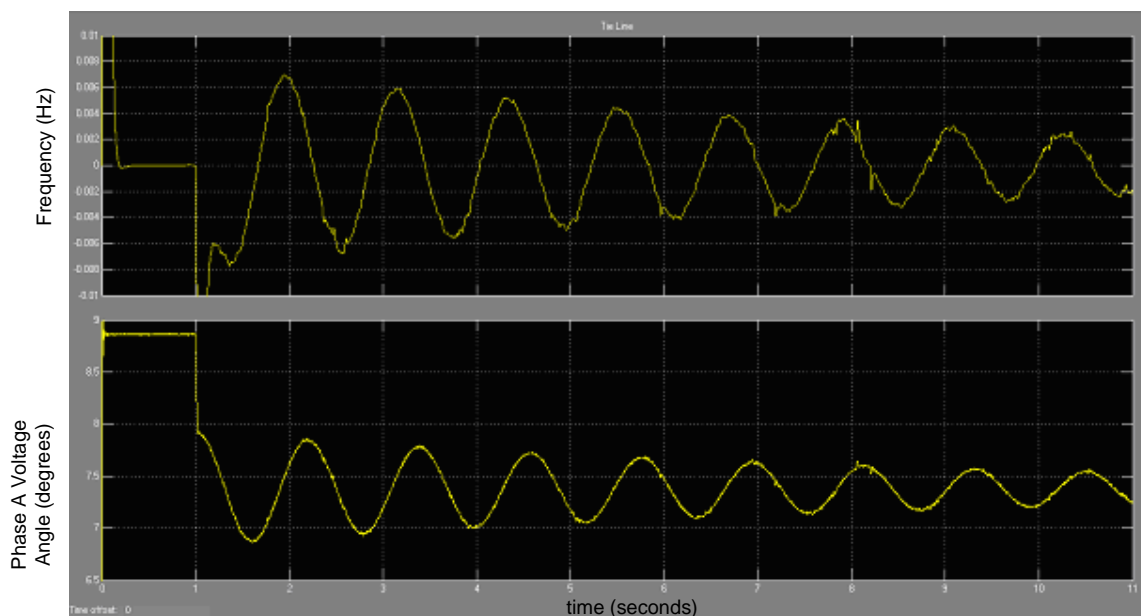


Figure 3.5: frequency and phase waveforms at tie line – machine 1 outage

The step in phase angle is due to the step in power flow into the tie line immediately after generator 1 is taken offline. This step in angle creates a corresponding spike in frequency at $t = 1.0$ seconds. The rest of the waveform may be observed to be a single-frequency sinusoid with a damping ratio of less than 0.1. The FFT of this

waveform is as shown in figure 3.6. The Y-axis is the magnitude on a 512-cycle, 10-second sample and the X-axis is frequency in hertz; the frequency resolution is 0.1 Hz.

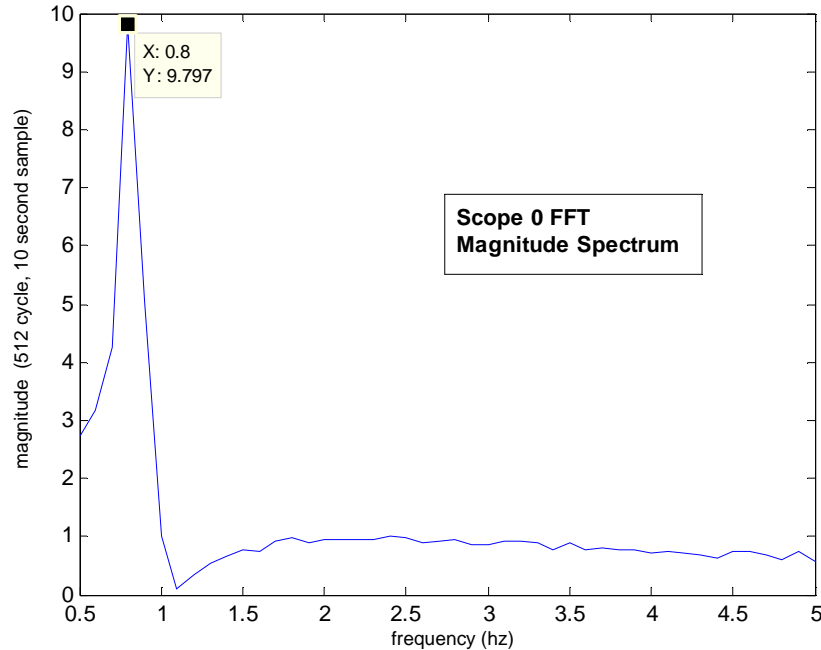


Figure 3.6: Magnitude Spectrum FFT of tie line frequency – machine 1 outage

Per Appendix II the eigenvalues for a generator 1 outage correspond to frequencies of 0.83 and 1.31Hz. The FFT's resolution is 0.1Hz and thus shows the frequency of 0.8Hz. This frequency is a manifestation of the interarea oscillation associated with a generator 1 outage. The intermachine oscillation is not visible at the tie line bus.

Scope 1 (81-1) shows the following waveform in figure 3.7

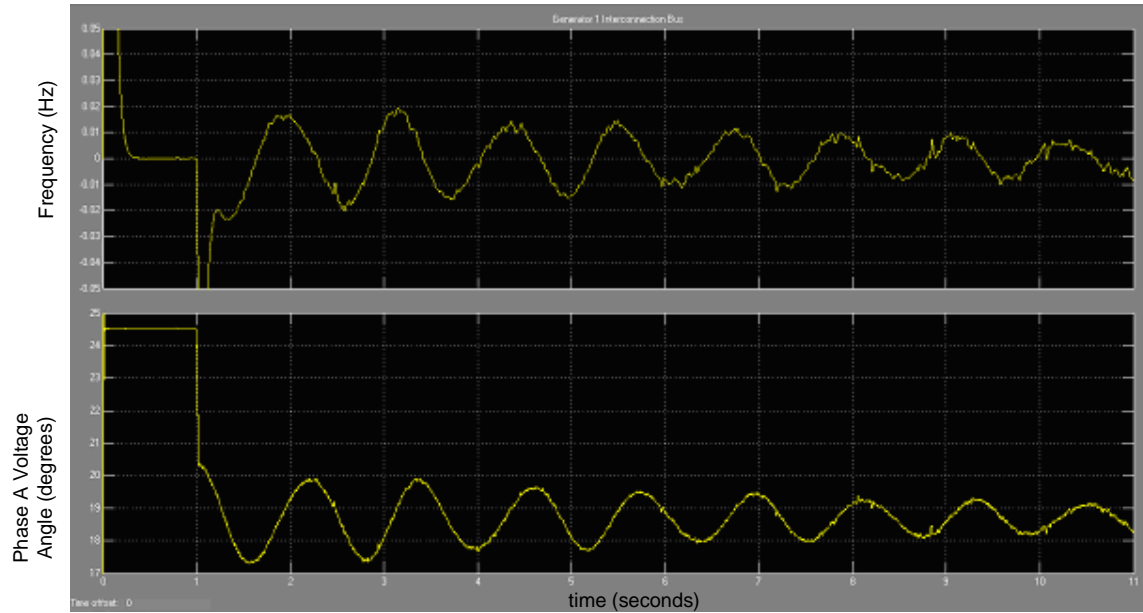


Figure 3.7: frequency and phase waveforms at machine 1’s inertia point – machine 1 outage

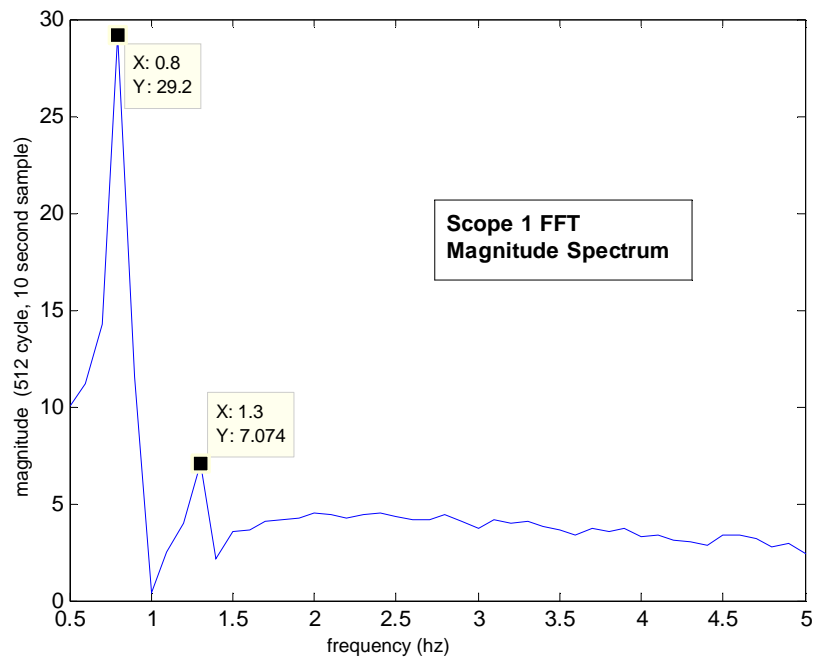


Figure 3.8: FFT of frequency waveform at machine 1’s inertia point – machine 1 outage

And Scope's 2 and 3 waveforms and FFT's are shown in figures 3.9 through 3.12.

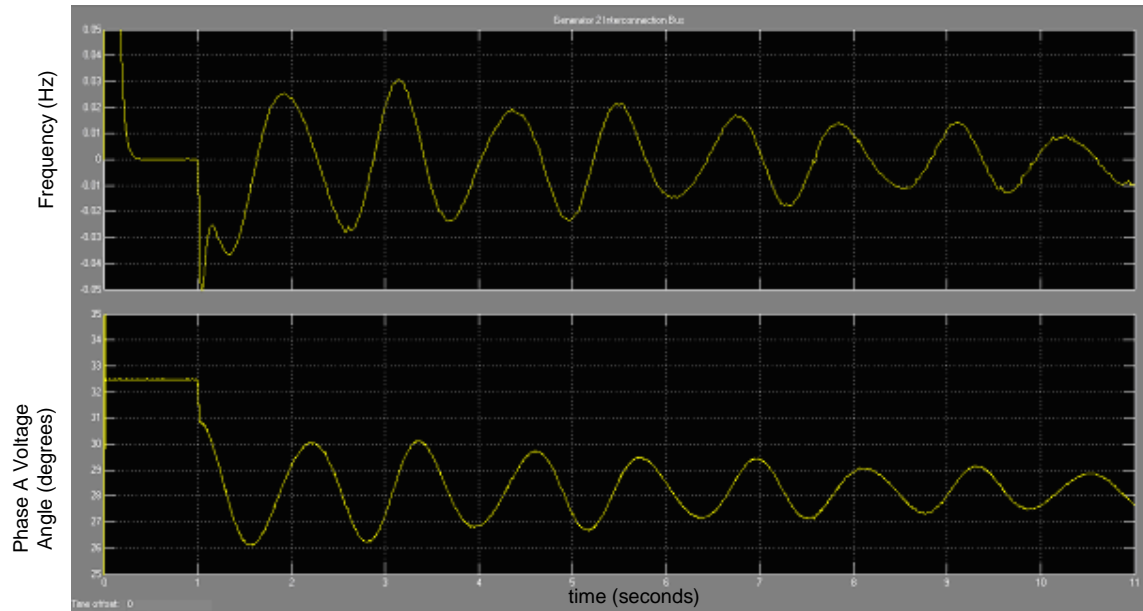


Figure 3.9: frequency and phase waveforms at machine 2's inertia point – machine 1 outage

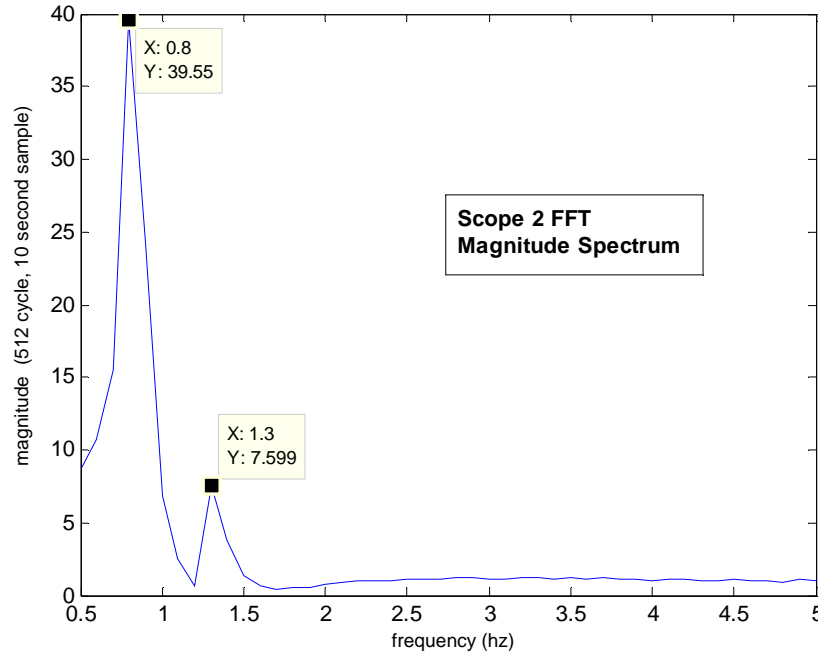


Figure 3.10: FFT of frequency waveform at machine 2's inertia point – generator 1 outage

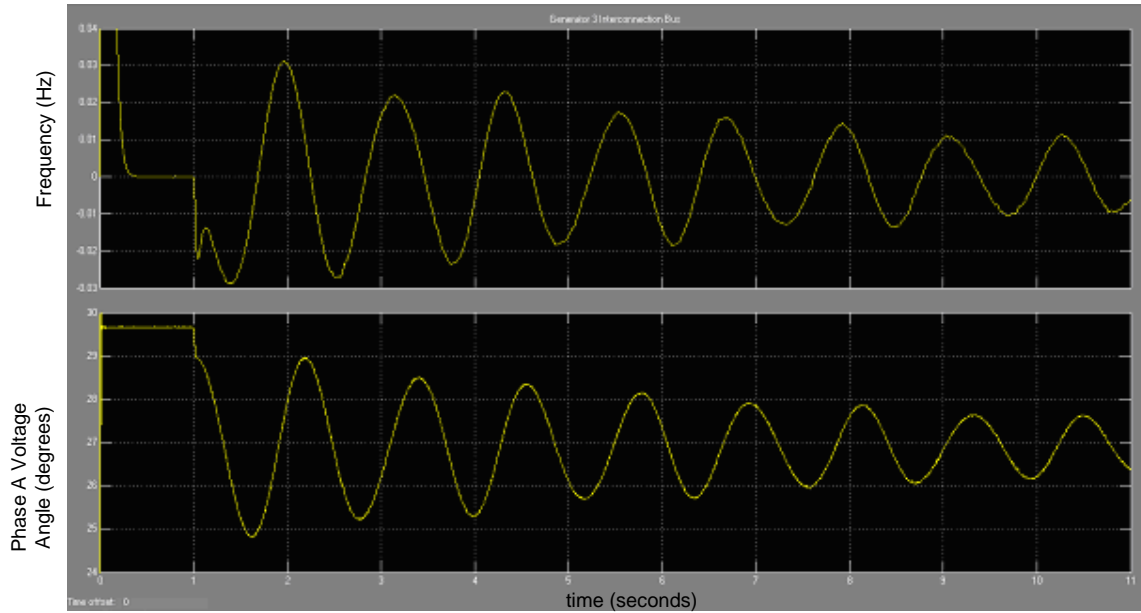


Figure 3.11: frequency and phase waveforms at machine 3's intertie point – machine 1 outage

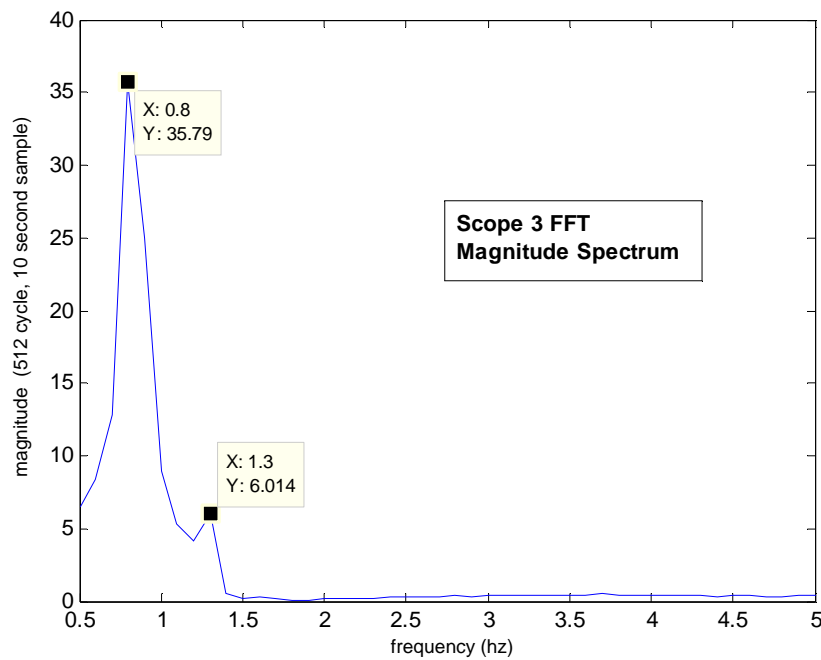


Figure 3.12: FFT of frequency waveform at machine 3's intertie point – machine 1 outage

The FFT data shows clearly that the interarea mode is prominent and the intermachine mode is at least observable especially at generator 2's interconnection point.

3.5.2 Machine 2 Outage

Looking at simulation data from a generator 2 outage, there is shown distinctly different modal activity as would be expected from the eigenanalysis of a generator 2 outage. The eigenvalues for this case correspond to frequencies of 1.73Hz and 1.03Hz and the right eigenvector modal matrix is

$$\Phi = \begin{bmatrix} -j0.091 & j0.091 & -j0.066 & j0.066 \\ j0.014 & -j0.014 & -j0.138 & j0.138 \\ 0.983 & 0.983 & 0.426 & 0.426 \\ -0.156 & -0.156 & 0.892 & 0.892 \end{bmatrix} \quad (3.15)$$

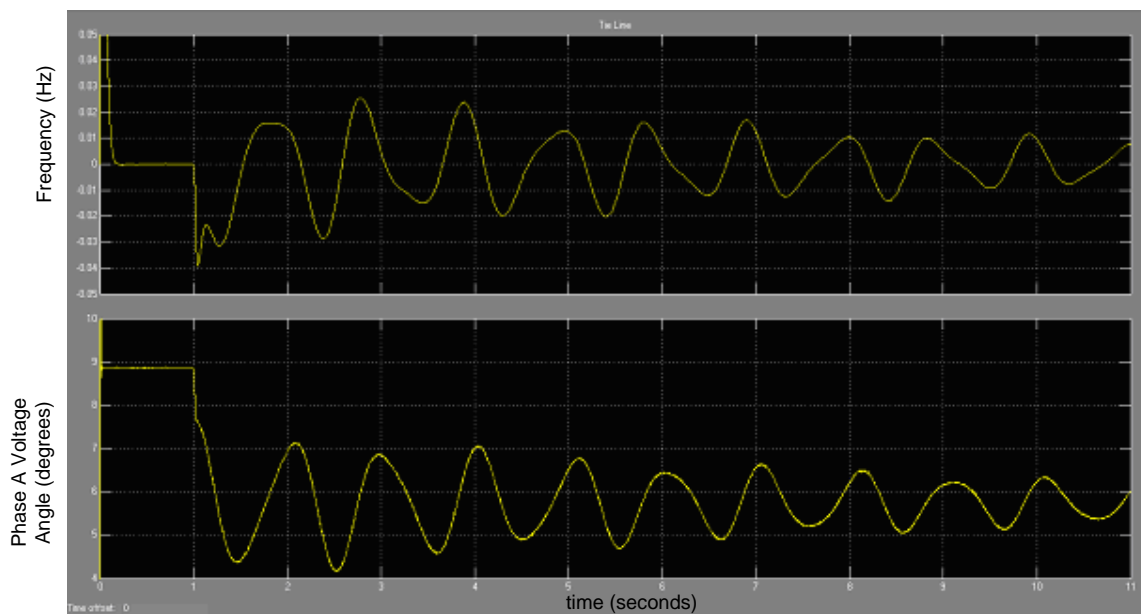


Figure 3.13: frequency and phase waveforms at tie line – machine 2 outage

Figure 3.13 shows the frequency and phase waveforms at the tie line. Figure 3.14 shows the FFT of this frequency waveform using the same sampling as in the machine 1 outage.

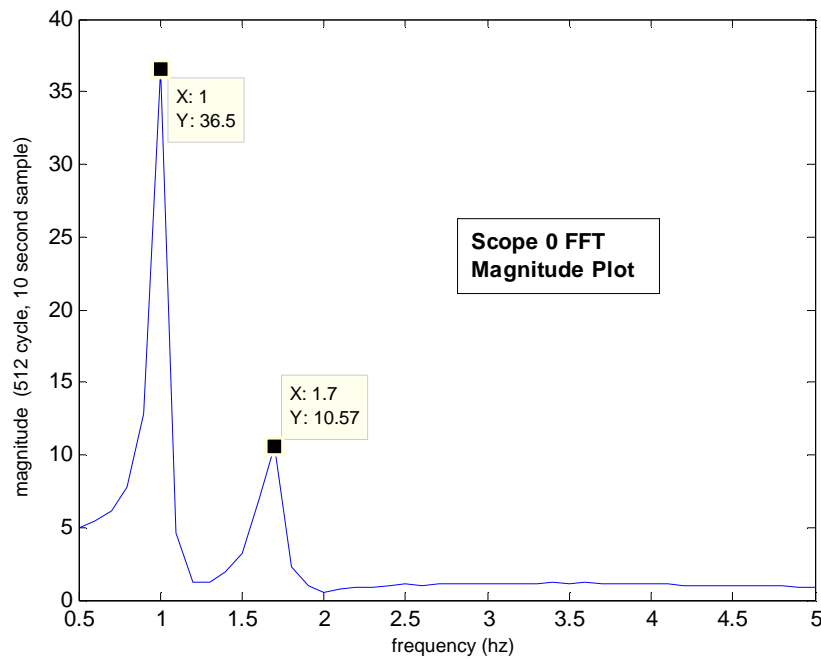


Figure 3.14: Magnitude Spectrum FFT of tie line frequency – machine 2 outage

From figure 3.14, both the 1.03Hz and the 1.73Hz modes are observable. Comparison of this FFT with the FFT shown in figure 3.10 shows that an outage of either machine 1 or machine 2 can be distinguished from each other based on the FFT of the tie frequency waveform. Even though the intermachine oscillation for the machine 1 outage case is not detectable at the tie line, the interarea mode can be used for the outage identification. Figure 3.15 shows the frequency and phase waveforms for scope 1, machine 1's interconnection point into the transmission system. Once again, the distinct oscillation frequencies are displayed in the FFT of figure 3.16. Figures 3.17 through 3.20 show the waveforms and FFT's for scope 2 and 3.

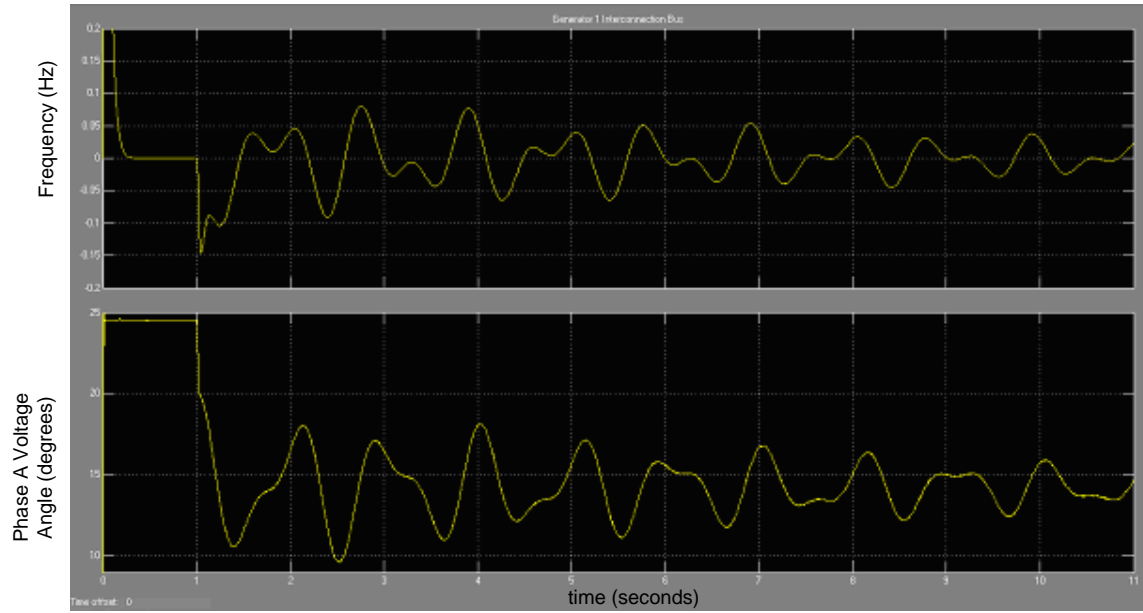


Figure 3.15: frequency and phase waveforms at machine 1’s inertia point – machine 2 outage

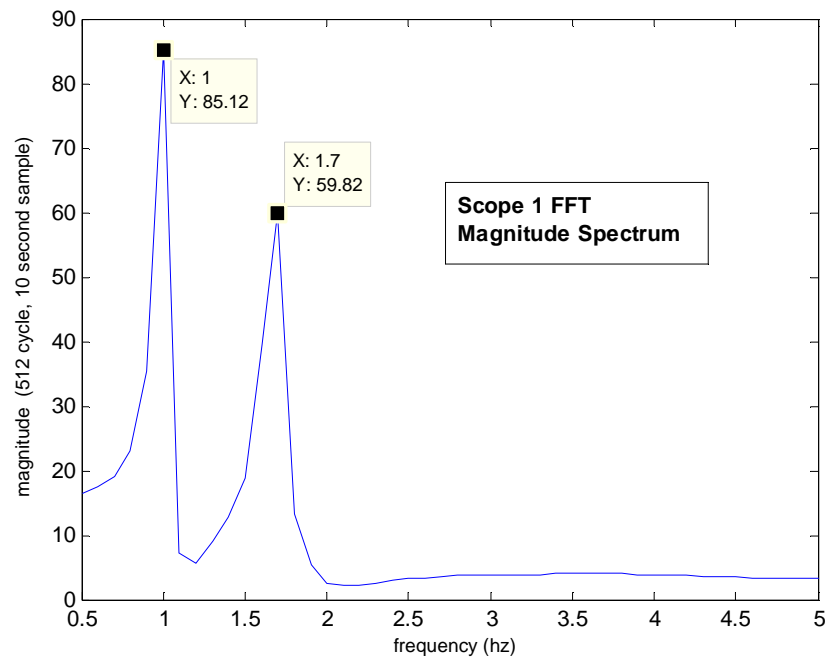


Figure 3.16: FFT of frequency waveform at machine 1’s inertia point – machine 2 outage

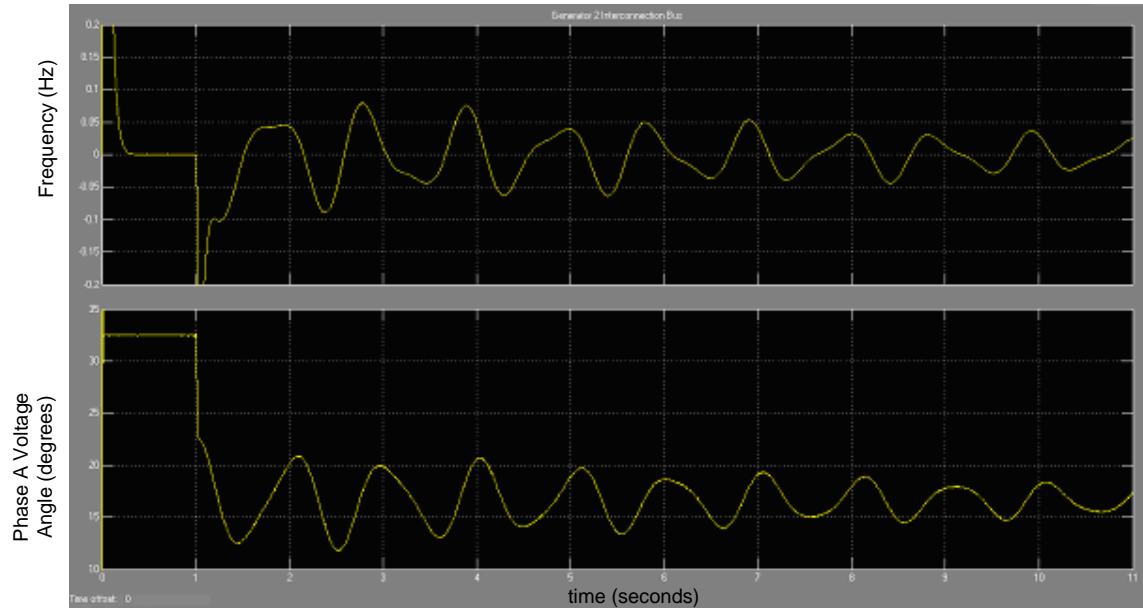


Figure 3.17: frequency and phase waveforms at machine 2’s intertie point – machine 2 outage

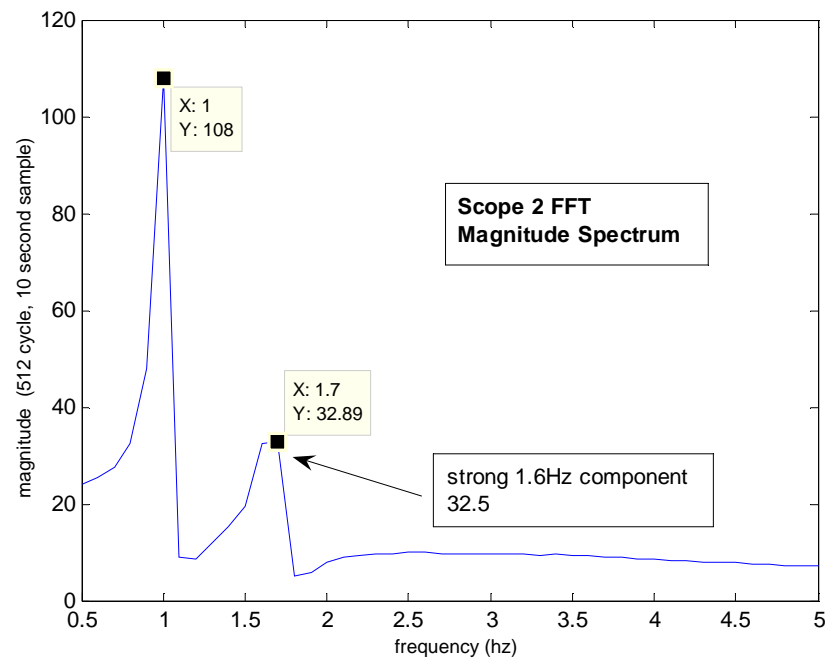


Figure 3.18: FFT of frequency waveform at machine 2’s intertie point – machine 2 outage

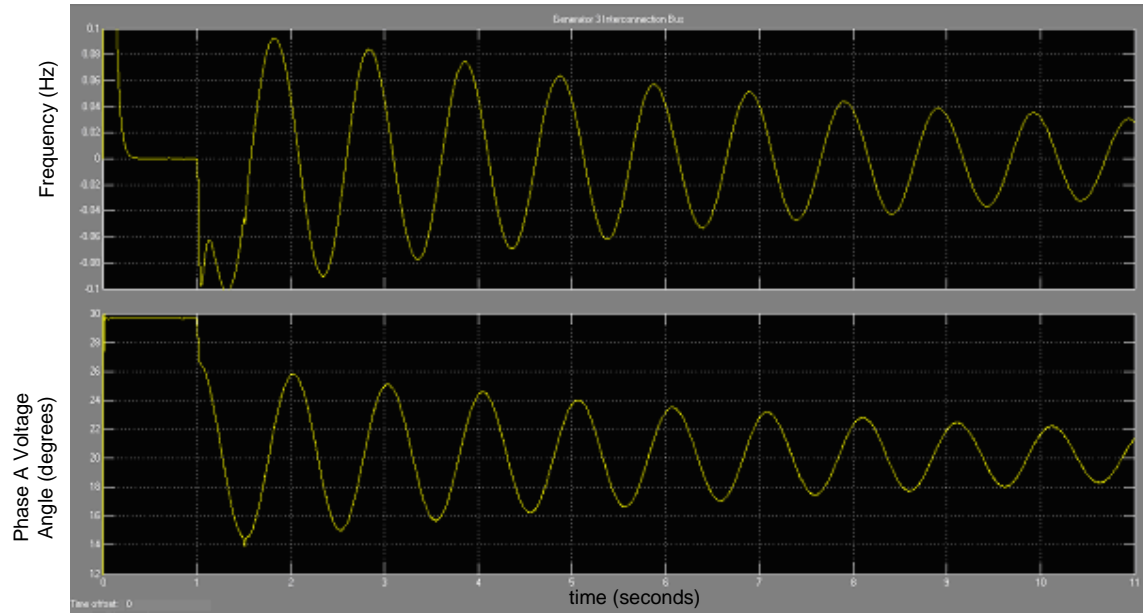


Figure 3.19: frequency and phase waveforms at machine 3’s inertia point – machine 2 outage

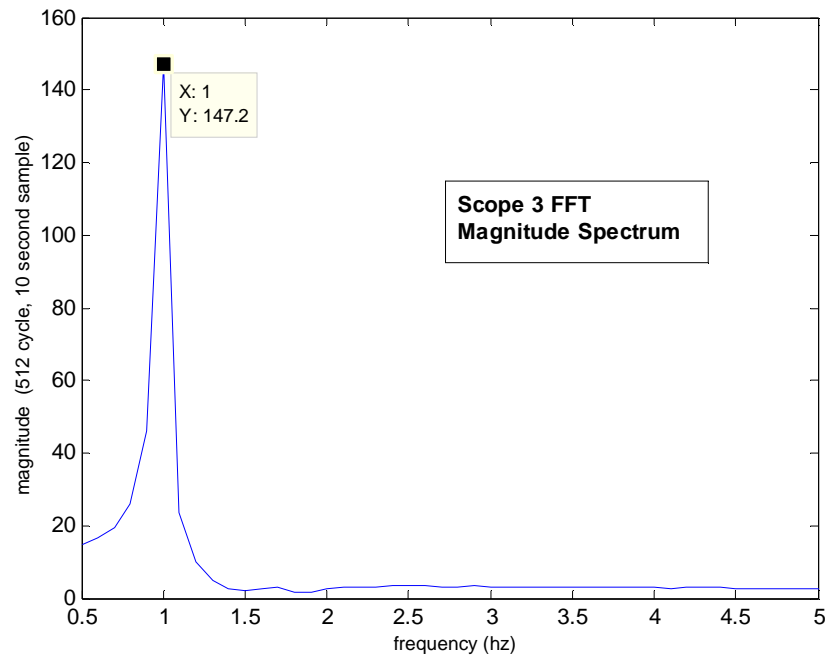


Figure 3.20: FFT of frequency waveform at machine 3’s inertia point – machine 2 outage

3.5.3 Machine 3 Outage

The eigenvalues for a generator 3 outage correspond to natural oscillation frequencies of 1.77Hz and 1.05Hz. Once again the frequencies are higher than in the case of the machines 1 and 2 outages mainly because the system is lighter than in the previous two outage cases. The right eigenvector modal matrix for the system after machine 3 is taken offline is

$$\Phi = \begin{bmatrix} -j0.086 & j0.086 & -j0.078 & j0.078 \\ j0.026 & -j0.026 & -j0.128 & j0.128 \\ 0.953 & 0.953 & 0.513 & 0.513 \\ -0.289 & -0.289 & 0.845 & 0.845 \end{bmatrix} \quad (3.16)$$

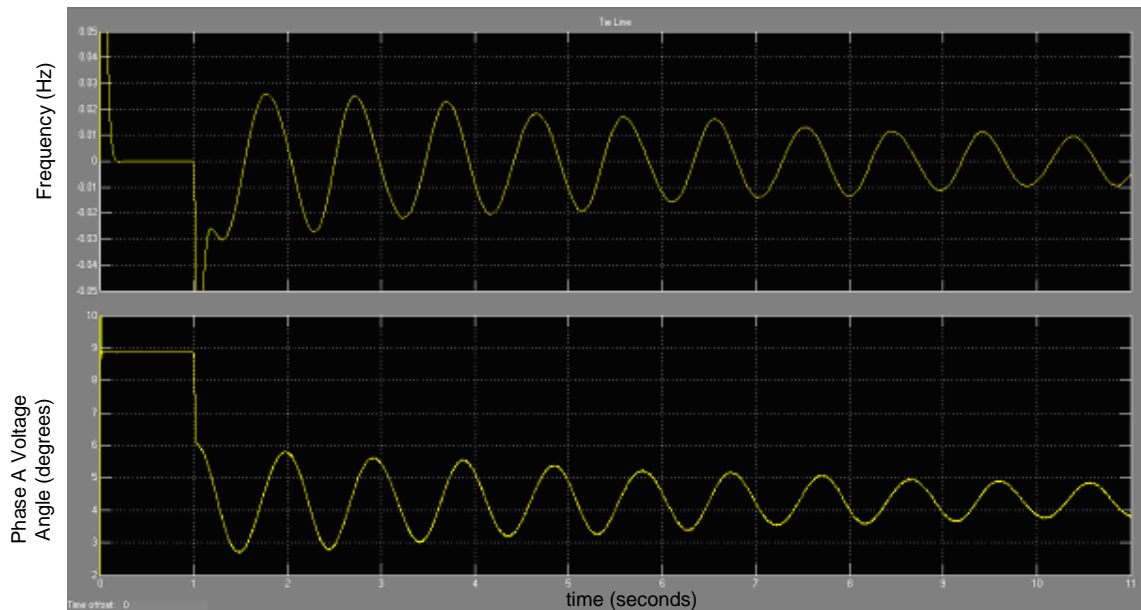


Figure 3.21: frequency and phase waveforms at tie line – machine 3 outage

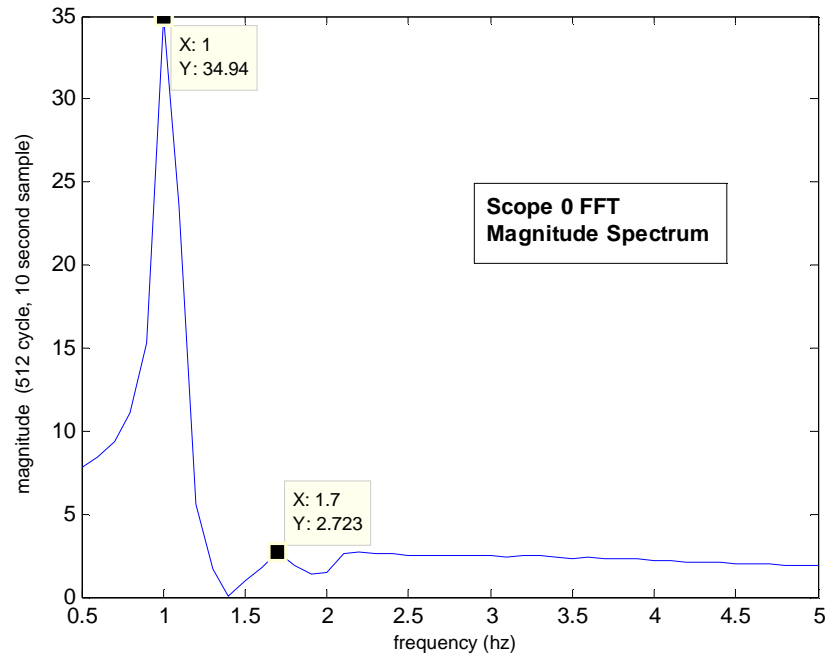


Figure 3.22: Magnitude Spectrum FFT of tie line frequency – machine 3 outage

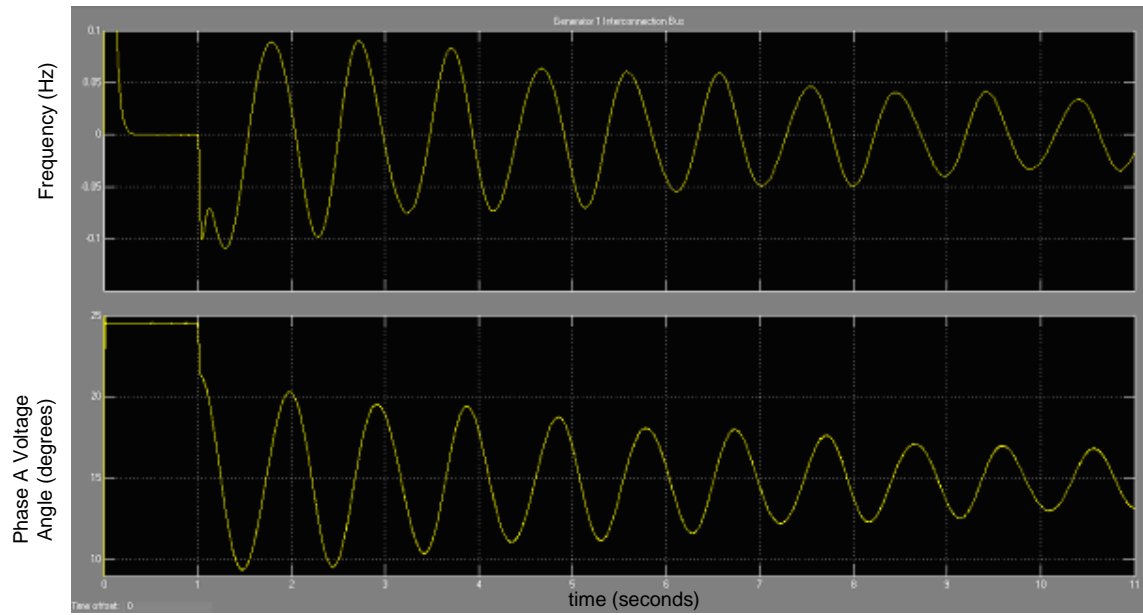


Figure 3.23: frequency and phase waveforms at machine 1's inertie point – machine 3 outage

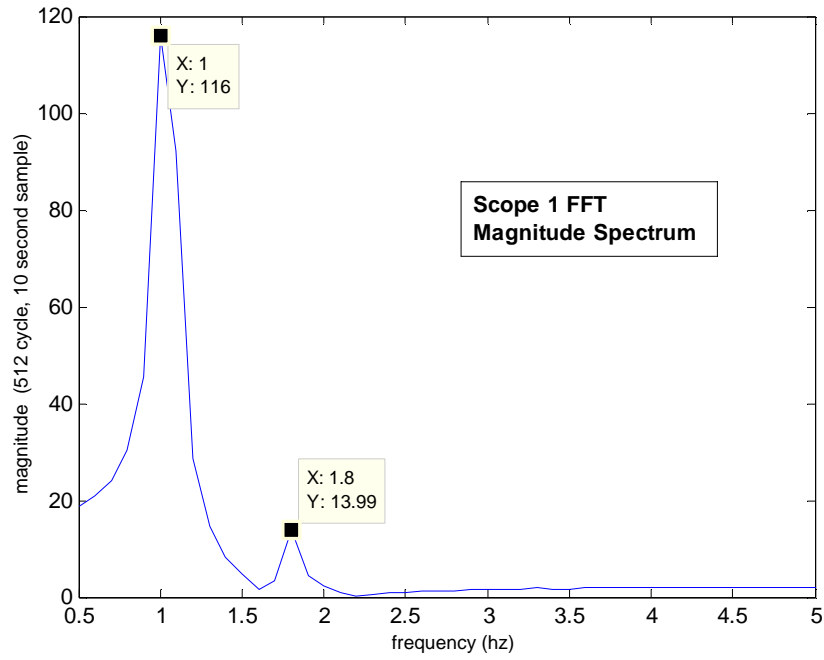


Figure 3.24: FFT of frequency waveform at machine 1’s intertie point – machine 3 outage

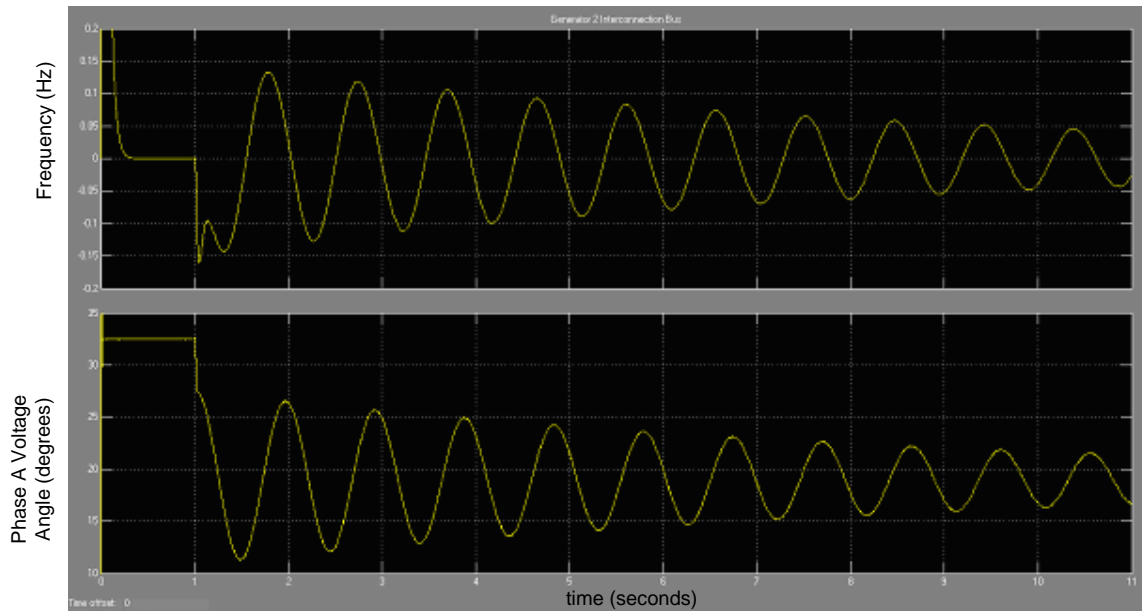


Figure 3.25: frequency and phase waveforms at machine 2’s intertie point – machine 3 outage

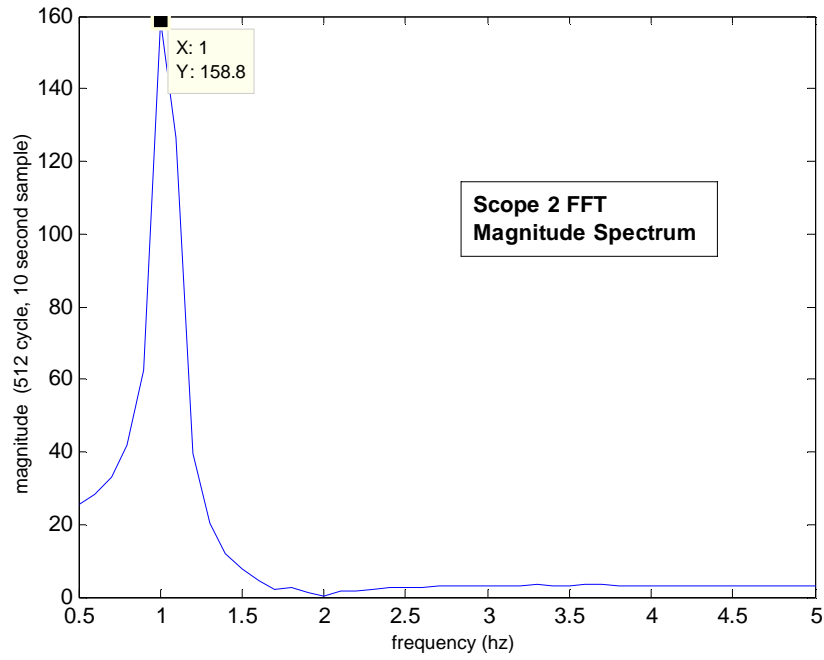


Figure 3.26: FFT of frequency waveform at machine 2's intertie point – machine 3 outage

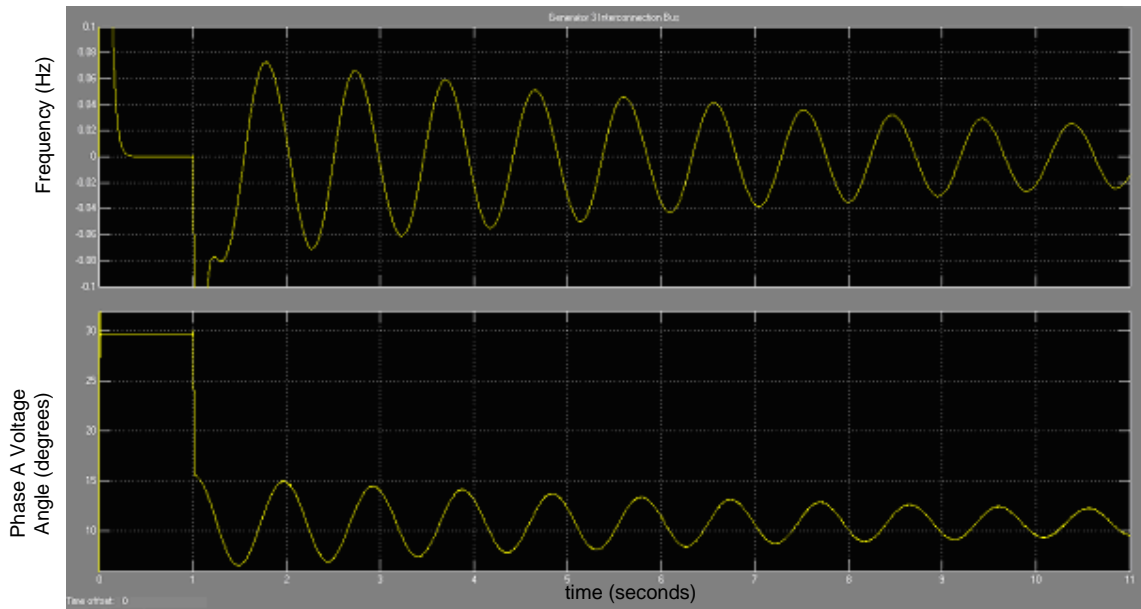


Figure 3.27: frequency and phase waveforms at machine 3's intertie point – machine 3 outage

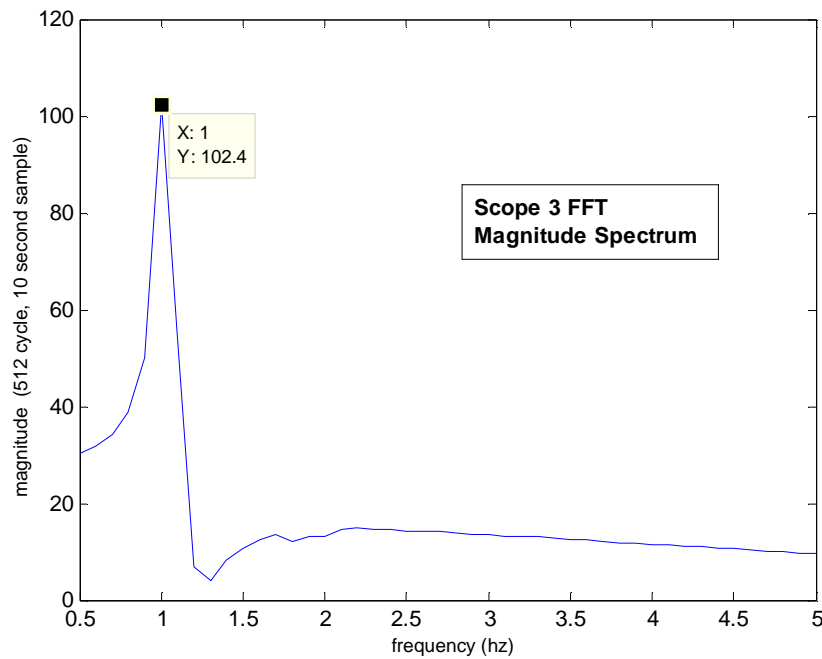


Figure 3.28: FFT of frequency waveform at machine 3's intertie point – machine 3 outage

Figures 3.22 and 3.28, FFT's for the tie line and machine 3 tie points, indicate that the intermachine oscillation frequency is 1.7Hz. This is a deficiency in the FFT algorithm since the FFT's are ran on a 10-second sample of the frequency waveform. When the FFT is ran on a 20-second waveform (resolution of 0.05Hz) both of these FFT's show up as 1.75Hz – closer to the calculated value of 1.77Hz. At the machine 3 tie point, the 1.77Hz mode is still basically not observable. The data from 20-second waveform FFT should be considered only for purposes of verifying the modal analysis results but may not be practical to use on real frequency measurements. A 20-second interval will typically be enough time for automatic generation controls to alter the waveform and these controls may or may not alter the natural frequency of the system. This automatic generation control topic will receive more rigorous treatment in chapter 4.

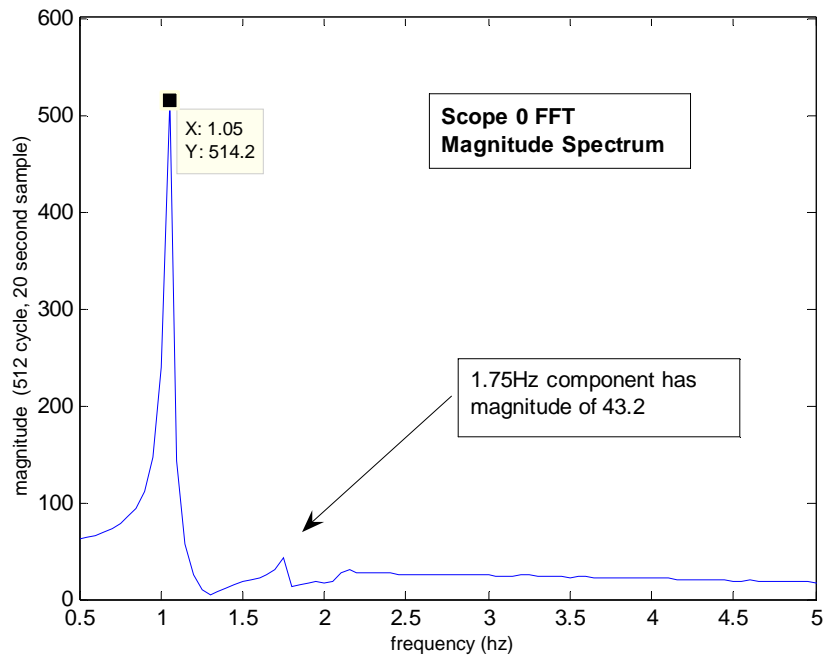


Figure 3.29: Magnitude Spectrum FFT of tie line frequency – machine 3 outage, 20-second waveform

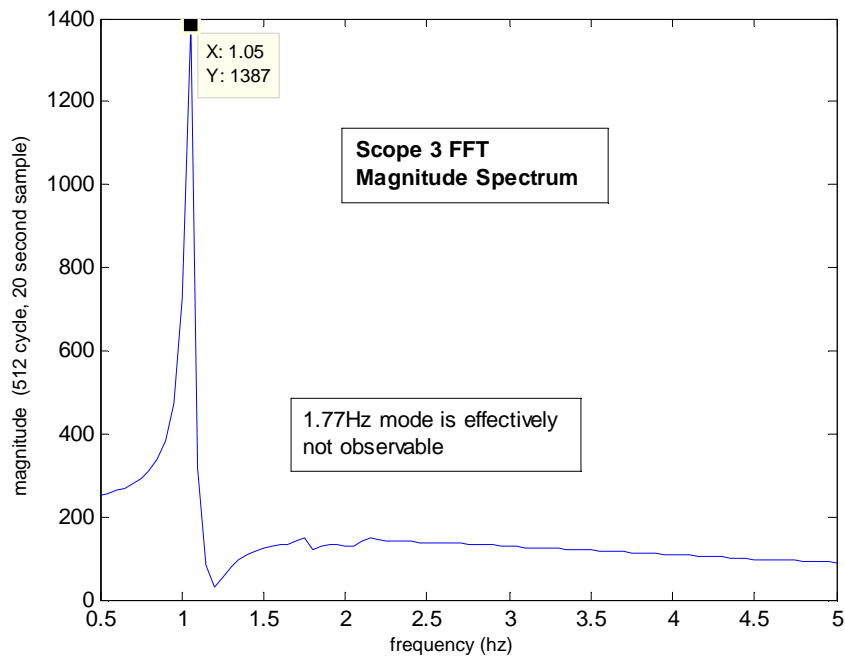


Figure 3.30: FFT of frequency waveform at machine 3's intertie point – machine 3 outage, 20-second waveform

This being the case, there may need to be a different method of identifying the mode(s) in addition to oscillation frequencies alone. In the next section, mode shapes will be investigated for the purpose of mode identification.

3.6 Comparison of Machine 2 and Machine 3 Outage Modal Characteristics

The eigenvalues for a machine 3 outage correspond to natural frequencies of 1.77Hz and 1.05Hz. Both of these natural frequencies are within a couple of percent of the machine 2 outage natural frequencies and using an FFT with a resolution of 0.1Hz will not give results that lead to confident outage identification based on the oscillations that result from the system's natural response. The additional information which should be present in the natural response measurements is in the mode shapes. Figures 3.31 and 3.32 show FFT's of machine 1 and machine 3 per-unit speeds for a machine 2 outage. Inspection of the magnitude of the 1.0Hz oscillation for both of these FFT's reveals that the mode shape ratio for machine 1 to machine 3 is $1.953/4.335$ or 0.4505 . The calculated value for this mode shape ratio, which is based on a right eigenvector for the interarea mode, is $0.426/0.892$ or 0.477 . The two ratios are within about 6 percent of each other, verifying the calculated mode shape. This same measured ratio for machine 1 to machine 2 in the machine 3 outage case is $2.703/4.345$ or 0.6221 . The calculated ratio from the corresponding eigenvector is $0.513/0.845$ or 0.607 . The measured and calculated ratios are within three percent of each other, once again verifying the mode shape predictor. But the significant fact is that the two ratios are far enough apart to be able to identify the mode in which the system oscillates. Since the mode shape is a function of the states, which cannot be measured by frequency meters, there needs to be a

way to somehow translate the system states into measurements using a transformation. A proposal for this transformation is presented in the next section of this chapter.

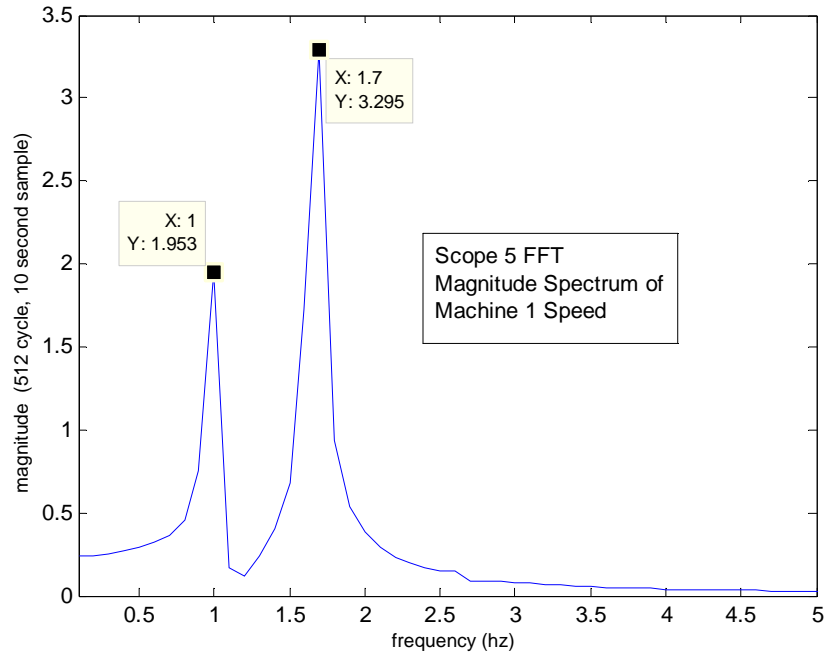


Figure 3.31: FFT of machine 1 per unit speed – machine 2 outage

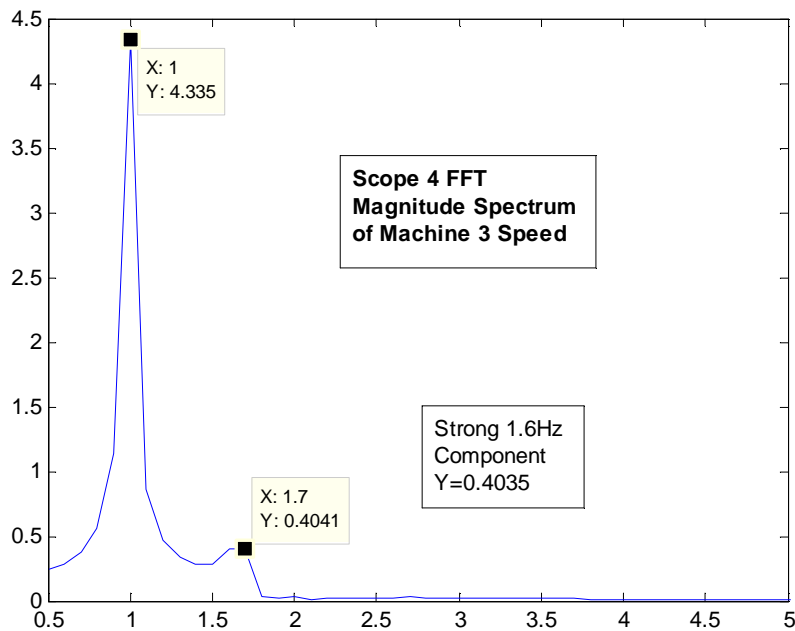


Figure 3.32: FFT of machine 3 per unit speed – machine 2 outage

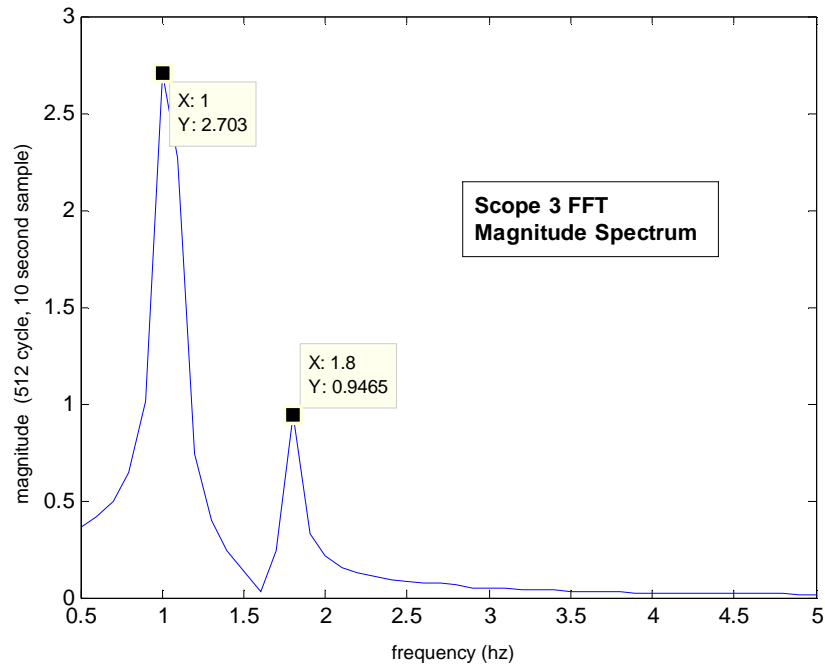


Figure 3.33: FFT of machine 1 per unit speed – machine 3 outage

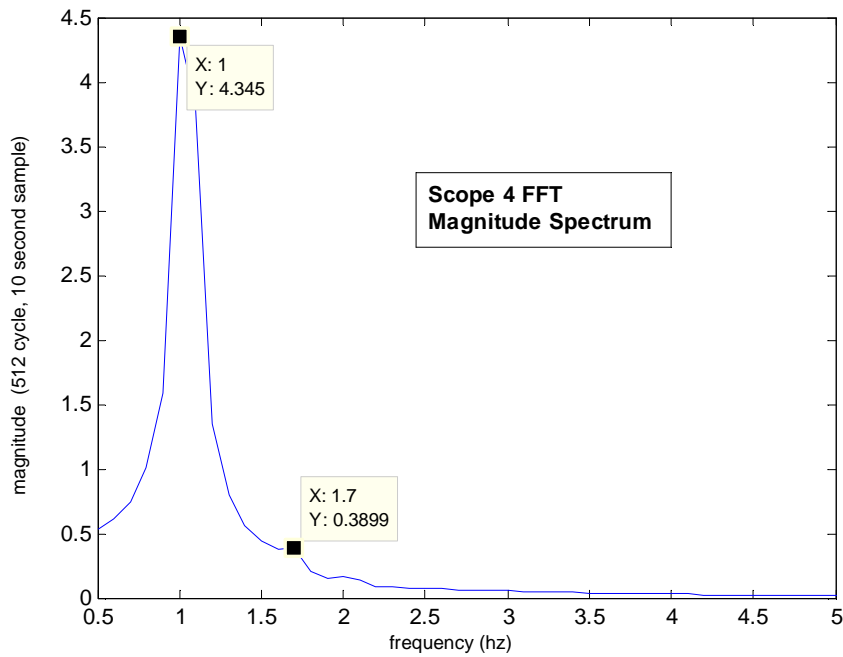


Figure 3.34: FFT of machine 2 per unit speed – machine 3 outage

3.7 Output matrix development for an n -Machine, m -Measurement point system

It may be clear from equation (3.9) that, since each of the states for the undamped (or underdamped) system is a linear combination of sinusoidal terms. As in the case of the SMIB system, one might expect that these sinusoidal terms, especially the machine speeds, will, in some specific way, manifest themselves as sinusoidal terms of the same frequency, perhaps scaled in magnitude, in the frequency measurements. If this is the case, examination of the measurements in terms of their frequency content should reveal what mode(s) the system is operating in as verified in section 3.5. Since particular generator outages result in specific modes, which have their own frequencies and mode shapes, and specific excitation magnitudes, it should, in principle, be possible to determine which generator was dropped offline based on the output measurements. This is the exact same theory as was used in the two-machine system that was simulated in section 3.1. In a multimachine system, the relationship must be more complicated, in general, than the two-machine system because the two-machine system only has one single mode that it may operate in after one of the units is dropped offline. In the multimachine case there will, in general, be multiple modes that are excited and thus there should be, in general, multiple frequencies that show up in the outputs (measurements). It may be good for the reader to recall one of the results of section 2.2 that demonstrated how certain modes may not be observable at certain points on the system via phasor angle or frequency measurements.

The initial method that I propose to use to develop the state-output relationship is via DC power flow relationships [24]. I selected this model initially because of its simplicity and its use of bus phasor angles as states.

To summarize the DC power flow model, the assumptions are stated first.

1) The system must be modeled as lossless. There are a couple of ways of modeling a lossy AC system as lossless. One way is to neglect the resistance in the series impedance calculation and assume that all of a line's series impedance is made up by the inductive reactance. Another is to calculate the magnitude of a line's series impedance and "force" the angle of the impedance to 90, thus making the model lossless. For the present case that I'll illustrate in this section, the original model is lossless and so the method of modeling isn't consequential. 2) The line models must not include shunt reactances. This feature of the model may render the DC power flow useless for widespread systems such as control areas in the WECC. 3) All of the voltage magnitudes at all of the buses in the system are modeled as having a value of 1.0 p.u. 4) The voltage angle difference across each line is low enough so that the power flow on each line, which is, in the full lossless AC power flow case, equal to

$$P_{ij} = V_i V_j b_{ij} \sin(\delta_i - \delta_j) \quad (3.17)$$

will, in the DC power flow, reduce to

$$P_{ij} = V_i V_j b_{ij} \bullet (\delta_i - \delta_j) \quad (3.18)$$

which further reduces to

$$P_{ij} = b_{ij} \bullet (\delta_i - \delta_j) \quad (3.19)$$

due to approximation number three above.

When equation (3.19) is written for each node, the total power injected at each node takes on the form

$$P_{ij} = \sum_{j=1}^n b_{ij} \bullet (\delta_i - \delta_j) \text{ for } i = 1, \dots, n \quad (3.20)$$

and this may be rewritten as a vector-matrix equation

$$\mathbf{P} = \mathbf{B}\boldsymbol{\delta} \quad (3.21)$$

where \mathbf{P} is an $n \times 1$ column vector whose i th entry is the power injected into the i th bus, $\boldsymbol{\delta}$ is an $n \times 1$ column vector whose i th entry is the voltage angle of the i th bus, and \mathbf{B} is an $n \times n$ susceptance matrix whose i - j th entry is the negative of the transfer admittance between the i and j th buses. Here n is the total number of buses on the system. Taking incremental changes in the elements of the bus angle vector, $\boldsymbol{\delta}$, yields

$$\Delta\mathbf{P} = \mathbf{B}\Delta\boldsymbol{\delta} \quad (3.22)$$

which begins to take on the form of an equation that could relate the system states, $\Delta\delta_i(t)$, with angles at each one of the buses where a frequency measurement is being taken. Partitioning the matrix and vectors in (3.22) as follows divides the states from the measurement quantities:

$$\begin{bmatrix} \Delta P_1 \\ \vdots \\ \Delta P_n \\ \Delta P_{n+1} \\ \vdots \\ \Delta P_p \end{bmatrix} = \begin{bmatrix} b_{11} & \cdots & b_{1n} & | & b_{1(n+1)} & \cdots & b_{1p} \\ \vdots & \ddots & \vdots & | & \vdots & \ddots & \vdots \\ b_{n1} & \cdots & b_{nn} & | & b_{n(n+1)} & \cdots & b_{np} \\ \hline b_{(n+1)1} & \cdots & b_{(n+1)n} & | & b_{(n+1)(n+1)} & \cdots & b_{(n+1)p} \\ \vdots & \ddots & \vdots & | & \vdots & \ddots & \vdots \\ b_{p1} & \cdots & b_{pn} & | & b_{p(n+1)} & \cdots & b_{pp} \end{bmatrix} \bullet \begin{bmatrix} \Delta\delta_1 \\ \vdots \\ \Delta\delta_n \\ \Delta\delta_{n+1} \\ \vdots \\ \Delta\delta_p \end{bmatrix} \quad (3.23)$$

Here the quantity $p-n$ is equal to the number of buses on the system that have measurements being taken. Thus, the lower partition of the column vectors in (3.23) may be considered to be quantities associated with the outputs. And since the upper partition of the vector $\Delta\boldsymbol{\delta}$ is part of the system state, then equation (3.23) describes a relationship

in between the system states and the outputs – if the outputs are bus phasor angles. Equation (3.23), in compact form, may be expressed as

$$\begin{bmatrix} \Delta \mathbf{P}_{states} \\ \Delta \mathbf{P}_{output} \end{bmatrix} = \begin{bmatrix} \mathbf{B}_{11} & \mathbf{B}_{12} \\ \mathbf{B}_{21} & \mathbf{B}_{22} \end{bmatrix} \bullet \begin{bmatrix} \Delta \boldsymbol{\delta}_{states} \\ \Delta \boldsymbol{\delta}_{output} \end{bmatrix} \quad (3.24)$$

In order to use (3.24) to explicitly relate the states to the outputs, the $(p-n) \times 1$ column vector, $\Delta \mathbf{P}_{output}$, must be approximated as zero. Such an approximation should hold in the small signal especially for lightly loaded systems where voltage magnitudes do not vary appreciably for small swings in voltage angle. However, in order for the small signal analysis to be a decent approximation, either the load at the measurement bus must not be highly frequency dependent and/or the deviations from rated frequency must be negligible compared to rated frequency.

With $\Delta \mathbf{P}_{output}$ approximated as zero, equation (3.24) becomes

$$\begin{bmatrix} \Delta \mathbf{P}_{states} \\ \mathbf{0} \end{bmatrix} = \begin{bmatrix} \mathbf{B}_{11} & \mathbf{B}_{12} \\ \mathbf{B}_{21} & \mathbf{B}_{22} \end{bmatrix} \bullet \begin{bmatrix} \Delta \boldsymbol{\delta}_{states} \\ \Delta \boldsymbol{\delta}_{output} \end{bmatrix} \quad (3.25)$$

and the following relationship may be extracted from (3.25)

$$-\mathbf{B}_{21} \Delta \boldsymbol{\delta}_{states} = \mathbf{B}_{22} \Delta \boldsymbol{\delta}_{output} \quad (3.26)$$

and if \mathbf{B}_{22} is invertible

$$\Delta \boldsymbol{\delta}_{output} = -\mathbf{B}_{22}^{-1} \mathbf{B}_{21} \Delta \boldsymbol{\delta}_{states} \quad (3.27)$$

The invertibility of the \mathbf{B}_{22} matrix is understood by the physical characteristics of the system from which the original matrix, \mathbf{B} , in (3.22) and (3.23) is derived. Since each node corresponding to the susceptances in the \mathbf{B}_{22} matrix is connected to a minimum of two circuit branches (transmission lines), then each diagonal element is greater in

magnitude than the sum of all of the other element magnitudes in the corresponding column or row. The only nodes in the circuit that are used to form the \mathbf{B} matrix in (3.22) that are connected to only one circuit branch are the generator internal voltage nodes. These internal voltage nodes are necessarily never measurement points and thus are not associated with the \mathbf{B}_{22} matrix. This arrangement of diagonal elements creates a collection of columns (or rows) which are linearly independent. Linear independence of all of the columns guarantees that the matrix has a left inverse and since \mathbf{B}_{22} is a square matrix it must also have a right inverse. Thus the \mathbf{B}_{22} matrix must always be invertible. Another viewpoint proves invertibility via diagonal dominance which is discussed earlier in this paragraph. The fact is that the \mathbf{B}_{22} matrix is strictly diagonally dominant and thus always invertible.

Since \mathbf{B}_{22} and \mathbf{B}_{21} have entries that do not vary with time and the time derivatives of the voltage angles are equal to the frequency deviations in radians per second, according to derivations in chapter 2, then taking the derivative of both sides of equation (3.27) yields

$$\Delta\omega_{output}(t) = -\mathbf{B}_{22}^{-1}\mathbf{B}_{21}\Delta\omega_{states}(t) \quad (3.28)$$

And so equation (3.28) gives a linear relationship between the states and the outputs. Thus (3.28) is an output equation.

The user must be careful in that buses that have neither state quantity nor output (measurement) quantity must be eliminated from both the matrix and the vectors in (3.23). This reduction may be performed via a reduction technique such as the technique

used in A3.b to reduce the \mathbf{Y}_{bus} matrix. In order to perform this reduction, the incremental injected power at the bus that is being eliminated must be assumed zero.

Notice that the intention here is to use a steady-state power system analysis technique (called load flow) for the purpose of performing a dynamic analysis. Inaccuracies in this model are implicit and should be quantified for each particular case where the output model is used. For this work, this model is being developed for didactic purposes which, hopefully, will be useful in describing the overarching characteristics of system behavior in terms of frequency measurements.

Using this approach, the output matrix for a generator 1 outage was determined in Appendix III to be

$$\mathbf{C}^r = \begin{bmatrix} 0.30 & 0.16 \\ 0.49 & 0.20 \\ 0.15 & 0.50 \\ 0.08 & 0.11 \end{bmatrix} \quad (3.29)$$

The r superscript refers to a reduced matrix per the appendix. Analysis of only the interarea mode (lower frequency mode), the 0.8 Hz component of the machine speeds are inserted into the state vector to obtain

$$\Delta \boldsymbol{\omega}_{states} = 60 * \begin{bmatrix} \Delta \omega_2(f = 0.8Hz) \\ \Delta \omega_3(f = 0.8Hz) \end{bmatrix} = 60 * \begin{bmatrix} 0.92 \\ 0.88 \end{bmatrix} \quad (3.30)$$

These 0.8Hz components of the machine speeds are multiplied by 60 because the machine speed FFT was performed on the per-unit machine speed. The factor of 60 converts the per-unit vector into a 60Hz frequency deviation. Pre-multiplying this reduced state vector by the reduced output matrix yields

$$\Delta\omega_{output}^{calc} = \mathbf{C}^r \Delta\omega_{states} = 60 * \begin{bmatrix} 0.30 & 0.16 \\ 0.49 & 0.20 \\ 0.15 & 0.50 \\ 0.08 & 0.11 \end{bmatrix} * \begin{bmatrix} 0.92 \\ 0.88 \end{bmatrix} = \begin{bmatrix} 24.8 \\ 37.5 \\ 34.8 \\ 9.9 \end{bmatrix} \quad (3.31)$$

and this may be compared with the measured (from simulation) output 0.8Hz vector

$$\Delta\omega_{output}^{meas} = \begin{bmatrix} \Delta\omega_4 \\ \Delta\omega_5 \\ \Delta\omega_6 \\ \Delta\omega_7 \end{bmatrix} = \begin{bmatrix} 29.2 \\ 39.6 \\ 35.8 \\ 9.8 \end{bmatrix} \quad (3.32)$$

The subscripts 4 through 7 in equation (3.32) indicate which bus the frequency measurement is being taken per figure AI.1. The error vector, based on the calculated values may be obtained as follows

$$error = \begin{bmatrix} 17.7\% \\ 5.6\% \\ 2.9\% \\ -1.0\% \end{bmatrix} \quad (3.33)$$

The error is substantial for the first element of the output vector. The errors in the last three elements might be considered small enough to at least claim some merit for the approach of using the output matrix based on DC load flow.

A generator 2 outage leads to the following predicted output vector:

$$\Delta\omega_{output}^{calc} = 60 * \begin{bmatrix} 0.36 & 0.18 \\ 0.25 & 0.32 \\ 0.09 & 0.54 \\ 0.07 & 0.12 \end{bmatrix} * \begin{bmatrix} 1.95 \\ 4.34 \end{bmatrix} = \begin{bmatrix} 88.1 \\ 113 \\ 150 \\ 39.7 \end{bmatrix} \quad (3.34)$$

and comparing this calculated output vector with the measured output vector

$$\Delta \omega_{output}^{meas} = \begin{bmatrix} \Delta \omega_4 \\ \Delta \omega_5 \\ \Delta \omega_6 \\ \Delta \omega_7 \end{bmatrix} = \begin{bmatrix} 85.1 \\ 108 \\ 147 \\ 36.5 \end{bmatrix} \quad (3.35)$$

The error based on the calculated values is

$$error = \begin{bmatrix} -3.4\% \\ -4.6\% \\ -2.1\% \\ -8.1\% \end{bmatrix} \quad (3.36)$$

A generator 3 outage leads to

$$\Delta \omega_{output}^{calc} = 60 * \begin{bmatrix} 0.32 & 0.24 \\ 0.16 & 0.50 \\ 0.11 & 0.27 \\ 0.07 & 0.08 \end{bmatrix} * \begin{bmatrix} 2.70 \\ 4.34 \end{bmatrix} = \begin{bmatrix} 113 \\ 155 \\ 87.2 \\ 33.4 \end{bmatrix} \quad (3.37)$$

The measured output vector is

$$\Delta \omega_{output}^{meas} = \begin{bmatrix} \Delta \omega_4 \\ \Delta \omega_5 \\ \Delta \omega_6 \\ \Delta \omega_7 \end{bmatrix} = \begin{bmatrix} 116 \\ 159 \\ 102 \\ 34.9 \end{bmatrix} \quad (3.38)$$

and this gives an error based on the calculated values of

$$error = \begin{bmatrix} -2.7\% \\ 2.6\% \\ 17.0\% \\ 4.5\% \end{bmatrix} \quad (3.39)$$

Chapter 4 Non - Idealized System Modeling

In chapter three the usefulness of modal analysis for identifying generator outages was demonstrated using an idealized system. The features of this system that make it idealized include 1) lossless transmission lines; 2) lack of generator damping; 3) lack of loads within the transmission mesh; 4) absence of generator governors and voltage regulators; 5) presence of an infinite bus; and 6) absence of line charging susceptance. In order to make the modal analysis technique more useful in a practical situation, transmission losses will be modeled, theory for including generator damping will be incorporated into the state model and loads will be modeled and incorporated into the system plant matrix. In addition, the plant matrix will also be developed for a system that has no infinite bus and that also has speed governors on generators. Each of these non-idealized features has implications concerning the system's natural response in terms of damping, synchronizing power coefficients, and in the no-infinite-bus case, there are the additions of the t-to-the-first-power and t-to-the-second-power modes. These two special modes exist in principle only (at least for a stable system) as a t^1 or t^2 characteristic in either machine angle or speed would result in a speed deviation so far from synchronous speed as to create a total system crash. However the theory that governs these two special non-oscillatory modes must be developed in order to understand machine/frequency measurement dynamics during the first two or three swings of the system following a disturbance.

It will be shown that the presence of transmission losses has the effect of increasing electromechanical coupling in between generators in the system thus tending to increase natural response frequencies. The losses will also be shown to add no

electromechanical damping to the system in the case where no generator damping is modeled. Both of these unexpected effects will be discussed further.

The incorporation of generator damping into the system's state equation is straightforward once a damping coefficient can be determined for each generator. Development of this incorporation with explanations of damping sources will be discussed.

The presence of loads within the transmission system will be included in the model by converting loads into impedances and incorporating these impedances into the system's short-circuit admittance matrix. This process, along with its approximation and justification will be discussed. It will be shown that, generally speaking, the presence of loads in a power system tend to decrease coupling in between machines, thus decreasing natural response frequencies. The decrease is due to a decrease in transfer admittance. This decrease in coupling is in addition to the decrease created by higher relative machine angles which must accompany increases in power flows across a system. It will also be shown that the presence of loads does not contribute to system damping.

And finally the development of the system plant matrix where the system has no infinite bus will be discussed. The lack of infinite bus has an obvious effect on the system frequency – namely that time-averaged frequency will not necessarily be equal to rated frequency. The two special non-oscillatory modes mentioned above characterize this lack of “synchronism” to synchronous speed. In systems that do have an infinite bus, the infinite bus will guarantee that time-average frequency will be equal to rated frequency because the infinite bus will maintain this frequency. Of course an exception would be in a system that where one or more of the machines losses synchronism. Loss

of synchronism is the result of very severe disturbances coupled with operation closer to steady-state instability than what systems are normally operated at. Thus loss of synchronism is considered more of a rare occurrence than a “routine” disturbance such as a line or generator outage. It may be expected that loss of synchronism should ensure operation deep in the system's non-linear region. Thus, modal analysis, in it's pure form as developed in this work, possibly cannot be used to identify very severe disturbances such as loss of synchronism. More research could be done in this problem but it will not be investigated here.

4.1 Modeling of Transmission Losses

Since the objective of this section is to incorporate losses into modal analysis, it is necessary to calculate electrical power flows into electrical ports (generator internal voltages) in the system with losses present. This may be done by calculating the power injections at each port in the same fashion as was done in chapter 3 and in a similar fashion as is done for conventional load flow calculations. The use of load flow for in formulating the state equations for any power system network may be summarized as follows: 1) calculate the complex power flow at each port, i , as $S_i^* = E_i^* I_i$. In this equation I_i may be calculated by using the bus admittance matrix relationship $\mathbf{Y}\mathbf{E} = \mathbf{I}$ where \mathbf{I} and \mathbf{E} without subscripts are $n \times 1$ column vectors and \mathbf{Y} is the $n \times n$ short-circuit admittance matrix; 2) taking the real part of S_i^* ; 3) the results from these two steps may be incorporated in the swing equation for each machine just as was done in chapter 3 and the resulting equations linearized.

In the following development all bold capital letters without subscripts represent vectors or matrices, all bold capital letters with subscripts represent complex scalar quantities and non-bold letters, capital or lowercase, represent real numbers. From the bus admittance relationship mentioned above, each of the \mathbf{I}_i 's may be expressed as

$$\mathbf{I}_i = \mathbf{Y}_{ii}\mathbf{E}_i + \sum_{\substack{j=1 \\ j \neq i}}^n \mathbf{Y}_{ij}\mathbf{E}_j \quad (4.1)$$

where each \mathbf{Y}_{ij} is the i - j th entry in the bus admittance matrix, \mathbf{Y} , and each \mathbf{E}_j is the voltage at the j th bus (which is the internal voltage of the j th machine). The quantity \mathbf{I}_i in (4.1) is the current injected into the port as opposed to current withdrawn.

Using (4.1), \mathbf{S}_i^* may be expressed as follows

$$\mathbf{S}_i^* = \mathbf{E}_i^* \mathbf{I}_i = \mathbf{E}_i^* (\mathbf{Y}_{ii}\mathbf{E}_i + \sum_{\substack{j=1 \\ j \neq i}}^n \mathbf{Y}_{ij}\mathbf{E}_j) = \mathbf{E}_i^* \mathbf{E}_i \mathbf{Y}_{ii} + \sum_{\substack{j=1 \\ j \neq i}}^n \mathbf{E}_i^* \mathbf{E}_j \mathbf{Y}_{ij} \quad (4.2)$$

which may be expressed as

$$\mathbf{S}_i^* = E_i^2 \mathbf{Y}_{ii} \angle \theta_{ii} + \sum_{\substack{j=1 \\ j \neq i}}^n E_i E_j \mathbf{Y}_{ij} \angle (-\delta_i + \delta_j + \theta_{ij}) \quad (4.3)$$

where $\mathbf{Y}_{ij} = Y_{ij} \angle \theta_{ij}$ is the i - j th complex entry of the \mathbf{Y} matrix expressed in polar form and

$E_i \angle \delta_i$ is \mathbf{E}_i expressed in polar form. Taking the real part of both sides of (4.3) gives

$$\Re\{\mathbf{S}_i^*\} = E_i^2 Y_{ii} \cos \theta_{ii} + \sum_{\substack{j=1 \\ j \neq i}}^n E_i E_j Y_{ij} \cos(-\delta_i + \delta_j + \theta_{ij}) \quad (4.4)$$

Decomposing the term $Y_{ij} \cos(-\delta_i + \delta_j + \theta_{ij})$ and defining δ_{ij} as $\delta_i - \delta_j$

$$Y_{ij} \cos(-\delta_i + \delta_j + \theta_{ij}) = Y_{ij} \cos \theta_{ij} \cos \delta_{ij} + Y_{ij} \sin \theta_{ij} \sin \delta_{ij} \quad (4.5)$$

Recognizing that $G_{ij} = Y_{ij} \cos(\theta_{ij})$ and $B_{ij} = Y_{ij} \sin(\theta_{ij})$ and then substituting (4.5) into (4.4) gives

$$P_{ei} = \Re\{S_i^*\} = E_i^2 G_{ii} + \sum_{\substack{j=1 \\ j \neq i}}^n E_i E_j [B_{ij} \sin \delta_{ij} + G_{ij} \cos \delta_{ij}] \quad (4.6)$$

where P_{ei} is the total amount of electrical power that is injected into bus i from the i th generator's internal voltage. In studying the effects of each term on the right-hand-side of (4.6) it is worth considering that the quantities B_{ij} and G_{ij} have the following inequality relationships for a system that has loads modeled as constant power loads and no shunt susceptances

$$B_{ij} \geq 0 \text{ for } i \neq j \quad (4.7)$$

and

$$G_{ij} \leq 0 \text{ for } i \neq j \quad (4.8)$$

Thus the presence of transmission losses in the system (represented as the G_{ij} components in the \mathbf{Y} matrix), as expected, decrease the power flows in the network for given power angles and voltages in the internal voltages of the machines. If there are no transmission losses in the network, equation (4.6) reduces to an expression of the form of equation (2.8).

$$P_{ei} = \sum_{\substack{j=1 \\ j \neq i}}^n E_i E_j B_{ij} \sin \delta_{ij} \quad (4.9)$$

It is important to remember at this point that the power flow into the i th bus is directed toward all of the other generators. The above equation insinuates this source-sink relationship because (4.1) above is based on an n-port analysis which does not

include the loads in the system – each B_{ij} term represents the transfer susceptance between the i and j machines. The loads must either be absorbed into the \mathbf{Y} matrix or treated as constant power loads. If all of the loads are treated as constant power loads, the system response due to disturbances must be small signal in the strictest sense. Load bus voltage magnitudes must necessarily remain very close to q-point voltages in order for the constant power approximation to hold. If the loads are modeled as constant impedances, then voltages at load buses may vary substantially from q-point voltages and the linearized model will hold since the load bus voltages are not state variables nor are the state variables explicit functions of load bus voltages. The second of these approaches to load modeling will be discussed further in the next section.

Equation (4.6) may be substituted into the swing equation for the i th machine to yield an equation of the form of (3.11) as follows

$$\frac{2H_i}{\omega_s} \frac{d^2 \delta_i(t)}{dt^2} = P_{mi} - P_{ei} = P_{mi} - (E_i^2 G_{ii} + \sum_{\substack{j=1 \\ j \neq i}}^n E_i E_j [B_{ij} \sin \delta_{ij} + G_{ij} \cos \delta_{ij}]) \quad (4.10)$$

which may be linearized by taking the first order Taylor series expansion of each side of the equation and eliminating the q-point quantities to yield

$$\frac{2H_i}{\omega_s} \frac{d^2 \Delta \delta_i(t)}{dt^2} = - \sum_{\substack{j=1 \\ j \neq i}}^n E_i E_j [B_{ij} \cos \delta_{ij_0} - G_{ij} \sin \delta_{ij_0}] \Delta \delta_{ij}(t) \quad (4.11)$$

where δ_{ij_0} is the quiescent angle between machines i and j . Defining the synchronizing power coefficient between buses i and j in a similar fashion as was done in chapter 2

$$S_{P_{ij}} = \left. \frac{\partial P_{eij}}{\partial \delta_{ij}} \right|_{\delta_{ij_0}} = E_i E_j [B_{ij} \cos \delta_{ij_0} - G_{ij} \sin \delta_{ij_0}] \quad (4.12)$$

the swing equation (4.11) may be written in a more compact form

$$\frac{2H_i}{\omega_s} \frac{d^2 \Delta \delta_i(t)}{dt^2} = - \sum_{\substack{j=1 \\ j \neq i}}^n S_{p_{ij}} \Delta \delta_{ij}(t) \quad (4.13)$$

Investigation of (4.11) through (4.13) reveals two features of the effects on transmission system losses on machine electromechanical coupling and oscillatory mode frequencies. The first is to notice from (4.12) that, due to the inequality relationships (4.7) and (4.8) it can be seen that for a given quiescent set of internal voltage angles, δ_{i_0} , which do not differ greatly from one another, that the synchronizing power coefficients are actually increased in the presence of transmission losses. An increase in these coefficients does not necessarily indicate that oscillatory modes will have higher frequencies than they will in the lossless case. This means that electromechanical coupling in between machines can actually be higher due to transmission losses. Conventional intuition states that the opposite should be true as higher losses would normally indicate lower coupling in between machines due to increased impedances. The second feature which can be seen from the form of equation (4.13) is that the presence of losses in the network does not add any damping to the swing equation for each machine. This can be seen from the fact that there are no first derivative terms in δ_i in the governing differential equation for each machine. This lack-of-damping also is contrary to intuition as the presence of losses is normally associated with damping and that higher losses will increase damping.

As a graphical demonstration, the power angle curve for machine i is shown in figure 4.1. The X-to-R ratio of the circuit for this demonstration is 1.0 which exaggerates the effect in order to make it more visible. The voltages and impedances for the system used to develop these curves were normalized to a value of 1.0. Examination of the curves shows that the synchronizing power is not increased because of the presence of

losses for all possible operating angles. However, over the typical operating range of machine angles (from the internal voltage, to say, the terminal of the interconnecting transmission line will typically be in the range of 15 to 30 degrees) there will be a slight increase in the derivative of the power with respect to the angle due to the losses. This derivative is by definition the synchronizing power of the generator. For higher power angles, in the range of, say, $\pi/3$ radians (60 degrees), it can be seen from the graph that the slope of the curve is substantially higher for the lossy system than it is for the lossless system. In practice, X/R ratios for interconnecting circuits are typically in the range of 15 to 20. Thus, in practice, losses will actually have very little effect on synchronizing power.

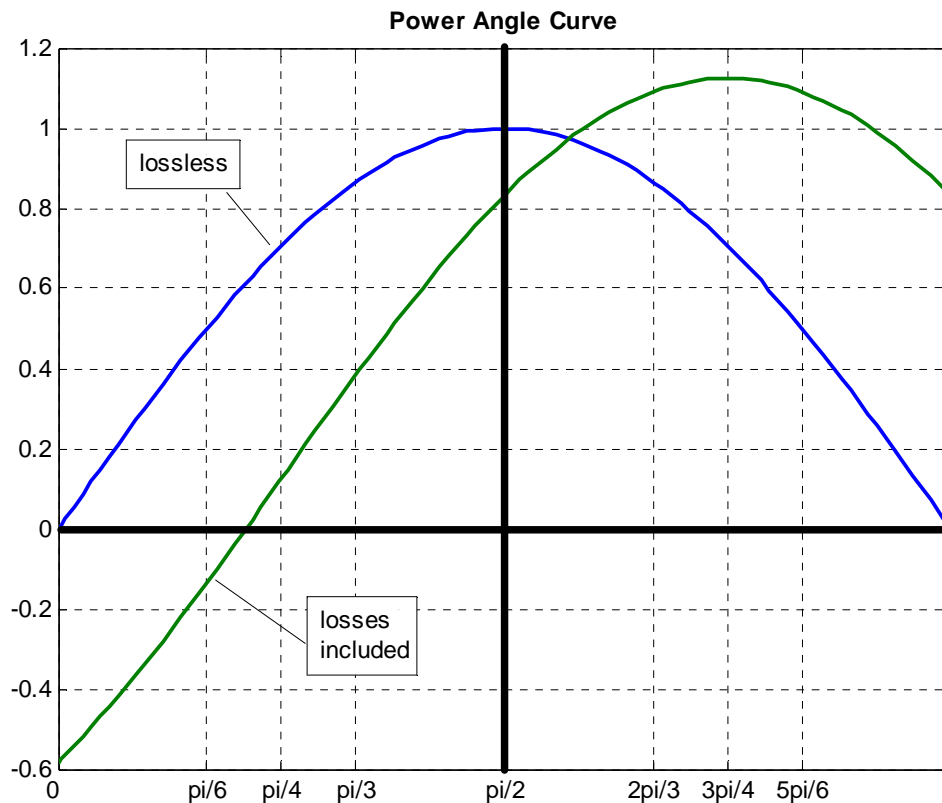


Figure 4.1: power-angle curve comparison between lossless and lossy systems

To further demonstrate the coupling effect, the single-machine infinite-bus system of chapter 2 shown in figure 4.2 is examined with variable X/R ratios in the interconnecting circuit as opposed to a pure reactance.

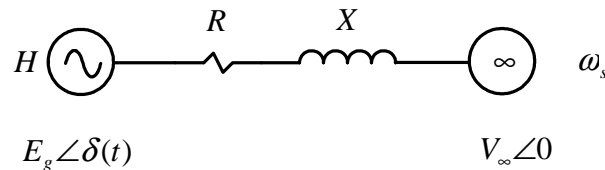


Figure 4.2: SMIB system

Table 4.1 shows that as the X/R ratio is decreased, the measured oscillation frequency does not change at least over the range of X/R ratios that are tested, thus verifying that the effect of losses is minimal for a realistic transmission system. The calculated frequency is seen to gradually rise above the lossless natural frequency and peaks somewhere between an X/R ratio of two and 100. The existence of the peak appears to have little consequence as the peak value may be expected to be very close to the lossless natural frequency. Further, in comparing the calculated and measured values of the natural frequencies, it is somewhat obvious that the effect of transmission system losses could easily be neglected (at least in the system used for this study) and still get good results in calculated values of natural frequency. The natural frequency then decreases as the X/R ratio decreases further. This peak effect may be explained by examination of the power angle curve in figure 4.1 as the green curve in this figure is shifted upward and to the right as the X/R ratio is decreased. The maximum coupling, and thus the maximum natural frequency, occurs when the transferred power corresponds to the maximum derivative of the green curve.

An important conclusion from the preceding development of transmission loss effects on dynamic behavior is that oscillation damping observed in frequency measurements need not be attributed to transmission system losses. Further, it can be expected that the presence of system losses will not have a substantial effect on the oscillation frequency itself and in many practical situations this effect may even be negligible.

Table 4. 1: variation in natural frequency with X/R ratio

X/R ratio	X	R	f_n (measured)	f_n (calc)
infinite	1.14	0	1.4	1.411
1000	1.14	1.14E-03	1.4	1.413
100	1.14	1.14E-02	1.4	1.415
10	1.13	0.113	1.4	1.435
2	0.408	0.204	1.4	1.430

4.2 Load Modeling

In order to incorporate electrical loads into modal analysis, the constant impedance load model will be used. The demerits of using a constant impedance load model include lack of both frequency sensitivity and appropriate voltage sensitivity especially in the case of induction motor loads. In the case of loads feed by power electronic processors, the load is, for all practical purposes, a constant power load in both the dynamic and steady state further rendering the constant impedance model inaccurate. These inaccuracies can be particularly acute in the case when a disturbance causes severe swings in load voltage.

In comparing the constant impedance model with a constant power model it is important to consider that constant power models are considered accurate in the steady state whereas a constant impedance model is substantially inaccurate in the steady state. The term steady state in this context can refer to a system that undergoes gradual changes in system voltages (over the course of hours or even minutes) that distribution transformer load tap changers and regulators can adequately respond to. The effect of the tap changers and regulators is to maintain load voltage close to a nominal voltage thus maintaining the power that the load draws from the transmission system. As an absolute rule, the under-load tap changers on these pieces of equipment do not respond to voltage excursions that last for less than 30 seconds. Many utilities will set the time limit higher than 30 seconds – typically 60 seconds is the standard for distribution utilities in the United States. Voltage excursions due to electromechanical dynamic activity will induce no response from load tap changers and regulators as the voltage excursions take place over the course of a few seconds – substantially less than 30 seconds. In addition, the oscillations due to an electromechanical disturbance will cause the voltage at a load bus to oscillate out-of and immediately back into the tap changer controller's nominal voltage bandwidth, thus continually setting and resetting the controller's timer. This continual resetting of the timer will render the tap changer / regulator inactive during the voltage excursions created by an electromechanical disturbance. The end result of a voltage excursion due to an electromechanical disturbance is that voltages on the actual loads are not regulated and thus must draw power according to the change in voltage. In the case of motor and lighting loads, it can be seen that the constant power model cannot be as accurate as the constant impedance model in the dynamic case.

In view of this voltage regulation scenario, it can be claimed that the constant impedance load model is a better model than the constant power model for dynamic studies. The constant impedance, though not frequency sensitive is able to vary its power drawn as voltage oscillates.

Typically when a utility or operator performs a dynamic simulation, the “50-50” load model is employed. The term “50-50” refers to the percentage of the load that is converted 1) into constant current and 2) constant impedance. The load is converted at initialization into 50% impedance and 50% constant current. The reason for using this type of load model is simply that lighting and other constant impedance loads behave like constant impedances; motor loads tend to behave like constant current loads (especially in the reactive portion of the current that a motor will draw).

The above dynamic load behavior is in reference to voltage excursions – not frequency excursions. Concerning frequency excursions, it is typical for load frequency sensitivity to be in the range of one to two percent [24], the extreme case being two percent. Load frequency sensitivity is defined as the percent power change per percent frequency change – for example a one percent decrease in frequency leads to a one percent decrease in power drawn by the load. In a typical small interconnection, for example ERCOT, a very large frequency excursion would be on the order of 300 mHz. This type of frequency excursion would be due to, say, a 2000MW unit trip – an extremely severe disturbance for the ERCOT interconnection. Taking into account that this is considered a severe disturbance, it is important to notice that the frequency change is only one-half of one percent. In terms of the change in load power, this frequency decrease would change, say, a total 30GW load (roughly speaking, the ERCOT

interconnection load) into a 29.7GW load. And this is a load change calculation based on the extreme case of two percent load frequency sensitivity. Similar arguments could be made for other interconnections. The eastern interconnection – the largest in the world – has severe frequency excursions on a much smaller scale than that of ERCOT. A 100mHz excursion in the Easter Interconnection would be considered extremely severe. The whole point of this preceding discussion on load frequency sensitivity is that load changes due to frequency changes for a typical interconnection could be considered negligible – especially in the small signal case.

All of the simulations performed from this point forward in this report will use the constant impedance load conversion. The calculations for modal analysis will also be performed using a constant impedance load.

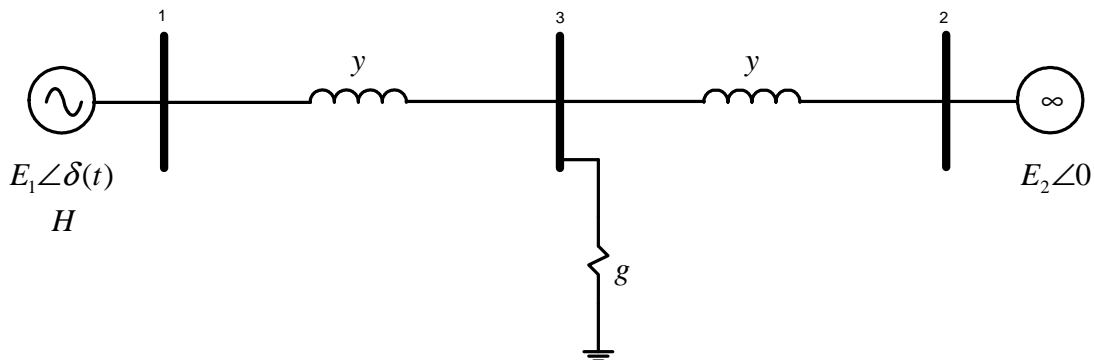


Figure 4.3: system used to present loading effects on electromechanical coupling

In order to present the effect of an electrical load on electromechanical dynamics, a SMIB case will be developed with a $\text{pf} = 1.0$ load located center-point on the branch that connects the generator to the infinite bus as shown in figure 4.3. The primary feature of the electrical load that will come out of this analysis is to show its effect on the electromechanical coupling between the two machines. The fact that the machine on the right hand side of the circuit is an infinite bus is actually not consequential in terms of the

machine being ideal instead of non-ideal. In fact the following theoretical development could be done with the infinite bus replaced with a finite-inertia machine.

The reduced admittance matrix for the system will be formulated below using the same technique as used in chapter three and described in more detail in appendix A3.b1. The purpose of formulating the reduced admittance matrix is to determine the transfer admittance in between the two buses that the internal voltages of the machines are connected to. Equation (4.12), the expression for the synchronizing power coefficient, is subscripted to fit the system in figure 4.3 as follows

$$S_{P_{12}} = \left. \frac{\partial P_{e12}}{\partial \delta_{12}} \right|_{\delta_{12_0}} = E_1 E_2 [B_{12} \cos \delta_{12_0} - G_{12} \sin \delta_{12_0}] \quad (4.14)$$

where the real and imaginary parts of the transfer admittance are B_{12} and G_{12} respectively.

Using bus numbering shown in the figure, the admittance matrix may be formulated as

$$\mathbf{Y}_{bus} = \left[\begin{array}{cc|c} y & 0 & -y \\ 0 & y & -y \\ \hline -y & -y & 2y+g \end{array} \right] \quad (4.15)$$

The \mathbf{Y}_{bus} matrix is partitioned in such a fashion so that the third row and third column may be eliminated in the reduction process. Repeating the matrix partition definitions and reduction process outlined in A3.b1, the upper left hand matrix is designated \mathbf{K} , the upper right is designated \mathbf{L} , the lower left, \mathbf{L}^t , and the lower right, \mathbf{M} . The reduced matrix is determined by

$$\mathbf{Y}_{bus}^r = \mathbf{K} - \mathbf{L}\mathbf{M}^{-1}\mathbf{L}^t \quad (4.16)$$

and so

$$\mathbf{Y}_{bus}^r = \begin{bmatrix} y & 0 \\ 0 & y \end{bmatrix} - \left(\frac{1}{2y+g} \right) \begin{bmatrix} -y \\ -y \end{bmatrix} \begin{bmatrix} -y & -y \end{bmatrix} \quad (4.17)$$

and eliminating algebraic steps to obtain the off-diagonal entries of \mathbf{Y}_{bus}^r leads to

$$Y_{12} = Y_{21} = \frac{-\frac{1}{2}y^2}{y + \frac{1}{2}g} \quad (4.18)$$

Normalizing this expression by setting $y = -j$ and further separating real and imaginary parts leads to

$$Y_{12} = Y_{21} = \frac{g}{g^2 + 4} + j \frac{2}{g^2 + 4} \quad (4.19)$$

thus

$$G_{12} = \frac{g}{g^2 + 4} \quad \text{and} \quad B_{12} = \frac{2}{g^2 + 4} \quad (4.20)$$

Both the real and imaginary parts of the transfer admittance, Y_{12} , are non-negative numbers. As seen by equation (4.14) a decrease in the transfer susceptance, B_{12} , has a direct effect on decreasing the synchronizing power coefficient. Increasing the load conductance decreases the transfer susceptance directly according to (4.20). Thus, the effect of a small increase in load power from zero power to some positive power (small increase in g) can be seen to decrease the value of the synchronizing power coefficient as defined in (4.14). Conversely, the same increase in the load conductance creates a decrease in the transfer conductance, G_{12} , thus having the effect of increasing the synchronizing power coefficient. It should be noted that the effect of increasing the load conductance has a more drastic effect on decreasing B_{12} than it does on decreasing G_{12} . The net effect, then, of increasing the load may be interpreted as decreasing the

synchronizing power coefficient. As explained above, a decrease in synchronizing power coefficient is tantamount to a decrease in electromechanical coupling, thus reducing the natural oscillation frequency of the system. This appears correct intuitively as noted in the case when the load conductance is increased to infinity – there can be no coupling at all in between the two machines in this case – they literally operate as two separate systems. In this infinite-conductance case, of course, there is no load on the system because the load bus is short-circuited. However, this limiting case illustrates the decoupling nature of an electrical load.

It is also interesting to observe that the swing equation for this system still takes on the form of equation (4.13)

$$\frac{2H}{\omega_s} \frac{d^2 \Delta \delta(t)}{dt^2} = -S_{p_{12}} \Delta \delta(t) \quad (4.21)$$

As in the case of modeling transmission system losses, the swing equation does not have a first order derivative term in the governing differential equation. Thus, the effect of loads within a transmission system should not be considered to have an effect on electromechanical oscillation damping. This statement concerning the damping effect of loads on oscillation damping is made here with reservation rather than assertion as the load model used to carry out this analysis, the constant impedance load model, is not considered totally accurate. It may, in fact, be determined, through a more thorough study of complicated load models, that loading does, indeed, have an effect on oscillation damping. Load modeling is a research subject all to itself that will not be explored any further in this work.

A further indirect effect that electrical loads have on the machine coupling is that as machine loading is increased, so does the power angle. Since any machine's

synchronizing power coefficient with respect to another machine is linearly proportional to the cosine of the difference in between the two machine's power angles, there must be a decrease in synchronizing power as the difference in between the two angles increases from zero towards 90 degrees.

4.3 System Modeling in the Absence of Infinite Bus and Basic Modal Characteristics of Line Outages

In order to establish a modeling procedure and explore the salient modal characteristics of a power system with no infinite bus, a two machine system with a single electrical load and a pair of parallel lines will be used. The system is shown in figure 4.4. Both of the machines have blocked governors. A line outage of one of the parallel lines will provide excitation for the electromechanical dynamic activity. Since line outage effects on electromechanical activity have not been treated thus far, at least some of their effects must be explored in this section. Both scenarios 1) line outage and; 2) line outage followed by reclosure will be used to provide excitation for this system and comparisons between these two scenarios will be made. The concept of generation-load mismatch will be used to analyze and explain dynamic phenomena due to line outages. This concept is useful for determining a “quasi – “ quiescent point for the system which will be shown to be a refined method of determining system q-point. This is a refinement to the method used in [19]. Once the q-point is determined, the plant matrix will be formulated for the two-machine system thus leading to eigenproperty information about the system. As stated earlier, at least one of the eigenvalues of the plant matrix must necessarily be identically equal to zero. This is, of course, using the state definition for angles as being the absolute angles and speeds themselves as opposed to using angle and

speed *differences* with respect to one machine in the system. Since a line outage on a power system (with blocked governors) will create at least an instantaneous generation-load mismatch (if not a sustained mismatch), the machine angles should be expected to drift away from the initial operating point in a monotonic fashion. This monotonic increase is intuitively associated with a zero eigenvalue and potentially a double-zero eigenvalue (the monotonic increase referred to here does, in general, have oscillation(s) superimposed upon it). For a single machine system, this concept may be understood by examining the swing equation for a single machine

$$\frac{2H}{\omega_s} \frac{d^2 \Delta \delta(t)}{dt^2} = \Delta P_a(t) \quad (4.20)$$

Assuming an arbitrary value for $\Delta P_a(t)$ and taking the Laplace transform of both sides of (4.20) reveals that this simple system does indeed have a pair of zero eigenvalues.

$$\frac{2H}{\omega_s} s^2 \Delta \delta(s) = \Delta P_a(s) \quad (4.21)$$

Equation (4.20) implies an input of $\Delta P_a(t)$ and an output of $\Delta \delta(t)$. For example a constant positive value of $\Delta P_a u(t)$ (a step input) will yield a “t-squared” response in $\Delta \delta(t)$ as

$$\Delta \delta(t) = \frac{\omega_s \Delta P_a}{2H} \mathcal{L}^{-1} \left\{ \frac{1}{s^3} \right\} = \frac{\omega_s \Delta P_a}{4H} t^2 u(t) \quad (4.22)$$

Since a stable AC interconnection is in synchronism, it should be expected that (4.22) describes the activity of an entire interconnection that is operating in a “t-squared” mode. Further, since the machine’s speed deviations are identical to the first derivatives of the corresponding machine angle deviations, it should be expected that a system that is

operating in a “t-squared” mode in *angle* states will also be operating in a “t-to-the-first-power” mode in *speed* states.

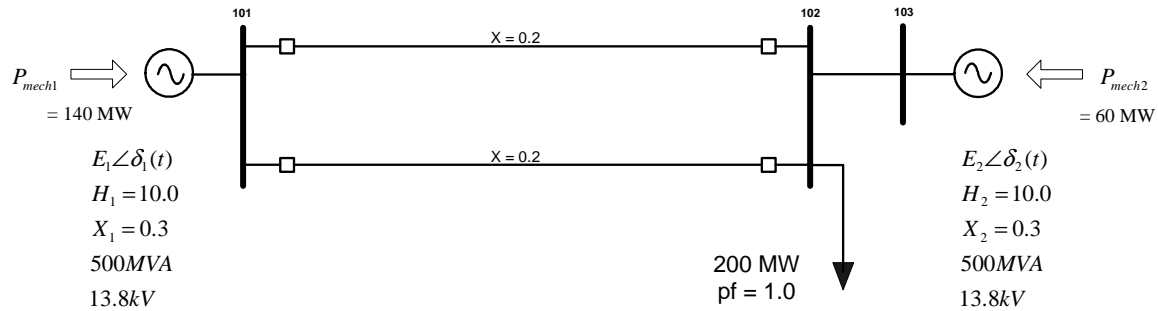


Figure 4.4: unregulated system without infinite bus

Before setting up the plant matrix for the system in figure 4.4 it must be determined whether the analysis is for a line outage with no reclosure or a line outage with reclosure. The most obvious difference in between these two analyses is that the admittance matrix must be different with the line out of service versus the line in service. With the line in service it should be expected that the oscillation frequency will be greater due to tighter coupling in between the two machines – vice versa for line outage with no reclosure. Another difference will be in the q-point for the two different cases. For a line outage with reclosure it may be expected that the q-point will be very close to, if not identically equal to, the initial operating point prior to the outage. It will be shown that the q-point for the line outage with reclosure case will not be exactly equal to the pre-outage operating point due to a slight sustained generation-load mismatch. In the case where the line outage is not followed by reclosure, it is evident that the angles in between the two machines must increase due to the decrease in transfer admittance between the two machines. This increase in angle will also tend to decrease oscillation frequencies. Further, it should be expected that in the case of a line outage with no reclosure that a

substantial generation-load mismatch must occur due to the immediate decrease in transfer capability of the transmission interface in between the two machines.

Plant matrix development for the line outage with no reclosure case will be covered first. The q-point for this case may be considered to be more of a quasi-q-point as opposed to a “conventional” q-point. The reason for this designation of quasi-q-point is that in the presence of a sustained generation-load mismatch, the machine speeds must necessarily be drifting away from synchronous speed in a fashion described in the discussion pertaining to equation (4.22). This notion is non-conventional because a q-point for any dynamic system is normally associated with a fixed point in the state space. If a state model were used where all of the system states were *differences* in between each machine angle and a reference machine angle such as the model developed in [19], the q-point could be considered to be a fixed point in the state space. The plant matrix would also not necessarily have any zero eigenvalues as the drift in average machine speed over the entire system could not be detected by looking at machine speed *differences*. The type of model developed in [19] does not give information about the absolute machine speeds and thus is not able to yield any information concerning the time-average frequency of the system being studied. Thus the model developed in [19] is not able to yield frequency measurement predictions and will not be used in any of the studies in this work.

The following key features of the system in figure 4.4 and modal properties of the line outage (with and without reclose action) will be examined in detail:

1) Since a line outage not followed by reclose will invariably cause the system to proceed to a new q-point, it is the difference between the initial operating point and the post fault q-point that provides dynamic excitation.

2) In the case of the system in figure 4.4 it is evident that machine 1 will have a positive acceleration power, P_{a1} , immediately following the line outage. Conversely machine 2 will have a negative acceleration power. These two instantaneous acceleration powers can be calculated in closed form using the system's admittance matrix. This is due to the fact that the machine angles will not change instantaneously (there can be no step in rotor angle). Internal voltage magnitudes will not change as flux magnitude cannot step either. Thus the system acceleration power may be calculated using linear network analysis as opposed to using an iterative load flow.

3) Due to the fact (2) above, the angle in between the two machines, δ_{12} , must increase. This increase in angle will invariably produce a voltage dip at the load bus (it will also produce a voltage dip at all other points on the system save the internal voltages of the two machines). This dip in load bus voltage causes an overall system generation-load mismatch. Thus the system must accelerate. Quantifying this mismatch and the dynamic characteristics of this mismatch will be discussed below. Further, due to the fact that after the line outage the average angle between the two machines must be greater than the pre-fault angle, the dip in voltage must be sustained. Thus the overall system generation-load mismatch will also be sustained. The voltage magnitude at the load bus is actually oscillatory in nature. This phenomenon will be explored below.

4) Following the line outage, the system state (machine angles and machine speeds) will proceed to deviate from the pre-fault state to a new q-point. Previously, dynamic studies used the initial operating point as the q-point [19]. This method should not yield accurate results, at least in determining oscillation frequencies, since the q-point, mathematically, cannot possibly be equal to the initial point. If the two points were equal, there would not be any modal excitation. The lack of excitation can be understood by examination of a simple first order homogeneous LTI differential equation that has an initial condition such that the dependent variable at time zero is exactly equal to zero – the particular solution to this first order system is zero for all time. In the work done by [19], an exact calculation of system eigenvalues is not of interest since the objective is to determine system stability and so therefore the assumption that the initial operating point is the q-point might give adequate accuracy for stability studies. In this present work, stability is not an issue so much as determining, as accurately as possible, the system natural frequencies. The practice of using the initial condition as the q-point will be abandoned here in lieu of a more refined determination of the system's post-fault q-point. Due to the facts that a) the system's admittance matrix changes between pre and post-fault and b) the system demand changes due to point (3) above, the system's new q-point may be substantially different from the initial operating point. Since the q-point determines the linearization point, the elements of the plant matrix depend on the q-point and thus the system's natural frequencies depend on the q-point. Since outage identification based on measured oscillation frequencies is the objective of this work, the determination of the

natural frequencies is crucial and so a very accurate determination of system q-point is desirable.

5) In determining the system's new q-point it needs to be recognized that due to the fact that there is a sustained generation-load mismatch, (point (3) above) there will be a drift in system frequency and thus the q-point actually drifts from the initial point indefinitely. The presence of this drift actually means that no q-point exists. However, it will be shown that the relative differences in the machine angles and machine speeds do not drift from one another and thus a quasi-q-point may be established. The notion of quasi-q-point may be thought of in terms of a nominal state *trajectory* that a state moves along in its state space. The linearization is actually performed about this nominal trajectory – as opposed to a specific point in the state-space - and the initial conditions on the system provide excitation for perturbations about the nominal trajectory. Due to the fact the all of the machines in the system are in synchronism with each other, all of the machines must accelerate at the exact same rate. This acceleration does not include instantaneous accelerations due to oscillatory behavior but instead is due to rigid body behavior – it is a type of time-averaged acceleration. Since all of the machines must accelerate at the same rate, they must all have the following quantity to be equal on all machines

$$\frac{d^2\Delta\delta'_i(t)}{dt^2} = \frac{d\Delta\omega'_i(t)}{dt} = \frac{\omega_s\Delta P_{ai}}{2H_i} \quad (4.23)$$

where $\Delta\delta'_i(t)$ and $\Delta\omega'_i(t)$ are the non-oscillatory components of $\Delta\delta_i(t)$ and $\Delta\omega_i(t)$.

Since ω_s and the factor 2 in (4.23) are the same in the swing equation for all machines, it follows that all machines must have the same ratio of

$$\frac{P_{ai}}{H_i} \quad (4.24)$$

hereafter referred to as *acceleration power ratio*. Determining the actual ratio for the system's new q-point is done iteratively as follows: calculate the electrical powers injected at a starting angle difference in between the two machines, then vary the angle in between the two machines until the acceleration power ratios of the two machines are equal to each other within a specified tolerance – this point where the ratios are equal is the new q-point of the system. The tolerance should be similar to a typical minimum power mismatch used in any load flow. When using this method on systems that have more than two machines, a slightly more elaborate process has to be used. A swing bus is selected, all power injections at all other generator buses are set so that their acceleration ratios are equal, then a load flow must be solved. The swing bus's ratio will invariably be different from the ratios of the rest of the machines on the system and so another ratio must be selected and the load flow reran. This procedure must be repeated until the swing bus ratio is equal to the ratios on the rest of the machines in the system. It should be understood that this load flow is not a conventional load flow in the sense that there are no load buses in the system. All loads are accounted for by including them in the admittance matrix as discussed above. Therefore this load flow is actually a solution of machine angles only. It is not a solution of load bus voltages. Load bus voltages may be determined by then solving the linear network after the load flow has been solved. It turns out that the load bus voltages are not consequential in determining the system q-point. The primary reason for needing the load bus voltages would be for determining the total system acceleration power. However this quantity may be solved for by using the load flow data obtained from the iterative process described above. An alternative

version of using constant impedance loads in lieu of, say, constant current or constant power (or combinations) could be incorporated into this process by considering that injected currents and/or powers into the load buses is no longer zero. These injections can then be included in the load flow algorithm. This refinement will not be considered in this work.

All five of the above points will be illustrated using the system in figure 4.4. The simple disturbance of removing one single line from the system will be used for excitation. The plant matrix will be formulated, overall system generation-load mismatch will be calculated and these two calculated values will be compared with simulation results. Following the line outage analysis, the line outage followed by reclose scenario will be examined.

In looking forward to analyzing and identifying line outages that are followed by reclose it is interesting to note that the initial operating point is the same as (or actually very close to) the q-point, however, the excitation is provided by the deviation in system state that occurred during the 5 to 10 cycles that the line was out of service before the reclose action. There are a couple of features of this disturbance that may create reservations in using eigenanalysis as a disturbance identification method. One is that the system admittance matrix is the same for all line outages, second is that the q-point is the same for all line outages. This necessarily indicates that the state matrix is *exactly* the same for all line outages that are followed by reclose action. The key to identification is that different line outages will excite different modes to differing degrees. It is this difference in mode excitation that must be used to identify the outage (mode shape may also be used).

It should be noticed by examination of figure 4.4 that this system is very lightly loaded. If each machine is considered to be an equivalent system, the power flow on the interface (the pair of parallel lines that connect bus 101 to 102) will be substantially low compared to each equivalent system's capacity. Thus the sample system in figure 4.4 is realistic in terms of capacity and power flow in between two equivalent systems.

4.3.1 Investigation of Line Outage Followed by no Reclose Action

The first step in determining the response due to a line outage is to run a load flow on the system. This will determine the initial condition of the system prior to line outage, the most important condition being the internal voltage of each machine. Reactive power and current flows are not consequential but are reported below for reference. The load flow was performed using PSS/E v29.

The results are as follows:

```

PTI INTERACTIVE POWER SYSTEM SIMULATOR--PSS/E      FRI, APR 06 2007  14:19
TEST CASE 4: TWO-MACHINES, TWO PARALLEL LINES AND A LOAD  RATING
BASE CASE                                               SET A

BUS  101 GENS      13.8 AREA CKT    MW    MVAR    MVA  %I 1.0000PU  0.00 101
GENERATION
TO  102 LOAD      13.8  1  1    140.0  10.8R  140.4 28 13.800KV
TO  102 LOAD      13.8  1  2    70.0   5.4   70.2  1
TO  102 LOAD      13.8  1  2    70.0   5.4   70.2  1

BUS  102 LOAD      13.8 AREA CKT    MW    MVAR    MVA  %I 0.9991PU -8.06 102
1
TO  LOAD-PQ
TO  101 GENS      13.8  1  1    200.0  0.0   200.0
TO  101 GENS      13.8  1  1    -70.0  4.5   70.1  1
TO  101 GENS      13.8  1  2    -70.0  4.5   70.1  1
TO  103 GEN2      13.8  1  1    -60.0 -8.9   60.7  1

BUS  103 GEN2      13.8 AREA CKT    MW    MVAR    MVA  %I 1.0000PU -7.71 103
GENERATION
TO  102 LOAD      13.8  1  1    60.0  9.3R  60.7 12 13.800KV
TO  102 LOAD      13.8  1  1    60.0  9.3   60.7  1

-----MACHINE INITIAL CONDITIONS-----
X----- BUS -----X ID  ETERM  EFD    POWER  VARS  P.F.  ANGLE  ID    IQ
101 GENS    13.8  1  1.0000 1.0100 140.00  10.77 0.9971  4.77 0.0448 0.2772
103 GEN2    13.8  1  1.0000 1.0062  60.00   9.31 0.9882 -5.66 0.0229 0.1193

```

The machine initial conditions that are listed at the bottom of the output printout are not the result of the load flow but instead are the result of initializing the system prior to dynamic simulation. These initial conditions are important because they represent the

initial system state. The load flow printout does not give this data because internal machine activity is not taken into account when performing a load flow.

The next step in the analysis is to construct the impedance diagram of the system, convert it into an admittance diagram and then construct the admittance matrix for the system. After the admittance matrix, a 3 x 3 matrix, is completed, it must be reduced to a 2 x 2 matrix using the procedure outlined in A3.b1.

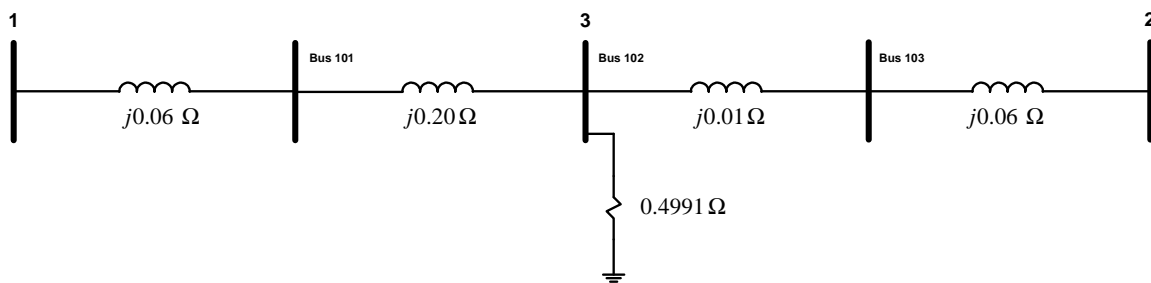


Figure 4.5: impedance diagram of system in figure 4.4 – line outage followed by no reclose action

The impedance in between buses 102 and 103 is 0.01 per unit on a 100MVA, 13.8kV base. Figure 4.5 shows the impedance diagram when one of the lines that connects bus 101 to 102 is taken out of service. The load was converted into an impedance according to the amount of power that it draws, the power factor of the load, and the pre-fault voltage at the load bus. Since the load bus voltage was 0.9991 per unit, the power factor is 1.0, and the power drawn is 2.0 per unit, the load converts into an impedance that is a pure resistance of 0.4991 ohms. Buses 1 and 2 of the impedance diagram represent the point in the network where internal voltages of the generators at buses 101 and 103 respectively are applied.

The circuit in figure 4.5 may be reduced and converted into an admittance diagram as shown in figure 4.6. The admittance matrix for the circuit in figure 4.6 is

$$\mathbf{Y}_{bus} = \left[\begin{array}{cc|c} -j3.846 & 0 & j3.846 \\ 0 & -j14.286 & j14.286 \\ \hline j3.846 & j14.286 & 2.0036 - j18.132 \end{array} \right] \quad (4.25)$$

and eliminating bus number three from the equations via Kron reduction yields

$$\mathbf{Y}_{bus}^r = \left[\begin{array}{cc} 0.089 - j3.040 & 0.331 + j2.994 \\ 0.331 + j2.994 & 1.229 - j3.166 \end{array} \right] \quad (4.26)$$

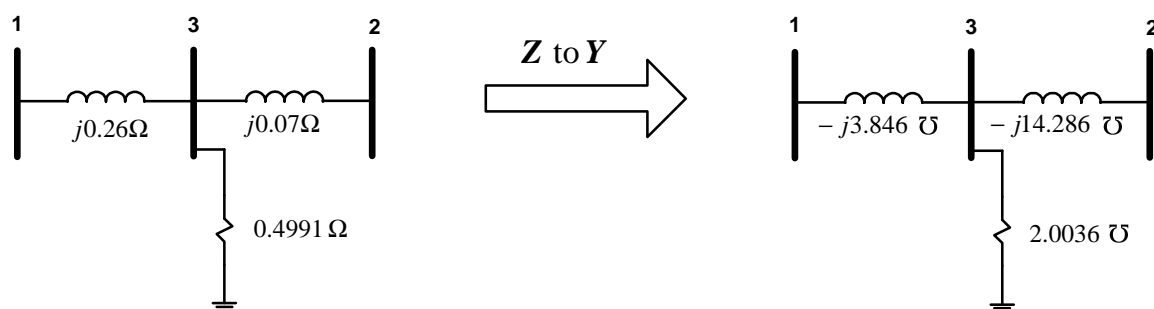


Figure 4.6: reduced impedance and admittance diagrams for system in figure 4.5

The next step in formulating the model for this system is constructing the governing differential equations for each machine. The procedure used for this two-machine two-line system is exactly the same as it was for the three-machine infinite bus system studied in chapter three – construct the swing equation for each machine, linearize these swing equations, and put the resulting equations in state-space form where the states are $\Delta\omega_i(t)$'s and $\Delta\delta_i(t)$'s.

The governing equation for each machine in this system is simply

$$\frac{2H_i}{\omega_s} \frac{d^2 \Delta\delta_i(t)}{dt^2} = \Delta P_{mi}(t) - \Delta P_{ei}(t). \quad (4.27)$$

and the term $\Delta P_{ei}(t)$ may be expressed as follows according to the derivations in section 4.1 above

$$\Delta P_{ei}(t) = \Delta \delta_{ij}(t) \left. \frac{\partial P_{ei}(\delta_{ij})}{\partial \delta_{ij}} \right|_{\delta_{ij}=\delta_{ij_0}} = E_i E_j [B_{ij} \cos(\delta_{ij_0}) - G_{ij} \sin(\delta_{ij_0})] \Delta \delta_{ij}(t). \quad (4.28)$$

Before proceeding with development of equation (4.28) for each machine, it should be evident that the q-point angles, δ_{ij_0} , must be determined. All of the other terms in (4.28) are known quantities: the susceptance and conductance terms, B_{ij} and G_{ij} , come directly from the admittance matrix and the voltages E_i and E_j are load flow outputs. At first glance it appears as though the system's q-point is such that the electrical power output of each machine is equal to the mechanical power input of each machine. It seems natural that this would be the q-point for when these two powers are equal to each other, each machine's synchronizing power is equal to zero – the lowest energy state possible. However, due to the fact that there is a sustained positive generation-load mismatch on the system, the system experiences an acceleration - machine speeds increase. This acceleration affects both of the machines in the system, and even though the acceleration will be shown to be non-constant (it will actually be "perturbed" about it's own trajectory in a fashion that is sinusoidal) the value of this acceleration is such that both of the machines in the system will have the exact same time-average acceleration on an individual machine basis. The q-point may be determined by recognizing the following relationship in between acceleration power and rotational acceleration

$$\Delta P_{mi}(t) = \Delta P'_{ei}(t) + \frac{1}{T} \int_{t_0}^{t_0+T} \frac{2H_i}{\omega_s} \frac{d^2 \Delta \delta_i(\tau)}{d\tau^2} d\tau \quad (4.29)$$

The second term on the right hand side of (4.29) is simply the time-average value of the acceleration in per unit since the integrand is unit-less. The quantity T in the two machine case is any integer multiple of the system's natural period – the inverse of the

system's natural frequency. The quantity $\Delta P'_{ei}(t)$ is the component of $\Delta P_{ei}(t)$ that is non-oscillatory.

If the average value of the acceleration may be determined, the electrical power output of each machine may be determined due to the fact that $\Delta P_{mi}(t)$ is known and constant (it is actually zero since the system is blocked). In order to determine the average system acceleration it must be recognized that both of the machines must accelerate at an equal rate on an average basis. This is due to the simple fact that both of the machines are in synchronism with each other. The reader may now recognize that this time-average acceleration is associated with a rigid body mode – both of the machines, in terms of their speeds, stick together in the rigid body mode. Any deviation in the machine's speeds with respect to each other is associated with another mode (or possibly modes) – specifically an oscillatory mode, assuming that the mode is not overdamped. In an oscillatory mode (there is only one oscillatory mode for this two-machine system), the machine speeds will oscillate in "antiphase" with each other. Thus there is a superposition of oscillatory and nonoscillatory modes.

In order to determine the average power for each machine at which both machines accelerate at the exact same rate it is necessary to determine the electrical powers of each machine corresponding to the following acceleration power ratio relationship which follows from equation (4.29)

$$\frac{\omega_s P_{a1}}{2H_1} = \frac{\omega_s P_{a2}}{2H_2} = \Delta \dot{\omega}_{avg} \quad (4.30)$$

In this simple two-machine system, this operating point may be determined by varying the angle in between the two machines, δ_{12} , until the acceleration power ratios of the two

machines are equal. This is to be done as a steady state analysis using equation (4.4) for each machine. Since the two machines have the exact same inertia constant, the solution to this iterative process is the point where the two acceleration powers, P_{a1} and P_{a2} , are equal to each other. A value of δ_{12} equal to 18.723 degrees yields equal acceleration powers. Thus

$$\delta_{12_0} = 18.723^\circ \quad (4.31)$$

and now all of the coefficients in (4.28) are known quantities – the expression on the right-hand side of (4.28) may now be calculated and the governing differential equation for each of the two machines, (4.27) may be set up.

The acceleration power of the system under the condition $\delta_{12_0} = 18.723^\circ$ corresponds to 0.0282 per unit on a 100MVA base according to (4.30) and at this acceleration power the following acceleration rate holds

$$\frac{\omega_s P_{a1}}{2H_1} = \frac{\omega_s P_{a2}}{2H_2} = \Delta \dot{\omega}_{avg} = 0.0532 \frac{\text{rad}}{\text{sec}^2} \quad (4.32)$$

In per unit this is 0.000141 per second.

Substituting (4.31) and the values for B_{12} , G_{12} , E_1 , E_2 into equation (4.27) and replacing the $\Delta \ddot{\delta}_1(t)$ term in (4.27) with $\Delta \dot{\omega}_1(t)$ yields the governing differential equation for machine 1 as

$$\Delta \dot{\omega}_1(t) = -10.4553 \Delta \dot{\delta}_1(t) + 10.4553 \Delta \dot{\delta}_2(t) \quad (4.33)$$

and for machine 2 using the same procedure with $\delta_{21_0} = -\delta_{12_0} = -18.723^\circ$

$$\Delta \dot{\omega}_2(t) = 11.2691 \Delta \dot{\delta}_1(t) - 11.2691 \Delta \dot{\delta}_2(t). \quad (4.34)$$

The remaining differential equations for each machine are

$$\Delta \dot{\delta}_1(t) = \Delta \omega_1(t) \quad \text{and} \quad \Delta \dot{\delta}_2(t) = \Delta \omega_2(t). \quad (4.35)$$

And finally the vector-matrix differential equation of (4.33) through (4.35) is

$$\frac{d}{dt} \begin{bmatrix} \Delta \delta_1(t) \\ \Delta \delta_2(t) \\ \Delta \omega_1(t) \\ \Delta \omega(t) \end{bmatrix} = \begin{bmatrix} 0 & 0 & 1 & 0 \\ 0 & 0 & 0 & 1 \\ -\alpha_1 & \alpha_1 & 0 & 0 \\ \alpha_2 & -\alpha_2 & 0 & 0 \end{bmatrix} \bullet \begin{bmatrix} \Delta \delta_1(t) \\ \Delta \delta_2(t) \\ \Delta \omega_1(t) \\ \Delta \omega(t) \end{bmatrix} \quad (4.36)$$

where $\alpha_1 = 10.4553$ and $\alpha_2 = 11.2691$.

The eigenvalues for the plant matrix are determined to be

$$\sigma(\mathbf{A}) = \{+j4.6609, -j4.6609, 0, 0\} \quad (4.37)$$

The two complex conjugate eigenvalues correspond to a frequency of 0.7418Hz and as discussed in chapter three, this frequency is the natural frequency of the system's oscillatory mode. It is interesting to note that, even though there are two machines present in the system, there is only one oscillatory mode. This is in contrast to the infinite bus system used above in chapter three which had, after one of the machines was taken offline, a total of two machines left on the system and the resulting modes were both oscillatory – thus the system had two oscillation modes. This "extra" mode is the result of the fact that the infinite bus in the chapter-three system does, in fact, behave like a machine – it has infinite inertia but it does affect the system as though it were a circuit element with all other characteristics of a synchronous machine. These characteristics include internal voltage, synchronizing power, and a \mathbf{Y}_{bus} matrix self-admittance.

Due to the fact that there is a pair of repeated eigenvalues, the solution to the state equation (4.35) may possibly not be expressed in the form presented in equation (3.9) repeated here for convenience.

$$\mathbf{x}(t) = \langle \boldsymbol{\Psi}_1, \mathbf{x}(t_0) \rangle \cdot \boldsymbol{\Phi}_1 \cdot e^{\lambda_1 t} + \dots + \langle \boldsymbol{\Psi}_n, \mathbf{x}(t_0) \rangle \cdot \boldsymbol{\Phi}_n \cdot e^{\lambda_n t} \quad (3.9)$$

Equation 3.9 represents the solution form of the linear state equation when all of the normalized eigenvectors of the plant matrix are able to span the entire state-space. When all of the eigenvalues are distinct, a total of n normalized and linearly independent eigenvectors of the plant matrix \mathbf{A} exist and so the solution to the state equation may be expressed in the same form as (3.9). However, as it turns out in (4.36), a set of four linearly independent eigenvectors does not exist and the solution must take on a different form from that of (3.9). Specifically the solution must be a linear combination of exponents multiplied by t raised to a particular power. In this case the power is one. The theoretical details behind the solution forms may be found in [23].

The solution form for (4.35) is

$$\mathbf{x}(t) = c_1 \cdot \boldsymbol{\Phi}_1 \cdot e^{\lambda_1 t} + c_2 \cdot \boldsymbol{\Phi}_2 \cdot e^{\lambda_2 t} + c_3 \cdot \boldsymbol{\Phi}_3 \cdot e^{\lambda_3 t} + c_4 [\boldsymbol{\Phi}_3 \cdot t \cdot e^{\lambda_3 t} + \boldsymbol{\beta} \cdot e^{\lambda_3 t}] \quad (4.38)$$

In (4.38) the constants c_i are arbitrary constants that depend on the system's initial state and the vectors $\boldsymbol{\Phi}_i$ are normalized eigenvectors of the plant matrix associated with their eigenvalues, λ_i . The vector $\boldsymbol{\beta}$ is a vector used to create a fourth linearly independent solution to (4.36) as four linearly independent solutions must exist for a 4 x 4 LTI system.

The relationship between the vector $\boldsymbol{\beta}$ and the system's plant matrix, \mathbf{A} , is

$$\mathbf{A}\boldsymbol{\beta} = \boldsymbol{\Phi}_3 \quad (4.39)$$

Since \mathbf{A} is not invertible (there are one or more eigenvalues equal to zero), the vector $\boldsymbol{\beta}$ is composed of elements that have at least one free parameter.

In the case of the system represented by (4.36) there are only a total of three linearly independent eigenvectors. The linearly independent normalized eigenvectors are the first three rows of the matrix obtained from matlab's diagonalization function

$$\Phi = \begin{bmatrix} +j0.1427 & -j0.1427 & -0.7071 & 0.7071 \\ -j0.1538 & +j0.1538 & -0.7071 & 0.7071 \\ -0.6650 & -0.6650 & 0 & 0 \\ +0.7168 & +0.7168 & 0 & 0 \end{bmatrix}. \quad (4.40)$$

The vector ϕ_i in (4.38) corresponds to the i th column of this matrix of eigenvectors.

Since the third eigenvalue of \mathbf{A} is zero, the last three terms in (4.38) reduce to

$$c_3 \cdot \phi_3 + c_4 [\phi_3 \cdot t + \beta] \quad (4.41)$$

and the vector β is determined to be

$$\beta = \begin{bmatrix} b \\ -b \\ 0.7071 \\ 0.7071 \end{bmatrix} \quad (4.42)$$

where the entry b is any arbitrary real number and is the free parameter mentioned above that is due to the singularity of \mathbf{A} .

Examination of (4.40), the non-oscillatory portion of the solution to (4.36), designated, $\Delta \mathbf{x}_m(t)$, reveals the modal characteristics of the states as

$$\Delta \mathbf{x}_m(t) = \begin{bmatrix} \Delta \delta_{1m}(t) \\ \Delta \delta_{2m}(t) \\ \Delta \omega_{1m}(t) \\ \Delta \omega_{2m}(t) \end{bmatrix} = c_1 \begin{bmatrix} \sqrt{2}/2 \\ \sqrt{2}/2 \\ 0 \\ 0 \end{bmatrix} + c_2 \left(\begin{bmatrix} \sqrt{2}/2 \\ \sqrt{2}/2 \\ 0 \\ 0 \end{bmatrix} t + \begin{bmatrix} b \\ -b \\ \sqrt{2}/2 \\ \sqrt{2}/2 \end{bmatrix} \right) \quad (4.43)$$

The vectors in (4.43) show that constant values of angle deviations from nominal can exist in the system's natural response. Angle ramps can also exist which are necessarily accompanied by constant values in speed deviations. These two proceeding statements are consistent with intuition concerning a relationship between speed and angle that states that a constant speed deviation from nominal must be accompanied by ramps in machine angles.

Figure 4.7 shows the frequency waveforms for the system in figure 4.4 with a line outage followed by no reclosure. The two measurements are taken at the two line terminals. The 0.74Hz oscillation as predicted by the plant matrix eigenvalues is evident in both of the frequency waveforms. A frequency ramp of equal magnitude in both waveforms is also visible. The equal ramp magnitude is as expected per the above discussion on AC synchronism that, in summary, states that the machine speeds must be equal when not taking into account oscillatory behavior. This slight ramp in frequency is expected from the standpoint that there is an overall generation-load mismatch in the system and that this mismatch forces the system to accelerate. The measured ramp rate is about 0.000158 per second – slightly higher than the calculated ramp using the acceleration power ratio method discussed above.

From the standpoint of equation (4.43) the ramp is unexpected. This is because of the fact that the system, with the sustained generation-load mismatch, is not truly homogeneous and thus (4.43) does not describe fully the system response. System response in terms of forced and natural responses can be examined separately if the system's state vector remains close to the nominal trajectory. The nominal trajectory, as discussed above, is a path in the state-space that has a frequency ramp associated with it.

Thus the simulation results are consistent with the analysis if the q-point is considered to be a trajectory in lieu of a fixed point in the state space. Determination of the trajectory, as done in this analysis must be completed before performing the linearization and formulation of the system's linear state equation. If the linearization is to be carried out around a fixed point in the state space, the waveform in figure 4.7 should be considered to be a combination of both forced and natural response. The input into the system would be a step in acceleration power (created by the generation-load mismatch) and it would be expected, without a detailed analysis, that the machine speeds, and thus the measured frequency, would participate in a 't-to-the first power' mode. Likewise, the angles would participate in a 't-squared' mode.

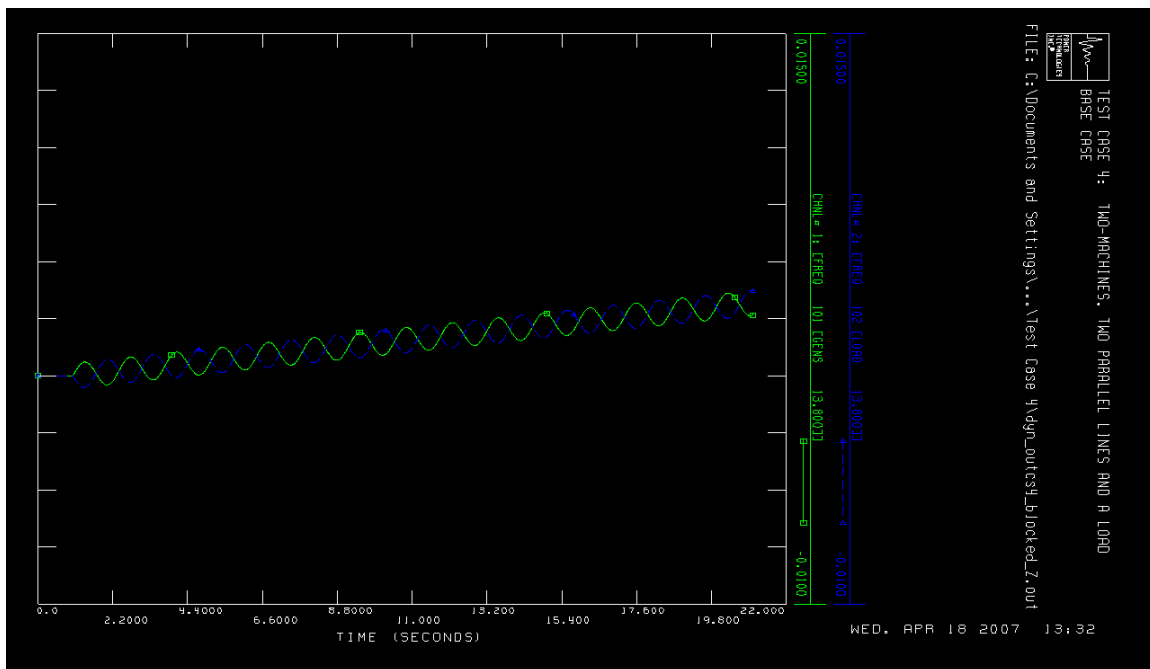


Figure 4.7: frequency waveforms for two-machine two line system following a line outage with no reclose

4.3.2 Investigation of Line Outage Followed by Reclose Action

As mentioned above, the modal characteristics of a disturbance created by a line outage not followed by reclose action should be expected to be different from a line outage followed by reclose. The reasons for the differences are 1) different admittance matrix for each scenario; 2) different q-point for each scenario; 3) difference in generation-load mismatch.

In formulating the state model for the system in figure 4.4, determining the admittance matrix and q-point for a line outage followed by reclose are trivial tasks as the q-point will be considered to be the initial operating point. Due to the fact that both of the machines in the system must either accelerate or decelerate during the 5-to-10 cycles of line outage, the machine angles must either advance or retard respectively – it is this deviation in angle from q-point which will provide modal excitation. Determination of the amount of deviation for each machine need not be determined as far as plant matrix formulation is concerned. It should be expected that the generation-load mismatch for each machine should be sustained and constant during the 5-to-10 cycle outage. This is an approximation and may be considered adequate due to the fact that 5-to-10 electrical cycles is a negligible amount of time compared to any dynamic electromechanical activity that will result from the line outage. It is an approximation, however, due to the fact that machine electrical power outputs must necessarily change as the angles deviate substantially from their angles at the time of the line outage. In this trivial case of a two-machine two-line system, the exact amount of excitation need not be determined as the oscillation frequency alone will be enough to distinguish in between a line outage followed by reclose versus no reclose.

The first step in formulating the state model will be to construct the admittance matrix for the system.

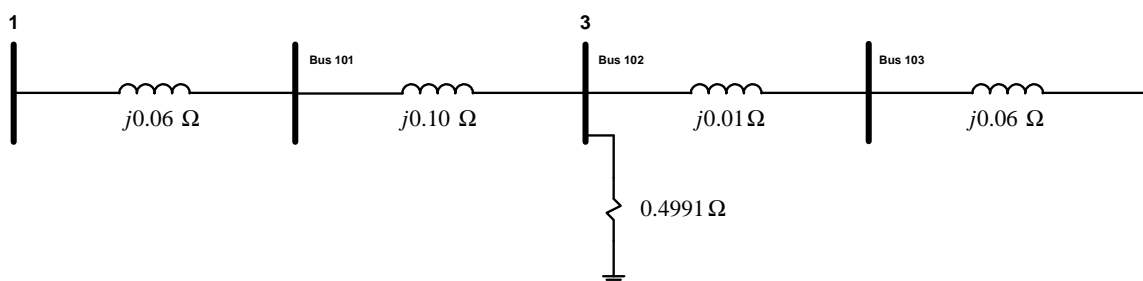


Figure 4.8: impedance diagram of system in figure 4.4 – line outage followed by reclose action

The impedance diagram shown in figure 4.8 is identical to the diagram in figure 4.5 (line outage with no reclose) except for the impedance of the interface in between the two machines. In figure 4.5 it was $j0.2 \Omega$ due to the line being out of service permanently after the outage.

As in section 4.3.1 the diagram in figure 4.8 may be reduced as follows in figure 4.9 and converted into an admittance diagram.

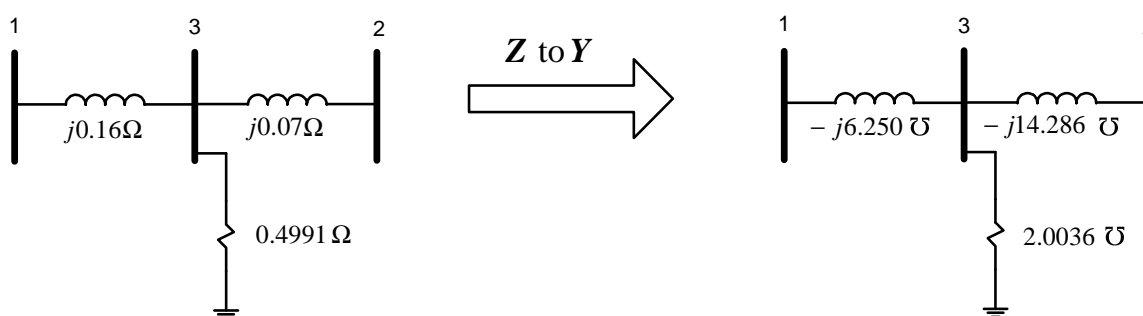


Figure 4.9: reduced impedance and admittance diagrams for system in figure 4.8

The \mathbf{Y}_{bus} for the admittance diagram in figure 4.9 is simply

$$\mathbf{Y}_{bus} = \left[\begin{array}{cc|c} -j6.250 & 0 & j6.250 \\ 0 & -j14.286 & j14.286 \\ \hline j6.250 & j14.286 & 2.0036 - j20.536 \end{array} \right], \quad (4.44)$$

and reducing to a two-port matrix via Kron reduction gives

$$\mathbf{Y}_{bus}^r = \begin{bmatrix} 0.184 - j4.366 & 0.420 + j4.307 \\ 0.420 + j4.307 & 0.961 - j4.442 \end{bmatrix}. \quad (4.45)$$

Comparison of (4.45) with (4.26), the \mathbf{Y}_{bus}^r matrix for the line outage followed by no reclosure verifies the intuitive conclusion that the two machines in the system are more tightly coupled together via the increased admittance in between the two machines. This increased admittance is mainly characterized by the quantity B_{12} in the \mathbf{Y}_{bus}^r matrix.

With $\delta_{12_0} = 10.43^\circ$, all of the quantities needed to compute the coefficients in equation (4.28) are known. The result of substituting (4.28) into (4.27) for each machine yields the state equation in $\Delta\omega_i(t)$. The results are

$$\dot{\Delta\omega}_1(t) = -15.9371\Delta\delta_1(t) + 15.9371\Delta\delta_2(t) \quad (4.46)$$

$$\dot{\Delta\omega}_2(t) = -16.5179\Delta\delta_1(t) + 16.5179\Delta\delta_2(t) \quad (4.47)$$

And finally the vector-matrix differential equation of (4.33) through (4.35) is

$$\frac{d}{dt} \begin{bmatrix} \Delta\delta_1(t) \\ \Delta\delta_2(t) \\ \Delta\omega_1(t) \\ \Delta\omega_2(t) \end{bmatrix} = \begin{bmatrix} 0 & 0 & 1 & 0 \\ 0 & 0 & 0 & 1 \\ -\alpha_1 & \alpha_1 & 0 & 0 \\ \alpha_2 & -\alpha_2 & 0 & 0 \end{bmatrix} \bullet \begin{bmatrix} \Delta\delta_1(t) \\ \Delta\delta_2(t) \\ \Delta\omega_1(t) \\ \Delta\omega_2(t) \end{bmatrix}, \quad (4.48)$$

where $\alpha_1 = 15.9371$ and $\alpha_2 = 16.5179$.

The eigenvalues for the plant matrix are determined to be

$$\sigma(\mathbf{A}) = \{+j5.6971, -j5.6971, 0, 0\} \quad (4.49)$$

The eigenvectors are the columns of

$$\Phi = \begin{bmatrix} +j0.1200 & -j0.1200 & -0.7071 & 0.7071 \\ -j0.1244 & +j0.1244 & -0.7071 & 0.7071 \\ -0.6838 & -0.6838 & 0 & 0 \\ +0.7088 & +0.7088 & 0 & 0 \end{bmatrix} \quad (4.50)$$

The two complex conjugate eigenvalues correspond to a natural frequency of 0.9067 Hz. This natural frequency is verified via simulation as measured oscillations are 0.907 Hz – see figure 4.10. The measured mode shape does not conform to the first two columns in the matrix of equation (4.50).

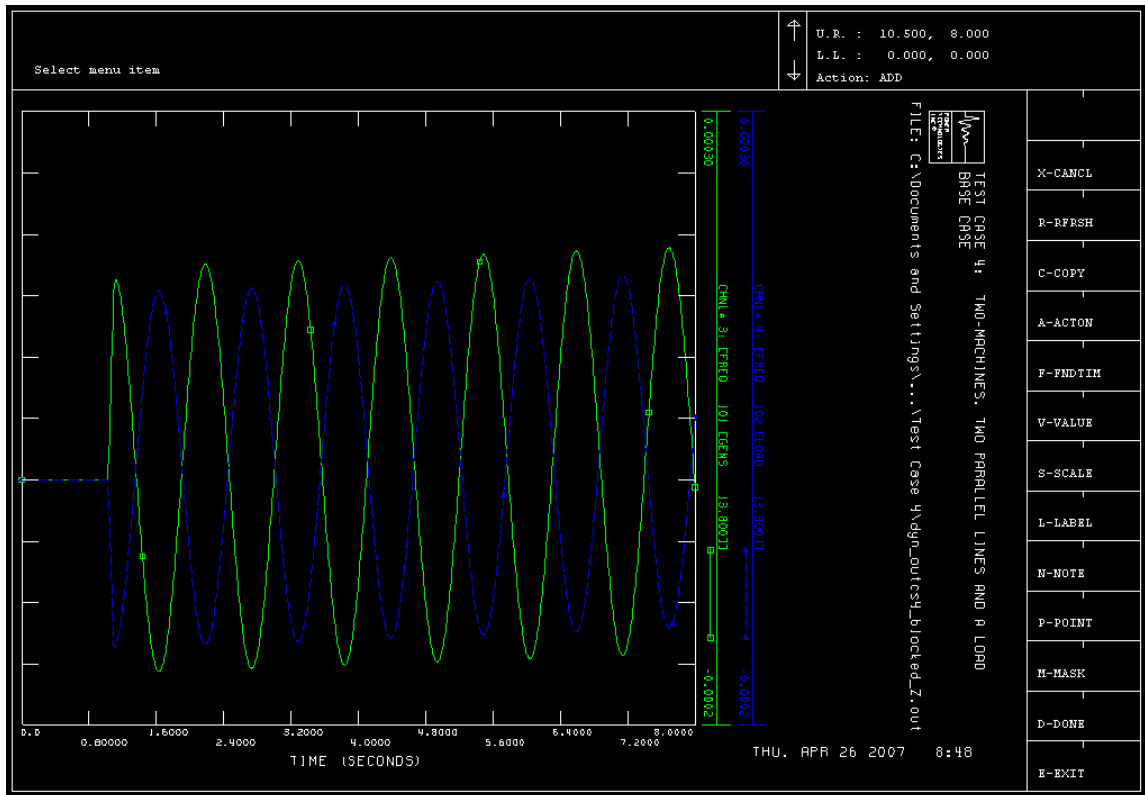


Figure 4.10: frequency waveforms for two-machine two line system following a line outage with successful reclose

The difference in apparent mode shape is due to the fact that there is a larger impedance in between machine two's internal voltage and it's frequency measurement compared to

the impedance in between machine one's internal voltage and it's measurement. Thus, the measurement is not actually a true mode shape.

Notice that during the time of line outage both of the machines undergo an acceleration that is apparently constant – machine 1 has a positive acceleration, machine 2 has negative. This preceding statement assumes that the machine speeds are in direct proportion to the measured frequency at their respective buses. This roughly constant acceleration during the time of line outage is to be expected.

Figure 4.11 zooms in on the line outage time to show that both machines do have roughly – but not exactly – a constant change in speed during the outage.

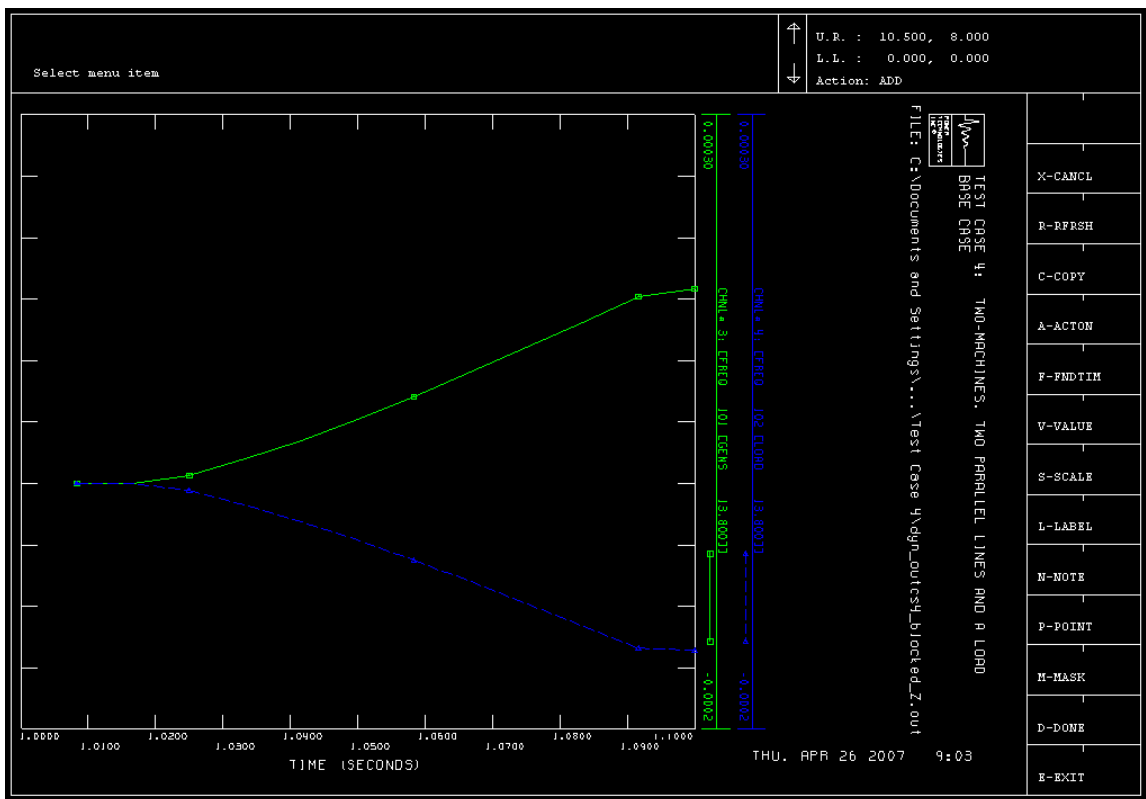


Figure 4.11: frequency waveforms for two-machine two line system following a line outage with successful reclose – zoomed in on line outage before reclose

The reason for the speed change is the same as the reason that the speed changes in the line outage that is not followed by reclose action – the electrical power transfer of each machine is instantly shifted to a quantity that is different from the mechanical input power – thus creating a speed change. The change in speed is, of course, arrested when the line is brought back into service. It would be expected that the machine accelerations would actually be reversed by the line being put back into service – such is not the case due to voltage sag at the load bus. The voltage sag at the load bus forces the load to absorb less power and thus machine 1 will not decelerate, even though its acceleration is arrested somewhat.

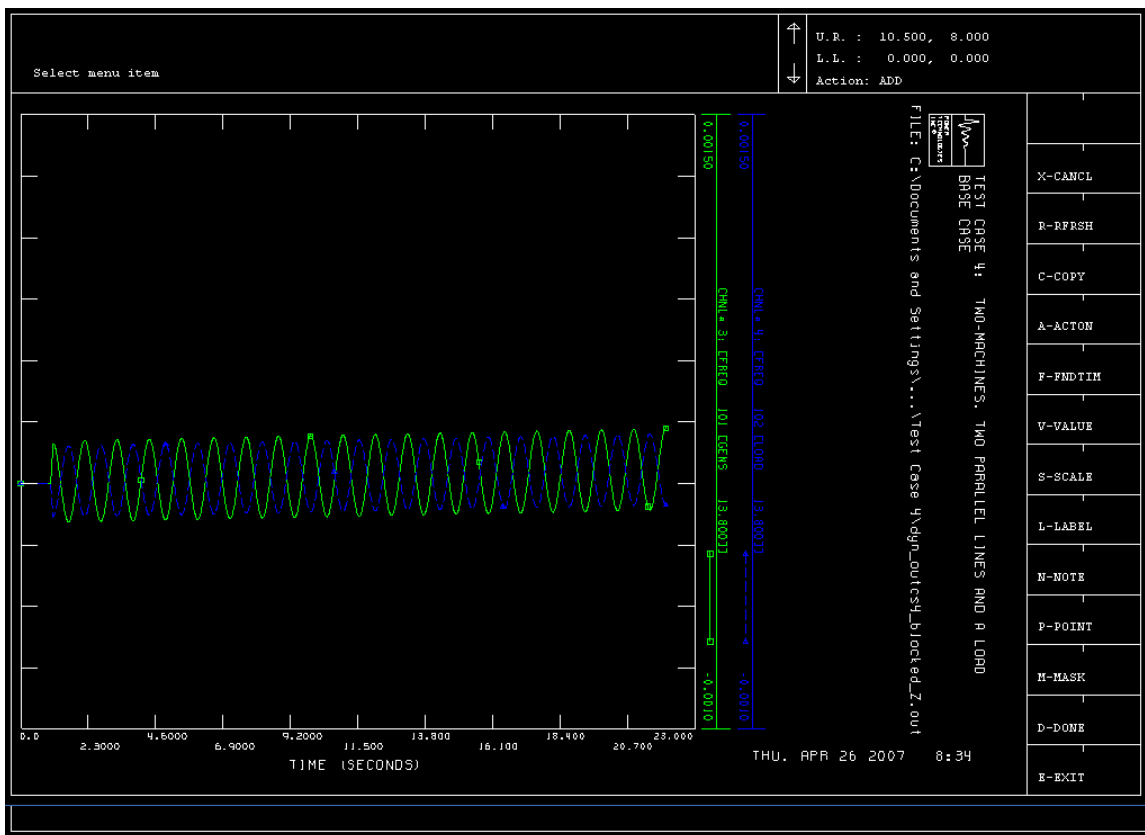


Figure 4.12: frequency waveforms for two-machine two-line system following a line outage with successful reclose – zoomed out to show system acceleration following reclose

There is a slight overall system generation-load mismatch visible in figure 4.10. The waveforms shown in figure 4.12 show the overall system mismatch more clearly. The reason for the slight mismatch is simply that during the angle swings of the two machines, the load voltage is decreased thus creating an average voltage that is lower than the voltage at steady state.

4.4 Speed Governor Modeling

Two different systems will be used derive the state model of a power system that has speed governors installed on one or more of the generators. The first system to be explored is the single-machine infinite-bus. A governing differential equation for the single machine system will be developed which will reveal damping effects created by the use of a speed governor. Intuitively one might understand that the use of a speed governor should, in fact, damp electromechanical oscillations due to the fact that speed governors tend to increase a machine's acceleration power when machine speed falls below synchronous speed and vice versa. The governor performs this change in acceleration power by directly increasing or decreasing the mechanical power injected into the machine via steam valve position adjustment. Governor action is normally considered to be slow compared to the dynamics associated with electromechanical dynamics [4], [19] and many engineers associate a time delay with governor action. It should be considered, however, that any speed governor is not equipped to operate with a time delay. Instead a governor has a time constant – type response. Thus governors do indeed react to machine speed changes instantly. Time constants of one-half second are typical and thus may be expected to take about two seconds for complete action to take place in response to, say, a step in machine speed. Of course, a step in machine speed

cannot take place due to machine inertia. Thus the slow reaction of the machine speed to, say, changes in electrical power drawn from the machine will tend to make governor action appear slow. The reason for pointing this out is to give the reader an understanding that speed governors should be taken into account when studying electromechanical activity which can be on the order of one hertz or lower as demonstrated in previous chapters. Thus speed governors that have time constants on the order of one-half of a second may be expected to affect oscillation damping.

Proof of electromechanical damping will be presented here by deriving a governing second order differential equation in machine angle which will contain a non-zero coefficient for the first order derivative. The existence of this non-zero coefficient does necessarily prove that positive damping exists. It should be recalled that the governing differential equations developed in previous sections do not have non-zero first order derivative coefficients.

It turns out that the presence of a speed governor on a generator necessitates the addition of at least one state variable for the machine that it is connected to. Use of s-domain function block diagrams will be used to determine the new state(s). Addition of a new state does mean that the state-space of a multimachine system must be equal to $2n + k$, where k is equal to the number of machines which have speed governors. As in chapter three, the plant matrix developed for the SMIB system will provide a prototype of the plant matrix for multimachine systems.

The second system to be used is the same two-machine system used in section 4.3 with a governor installed on machine number two. The plant matrix for this system will be developed using the same differential equations per machine as used on the SMIB

system. It is interesting to point out the differences in between this new plant matrix for the two-machine system – the main one being the exclusion of double-zero-eigenvalue modes. The two-machine system with a governor installed will be shown to have only a single zero eigenvalue. This lack of double-zero eigenvalues necessarily means that the system speed cannot deviate from q-point speed. This is consistent with physical interpretation as any speed governors in the system will arrest frequency changes and thus establish a steady frequency after all transients have died out. It is this steady frequency which is used as the system q-point frequency. An analogy of this two-machine system with speed governor installed will be drawn with the "position" model of a force-mass-friction system. The non-oscillatory eigenproperties of both the power system and the force mass systems are qualitatively identical.

The two-machine system will be analyzed quantitatively by forming the system plant matrix and computing it's eigenvalues. The system, as in section 4.3, will be excited by line outage. The natural oscillation frequency and damping ratio for the oscillatory mode that is computed from the eigenanalysis will be compared with measured values in oscillation frequency. Previously measured values of oscillation frequency were obtained using the Fourier transform. This transform is suitable in the sense that it is actually frequency *content* of the waveform that identifies the excited modes and thus the disturbance. In the work done in this present chapter and in following chapters, a different technique, which is more suitable for identifying the modes and thus the frequency content of the waveform, will be used. This technique is formally known as a Matrix Pencil technique [25]. The decomposition performed by matrix pencil is able to identify both oscillation frequencies and damping for each mode

in a similar way to the decomposition that results from a Laplace transform. The matrix pencil literally identifies poles (eigenvalues) and residues (complex amplitudes) of a signal by decomposing the signal into a collection of exponential functions. These functions, in general, have both pure real and complex arguments. Thus the matrix pencil may be used to identify non-oscillatory modes associated with pure real eigenvalues as well as oscillatory modes which are associated with complex eigenvalues. In addition, the damping ratio for each oscillatory mode is determined. Since the Matrix pencil has the ability to compute residues, thus determining both phase and magnitude of each oscillatory component, it is able to provide a full complement of a signal's spectral information.

It should be pointed out that, in terms of MW capacity, most of the machines in a power system do not have speed governors in service. This is due to both technical and economic reasons. Most of the MW capacity on a typical power system is composed of so-called base-load units. Base load units are operated at rated power and thus have no room to increase power output to provide system speed regulation. For the most part speed regulation is provided by smaller units, which, due to their lack of efficiency, are ran at power outputs that are lower than rated load. Also, it turns out that base loaders are not able to change power output as quickly as smaller inefficient units. Nuclear units are a prime example – it may take an entire day for a nuclear unit to ramp it's output power from zero to full power. Gas units, on the other hand can provide adequate speed regulation by ramping output power in a matter of seconds.

4.4.1 Single-Machine Infinite Bus System

The diagram for the system used previously in section 4.1 is repeated below for reference. A state model for this single-machine infinite-bus system will be developed to provide a prototype for multimachine systems and to present some of the details behind governor operation and its relationship to system modal characteristics. The primary deficiency using the SMIB system for concept presentation is that the infinite-bus forces the plant matrix to be non-singular and thus any rigid body activity as discussed in section 4.3 cannot exist. Nonetheless, this system does present the basic modal features that a simple system will exhibit when a speed governor is in use.

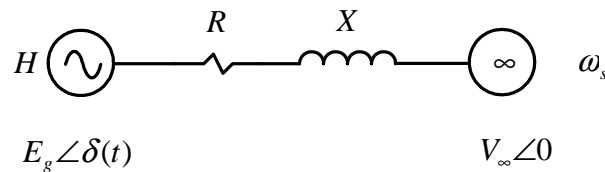


Figure 4.2: SMIB system

Before developing any differential equations for this system, a pair of s-domain function blocks are presented in figure 4.13. The two blocks represent the effects of generator mass and the synchronizing power coefficient. These two function blocks will be used in conjunction with a governor block to determine what the system states should be for the SMIB system. It has already been established that machine speed and angle deviation are two of the states for the system. Angle deviation is built in to the

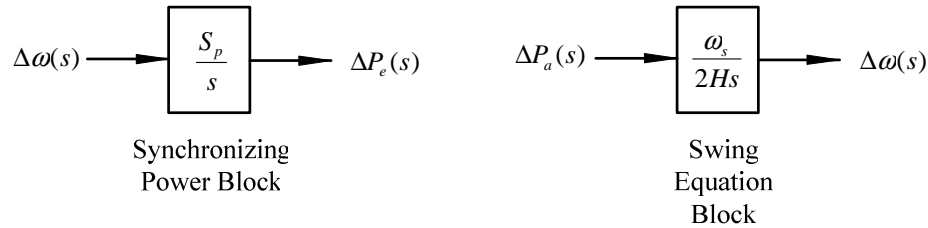


Figure 4.13: function block diagrams for SMIB system

synchronizing power block as the machine speed is integrated in the block. As previously stated, $\Delta P_e = S_p * \Delta \delta$, thus the synchronizing power block is consistent with this relationship. Likewise, the swing equation block is consistent with the swing equation as the second derivative of the angle deviation is directly proportional to the acceleration power.

A third block diagram, presented in figure 4.14, represents the governor model used by PSS/E, model TGOV1. This is a steam governor model and it includes a speed droop parameter, R , and a governor time constant, τ . The droop parameter determines the steady-state difference in frequency for a given change in electrical power. This relationship is not obvious from the diagram and the reader is referred to [4], [24] for details on the mechanisms behind this relationship. The one-over ω_s block is necessary to convert the machine speed which is calculated in radians per second in the swing equation to per unit speed which is specified by PSS/E for all machine quantities. The droop parameter also is specified in per unit speed change per per-unit power change on the machine's base MVA. And finally the first order lag block represents the actual valve assembly that controls steam flow. The output of the entire function block diagram may be interpreted as either mechanical power injected into the machine or valve position.

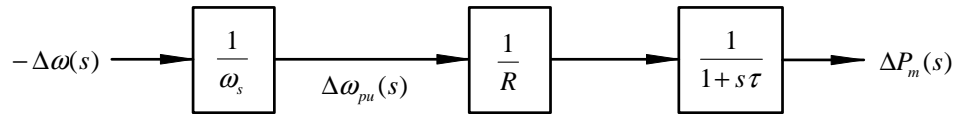


Figure 4.14: function block diagram for governor TGOV1

The system shown in figure 4.14 does not include a model of turbine reheat characteristics. The typical model used for the reheat characteristic is a lead-lag block with a time constant on the order of 5 to 10 seconds. In cases where a generating unit that has its entire steam system subject to reheat, the machine will react slowly enough to electromechanical swings so as to exclude them from the model used to predict electromechanical behavior [26]. Additionally, a generating unit with a reheat cycle will be more efficient and thus more likely to be a base loader, thus non-speed regulated. In special cases where the reheat cycle effects need to be included in the study, a lead-lag block should be inserted in series with the string of blocks in figure 4.14 either immediately in front of or behind the first order lag block.

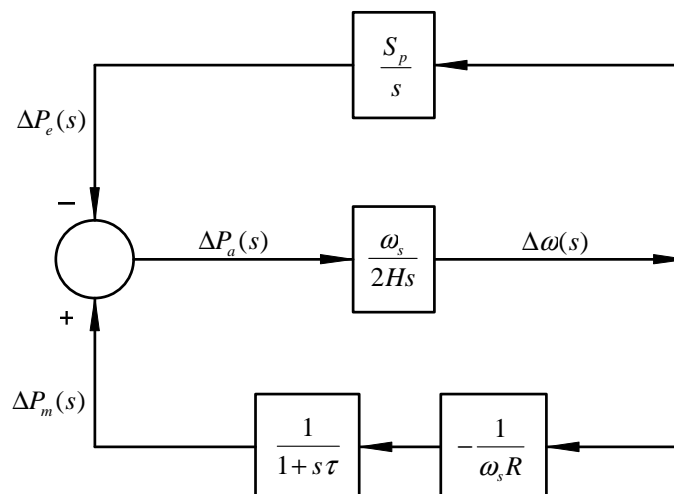


Figure 4.15: function block diagram of entire electromechanical system for SMIB

Figure 4.15 shows how the function blocks of figures 4.13 and 4.14 are to be arranged together to analyze the system. It is interesting to note that there are no inputs into this system. Excitation is not provided by an input per se, but instead is provided by non-zero initial conditions. As in previous derivations in this chapter, the initial conditions must necessarily be non-zero *deviations* in at least one of the system states. The only system state that is visible in the diagram of figure 4.15 is the machine's speed deviation. At present, the only other known state is the machine's angle deviation. There is one other state in the system that is not known. A method of determining a convenient variable for the remaining state is to decompose the entire system in 4.15 into a network of multipliers and integrators. After this step is performed the states may be chosen as the variables that are outputs of the integrators. The system may be decomposed as shown in figure 4.16.

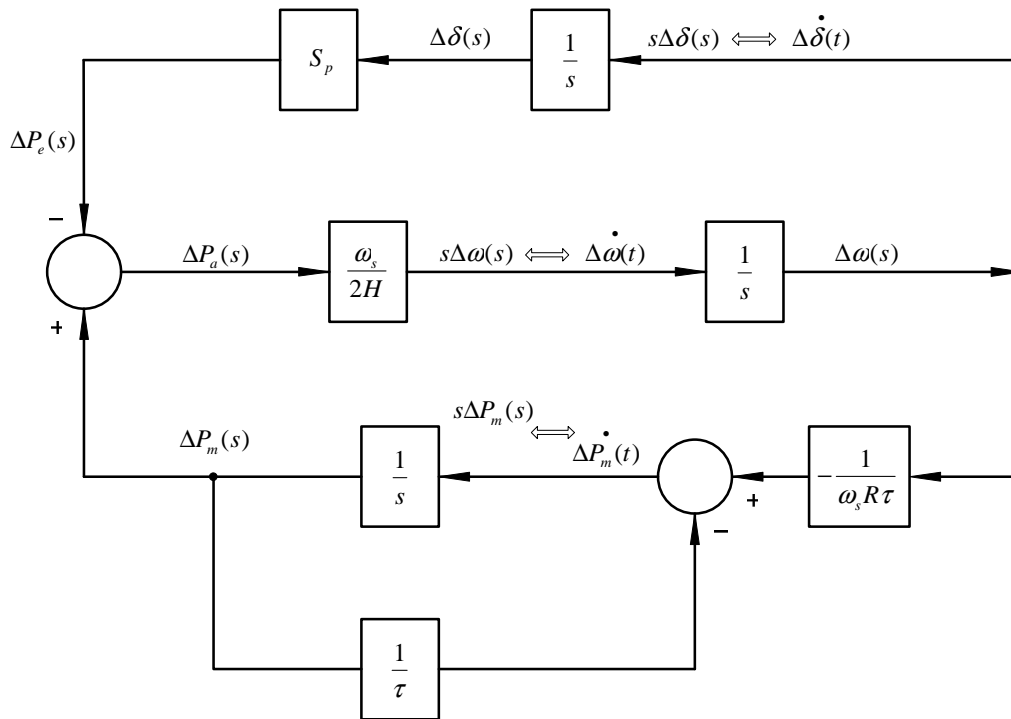


Figure 4.16: function block diagram of entire electromechanical system for SMIB decomposed into a collection of integrators and multipliers

Two of the states, $\Delta\delta$ and $\Delta\omega$, appear as integrator outputs as expected. The third state, ΔP_m , the deviation in mechanical power injected, may create some reservation intuitively as power is usually associated with a flow variable as opposed to an energy-storage variable. However, considering that mechanical power is directly related to torque, which has the same units of energy, N.m, should alleviate these reservations. Further, both the mechanical and electrical power in the machine's swing equation do actually represent mechanical and magnetically developed torque in a per unit sense.

The first derivatives with respect to time of each of the three state variables may be expressed as linear combinations of each of the states.

$$\begin{aligned}\Delta\dot{\delta}(t) &= \Delta\omega(t) \\ \Delta\dot{\omega}(t) &= \frac{\omega_s}{2H}\Delta P_m(t) - \frac{\omega_s S_p}{2H}\Delta\delta(t) \\ \Delta\dot{P}_m(t) &= -\frac{1}{\omega_s R\tau}\Delta\omega(t) - \frac{1}{\tau}\Delta P_m(t)\end{aligned}\tag{4.51}$$

And in vector-matrix form

$$\begin{bmatrix} \Delta\dot{\delta}(t) \\ \Delta\dot{\omega}(t) \\ \Delta\dot{P}_m(t) \end{bmatrix} = \begin{bmatrix} 0 & 1 & 0 \\ -\frac{\omega_s S_p}{2H} & 0 & \frac{\omega_s}{2H} \\ 0 & -\frac{1}{\omega_s R\tau} & -\frac{1}{\tau} \end{bmatrix} \bullet \begin{bmatrix} \Delta\delta(t) \\ \Delta\omega(t) \\ \Delta P_m(t) \end{bmatrix}\tag{4.52}$$

The form of the plant matrix does not directly yield damping information. In order to prove that the presence of the governor does provide damping, a governing differential equation in $\Delta\delta$ is developed by combining the s-domain relationships that govern all three state variables. The first of these equations is the s-domain relationship between $\Delta\delta$ and the acceleration power.

$$\frac{2H}{\omega_s} s^2 \Delta\delta(s) = \Delta P_m(s) - \Delta P_e(s) \quad (4.53)$$

and the remaining two equations which are transfer function representations of the two different components of acceleration power are

$$\Delta P_m(s) = -\frac{1}{\omega_s R} \left[\frac{1}{1+s\tau} \right] \Delta\omega(s) \quad (4.54)$$

$$\Delta P_e(s) = S_p \Delta\delta(s) \quad (4.55)$$

Substituting (4.54) and (4.55) into (4.53) yields

$$\frac{2H}{\omega_s} s^2 \Delta\delta(s) = -\frac{1}{\omega_s R} \left[\frac{1}{1+s\tau} \right] \Delta\omega(s) - S_p \Delta\delta(s) \quad (4.56)$$

The following two values are substituted to simplify the constants

$$K_1 = \frac{2H}{\omega_s} \quad \text{and} \quad K_2 = \frac{1}{\omega_s R} \quad (4.57)$$

And substituting (4.57) into (4.56) yields

$$K_1 s^2 \Delta\delta(s) = \frac{-K_2}{1+s\tau} s \Delta\delta(s) - S_p \Delta\delta(s) \quad (4.58)$$

Multiplying through by $1+s\tau$ yields

$$K_1 \tau s^3 \Delta\delta(s) + K_1 s^2 \Delta\delta(s) + (K_2 + \tau S_p) s \Delta\delta(s) + S_p \Delta\delta(s) = 0 \quad (4.59)$$

and dividing through by $K_1 \tau$ gives

$$s^3 \Delta\delta(s) + \frac{1}{\tau} s^2 \Delta\delta(s) + \frac{(K_2 + \tau S_p)}{K_1 \tau} s \Delta\delta(s) + \frac{S_p}{K_1 \tau} \Delta\delta(s) = 0 \quad (4.60)$$

It may be shown that if the product of the first and second order coefficients is identically equal to the zero-order coefficient that the system described by 4.60 has a pole pair on the imaginary axis. In the case where this special coefficient condition does hold the oscillatory mode associated with these two poles is completely undamped. If the

condition does not hold, the system is necessarily damped – however the damping may either be positive or negative. The coefficient condition for (4.60) is stated as

$$\frac{(K_2 + \tau S_p)}{K_1 \tau^2} = \frac{S_p}{K_1 \tau} \quad \text{or} \quad \frac{K_2}{\tau} + S_p = S_p \quad (4.61)$$

and substituting the value for K_2 back into (4.61) gives the relationship

$$\frac{1}{\tau R \omega_s} + S_p = S_p \quad (4.62)$$

Equation (4.62) holds true only if either τ or R are infinite. Either of these two conditions corresponds to no governor action at all. Thus equation (4.62) must never hold true if a governor is installed on the SMIB system and further the governor must provide damping.

4.4.2 Two-Machine System

The two-machine two-line system used in section 4.3 will be used to investigate speed governor effects on a system with no infinite bus. Excitation will be provided by a line outage followed by no reclose action. The machine connected to bus 103 will have a TGOV1 governor installed on it with a speed droop of 5 percent – corresponding to $R = 0.05$ for the initial tests. The purpose of varying these quantities is to show their effect on oscillation damping ratio. The time constant will be varied over the “typical” range of PSSE values for the TGOV1 time constant. “Typical” here refers to the range of values that PSSE uses to check for errors in dynamic read files. The range is 0.05 to 0.5 seconds.

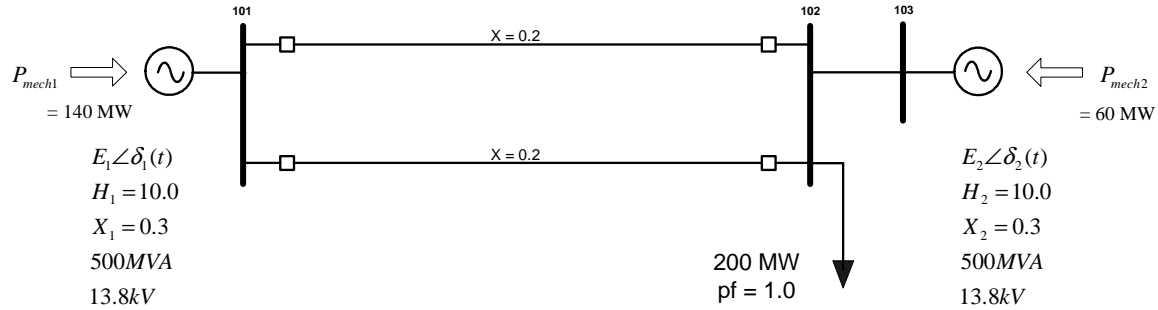


Figure 4.4: unregulated system without infinite bus

Figure 4.4 is repeated above for reference. In order to determine the system's q-point, it is necessary to determine what the steady-state power output of each machine will be after the line is tripped. Due to the fact that the load voltage must drop following the line outage and consequently must draw less power, the system must accelerate forcing the speed governor to decrease the power output on machine number two. This governor action will force the system to steady out at a new frequency according to the relationship

$$\Delta\omega = -\frac{\Delta P_L}{\frac{1}{R} + D} \quad (4.63)$$

where $\Delta\omega$ is per unit speed deviation, ΔP_L is the change in load power, R is the governor's speed droop and D is the load's frequency sensitivity [24]. Load frequency sensitivity will not be considered here as typical worst-case values for load sensitivity will be around two percent per percent change in frequency. To put load frequency sensitivity into perspective, consider that a 60 mHz change in frequency on a 60 Hz system is a 0.1% change in frequency. Sixty millihertz is generally considered a large deviation as far as oscillations are concerned, even in smaller interconnections. This 60 mHz change in frequency would correspond to a 0.2% change in load power – for all

practical purposes, negligible. Thus the neglect of load frequency sensitivity is justified. Examples associated with load frequency sensitivity are discussed in the previous section, 4.3.

Using the decrease in power drawn by the load calculated in section 4.3 as an estimate will yield an approximate speed deviation per equation 4.63. For line outages it will be expected that interconnection power demand changes will be small and thus should not affect synchronizing power coefficients substantially. For this present analysis, however it will be taken into account to demonstrate the precision that may be obtained using the electromechanical state model.

In calculating the synchronizing power coefficients for the system, the same transfer admittances as were used in section 4.3.1 must also be used here. They may be summarized as follows

$$\begin{aligned} B_{12} = B_{21} &= 2.994 \\ G_{12} = G_{21} &= 0.331 \end{aligned} \tag{4.64}$$

In order to calculate the steady-state angle difference in between the two machines, a calculated voltage drop at the load bus may be used in conjunction with the power angle equation as applied to each of the machines. This is a different procedure from the one used in section 4.3 where there was no governor and the system was subjected to a sustained generation-load mismatch. In this present case where there is a governor installed on machine number two, there is no generation-load mismatch and the power decrease on machine two due to governor action is approximated by the same mismatch power as determined in section 4.3. It is expected that the mismatch in power that would exist in the absence of the speed governor will be matched by the presence of the speed governor. This type of approximation will be superseded by a more elaborate method

developed in chapter 5 for a larger system. For this small system, this type of approximation suffices as will be demonstrated via comparison of simulation result with calculated values. Thus the system in steady state is described by the diagram in figure 4.17.

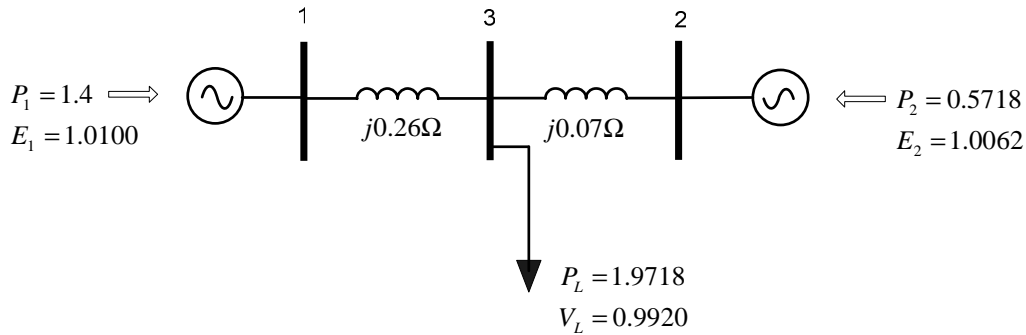


Figure 4.17: regulated system in steady state

The voltage at the load bus, bus number 3, may be approximated by using the relationship $P = \frac{V^2}{R}$ and thus may be determined to be 0.9921 pu. Using the power angle equation to solve for the angles as

$$\frac{E_1 V_L}{X_{1L}} \sin \delta_1 = 1.400 \text{ pu} \quad \text{and} \quad \frac{E_2 V_L}{X_{2L}} \sin \delta_2 = 0.5718 \text{ pu}$$

where the angle of the load bus is zero degrees. The difference between the two angles will be used to determine the synchronizing power coefficients, S_{p12} and S_{p21} . The solution is $\delta_{12_0} = 19.004^\circ$. Thus the synchronizing power coefficients may be calculated as

$$\begin{aligned} S_{p12} &= E_1 E_2 [B_{12} \cos \delta_{12_0} - G_{12} \sin \delta_{12_0}] = 2.7673 \\ S_{p21} &= E_2 E_1 [B_{21} \cos \delta_{21_0} - G_{21} \sin \delta_{21_0}] = 2.9863 \end{aligned} \quad (4.65)$$

and so the α_i constants that will be entered into the plant matrix will be

$$\begin{aligned}\alpha_1 &= \frac{\omega_s S_{p12}}{2H_1} = 10.4327 \\ \alpha_2 &= \frac{\omega_s S_{p21}}{2H_2} = 11.2587\end{aligned}\tag{4.66}$$

All of the differential equations for this multimachine system may be formulated as was done in equation (4.51) except that the unregulated machine speed's rate function will not depend on mechanical power. This is due to the fact that the governor directly affects machine two's speed only. Any speed governor's effect must not be coupled to any machine except it's own in the differential equation formulation. The same statements hold true concerning the mechanical power's rate function – it is only dependent upon it's own machine's speed and not any other machine speeds in the system. Looking forward to multiple governor systems, it may then be expected that the presence of multiple governors in a system will result in a pair of diagonal matrices that are submatrices of the plant matrix. For example in equation (4.52), the terms $-\frac{1}{\omega_s R \tau}$ and $-\frac{\omega_s}{2H}$ should be expected to correspond to diagonal matrices with the corresponding i th machine and governor inertias, speed droops, and time constants placed on the diagonals.

In this two-machine single governor case the differential equations will take on the form

$$\begin{aligned}
\Delta \dot{\delta}_1(t) &= \Delta \omega_1(t) \\
\Delta \dot{\delta}_2(t) &= \Delta \omega_2(t) \\
\Delta \dot{\omega}_1(t) &= -\alpha_1 \Delta \delta_1(t) + \alpha_2 \Delta \delta_2(t) \\
\Delta \dot{\omega}_2(t) &= \alpha_1 \Delta \delta_1(t) - \alpha_2 \Delta \delta_2(t) + \frac{\omega_s}{2H_2} \Delta P_m(t) \\
\Delta \dot{P}_{m2}(t) &= -\frac{1}{\omega_s R_2 \tau_2} \Delta \omega_2(t) - \frac{1}{\tau_2} \Delta P_{m2}(t)
\end{aligned} \tag{4.67}$$

The speed droop in the mechanical power's rate equation must be specified on the electrical MVA base and not on the machine's base. The equation set of (4.67) may be expressed in vector-matrix format as

$$\begin{bmatrix} \Delta \dot{\delta}_1(t) \\ \Delta \dot{\delta}_2(t) \\ \Delta \dot{\omega}_1(t) \\ \Delta \dot{\omega}_2(t) \\ \Delta \dot{P}_{m2}(t) \end{bmatrix} = \begin{bmatrix} 0 & 0 & 1 & 0 & 0 \\ 0 & 0 & 0 & 1 & 0 \\ -\alpha_1 & \alpha_1 & 0 & 0 & 0 \\ \alpha_2 & -\alpha_2 & 0 & 0 & \frac{\omega_s}{2H_2} \\ 0 & 0 & 0 & -\frac{1}{\omega_s R_2 \tau_2} & -\frac{1}{\tau_2} \end{bmatrix} \bullet \begin{bmatrix} \Delta \delta_1(t) \\ \Delta \delta_2(t) \\ \Delta \omega_1(t) \\ \Delta \omega_2(t) \\ \Delta P_{m2}(t) \end{bmatrix} \tag{4.68}$$

The first test to run on this system will be with a time constant, τ_2 , equal to 0.05 seconds. The corresponding plant matrix is then

$$\mathbf{A} = \begin{bmatrix} 0 & 0 & 1 & 0 & 0 \\ 0 & 0 & 0 & 1 & 0 \\ -10.4327 & 10.4327 & 0 & 0 & 0 \\ 11.2587 & -11.2587 & 0 & 0 & 3.77 \\ 0 & 0 & 0 & -5.3050 & -20.0 \end{bmatrix} \tag{4.69}$$

The eigenvalues of \mathbf{A} are

$$\sigma(\mathbf{A}) = \{0, -0.4993, -18.9722, -0.2617 \pm j4.6852, \} \tag{4.70}$$

and the associated eigenvectors are (listed in order of the values in (4.70))

$$\begin{bmatrix} 0.7071 & -0.6228 & 0.0003 & -0.0359 - j0.1314 & -0.0359 + j0.1314 \\ 0.7071 & -0.6376 & 0.0100 & 0.0085 + j0.1526 & 0.0085 - j0.1526 \\ 0.0000 & 0.3110 & -0.0053 & 0.6249 - j0.1339 & 0.6249 + j0.1339 \\ 0.0000 & 0.3184 & -0.1893 & -0.7173 & -0.7173 \\ 0.0000 & -0.0866 & 0.9819 & 0.1825 - j0.0433 & 0.1825 + j0.0433 \end{bmatrix} \quad (4.71)$$

The zero eigenvalue and its associated eigenvector may be associated with a zero-frequency mode, in other words a DC mode. As might be expected, only the machine angles may participate in this rigid-body mode. A rigid-body mode for a power system with at least one speed regulator may be compared to a single-body $F = ma + kv$ system where k is the friction coefficient of the mass in it's environment and v is the mass' velocity. This is, of course, a second order system when employing a position model as opposed to a velocity model. The governing differential equation is

$$f(t) = m \frac{d^2 x(t)}{dt^2} + k_v \frac{dx(t)}{dt} \quad (4.72)$$

However, it has a single pole located at the origin and another pole located at $-\frac{k_v}{m}$.

Excitation of this system provided by initial conditions of $\dot{x}(0) = \frac{1}{m}$ and $x(0) = 0$ will

yield the following responses in position, $x(t)$ and velocity, $v(t)$.

$$x(t) = \frac{1}{k_v} \left[1 - e^{-\frac{k_v}{m}t} \right] u(t) \quad (4.73)$$

$$v(t) = \dot{x}(t) = \frac{1}{m} \left[e^{-\frac{k_v}{m}t} \right] u(t) \quad (4.74)$$

As seen by this pair of equations, the position has both a DC term and an exponential term with a pure real argument. These two terms correspond to a zero-frequency mode

and a pure-real eigenvalue mode. The velocity, however, contains no DC term which is to be expected in the system's natural response. The first column eigenvector in (4.71) reveals the same characteristic for the two-machine power system with a single governor installed. This may be contrasted with equation (4.43), the natural response of the unregulated two-machine system which has a double zero eigenvalue. In (4.43) it may be seen that the speed variables can participate in a zero-frequency mode. The absence of a speed governor allows this type of behavior. The blocked system, as stated before, may be compared to an $F = ma$ system, one with no friction component in the force.

The second column vector in (4.71) is the eigenvector that may be associated with the decay in state variables due to synchronizing power – in other words, a mode driven by purely electrical forces, forces that tend to bring the machine speeds and angles back to the q-point following a disturbance that causes a deviation from the q-point. The lack of mechanical response is seen by the smaller magnitude of the last element in this eigenvector. The third column vector in (4.71) is the eigenvector that may be associated with almost purely mechanical activity and may be expected to be dominated by the governor's time constant as seen by the eigenvalue associated with this mode. Notice that there is very little participation of the speed and angle variables. And finally the last two eigenvectors are to be associated with the pair of complex eigenvalues which indicate oscillatory response with positive damping. Notice that the elements of the eigenvectors associated with this mode do not indicate damping but instead indicate phase and amplitude of the state variables with respect to each other. Damping is determined exclusively by the angle of the eigenvalue – not from any angles in the eigenvector

elements. Notice also that in the blocked system that was analyzed in section 4.3.1 that damping did not exist as was shown by the purely imaginary eigenvalues.

Figure 4.18 shows the measured frequency at the generator number two bus of the system in figure 4.17 when running the simulation with a governor time constant equal to 0.05 seconds. Comparing the oscillation in the waveform with the complex eigenvalues shows that there is consistency in between the measured and calculated oscillatory modes. The calculated oscillation frequency is 0.7457 Hz. Matrix Pencil analysis on the waveform gives an oscillation frequency of 0.7450 Hz, an error of 0.09%. The calculated damping ratio is 5.576% and the measure value through the Matrix Pencil is 5.550%, an error of 0.46%.

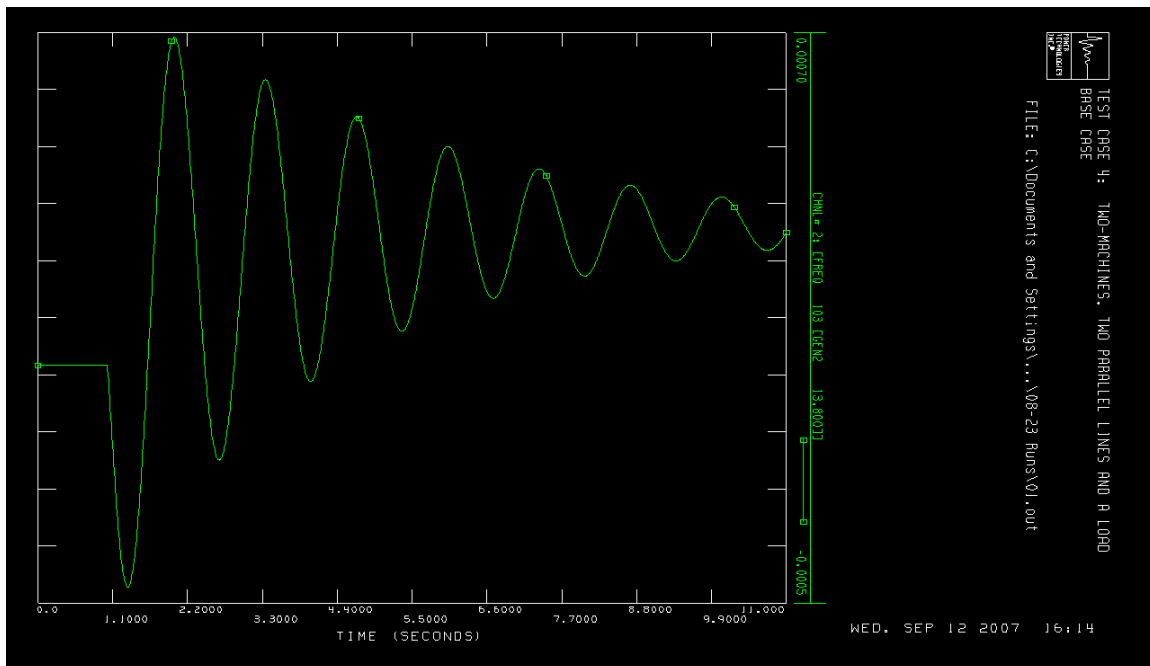


Figure 4.18: frequency following line outage; $\tau_2 = 0.05$ seconds

Changing the governor's time constant to 0.3 seconds reveals a decrease in damping and an increase in oscillation frequency. Figure 4.19 shows the waveform. The

calculated and measured oscillation frequencies are 0.7616 Hz and 0.7616 Hz respectively. The damping ratios are 1.982% and 1.984% respectively. Although not a substantial change in frequency, the decrease in damping ratio, 3.5 percentage points, is a drop of over 64%. The effect of changing time constants on generator governors in areas of a power system where damping is a problem could be to improve system reliability.

Increasing the time constant further to 0.5 seconds shows a corresponding decrease in damping however the oscillation frequency begins to drop again. It may be expected to approach the value of 0.7418 Hz determined in section 4.3.1 for an unregulated system as the time constant approaches infinity. Of course a time constant of infinity corresponds to no governor action at all. The frequency waveform form is shown in figure 4.20. The calculated and measured values for oscillation frequency and damping are 0.7567 Hz, 0.7566 Hz, 0.887%, 0.888% respectively.

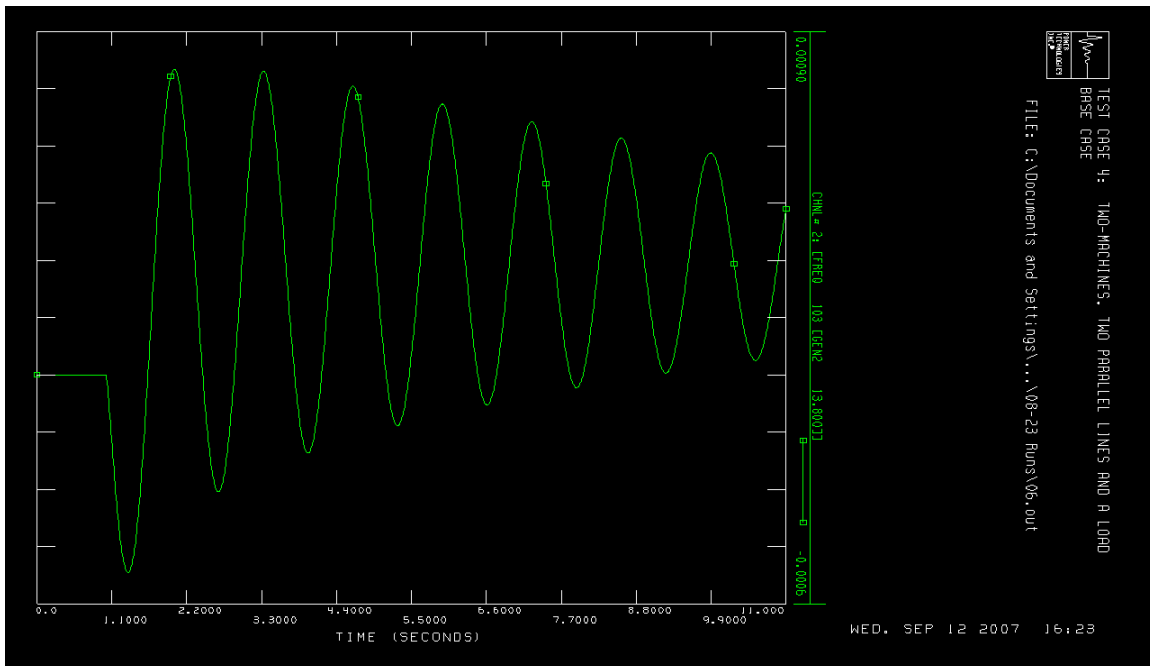


Figure 4.19: frequency following line outage; $\tau_2 = 0.3$ seconds

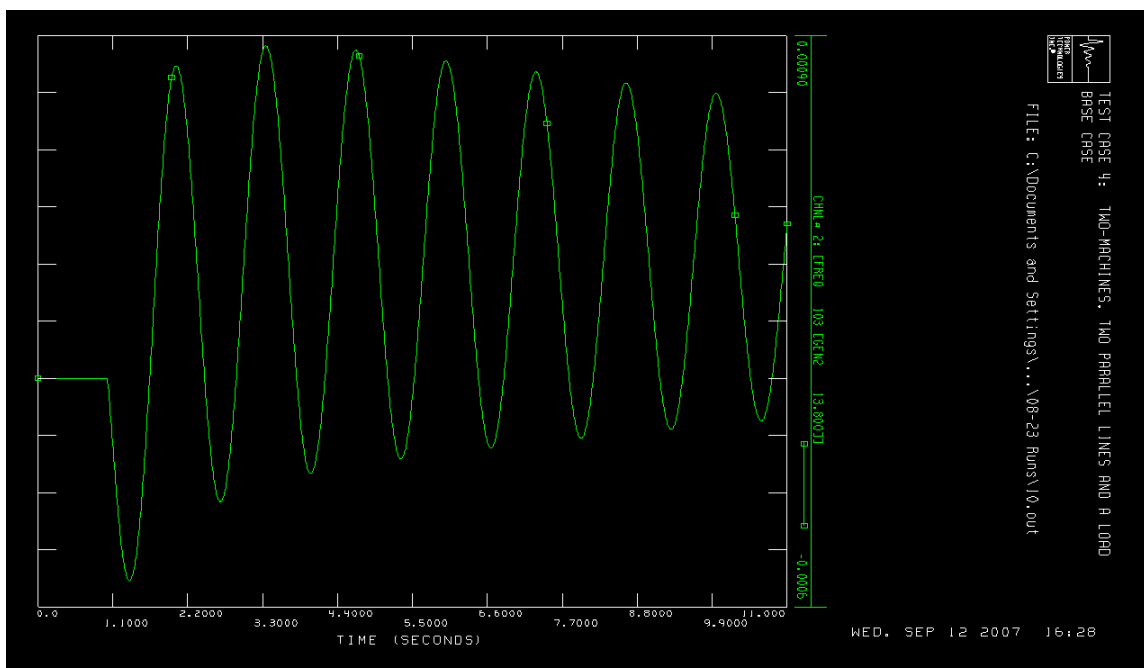


Figure 4.20: frequency following line outage; $\tau_2 = 0.5$ seconds

Table 4.2: mode data for unblocked two-machine two line system with line outage followed by no reclosure action. Governor time constant is varied.

					matrix pencil	matrix pencil
τ_2	$\text{Re}\{\lambda_{\text{osc}}\}$	$\text{Im}\{\lambda_{\text{osc}}\}$	oscill calc (Hz)	DR calc	oscill meas	DR meas
0.05	-0.2617	4.6852	0.7457	0.05576	0.7450	0.05550
0.10	-0.2373	4.7419	0.7547	0.04997	0.7543	0.04973
0.20	-0.1545	4.7903	0.7624	0.03223	0.7621	0.03218
0.30	-0.0949	4.7855	0.7616	0.01982	0.7616	0.01984
0.40	-0.0614	4.7696	0.7591	0.01286	0.7591	0.01288
0.50	-0.0422	4.7545	0.7567	0.00887	0.7566	0.00888

Table 4.2 shows how the oscillatory mode characteristics change as the governor's time constant is varied. It also gives a comparison of calculated modal frequencies and damping ratios vs. measured frequencies and damping ratios. This is done by applying the matrix pencil to the load bus's frequency measurement. The accuracy of the eigenanalysis is evident by the small errors in frequency and damping ratio. The

damping ratio continues to decline as governor time constant is increased which may be expected to approach zero as the time constant approaches infinity.

4.5 Modeling of Machine Damping

There are two major sources of damping in a synchronous generator, both of which may be modeled as a first-order-derivative term in the machine's swing equation. The first source of machine damping to mention is damping due to friction and windage losses. The second is damping due to electrical effects of amortisseur windings (also called damper windings). Damper windings, short circuits built into the machine's rotor, contribute no effect to machine torque when the machine is running at synchronous speed. As the machine deviates from synchronous speed, the damper windings have voltages induced on them, thus creating a current in the winding that results in an opposing electrical torque that tends to bring the machine's speed back toward synchronous. The physical mechanisms that create the effects of damper windings are described in machine texts such as [2], [4]. The main point is that the damping forces due to the windings are proportional (and thus in phase with) the speed deviation as

$$\tau_d = K_d \Delta \omega \quad (4.75)$$

The equation governing damping torque due to windage and friction losses takes on the same form as (4.75). Thus, the two effects, mechanical and electrical damping, may be lumped together into a single damping effect.

Since damping is not coupled from one machine to another, each machine's swing equation may be written as

$$\frac{2H_i}{\omega_s} \Delta \ddot{\delta}_i(t) + D_p \Delta \dot{\delta}_i(t) + \sum_{i=1}^n S_{pij} \Delta \delta_{ij}(t) = \Delta P_{mi} \quad (4.76)$$

This may be rewritten as the i th state equation in $\Delta\omega_i(t)$ as follows

$$\Delta\dot{\omega}_i(t) = -\frac{\omega_s}{2H_i} \sum_{j=1}^n S_{pij} \Delta\delta_{ij}(t) - \frac{\omega_s D_p}{2H_i} \Delta\omega_i(t) + \frac{\omega_s}{2H_i} \Delta P_{mi}(t) \quad (4.77)$$

To get a feel for how the damping power terms will appear in the plant matrix, setting the mechanical powers equal to zero for each machine and casting all state equations into vector-matrix format yields

$$\begin{bmatrix} \Delta\dot{\delta}_1(t) \\ \vdots \\ \Delta\dot{\delta}_n(t) \\ \Delta\dot{\omega}_1(t) \\ \vdots \\ \Delta\dot{\omega}_n(t) \end{bmatrix} = \begin{bmatrix} 0 & \cdots & 0 & | & 1 & \cdots & 0 \\ \vdots & \ddots & \vdots & | & \vdots & \ddots & \vdots \\ 0 & \cdots & 0 & | & 0 & \cdots & 1 \\ \hline \alpha_{11} & \cdots & \alpha_{1n} & | & d_{11} & \cdots & 0 \\ \vdots & \ddots & \vdots & | & \vdots & \ddots & \vdots \\ \alpha_{n1} & \cdots & \alpha_{nn} & | & 0 & \cdots & d_{n1} \end{bmatrix} * \begin{bmatrix} \Delta\delta_1(t) \\ \vdots \\ \Delta\delta_n(t) \\ \Delta\omega_1(t) \\ \vdots \\ \Delta\omega_n(t) \end{bmatrix} \quad (4.78)$$

The lower-right matrix in (4.78) is composed of the damping power terms in (4.77) and is a diagonal matrix due to the fact that damping is not coupled from one machine to another. Thus the addition of machine damping is simple to implement into the state model and results in the exact same vector-matrix equation as was developed in chapter three, written in compact form as

$$\begin{bmatrix} \dot{\Delta\delta} \\ \dot{\Delta\omega} \end{bmatrix} = \begin{bmatrix} \mathbf{0} & \mathbf{I} \\ \mathbf{S}_p & \mathbf{D}_p \end{bmatrix} * \begin{bmatrix} \Delta\delta \\ \Delta\omega \end{bmatrix} \quad (4.79)$$

where $\Delta\delta$ and $\Delta\omega$ are each vectors composed of machine angle and speed components and each element of the 2×2 matrix in (4.79) is an $n \times n$ matrix, where \mathbf{S}_p may be called a synchronizing power matrix and \mathbf{D}_p , the damping matrix.

It tends to be a common practice among utilities and other members of the power industry to count all damping terms as zero. However as stated in [19] damping factors

may typically be found to be on the order of 1 to 3 per unit and in some cases as high as 25. It may be reasonable to assume that the damping that utilities model in their studies as zero is the damping due to mechanical effects and not the electrical effects. The electrical effects are actually modeled when including the salient characteristics of the machine. Salient features are not included in this present work's electrical model as the classical machine model is being used. However, [27] provides a rigorous calculation in closed form of machine damping coefficient in terms of transient and subtransient reactances and time constants. These damping coefficients are intended for use with the classical machine model. Thus, they may be inserted directly (with the appropriate change of basis) into equation (4.77).

Chapter 5 Theory Verification Using a Non-trivial System

Chapter five is to be completely dedicated to verifying the theories developed in chapters three and four by analyzing a non-trivial 23-bus, six-machine system. Non-trivial, in this sense, refers to the system's inclusion of non-idealizations for which the theory was developed in chapter four. In addition the system is large enough so as not to be considered a "text-book" academic case such as the single-machine infinite-bus. The non-idealizations in this system include 1) line losses; 2) lack of infinite bus; 3) loads are part of the network as opposed to having an infinite bus as a load; 4) generator governors are present (the system is not blocked with respect to speed regulation); 5) line charging susceptance is included in the system model. The theory governing the latter of these non-ideal characteristics was not developed in chapter four. However, the principles that underlie load modeling (section 4.2) apply to line charging susceptance as both the loads and the charging susceptances may be treated as shunt elements and included in the system's short-circuit admittance matrix. The modal characteristics influenced by the presence of a power system load as examined in section 4.2 may be expected to follow for charging susceptances. A preliminary conclusion regarding the influence may be drawn from the fact that charging susceptance for a lightly loaded system will tend to increase synchronizing powers across the system via increases in voltages, thus increasing oscillation frequencies. Other conclusions may be drawn for more heavily loaded systems, namely the presence of the charging susceptance may actually decrease synchronizing powers thus decreasing coupling and corresponding oscillation frequencies. Though these characteristics should not be considered irrelevant, they will not be examined with the rigor that was employed in chapter four for load modeling.

5.1 System Description and State Equation Development

The 23-bus system that will be tested will have a total of three generators that have speed governors in service. In accordance with the plant matrix development in section 4.4, it may be assumed that the total number of states that need to be modeled for this system will be 12 (angle and speed for each machine) plus three states for the speed governors – a total of 15 states. The state equation with its plant matrix, must then take on a form similar to the one in equation (4.68) as follows

$$\begin{bmatrix} \dot{\Delta\delta} \\ \dot{\Delta\omega} \\ \dot{\Delta P_m} \end{bmatrix} = \begin{bmatrix} \mathbf{0} & \mathbf{I} & \mathbf{0} \\ \mathbf{S}_p & \mathbf{0} & \mathbf{H}^{-1} \\ \mathbf{0} & \mathbf{R}^{-1} & \Lambda \end{bmatrix} \bullet \begin{bmatrix} \Delta\delta \\ \Delta\omega \\ \Delta P_m \end{bmatrix} \quad (5.1)$$

The state vector in (5.1) is decomposed into three vector partitions, a vector of six machine angles, $\Delta\delta$, a vector of six machine speeds, $\Delta\omega$, and a vector of three machine mechanical powers, ΔP_m . Each partition in the plant matrix may be explained as follows: The zero-matrix in the upper left-hand corner is six-by-six. All entries must be zero as the derivative of each angle is not proportional to the angles themselves. The identity matrix in the top row is six-by-six and is present as the derivatives of the angles are identically equal to the corresponding machine speeds. The synchronizing power matrix, \mathbf{S}_p , is six-by-six and, as with all other previous derivations, relates the derivative of each machine speed with linear combinations of machine angles. Likewise, the six-by-six matrix \mathbf{D} , which may be called a damping power matrix, relates the derivative of each machine speed with its own speed. The damping power matrix is a diagonal matrix, as machine damping cannot be coupled with other machines (see swing equation development that was done in section 4.5). For the analysis conducted on the sample

system, \mathbf{D} will be a zero matrix. The matrix \mathbf{H}^{-1} may be called an inverse inertia matrix. This term is chosen as the entries in this matrix relate machine acceleration with machine mechanical power thus representing the inverse of mass in the swing equations. Due to the fact that not all machines in the system have speed governors, the \mathbf{H}^{-1} matrix is six-by-three in size. Further, due to the fact that no intermachine coupling exists in the relationship between mechanical power and machine acceleration, the matrix contains no coupling terms – it only has one non-zero entry per row. The matrix \mathbf{R}^{-1} referred to as a droop matrix is three-by-six and relates each speed-regulated machine's mechanical power derivative with its own speed. This relationship is per the development in section 4.4 for the differential equation that governs the relationship between mechanical power and speed. Again there is no intermachine coupling and thus each row of the \mathbf{R}^{-1} matrix has only one non-zero term. The matrix $\mathbf{\Lambda}$ contains the inverse of governor time constants (thus the symbol $\mathbf{\Lambda}$ was chosen). It will be referred to as the time constant matrix. It is a diagonal three-by-three matrix that relates mechanical power derivatives to their corresponding mechanical powers. Once again there is no intermachine coupling associated with the time constant matrix $\mathbf{\Lambda}$.

Before listing the actual submatrices mentioned in the above paragraph, some of the pertinent details associated with the 23-bus test power system will be covered here. A one-line diagram of the power system is shown in figure 5.1. Machines at buses one, two, and four have speed regulators in service as indicated by the regulation constant symbol, R_i , beside the generator symbol. All other machines in the system have no speed governors and are thus blocked. Each bus has two different numbers, the larger boldface number is the PTI designation

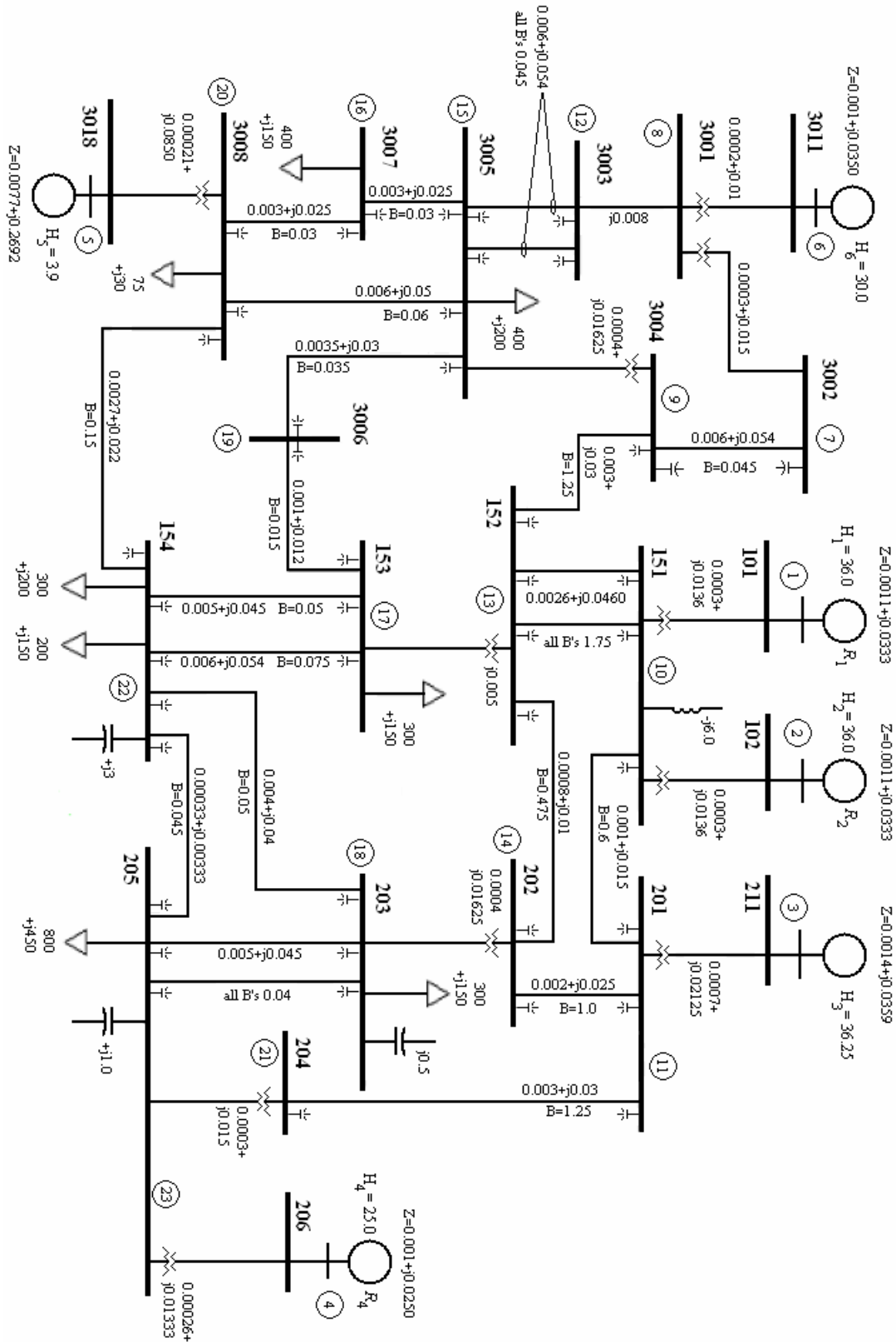


Figure 5.1: single-line diagram of 23-bus test system

and the smaller number enclosed in a circle is the number used to formulate the system's bus admittance matrix. The generator terminal buses do not have a corresponding admittance matrix bus as they are eliminated from the calculation. Each generator bus that does have an admittance matrix bus number actually represents the machine's internal voltage as was done in chapters three and four. All transformer and line series impedances along with charging susceptances and power factor correction reactors are listed in per-unit impedance on a 100MVA base. Loads are listed in MW and MVARs. Generator inertias are listed in per unit on a 100MVA base.

In order to develop the plant matrix for this system, first the admittance matrix must be constructed. Before building the admittance matrix, the loads, charging susceptances, and power factor correction reactors must be converted into admittances. After this conversion is complete, the 23 x 23 admittance matrix may be built and immediately reduced to a 6 x 6 admittance matrix using the Kron reduction technique used repeatedly throughout chapters three and four. This reduction converts the entire power system into a 6-port linear network that may be analyzed using linear network analysis techniques. See figure 5.2. It is important to understand that load flow calculations performed on this system are not linear as power relations are not linear in either current or voltage. Instead the linearity is in the voltage relationships to the current injections. This is standard theory of any network composed of linear elements – resistors, capacitors, and inductors. In the reduction process described here, any bus having a number that is higher than six are eliminated from calculations. The effect of all series and shunt elements are included in the reduced matrix. The resulting matrix yields the conductance and susceptance terms needed to calculate the elements of the

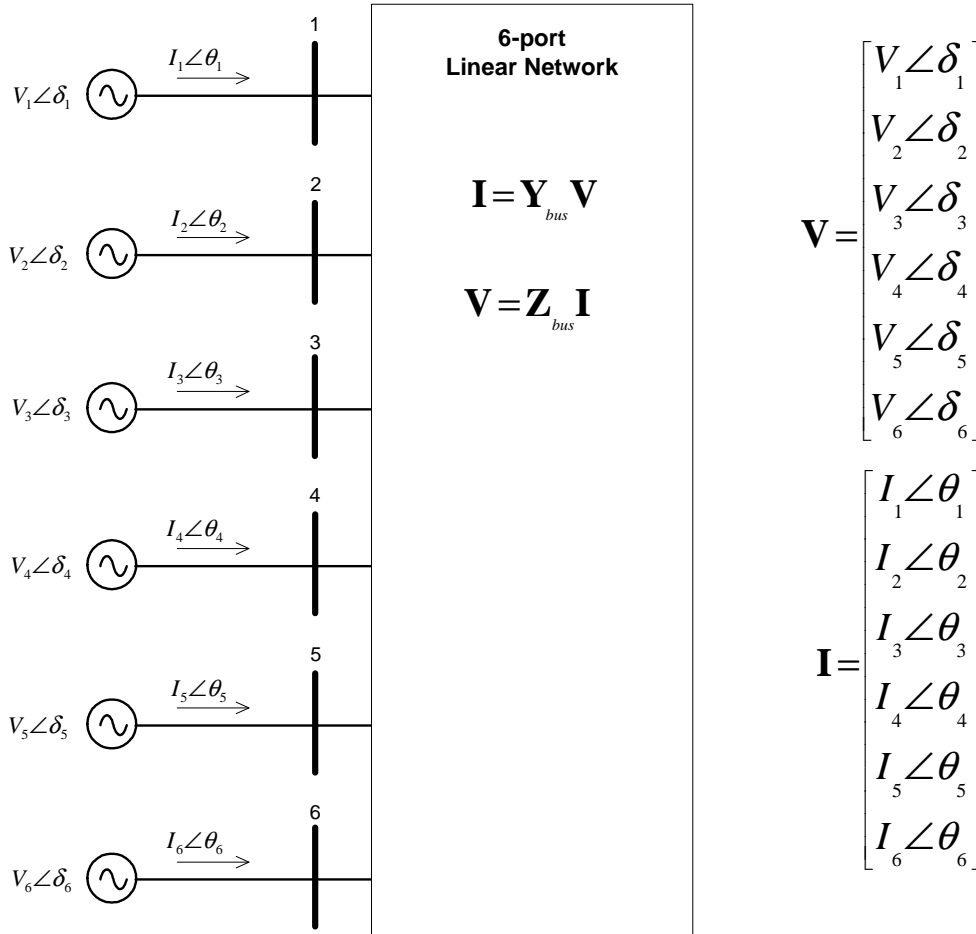


Figure 5.2: Representation of Power System as a Six-Port Network

synchronizing power matrix \mathbf{S}_p . Each off-diagonal term in the synchronizing power matrix will take on the familiar form

$$\alpha_{ij} = \frac{\omega_s}{2H_i} S_{pij} = \frac{\omega_s}{2H_i} E_i E_j [B_{ij} \cos \delta_{ij0} + G_{ij} \sin \delta_{ij0}] \quad (5.2)$$

and each diagonal term will take on the form

$$\alpha_{ii} = \frac{\omega_s}{2H_i} S_{pii} = -\frac{\omega_s}{2H_i} \sum_{\substack{j=1 \\ j \neq i}}^n E_i E_j [B_{ij} \cos \delta_{ij0} + G_{ij} \sin \delta_{ij0}] \quad (5.3)$$

The vector-matrix equation corresponding to the "middle row" partition of equation (5.1) may be expressed as

$$\dot{\Delta\omega} = \mathbf{S}_p \Delta\delta + \mathbf{H}^{-1} \Delta\mathbf{P}_m \quad (5.4)$$

and as stated before, since there is no intermachine coupling in speed and mechanical power, the inverse inertia matrix must take on the form

$$\mathbf{H}^{-1} = \begin{bmatrix} \frac{\omega_s}{2H_1} & 0 & 0 \\ 0 & \frac{\omega_s}{2H_2} & 0 \\ 0 & 0 & 0 \\ 0 & 0 & \frac{\omega_s}{2H_4} \\ 0 & 0 & 0 \\ 0 & 0 & 0 \end{bmatrix} \quad (5.5)$$

The vector-matrix equation corresponding to the "bottom row" partition of equation (5.1) may be expressed as

$$\Delta\dot{\mathbf{P}}_m = \mathbf{R}^{-1} \Delta\omega + \Lambda \Delta\mathbf{P}_m \quad (5.6)$$

The relationship in between machine speed and the derivative of mechanical power yields the droop matrix as

$$\mathbf{R}^{-1} = \begin{bmatrix} -\frac{1}{\omega_s R_1 \tau_1} & 0 & 0 & 0 & 0 & 0 \\ 0 & -\frac{1}{\omega_s R_2 \tau_2} & 0 & 0 & 0 & 0 \\ 0 & 0 & 0 & -\frac{1}{\omega_s R_4 \tau_4} & 0 & 0 \end{bmatrix} \quad (5.7)$$

It must be pointed out that the nomenclature and symbol for the "inverse" inertia and droop matrices should not be considered mathematical operators in the sense that they

are the inverse of some matrix. They are called inverse matrices because of the relationship in between the inverse of their entries and the corresponding governing scalar equations. An analogy would be the expression of acceleration as being linearly proportional to force where the proportionality constant is the inverse of the body's mass. The droop and inverse inertia matrices are, in fact, matrices that have right and left inverse matrices that do exist but this fact is not relevant in the present analysis.

Finally the diagonal time constant matrix, Λ , that relates mechanical power derivatives with mechanical power is

$$\Lambda = \begin{bmatrix} -\frac{1}{\tau_1} & 0 & 0 \\ 0 & -\frac{1}{\tau_2} & 0 \\ 0 & 0 & -\frac{1}{\tau_4} \end{bmatrix} \quad (5.8)$$

As seen by the entries in the matrix partitions above, none of elements of the matrices will change due to any line outage save the elements of the \mathbf{S}_p matrix. This is due to the fact that the \mathbf{S}_p matrix contains terms that depend on 1) the elements of the system's reduced admittance matrix and 2) the q-point machine angles. Both of these sets of quantities must necessarily be different for different line outages. Thus, the only quantities that need to be calculated after an initial plant matrix development are the synchronizing power coefficients. It must be pointed out that if generator outages were to be analyzed, the state-space dimension must decrease by at least two and so all of the matrix partitions must be rebuilt for each generator outage analysis.

There will be a total of four line outages that will be examined and it will be verified via comparison of matrix pencil analysis with modal analysis that the outages

themselves can be distinguished via the mode matching technique that was explained in chapter three. The four lines that will be taken out of service and their corresponding pre-fault megawatt flows are as follows in table 5.1:

Table 5.1: selected line outages for the system in figure 5.1 with pre-fault power flows

Line ID	MW Flow
151-152 circuit 1	304
201-204	369
3003-3005 circuit 1	267
3005-3006	27

These lines were selected to provide a variety of magnitudes of MW interruptions. The system demand is approximately 2800MW and thus, percentage-wise, the interruptions range from about 1% to over 10% of system demand. It turns out that the linearized electromechanical model of the system predicts oscillation frequencies of the natural response within 0.5% error for all of the above disturbances. This is significant as normally a linearized model is expected to yield accurate results for disturbances of no more than 1% of system demand [19].

5.2 Q-point Determination Method

Equations (5.2) and (5.3) are not of practical use without knowing the quantities δ_{ij0} , the difference in between machine i and j in post-fault steady-state, in other words, the q-point angle differences. It should be expected that for each different disturbance applied to the power system that there will be different q-point angles, thus the plant matrix must be recalculated for each disturbance. In order to calculate these numbers for each disturbance, a load flow needs to be ran that will take into account the change in system topology due to the line outage. As explained in section 4.2, the system demand

must change following a line outage due to voltage changes (normally expected to be decreases in voltage) and, of course, the total system losses should be expected to change due to the fact that a line is no longer in service. The change in system demand must require that the steady-state system frequency change per equation (4.63) modified as follows to neglect load frequency sensitivity and take into account multiple speed governors,

$$\Delta\omega = -\frac{\Delta P_L}{\frac{1}{R_1} + \frac{1}{R_2} + \frac{1}{R_4}} \quad (5.9)$$

and that each speed-governed machine mechanical power must change per a similar relationship, equation (4.54)

$$\Delta P_{mi} = -\frac{\Delta\omega}{1/R_i} = -R_i\Delta\omega \quad (5.10)$$

The quantity $\Delta\omega$ in equations (5.9) and (5.10) represents steady-state machine speeds for all machines, regardless of whether they are speed-governed or not (the system is in synchronism) and the unit of $\Delta\omega$ is per unit speed. Of course, all of the machines that are not equipped with speed governors will have a post-fault steady-state power output equal to their pre-fault power output.

Using equations (5.9) and (5.10) will result in being able to determine q-point powers thus allowing one to perform a load flow analysis which will yield q-point angles. The swing bus in the test system is machine six (top left-hand corner of figure 5.1). The post-fault power of this machine must be equal to the pre-fault power due to the fact that it is an unregulated machine. In order to obtain equal pre- and post-fault power outputs for the swing bus a four-step process must be carried out – 1) a quantity for $\Delta\omega$ is chosen

as a first guess speed deviation; 2) all speed-governed machine power outputs are calculated using (5.8); 3) load flow is ran; 4) compare swing bus pre- and post-fault powers. After comparison is made, a new guess for $\Delta\omega$ must be made. This process must be carried out until the two power quantities are equal within a specified amount. A process flow chart is shown in figure 5.3.

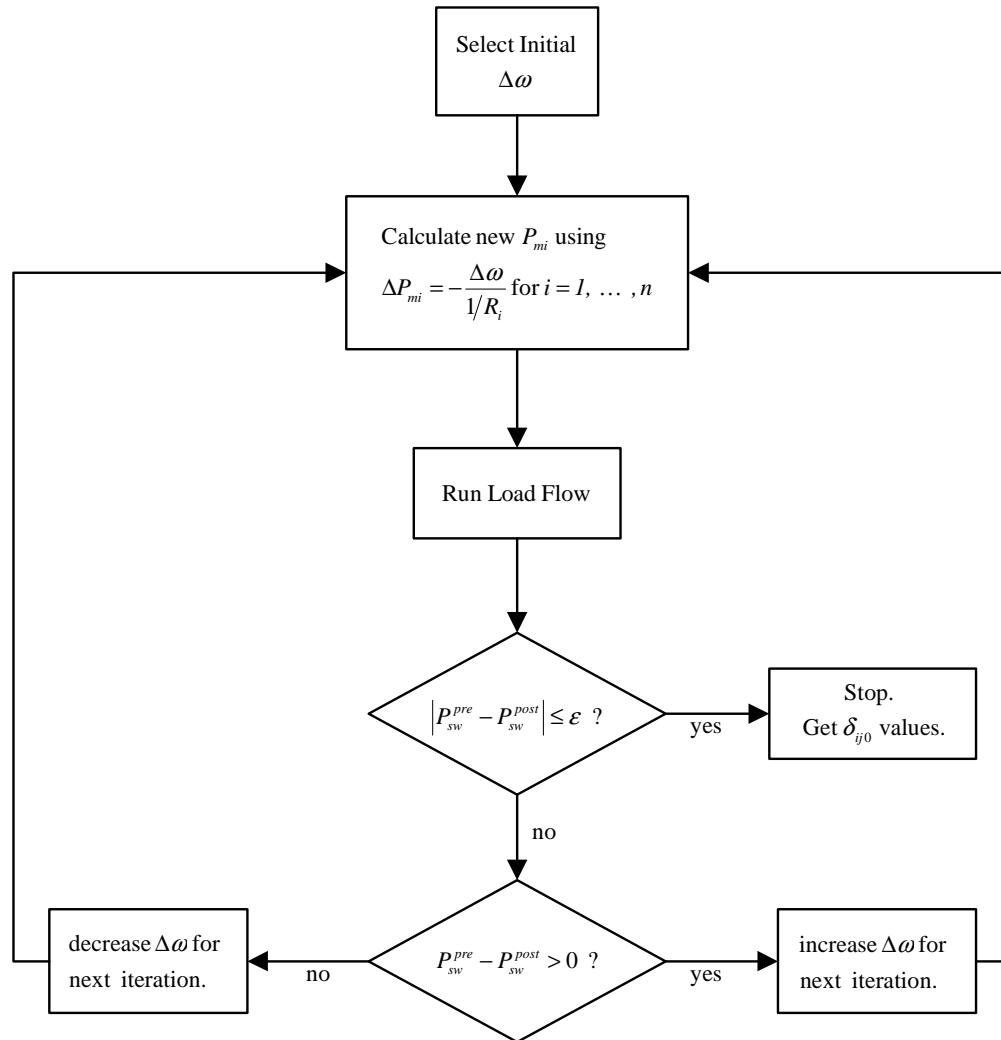


Figure 5.3: Iteration scheme for q-point calculation

For the test system, the load flow was run using the reduced system shown in figure 5.2 and conventional power flow equations for each machine. The only quantities that require solving for this load flow happen to be the generator angles and due to the

fact that this system is appropriately reduced, the generator angles are the internal voltage angles. All 23 of the bus voltage angles and magnitudes are not solved for during this load flow. The voltages may be solved for after the load flow is complete using linear network analysis on the full, unreduced 23-bus system. This solution will not be treated here as bus voltages are not needed in the modal analysis, save the machine internal voltages that are already solved for. They will need to be solved, at least certain bus voltages for the case where a full AC load flow – based output matrix must be developed similar to what was done in chapter three.

After completing the scheme shown in figure 5.3, the q-point is known and thus the elements of the synchronizing power matrix may be calculated. Modal analysis may then be performed.

5.3 Modal Analyses and Comparison with Simulation Results

5.3.1 151-152 line outage

The first disturbance to be analyzed is the 151-152 single line outage, a 304 MW interruption. The process outlined in figure 5.4 yielded a $\Delta\omega$ value of 0.00318800 p.u. which corresponds to 191.3 mHz. The steady state post-disturbance angles for the system were calculated to be

$$\begin{aligned}
 \delta_1 &= 8.2796^\circ \\
 \delta_2 &= 8.2796^\circ \\
 \delta_3 &= 5.6469^\circ \\
 \delta_4 &= -5.4753^\circ \\
 \delta_5 &= 0.7934^\circ \\
 \delta_6 &= 13.680^\circ
 \end{aligned}
 \tag{5.11}$$

Since this set of angles was obtained via load flow analysis, the angles should be considered to be relative angles and not absolute angles. The process that was carried out entailed setting the reference bus (machine six) at its original pre-fault value which was 13.680° . All other angles were solved for relative to this angle. The fact that these are not absolute angles is not consequential in the modal analysis due to the fact that the elements of the synchronizing power matrix require knowledge of angle *differences*. The synchronizing power, inverse inertia, droop, and time constant matrices were determined as follows:

$$\mathbf{S}_p = \begin{bmatrix} -77.5159 & 32.8827 & 18.5599 & 14.2981 & 1.7334 & 10.0419 \\ 32.8827 & -77.5159 & 18.5599 & 14.2981 & 1.7334 & 10.0419 \\ 18.6545 & 18.6545 & -67.0964 & 17.2241 & 1.9545 & 10.6088 \\ 24.4640 & 24.4640 & 28.6409 & -114.8821 & 7.0559 & 30.2573 \\ 17.8218 & 17.8218 & 19.5082 & 41.0174 & -132.3351 & 36.1658 \\ 11.3087 & 11.3087 & 11.5828 & 18.3791 & 3.9508 & -56.5302 \end{bmatrix} \quad (5.12)$$

$$\mathbf{H}^{-1} = \begin{bmatrix} 5.2360 & 0 & 0 \\ 0 & 5.2360 & 0 \\ 0 & 0 & 0 \\ 0 & 0 & 7.5398 \\ 0 & 0 & 0 \\ 0 & 0 & 0 \end{bmatrix} \quad (5.13)$$

$$\mathbf{R}^{-1} = \begin{bmatrix} -0.9549 & 0 & 0 & 0 & 0 & 0 \\ 0 & -0.9549 & 0 & 0 & 0 & 0 \\ 0 & 0 & 0 & -1.0610 & 0 & 0 \end{bmatrix} \quad (5.14)$$

$$\mathbf{A} = \begin{bmatrix} -2.0000 & 0 & 0 \\ 0 & -2.0000 & 0 \\ 0 & 0 & -2.0000 \end{bmatrix} \quad (5.15)$$

Due to the fact that the plant matrix is 15 x 15, one may expect that the maximum number of oscillatory modes would be seven – there is a pair of complex eigenvalues for each oscillatory mode. The eigenvalues of the plant matrix formed by these partitions are

$$\begin{aligned} \sigma(\mathbf{A}) = \{ & \lambda_1 = -0.0285 \pm j12.1443, \lambda_2 = -0.0224 \pm j11.2313, \\ & \lambda_3 = -0.0420 \pm j10.7348, \lambda_4 = -0.0199 \pm j9.2687, \\ & \lambda_5 = -0.0143 \pm j8.0935, \lambda_6 = 0.0000, \lambda_7 = -0.9712 \pm j1.4709, \\ & \lambda_8 = -1.9160, \lambda_9 = -1.8876 \} \end{aligned} \quad (5.16)$$

The calculated and measured oscillation frequencies, normalized eigenvectors (speed components only) with amplitude and phase for select complex eigenvalues in $\sigma(\mathbf{A})$ are in tables 5.2 through 5.5. Mode three in (5.14), the mode associated with λ_3 , is not listed in the tables as it is a mode in which only machines one and two participate, thus it is not observable in frequency measurements. And it is a mode that cannot be excited via line outages in the transmission network. Thus it will not be investigated further as a means of distinguishing disturbances from one another.

Mode seven, which is the dominant mode, turns out to be a common mode for all four of line outages listed in table 5.1. All of the speed and angle states participate equally in this mode and the damped frequency, around 0.2341Hz for the 151-152 outage, is nearly constant regardless of which line outage occurs. This type of mode could possibly be used on a power system to sift disturbances, say, line outage with no reclose vs. generator outage vs. line outage with reclose, etc. A special feature of this mode is that all of the machines oscillate together – not against one another.

Table 5.2: comparison of modal properties for 151-152 line outage, mode 1

Calculated Values			Simulation Values			f_{damp} average error
$ \Delta\omega_i $	$\angle\Delta\omega_i$	f_{damp} (Hz)	$ \Delta\omega_i $	$\angle\Delta\omega_i$	f_{damp} (Hz)	
1.000	0	1.9328	1.000	0	1.9369	-0.0023
1.000	0		1.000	0	1.9373	
1.478	-1		1.489	3	1.9373	
12.849	-181		12.956	-179	1.9372	
28.278	-4		28.264	3	1.9372	
0.934	2		1.040	-9	1.9372	

$$\lambda_1 = -0.0285 \pm j12.1443$$

Table 5.3: comparison of modal properties for 151-152 line outage, mode 2

Calculated Values			Simulation Values			f_{damp} average error
$ \Delta\omega_i $	$\angle\Delta\omega_i$	f_{damp} (Hz)	$ \Delta\omega_i $	$\angle\Delta\omega_i$	f_{damp} (Hz)	
1.000	0	1.7875	1.000	0	1.7908	-0.0019
1.000	0		1.000	0	1.7908	
1.523	-1		1.561	2	1.7908	
6.560	-181		6.679	-178	1.7908	
19.607	-178		20.129	-182	1.7908	
2.265	0		2.316	-1	1.7908	

$$\lambda_2 = -0.0224 \pm j11.2313$$

Table 5.4: comparison of modal properties for 151-152 line outage, mode 4

Calculated Values			Simulation Values			f_{damp} average error
$ \Delta\omega_i $	$\angle\Delta\omega_i$	f_{damp} (Hz)	$ \Delta\omega_i $	$\angle\Delta\omega_i$	f_{damp} (Hz)	
1.000	0	1.4752	1.000	0	1.4783	-0.0021
1.000	0		1.000	0	1.4783	
1.904	-181		1.907	-178	1.4783	
0.117	-187		0.121	-174	1.4783	
0.085	-185		0.089	-174	1.4786	
0.069	-22		0.067	-8	1.4780	

$$\lambda_4 = -0.0199 \pm j9.2687$$

Table 5.5: comparison of modal properties for 151-152 line outage, mode 5

Calculated Values			Simulation Values			f_{damp} average error
$ \Delta\omega_i $	$\angle\Delta\omega_i$	f_{damp} (Hz)	$ \Delta\omega_i $	$\angle\Delta\omega_i$	f_{damp} (Hz)	
1.000	0	1.2881	1.000	0	1.2890	-0.0007
1.000	0		1.000	0	1.2890	
0.925	4		0.925	-3	1.2890	
0.265	-183		0.265	-176	1.2890	
0.868	-180		0.871	-176	1.2890	
2.788	-179		2.793	-181	1.2890	

$$\lambda_5 = -0.0143 \pm j8.0935$$

The waveforms of figure 5.4 (a) show the per unit speed deviation of machine five (which quantity is also equal to the frequency deviation of its internal voltage) following the 151-152 line outage. The waveforms in figure 5.4(a) need to be interpreted as follows: The green waveform is the estimated signal based on Matrix Pencil's superposition of exponentials; the blue waveform, barely visible behind the green waveform, is the actual measured signal directly from the simulation. Close examination of figure 5.4(a) shows that the two waveforms are very nearly equal and thus the Matrix Pencil algorithm appears to have successfully duplicated the measured signal via a superposition of exponentials. The red waveform (constant waveform) in figure 5.4 (a), which is the Matrix Pencil's estimated signal mean value, is about 0.0032 p.u. This number may be interpreted as a steady state post-disturbance frequency deviation and may also be associated with mode number six, the zero-frequency mode. Its value agrees with the calculated value of 0.003188 p.u. (191.3 mHz) obtained using the iteration scheme shown in the flowchart of figure 5.3. This agreement verifies the generation-load mismatch theory described in section 5.2. The accuracy of the damped oscillation frequencies shown in tables 5.2 through 5.5 well verifies the validity of q-

point determination method described in section 5.2. The accuracy of the calculated steady-state post-disturbance frequency deviation further verifies the method.

The machine 5 waveforms are shown first here because this generator tends to participate heavily in each of the modes. Thus multiple sine waves, shown in the signal gallery, figure 5.4 (b), make up the components of the estimated waveform. The 0.2341Hz mode may be seen clearly as the red waveform in figure 5.4 (b).

Notice from the mode shape data listed in the tables above, that generators one and two participate equally in each mode – both in magnitude and phase. This is due to the fact that they are identical machines with identical predisturbance loading. The two machines literally behave as though they were one machine. Figure 5.5 shows the speed waveforms for these two machines. Notice how the oscillatory activity for machines one and two is much less than machine five. Part of this may be attributed to the fact that machine five is the lightest machine on the system (130MVA).

Figures 5.6 and 5.7 show speed deviation for machines three and four respectively. It may be discerned again that the amount of oscillatory activity in machine four is less than that in machine three, and, once again the amounts of oscillatory activity in terms of oscillation amplitude may be attributed to a machine's greater or lesser mass. This association between mass and oscillatory amplitude is coupled with other physical conditions such as the differences in between pre- and post- angles and steady-state speeds and the amount of electromechanical coupling in between machines as determined by the synchronizing power coefficients.

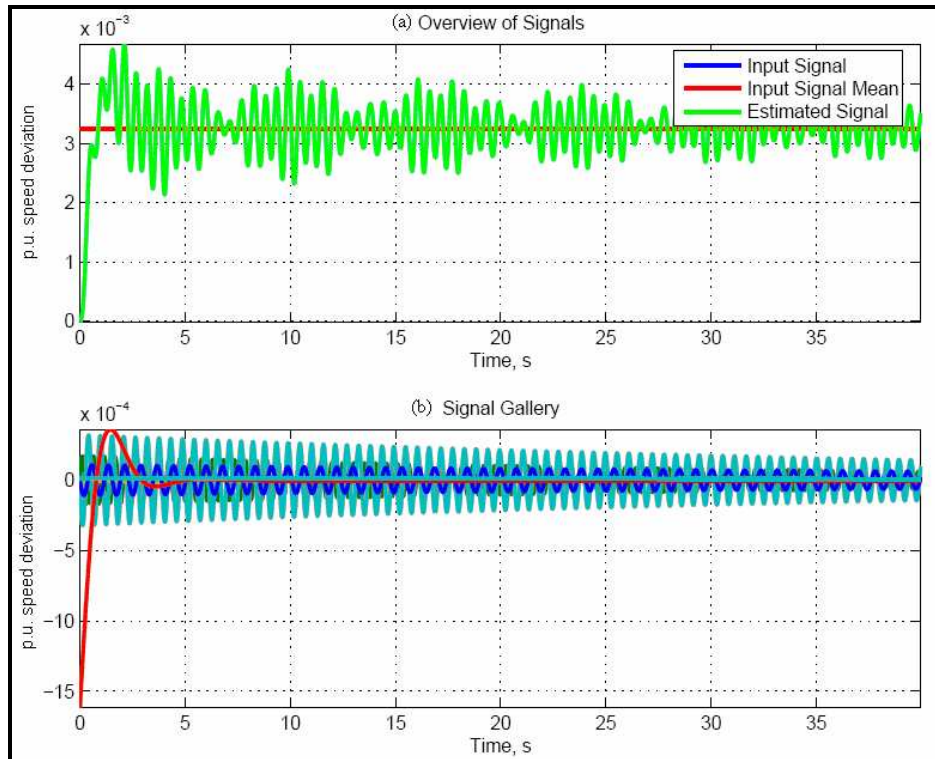


Figure 5.4: 151-152 line outage: (a) machine 5 estimated vs. measured speed signal; (b) display of each oscillatory component

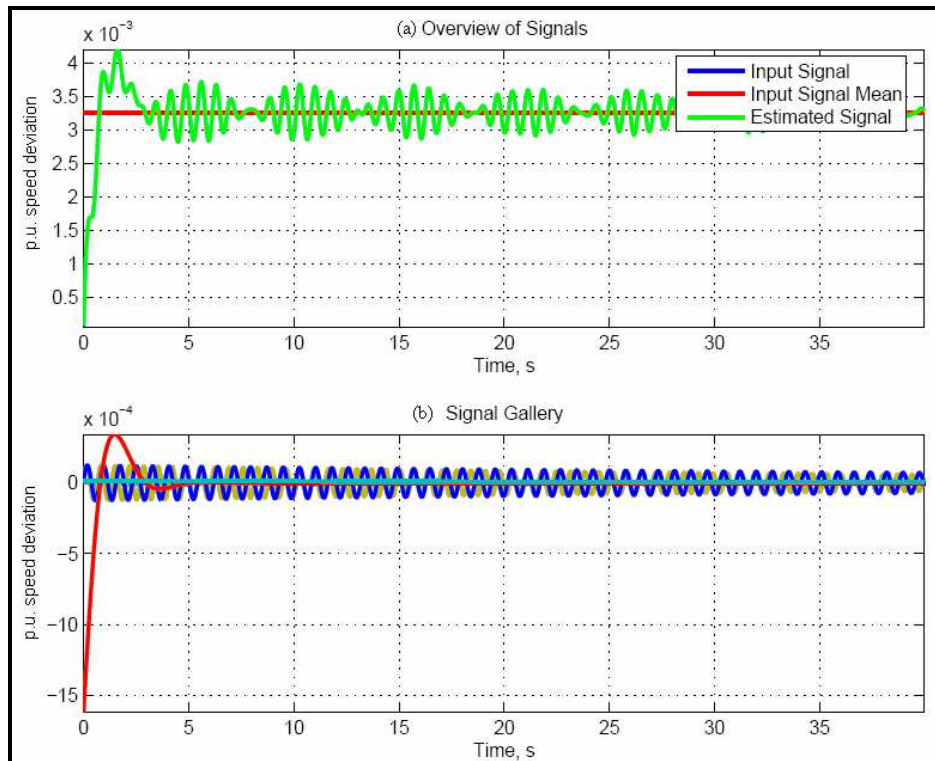


Figure 5.5: 151-152 line outage: (a) machines 1 and 2 estimated vs. measured speed signal; (b) display of each oscillatory component

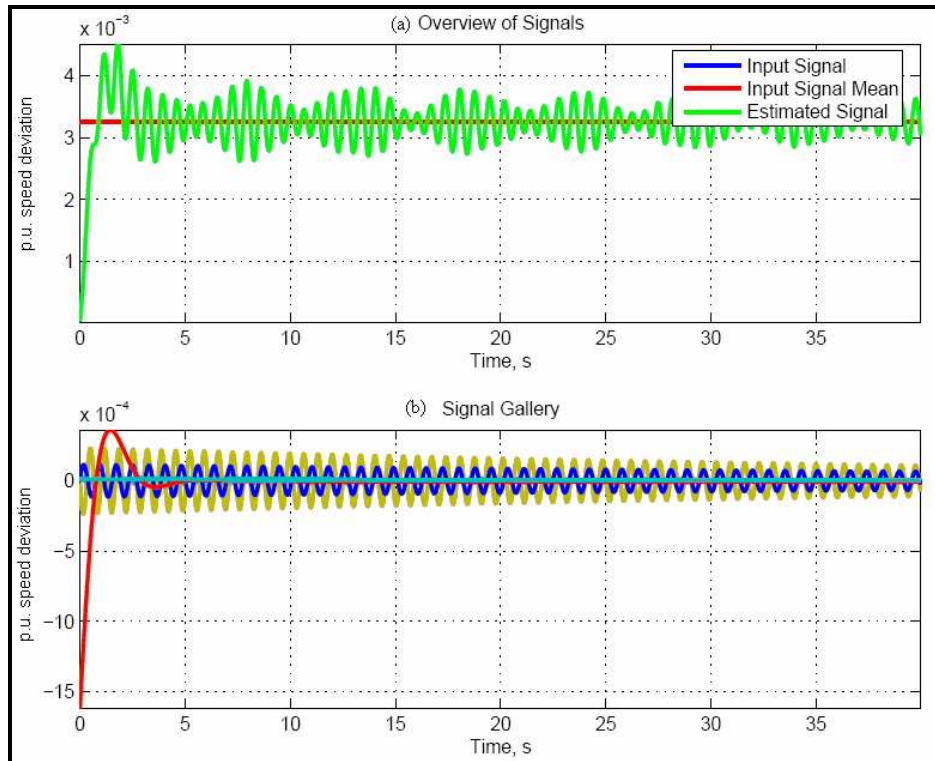


Figure 5.6: 151-152 line outage: (a) machine 3 estimated vs. measured speed signal; (b) display of each oscillatory component

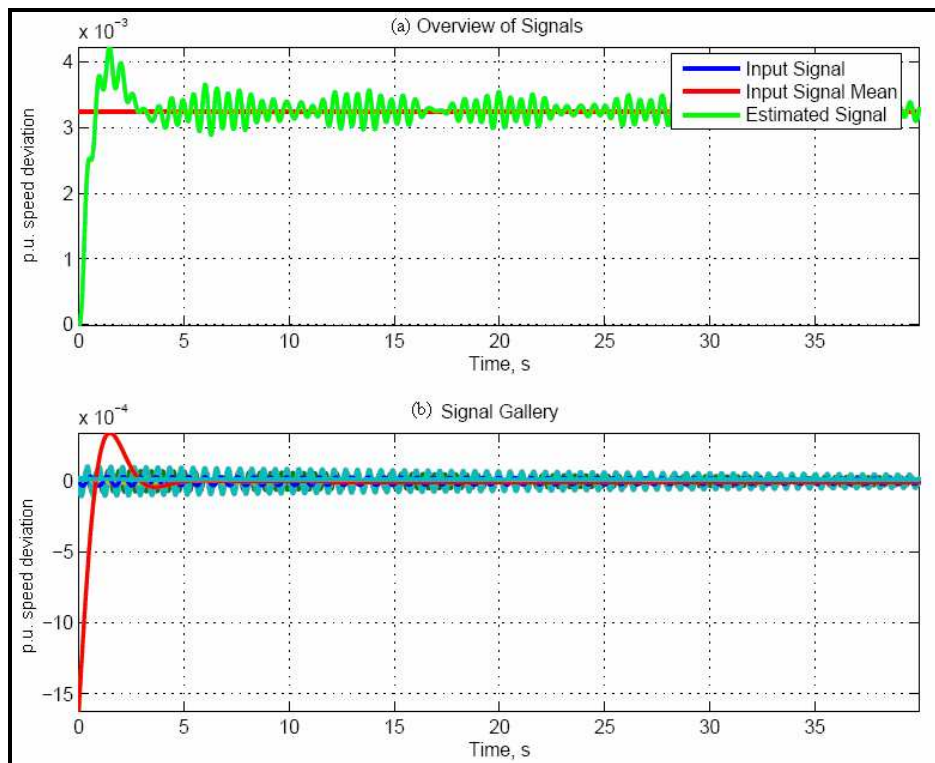


Figure 5.7: 151-152 line outage: (a) machine 4 estimated vs. measured speed signal; (b) display of each oscillatory component

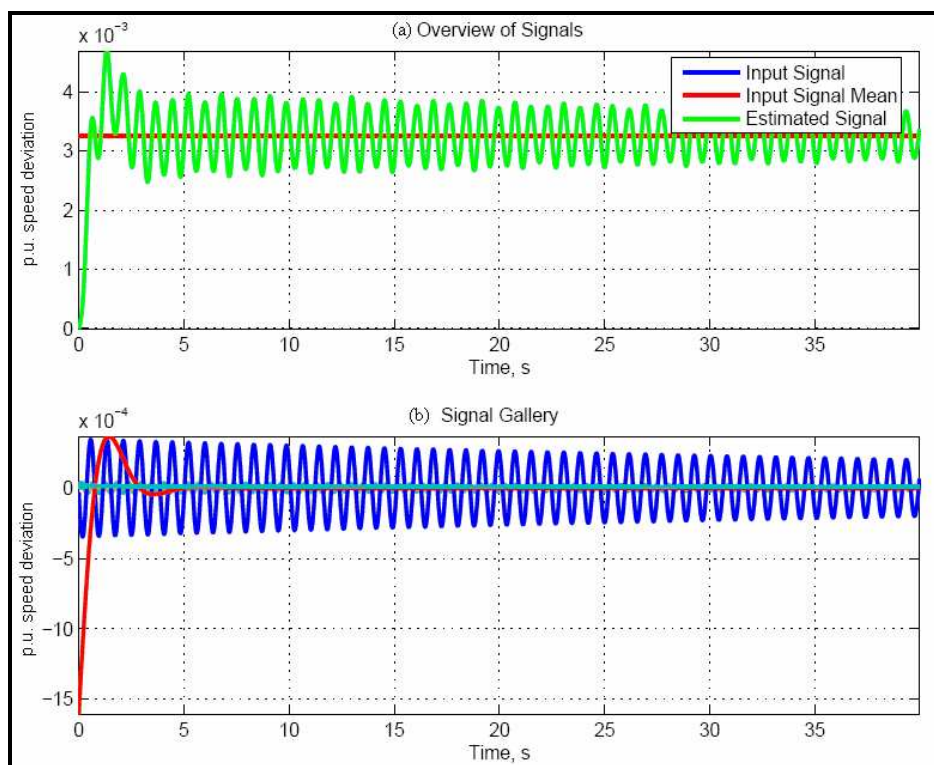


Figure 5.8: 151-152 line outage: (a) machine 6 estimated vs. measured speed signal; (b) display of each oscillatory component

5.3.2 201-204 line outage

The 201-204 line outage is a 369 MW interruption in flow. The q-point calculation for this disturbance yields a $\Delta\omega$ value of 0.00352950 p.u. which corresponds to 211.8 mHz. The measured value of steady-state post disturbance frequency deviation from simulation is about 0.00367 p.u. (220.2 mHz), thus verifying again the q-point determination procedure outlined in the flowchart figure 5.3. The steady-state post-disturbance angles for the system were calculated to be

$$\begin{aligned}
 \delta_1 &= 7.1461^\circ \\
 \delta_2 &= 7.1461^\circ \\
 \delta_3 &= 7.5097^\circ \\
 \delta_4 &= -7.8368^\circ \\
 \delta_5 &= 0.0917^\circ \\
 \delta_6 &= 13.6800^\circ
 \end{aligned}
 \tag{5.17}$$

The synchronizing power matrix was determined to be

$$\mathbf{S}_p = \begin{bmatrix} -80.0423 & 32.9657 & 20.5188 & 13.4093 & 1.8305 & 11.3179 \\ 32.9657 & -80.0423 & 20.5188 & 13.4093 & 1.8305 & 11.3179 \\ 20.3490 & 20.3490 & -65.1688 & 12.7176 & 1.6755 & 10.0778 \\ 23.8089 & 23.8089 & 22.7734 & -107.6052 & 7.3302 & 29.8837 \\ 18.7578 & 18.7578 & 17.3832 & 41.6135 & -131.8281 & 35.3157 \\ 12.6508 & 12.6508 & 11.3715 & 17.3194 & 3.8202 & -57.8127 \end{bmatrix} \quad (5.18)$$

The inverse inertia, droop, and time constant matrices are identical to the matrices listed in equations (5.13) through (5.15). The eigenvalues of the plant matrix formed by these partitions are

$$\begin{aligned} \sigma(\mathbf{A}) = \{ & \lambda_1 = -0.0202 \pm j11.9869, \lambda_2 = -0.0411 \pm j10.8558, \\ & \lambda_3 = -0.0347 \pm j10.9763, \lambda_4 = -0.0219 \pm j9.3981, \\ & \lambda_5 = -0.0101 \pm j8.1607, \lambda_6 = 0.0000, \lambda_7 = -0.9713 \pm j1.4573, \\ & \lambda_8 = -1.9178, \lambda_9 = -1.8837 \} \end{aligned} \quad (5.19)$$

Table 5.6: comparison of modal properties for 201-204 line outage, mode 1

Calculated Values			Simulation Values			f_{damp} average error
$ \Delta\omega_i $	$\angle\Delta\omega_i$	f_{damp} (Hz)	$ \Delta\omega_i $	$\angle\Delta\omega_i$	f_{damp} (Hz)	
1.000	0	1.9078	1.000	0	1.9108	-0.0016
1.000	0		1.000	0	1.9108	
0.838	-1		0.812	8	1.9111	
14.845	178		14.979	-175	1.9109	
46.066	-5		46.023	8	1.9109	
0.551	7		0.667	0	1.9108	

$$\lambda_1 = -0.0202 \pm j11.9869$$

Table 5.7: comparison of modal properties for 201-204 line outage, mode 3

Calculated Values			Simulation Values			f_{damp} average error
$ \Delta\omega_i $	$\angle\Delta\omega_i$	f_{damp} (Hz)	$ \Delta\omega_i $	$\angle\Delta\omega_i$	f_{damp} (Hz)	
1.000	0	1.7469	1.000	0	1.7491	-0.0012
1.000	0		1.000	0	1.7491	
0.694	-2		0.690	3	1.7492	
6.127	-181		6.111	-179	1.7491	
12.148	-178		12.231	-182	1.7491	
1.904	-1		1.920	1	1.7491	

$$\lambda_3 = -0.0347 \pm j10.9763$$

Table 5.8: comparison of modal properties for 201-204 line outage, mode 4

Calculated Values			Simulation Values			f_{damp} average error
$ \Delta\omega_i $	$\angle\Delta\omega_i$	f_{damp} (Hz)	$ \Delta\omega_i $	$\angle\Delta\omega_i$	f_{damp} (Hz)	
1.000	0	1.4958	1.000	0	1.4992	-0.0023
1.000	0		1.000	0	1.4992	
1.695	179		1.706	182	1.4993	
0.076	7		0.077	-4	1.4999	
0.057	10					
0.248	183		0.248	173	1.4988	

$$\lambda_4 = -0.0219 \pm j9.3981$$

Table 5.9: comparison of modal properties for 201-204 line outage, mode 5

Calculated Values			Simulation Values			f_{damp} average error
$ \Delta\omega_i $	$\angle\Delta\omega_i$	f_{damp} (Hz)	$ \Delta\omega_i $	$\angle\Delta\omega_i$	f_{damp} (Hz)	
1.000	0	1.2988	1.000	0	1.2996	-0.0006
1.000	0		1.000	0	1.2996	
1.607	3		1.598	-2	1.2996	
0.534	178		0.526	-175	1.2996	
1.176	180		1.173	-175	1.2996	
3.397	181		3.387	-181	1.2996	

$$\lambda_5 = -0.0101 \pm j8.1607$$

Tables 5.6 through 5.9 list the modal characteristics of all of the oscillatory modes shown in equation (5.19). As in section 5.3.1, the second mode listed in equation (5.19) is a mode in which only machines one and two are able to participate and for the same reason previously described, this mode will not be included in the tables (this two-machine only mode is actually mode three in the 151-152 outage). Likewise mode seven is not included. A blank cell in table 5.8 (mode 4) indicates that activity corresponding to mode four was not detected by the Matrix Pencil. Figures 5.9 through 5.13 show the speed deviation waveforms for each of the six machines. As in the previous disturbance, 151-152 line outage, machine five's heavy participation in several of the oscillatory modes is evident.

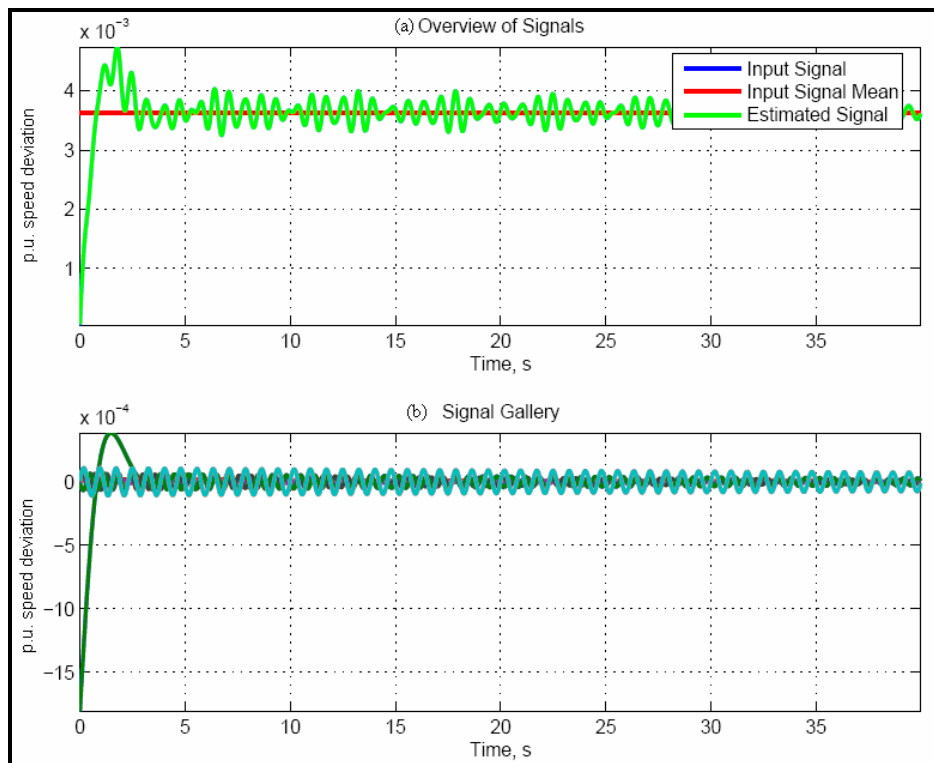


Figure 5.9: 201-204 line outage: (a) machines 1 and 2 estimated vs. measured speed signal; (b) display of each oscillatory component

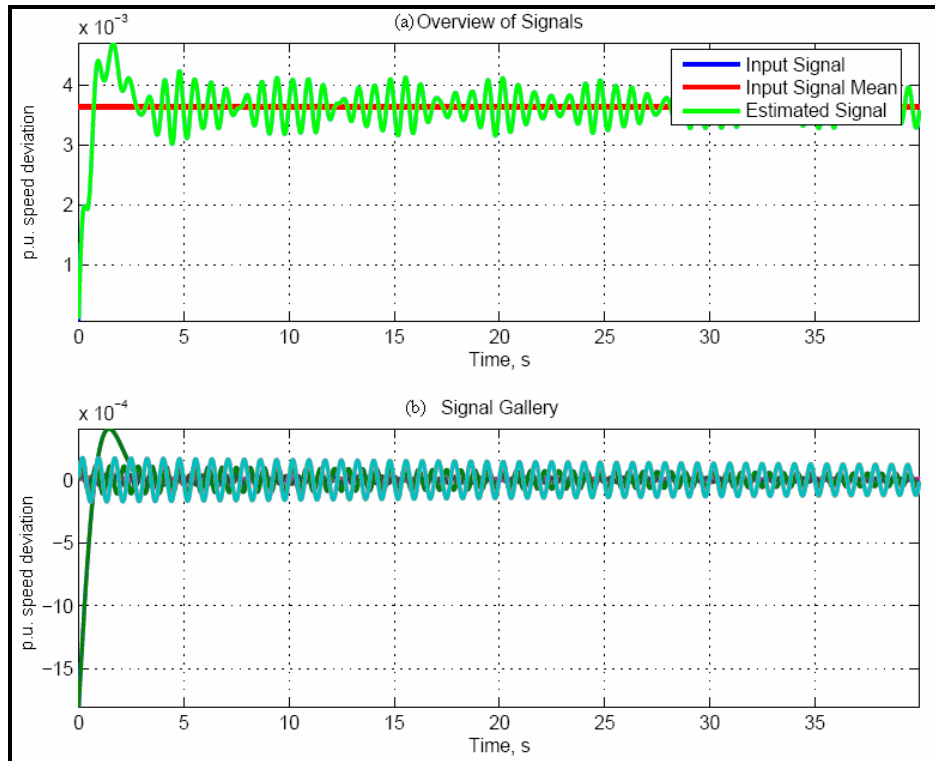


Figure 5.10: 201-204 line outage: (a) machine 3 estimated vs. measured speed signal; (b) display of each oscillatory component

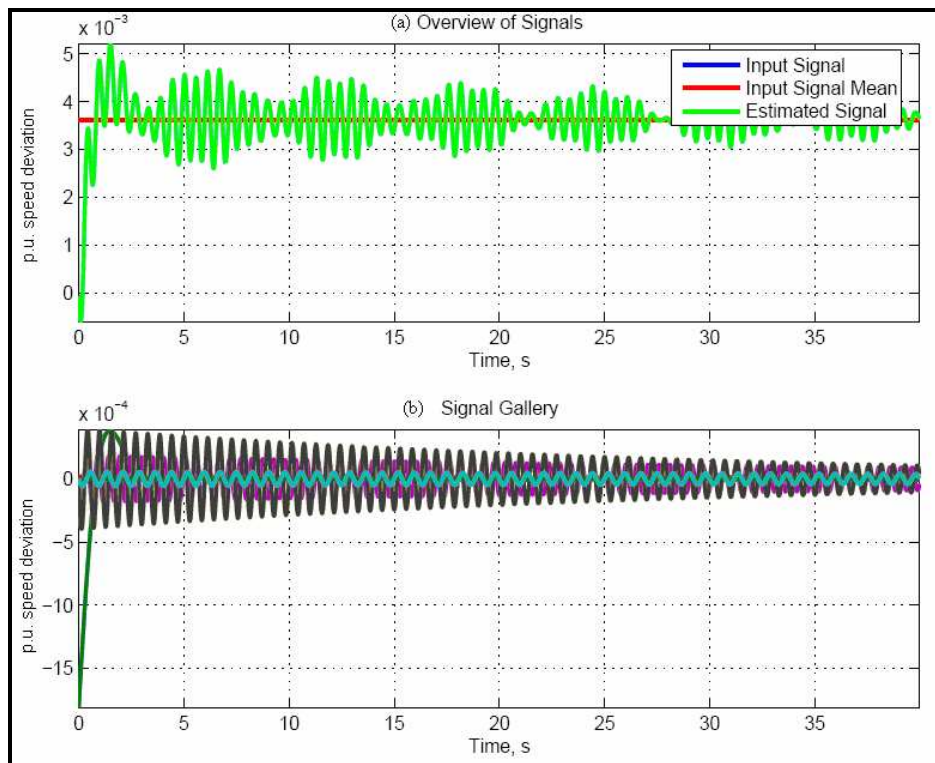


Figure 5.11: 201-204 line outage: (a) machine 4 estimated vs. measured speed signal; (b) display of each oscillatory component

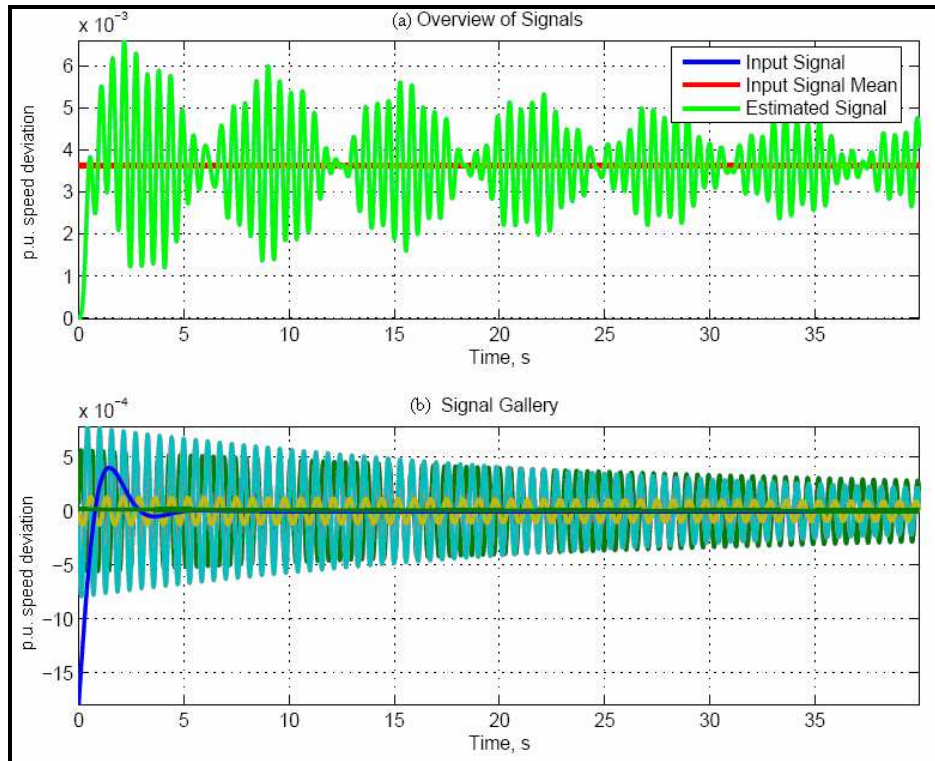


Figure 5.12: 201-204 line outage: (a) machine 5 estimated vs. measured speed signal; (b) display of each oscillatory component

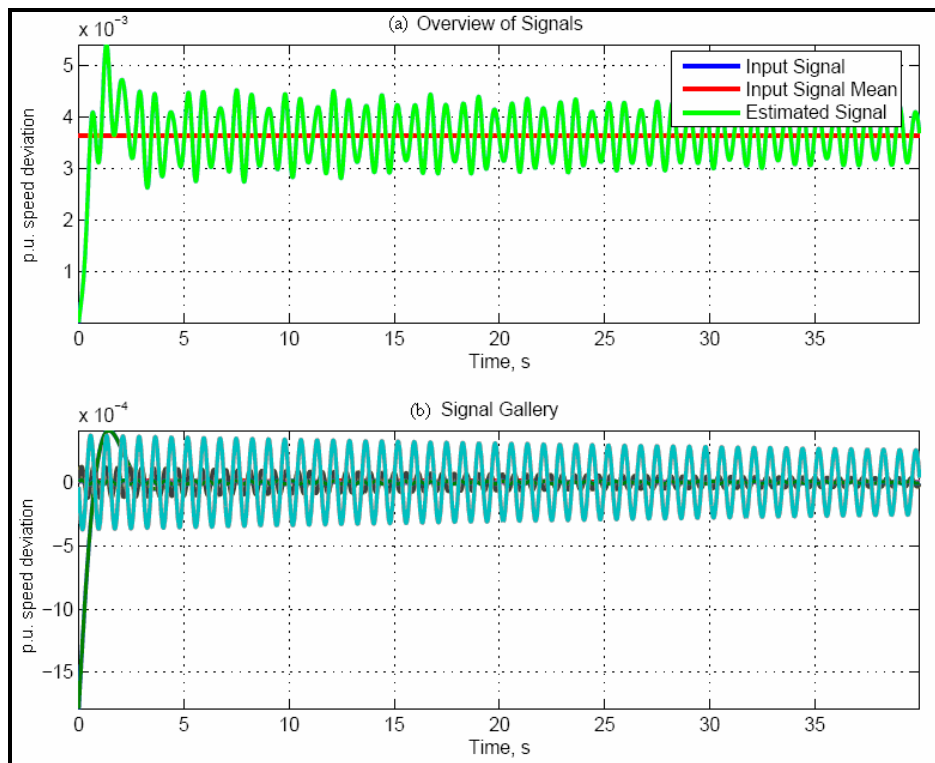


Figure 5.13: 201-204 line outage: (a) machine 6 estimated vs. measured speed signal; (b) display of each oscillatory component

5.3.3 3003-3005 line outage

The 3003-3005 line outage is a 267 MW interruption in flow. The q-point calculation for this disturbance yields a $\Delta\omega$ value of 0.00077830 p.u. which corresponds to 46.7 mHz. The measured value from the simulation was 0.000867 p.u. (52.1 mHz).

The steady state post-disturbance angles for the system were calculated to be

$$\begin{aligned}
 \delta_1 &= 2.6774^\circ \\
 \delta_2 &= 2.6774^\circ \\
 \delta_3 &= 0.1375^\circ \\
 \delta_4 &= -8.4066^\circ \\
 \delta_5 &= -3.3831^\circ \\
 \delta_6 &= 13.6800^\circ
 \end{aligned} \tag{5.20}$$

The synchronizing power matrix was determined to be

$$\mathbf{S}_p = \begin{bmatrix} -81.8046 & 32.6271 & 19.3181 & 16.7399 & 2.0722 & 11.0472 \\ 32.6271 & -81.8046 & 19.3181 & 16.7399 & 2.0722 & 11.0472 \\ 19.4550 & 19.4550 & -69.7022 & 18.4222 & 2.0963 & 10.2737 \\ 27.8080 & 27.8080 & 29.6836 & -119.0923 & 7.0205 & 26.7721 \\ 20.8991 & 20.8991 & 20.5203 & 41.6162 & -135.7732 & 31.8386 \\ 11.7109 & 11.7109 & 10.5332 & 15.5751 & 3.2877 & -52.8179 \end{bmatrix} \tag{5.21}$$

The eigenvalues of the plant matrix formed by the partitions are

$$\begin{aligned}
 \sigma(\mathbf{A}) = \{ &\lambda_1 = -0.0293 \pm j12.3221, \lambda_2 = -0.0210 \pm j11.3853, \\ &\lambda_3 = -0.0406 \pm j10.9213, \lambda_4 = -0.0202 \pm j9.5083, \\ &\lambda_5 = -0.0107 \pm j8.0185, \lambda_6 = 0.0000, \lambda_7 = -0.9709 \pm j1.4636, \\ &\lambda_8 = -1.9188, \lambda_9 = -1.8958 \}
 \end{aligned} \tag{5.22}$$

Table 5.10: comparison of modal properties for 3003-3005 line outage, mode 1

Calculated Values			Simulation Values			f_{damp} average error
$ \Delta\omega_i $	$\angle\Delta\omega_i$	f_{damp} (Hz)	$ \Delta\omega_i $	$\angle\Delta\omega_i$	f_{damp} (Hz)	
1.000	0	1.9611	1.000	0	1.9679	-0.0035
1.000	0		1.000	0	1.9679	
1.211	-1		1.193	2	1.9680	
10.222	-181		10.770	-179	1.9680	
21.249	-4		22.136	4	1.9680	
0.539	2					

$$\lambda_1 = -0.0293 \pm j12.3221$$

Table 5.11: comparison of modal properties for 3003-3005 line outage, mode 2

Calculated Values			Simulation Values			f_{damp} average error
$ \Delta\omega_i $	$\angle\Delta\omega_i$	f_{damp} (Hz)	$ \Delta\omega_i $	$\angle\Delta\omega_i$	f_{damp} (Hz)	
1.000	0	1.8120	1.000	0	1.8175	-0.0030
1.000	0		1.000	0	1.8175	
1.129	-1		1.136	2	1.8175	
4.692	179		4.717	-179	1.8175	
15.230	182		15.387	-182	1.8175	
1.142	0		1.137	1	1.8174	

$$\lambda_2 = -0.0210 \pm j11.3853$$

Table 5.12: comparison of modal properties for 3003-3005 line outage, mode 4

Calculated Values			Simulation Values			f_{damp} average error
$ \Delta\omega_i $	$\angle\Delta\omega_i$	f_{damp} (Hz)	$ \Delta\omega_i $	$\angle\Delta\omega_i$	f_{damp} (Hz)	
1.000	0	1.5133	1.000	0	1.5186	-0.0035
1.000	0		1.000	0	1.5186	
1.806	-181		1.748	177	1.5186	
0.027	-213					
0.017	64					
0.110	-173					

$$\lambda_4 = -0.0202 \pm j9.5083$$

Table 5.13: comparison of modal properties for 3003-3005 line outage, mode 5

Calculated Values			Simulation Values			f_{damp} average error
$ \Delta\omega_i $	$\angle\Delta\omega_i$	f_{damp} (Hz)	$ \Delta\omega_i $	$\angle\Delta\omega_i$	f_{damp} (Hz)	
1.000	0	1.2762	1.000	0	1.2781	-0.0015
1.000	0		1.000	0	1.2781	
1.258	2		1.252	-2	1.2781	
0.079	10		0.085	-10	1.2781	
0.425	178		0.419	182	1.2781	
3.178	180		3.172	180	1.2781	

$$\lambda_5 = -0.0107 \pm j8.0185$$

Tables 5.10 through 5.13 list the modal characteristics of all of the oscillatory modes shown in equation (5.21). As in section 5.3.1 and 5.3.2 there exists a two-machine-only mode, that is, a mode in which only machines one and two participate. It is mode three for this particular disturbance and not listed in the tables. Mode seven, once again, is not included in the tables and blank spaces in cells of the mode four table indicate that no activity for these states was detectable.

Figures 5.14 through 5.18 show the speed deviation waveforms for each of the six machines.

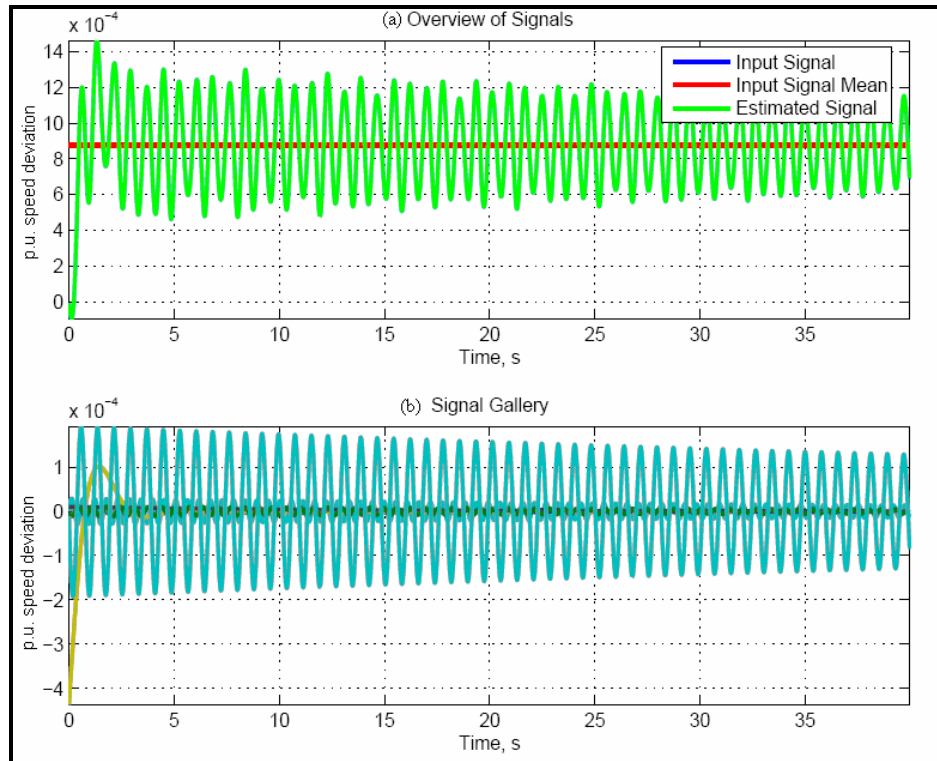


Figure 5.14: 3003-3005 line outage: (a) machines 1 and 2 estimated vs. measured speed signal; (b) display of each oscillatory component

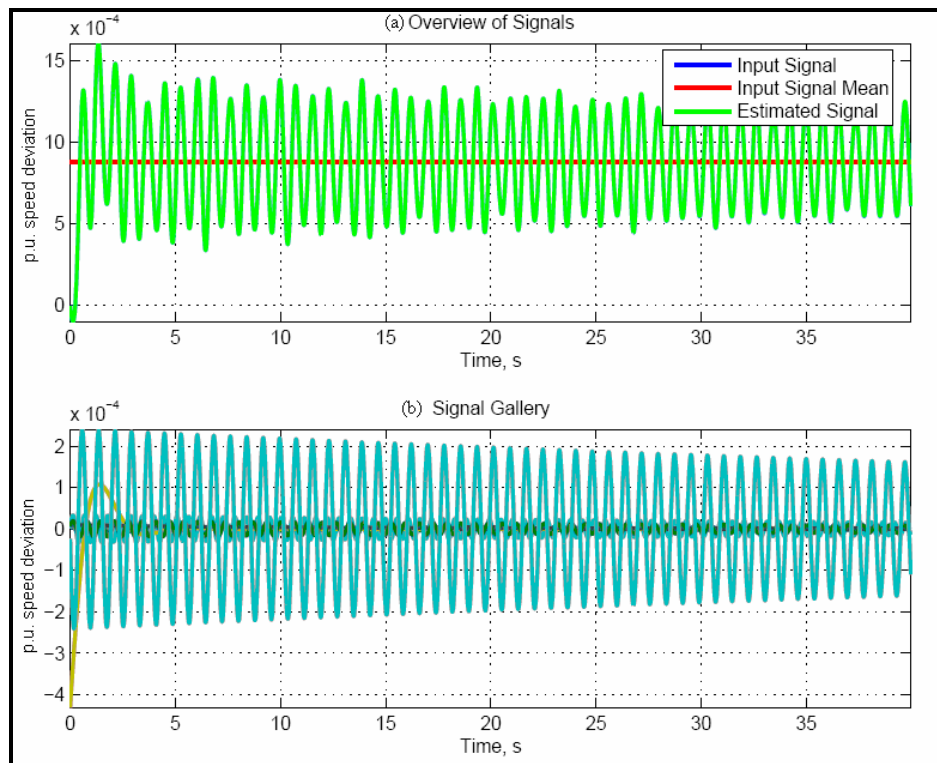


Figure 5.15: 3003-3005 line outage: (a) machine 3 estimated vs. measured speed signal; (b) display of each oscillatory component

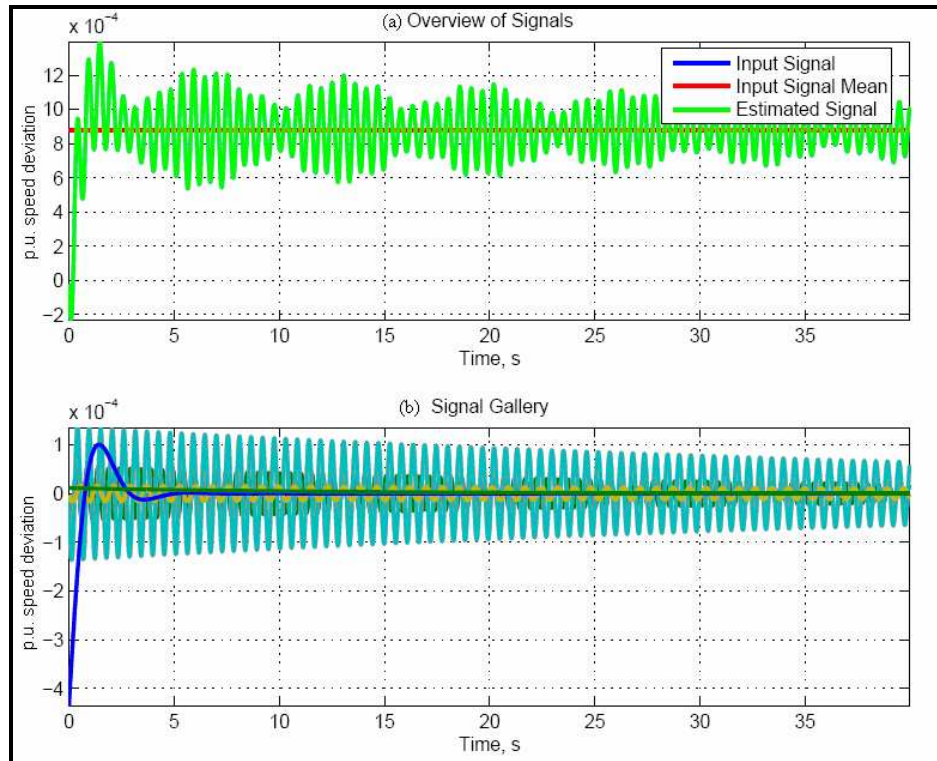


Figure 5.16: 3003-3005 line outage: (a) machine 4 estimated vs. measured speed signal; (b) display of each oscillatory component

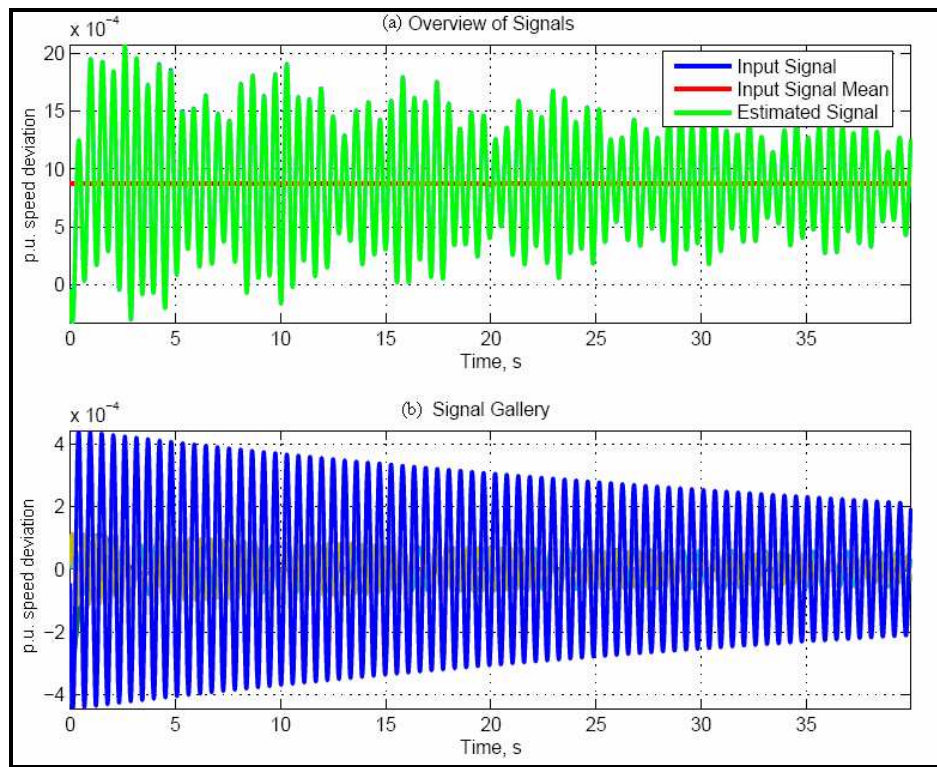


Figure 5.17: 3003-3005 line outage: (a) machine 5 estimated vs. measured speed signal; (b) display of each oscillatory component

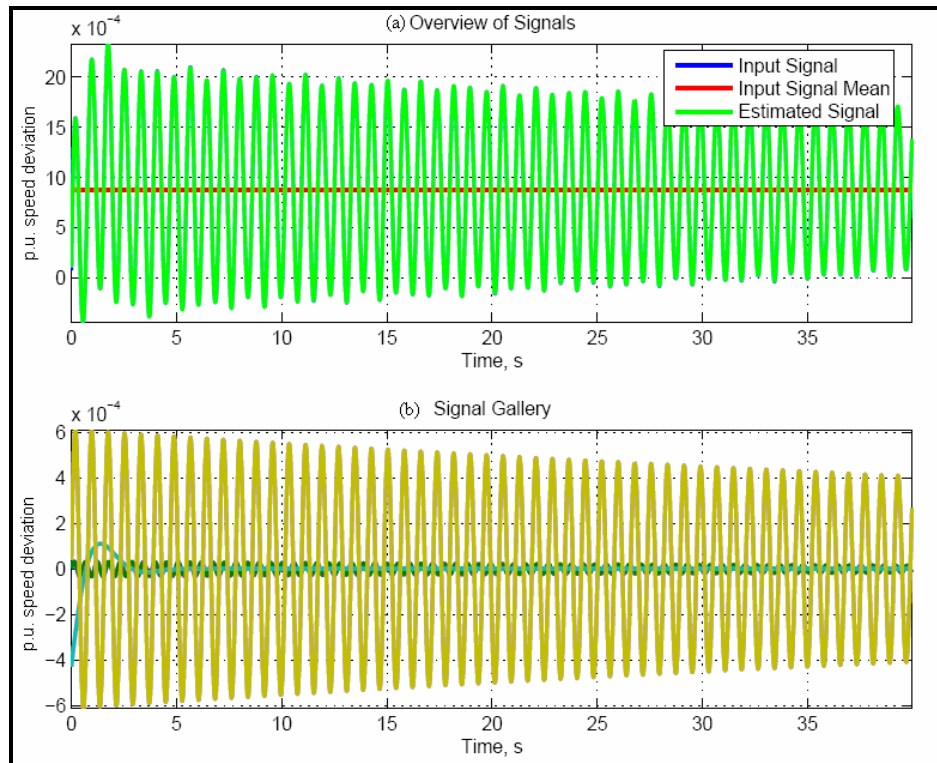


Figure 5.18: 3003-3005 line outage: (a) machine 6 estimated vs. measured speed signal; (b) display of each oscillatory component

5.3.4 3005-3006 line outage

The 3005-3006 line outage is a 27 MW interruption in flow, the smallest interruption of all of the test cases. In terms of interconnection disturbances this interruption accounts for about one percent of system demand, thus making it possibly the most realistic of all of the interruptions at least in comparison to North American interconnections. The q-point calculation for this disturbance yields a $\Delta\omega$ value of 0.0000796 p.u. which corresponds to 4.8 mHz. The measured value from the simulation was 0.0000155 p.u. (9.3 mHz). The steady state post-disturbance angles for the system were calculated to be

$$\begin{aligned}\delta_1 &= 7.5268^\circ \\ \delta_2 &= 7.5268^\circ\end{aligned}$$

$$\begin{aligned}
\delta_3 &= 4.6076^\circ \\
\delta_4 &= -3.6027^\circ \\
\delta_5 &= 1.0338^\circ \\
\delta_6 &= 13.6800^\circ
\end{aligned} \tag{5.23}$$

The synchronizing power matrix was determined to be

$$\mathbf{S}_p = \begin{bmatrix} -82.1001 & 32.8817 & 19.5016 & 16.9232 & 1.9410 & 10.8526 \\ 32.8817 & -82.1001 & 19.5016 & 16.9232 & 1.9410 & 10.8526 \\ 19.6643 & 19.6643 & -70.1836 & 18.6157 & 1.9859 & 10.2533 \\ 27.9493 & 27.9493 & 29.7513 & -120.4148 & 6.7749 & 27.9900 \\ 19.6839 & 19.6839 & 19.4435 & 40.4537 & -136.8886 & 37.6236 \\ 12.0908 & 12.0908 & 11.0232 & 17.5323 & 4.1466 & -56.8836 \end{bmatrix} \tag{5.24}$$

The eigenvalues of the plant matrix formed by the partitions are

$$\begin{aligned}
\sigma(\mathbf{A}) = \{ &\lambda_1 = -0.0300 \pm j12.3584, \lambda_2 = -0.0193 \pm j11.4970, \\ &\lambda_3 = -0.0404 \pm j10.9465, \lambda_4 = -0.0200 \pm j9.5387, \\ &\lambda_5 = -0.0104 \pm j8.2007, \lambda_6 = 0.0000, \lambda_7 = -0.9721 \pm j1.4778, \\ &\lambda_8 = -1.9191, \lambda_9 = -1.8963 \}
\end{aligned} \tag{5.23}$$

Tables 5.14 through 5.17 list the corresponding modal characteristics and figures 5.19 through 5.23 show associated speed waveforms.

Table 5.14: comparison of modal properties for 3005-3006 line outage, mode 1

Calculated Values			Simulation Values			f_{damp} average error
$ \Delta\omega_i $	$\angle\Delta\omega_i$	f_{damp} (Hz)	$ \Delta\omega_i $	$\angle\Delta\omega_i$	f_{damp} (Hz)	
1.000	0	1.9669	1.000	0	1.9749	-0.0041
1.000	0		1.000	0	1.9749	
1.211	-1		1.199	1	1.9749	
10.222	-181		9.845	-179	1.9749	
21.249	-4		19.880	4	1.9750	
0.539	2		0.551	-4	1.9748	

$$\lambda_1 = -0.0300 \pm j12.3584$$

Table 5.15: comparison of modal properties for 3005-3006 line outage, mode 2

Calculated Values			Simulation Values			f_{damp} average error
$ \Delta\omega_i $	$\angle\Delta\omega_i$	f_{damp} (Hz)	$ \Delta\omega_i $	$\angle\Delta\omega_i$	f_{damp} (Hz)	
1.000	0	1.8298	1.000	0	1.8366	-0.0037
1.000	0		1.000	0	1.8366	
1.153	-1		1.156	2	1.8367	
5.028	-182		5.031	-178	1.8367	
17.073	-178		17.057	-182	1.8367	
1.619	0		1.619	0	1.8367	

$$\lambda_2 = -0.0193 \pm j11.4970$$

Table 5.16: comparison of modal properties for 3005-3006 line outage, mode 4

Calculated Values			Simulation Values			f_{damp} average error
$ \Delta\omega_i $	$\angle\Delta\omega_i$	f_{damp} (Hz)	$ \Delta\omega_i $	$\angle\Delta\omega_i$	f_{damp} (Hz)	
1.000	0	1.5181	1.000	0	1.5238	-0.0038
1.000	0		1.000	0	1.5238	
1.810	-181		1.808	181	1.5239	
0.032	-205		0.000			
0.024	-205		0.000			
0.108	-172		0.000			

$$\lambda_4 = -0.0200 \pm j9.5387$$

Table 5.17: comparison of modal properties for 3005-3006 line outage, mode 5

Calculated Values			Simulation Values			f_{damp} average error
$ \Delta\omega_i $	$\angle\Delta\omega_i$	f_{damp} (Hz)	$ \Delta\omega_i $	$\angle\Delta\omega_i$	f_{damp} (Hz)	
1.000	0	1.3052	1.000	0	1.3091	-0.0030
1.000	0		1.000	0	1.3091	
1.241	3		1.238	-2	1.3091	
0.054	-195		0.053	-164	1.3091	
0.858	-180		0.859	-179	1.3091	
3.220	-179		3.218	-180	1.3091	

$$\lambda_5 = -0.0104 \pm j8.2007$$

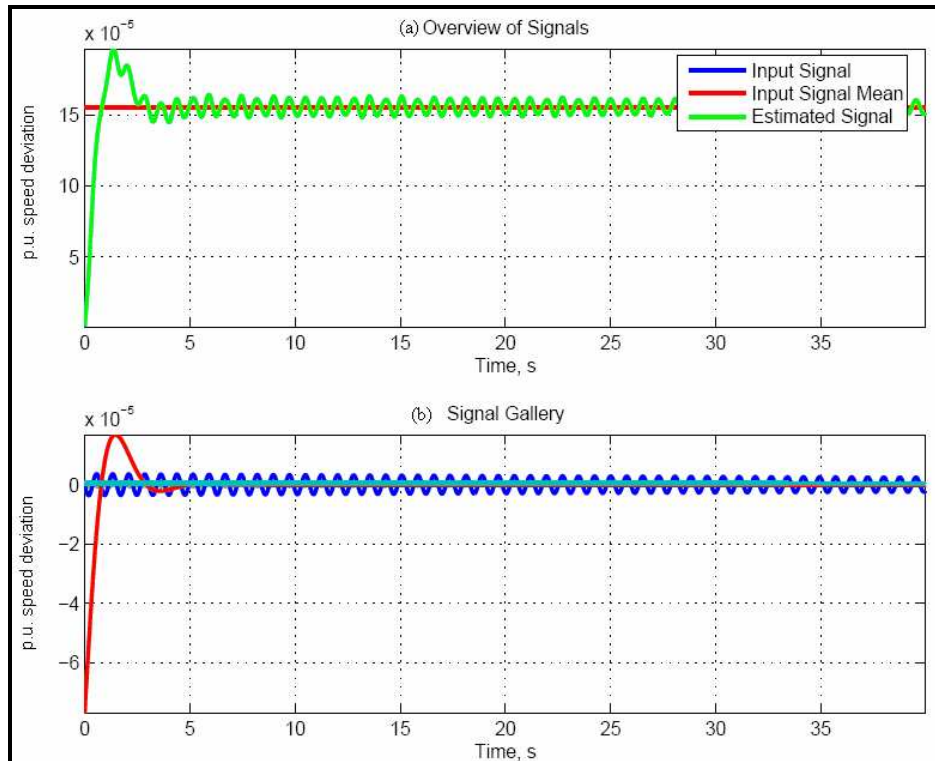


Figure 5.19: 3005-3006 line outage: (a) machines 1 and 2 estimated vs. measured speed signal; (b) display of each oscillatory component

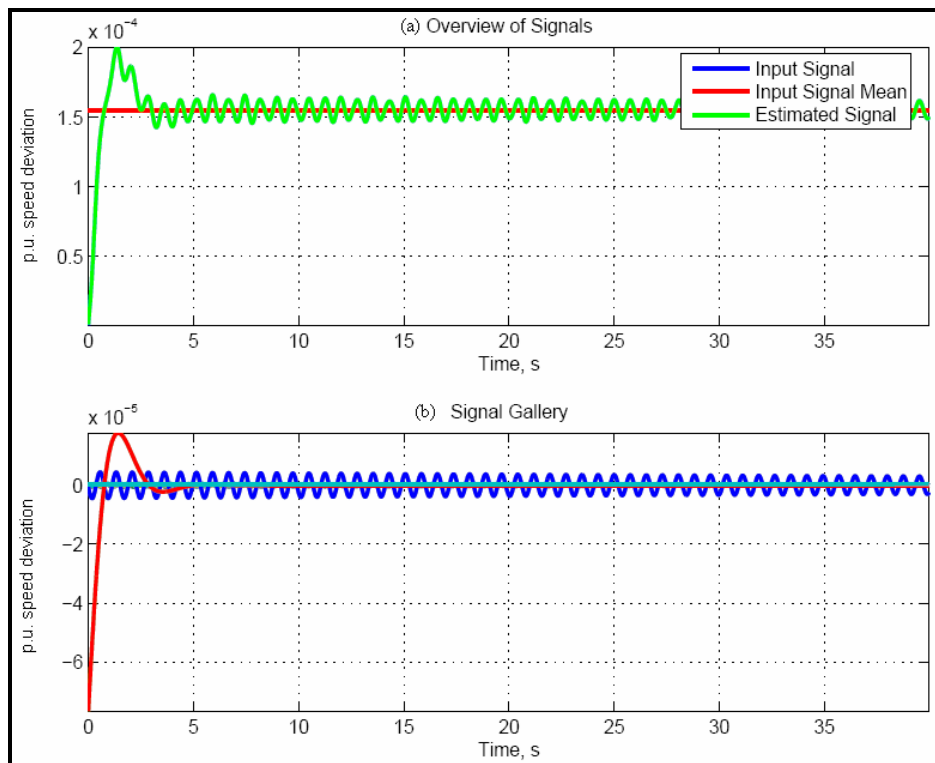


Figure 5.20: 3005-3006 line outage: (a) machine 3 estimated vs. measured speed signal; (b) display of each oscillatory component

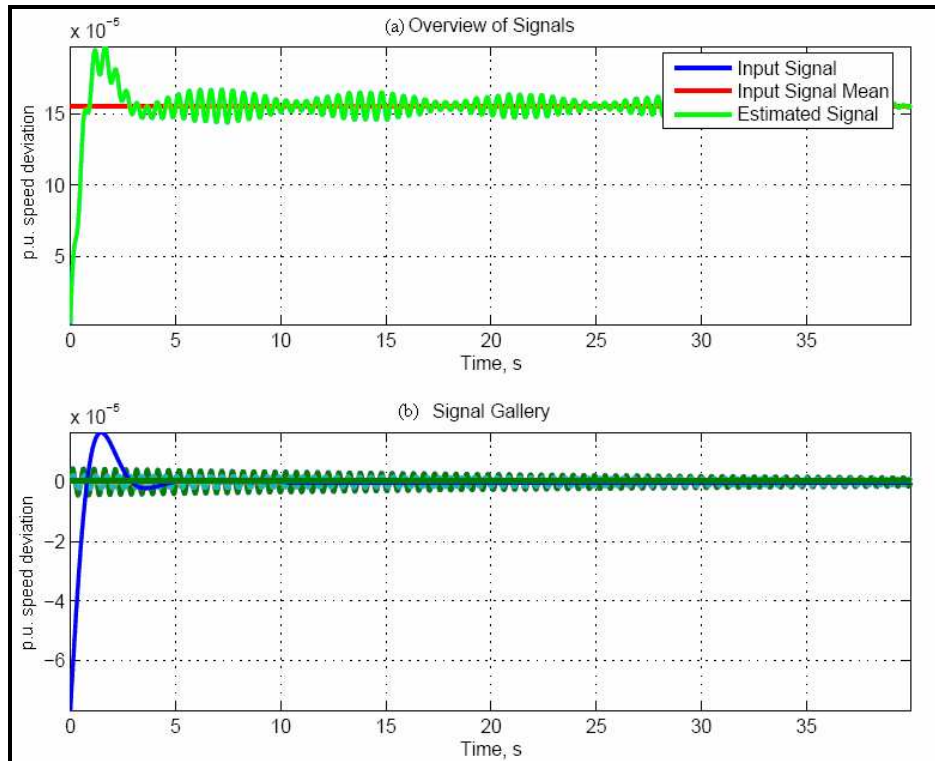


Figure 5.21: 3005-3006 line outage: (a) machine 4 estimated vs. measured speed signal; (b) display of each oscillatory component

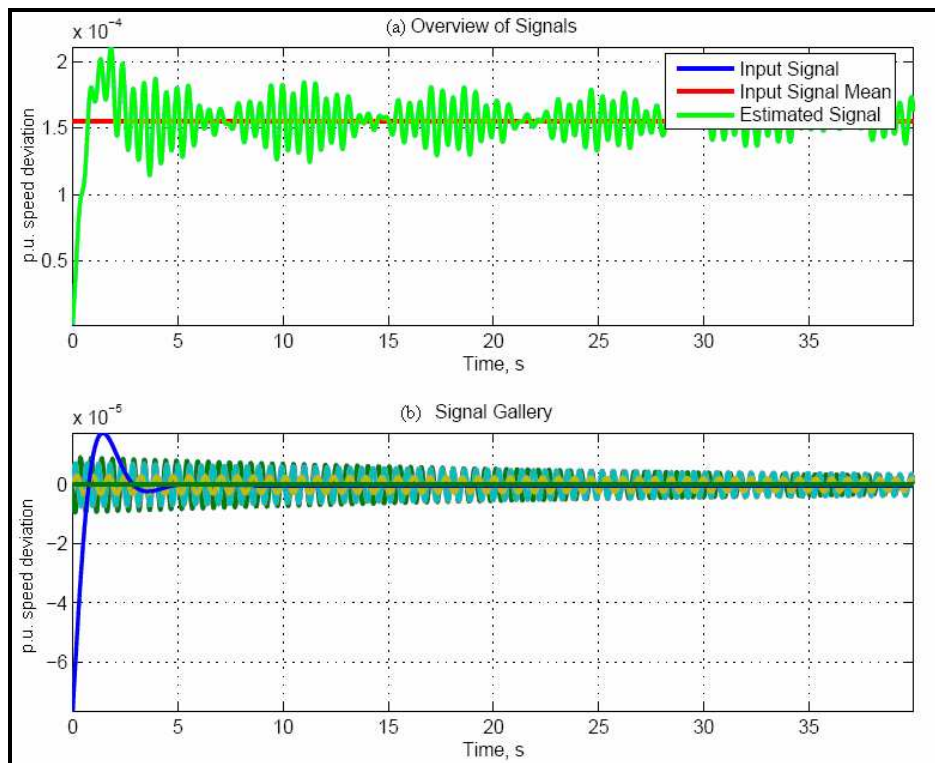


Figure 5.22: 3005-3006 line outage: (a) machine 5 estimated vs. measured speed signal; (b) display of each oscillatory component

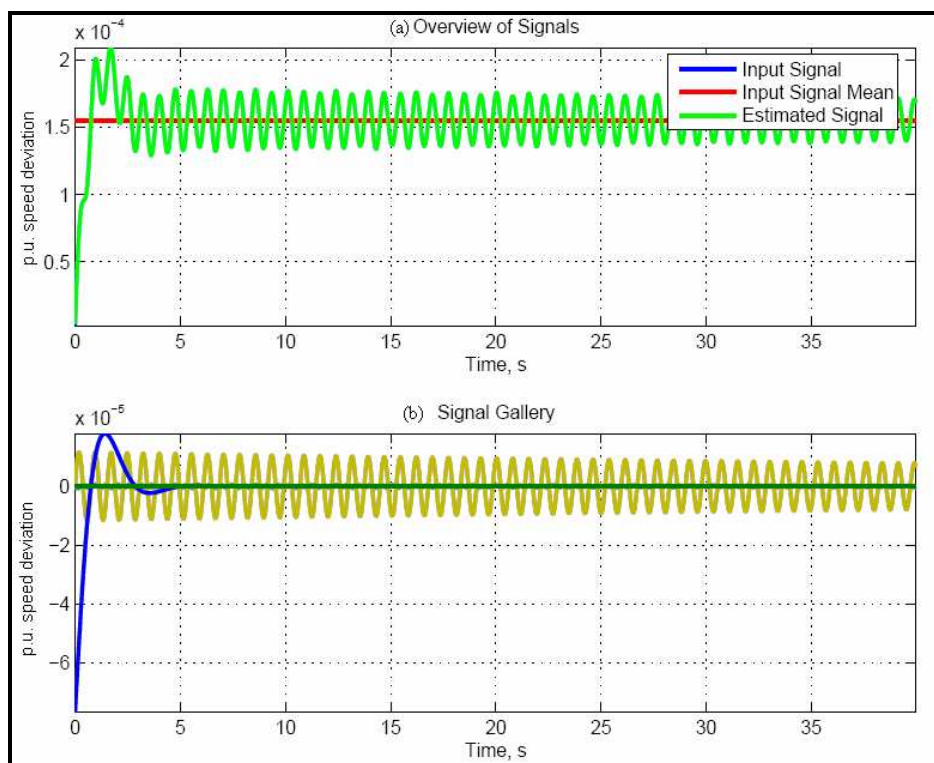


Figure 5.23: 3005-3006 line outage: (a) machine 6 estimated vs. measured speed signal; (b) display of each oscillatory component

5.3.5 Final Remarks and Conclusions Concerning Predicted and Simulated Results

All of the preceding subsections of section 5.3 demonstrate the accuracy of the state-space model used to predict oscillation frequencies, and mode shapes – including both magnitude and phase – of the generator speeds for the line outages listed in table 5.1. Since the model used is a small-signal model, it is a curious feature of the simulation results that the more severe disturbances actually have better oscillation frequency accuracies than the least severe disturbance, the 27MW 3005-3006 outage. It is my belief that the reason for this greater accuracy is due to the more accurate q-point determinations for more severe disturbances. The lack of accuracy for lesser disturbances may be attributable to a very slight inaccuracy – or possibly just an inconsistency in the 23-bus system's admittance matrix. A slight mismatch in calculated

power drawn by the system from the six generators will lead to greater and greater errors percentage-wise in the q-point frequency as the disturbance level approaches zero MW. For example all of the disturbances have a difference in q-point frequency (between calculated and measured from simulation) of about five to ten mHz. If the disturbance results in a 200mHz change in frequency, the error in q-point speed is a few percent. If the disturbance results in a 10mHz change in frequency, the error is over 100%. However, the calculated q-point still yields results that may be considered decent since the errors are less than five percent.

Use of the oscillation frequencies alone for disturbance identification appears feasible except possibly in the case of distinguishing in between the two line outages that are connected to bus 3005. The mode shapes for these two outages are also very similar – however they are distinguishable from the other two outages. And, they could possibly be distinguished from each other on the basis of the q-point calculation – there is a drastic difference in q-point frequency deviation.

The result of the entire process of using natural response frequencies as a disturbance identifier should be expected to result in distinguishing groups of disturbances instead of necessarily being able to distinguish between each of the individual disturbances. It can be expected, however, that on certain systems, there is a particular set of disturbances that occur more frequently than others. This fact should allow more confidence in using this method as statistical analysis could be coupled with modal analysis in disturbance identification.

It is most important to point out that the results presented in section 5.3 are only a verification of the state-space model. They do not present any verification of measured

values, measured values being the frequencies at a collection of buses. The states are not frequencies and thus cannot be assumed to be measured values. In fact all of the developments in the work presume the availability of frequency measurements and it has been assumed in all of section 5.3 that the frequency measurements should be related to machine speed (the states) in a linear fashion. This assumption is per the developments in chapter two.

In order to verify the assumption as was done in chapter three for the idealized system, a set of frequency measurements and their oscillation frequencies are presented in tables 5.18 through 5.21. Frequency measurement units are placed at buses 151, 201, 205, 3008, and 3001. For each mode, the calculated frequency is shown in bold-face type above the sub-chart for the corresponding mode. The measured oscillation frequency at each one of the buses is displayed with its error on the calculated oscillation frequency base. Wherever an “x” is listed in the table, the corresponding oscillatory component was undetected by the Matrix Pencil at that bus. It may be seen that the four disturbances can be distinguished from each other by the measured oscillation frequencies. The 3003-3005 and 3005-3006 disturbances have close oscillation frequencies in all of the modes save the lowest frequency mode. All other disturbances have at least noticeable, if not substantial differences in all oscillation frequencies for all modes.

As with the *state* oscillation frequencies that were examined in section 5.3, the *measurement* oscillation frequencies also fall within less than one half of one percent of the calculated oscillation frequencies. Thus the simulation results verify the hypothesis proposed in chapter two that frequency measurements are linearly proportional to

machine speeds. Thus, frequency measurements may be used to identify modes in which machine speeds participate. Not shown in the charts is a 2.556 Hz mode that was detected at buses 205 and 3008 this frequency is, for all practical purposes, right at double the natural frequency of the 1.2762 Hz mode. The very high frequency mode may indicate that the system is being pushed far enough away from the q-point to exhibit non-linear behavior. One must be careful in this case concerning non-linearities as such behavior should show up in the states even more prominently than in the measurements. This double-frequency mode does not, in fact, show up in the states. Thus the 2.556 Hz - mode may be attributable to signal processing problems. The magnitudes of the 2.556 Hz measurement quantities are on the order of 10 microhertz thus they are not included in the data shown here.

Table 5.18: oscillation frequency of simulated measurements: 151-152 outage

151-152 Outage					
1.9328 Hz mode			1.7875 Hz mode		
Bus	Measured f	error	Bus	Measured f	error
151	1.9384	-0.0029	151	1.7920	-0.0025
201	1.9377	-0.0025	201	1.7912	-0.0020
205	1.9374	-0.0024	205	1.7909	-0.0019
3008	1.9378	-0.0026	3008	1.7909	-0.0019
3001	x		3001	x	
1.4752 Hz mode			1.2881 Hz mode		
Bus	Measured f	error	Bus	Measured f	error
151	1.4782	-0.0020	151	1.2890	-0.0007
201	1.4784	-0.0022	201	1.2890	-0.0007
205	1.4785	-0.0023	205	1.2891	-0.0008
3008	1.4788	-0.0024	3008	1.2891	-0.0008
3001	1.4783	-0.0021	3001	1.2890	-0.0007

Table 5.19: oscillation frequency of simulated measurements: 201-204 outage

201-204 Outage		
1.9078 Hz mode		
Bus	Measured f	error
151	1.9114	-0.0019
201	1.9112	-0.0018
205	1.9109	-0.0016
3008	1.9112	-0.0018
3001	1.9112	-0.0018
1.4958 Hz mode		
Bus	Measured f	error
151	1.4994	-0.0024
201	1.4988	-0.0020
205	1.5001	-0.0029
3008	1.5012	-0.0036
3001	1.4982	-0.0016
1.7469 Hz mode		
Bus	Measured f	error
151	1.7498	-0.0017
201	1.7493	-0.0014
205	1.7491	-0.0013
3008	1.7491	-0.0013
3001	1.7482	-0.0007
1.2988 Hz mode		
Bus	Measured f	error
151	1.2995	-0.0006
201	1.2995	-0.0006
205	1.2996	-0.0006
3008	1.2996	-0.0006
3001	1.2996	-0.0006

Table 5.20: oscillation frequency of simulated measurements: 3003-3005 outage

3003-3005 Outage		
1.9611 Hz mode		
Bus	Measured f	error
151	1.9680	-0.0035
201	1.9680	-0.0035
205	1.9680	-0.0035
3008	1.9680	-0.0035
3001	x	
1.5133 Hz mode		
Bus	Measured f	error
151	1.5185	-0.0035
201	1.5185	-0.0034
205	x	
3008	x	
3001	x	
1.8120 Hz mode		
Bus	Measured f	error
151	1.8174	-0.0030
201	1.8175	-0.0030
205	1.8175	-0.0030
3008	1.8175	-0.0030
3001	x	
1.2762 Hz mode		
Bus	Measured f	error
151	1.2781	-0.0015
201	1.2781	-0.0015
205	1.2781	-0.0015
3008	1.2781	-0.0015
3001	1.2781	-0.0015

Table 5.21: oscillation frequency of simulated measurements: 3005-3006 outage

3005-3006 Outage					
1.9669 Hz mode			1.8298 Hz mode		
Bus	Measured f	error	Bus	Measured f	error
151	1.9741	-0.0037	151	1.8352	-0.0030
201	1.9746	-0.0039	201	1.8362	-0.0035
205	1.9748	-0.0040	205	1.8365	-0.0037
3008	1.9744	-0.0038	3008	1.8365	-0.0037
3001	x		3001	x	
1.5181 Hz mode			1.3052 Hz mode		
Bus	Measured f	error	Bus	Measured f	error
151	x		151	1.3091	-0.0030
201	x		201	1.3091	-0.0030
205	x		205	1.3087	-0.0027
3008	x		3008	1.3090	-0.0029
3001	x		3001	1.3091	-0.0030

5.4 Output Matrix Development and Simulation Results

In an effort to supplement the modeling and identification problems presented in the previous sections, this section will focus on forming an output matrix which attempts to translate machine speeds into frequency measurements. A procedure similar to the one used for the simple three-machine system studied in chapter three will be used. The idea behind transforming machine speeds into frequency measurements is that machine angles may be solved for using a load flow analysis. These machine angles, in principle, should be able to be translated into bus angles via linear network analysis and in turn the time-derivatives of the angles will yield machine speeds and bus frequency data. The linearized power flow equations will yield linear relationships between each angle to be determined, whether bus angles or internal voltage angles. The collective

coupled linear equations form a vector-matrix equation in power and angle, thus yielding a matrix transformation from speeds to angles.

For the system shown in figure 5.1 there are a total of 11 buses on the system that require power flow equations to be formulated – six buses are machine internal voltages and five are physical buses on the power system that have frequency meters. After formulating the power equations, linearizing, and assembling the equations in vector-matrix form, the resulting equation may be partitioned to yield the relationship between machine speed and bus frequency.

For each bus, the full AC power flow equation is written as

$$P_i = E_i^2 G_{ii} + \sum_{\substack{j=1 \\ j \neq i}}^n E_i E_j [B_{ij} \sin \delta_{ij} + G_{ij} \cos \delta_{ij}] \quad (5.25)$$

and may be linearized as

$$\Delta P_i(t) = \sum_{\substack{j=1 \\ j \neq i}}^n E_i E_j [B_{ij} \cos \delta_{ij_0} - G_{ij} \sin \delta_{ij_0}] \Delta \delta_{ij}(t) \quad (5.26)$$

and assembled in vector-matrix form for the equivalent 11-bus system as

$$\begin{bmatrix} \Delta P_1 \\ \vdots \\ \Delta P_6 \\ \Delta P_7 \\ \vdots \\ \Delta P_{11} \end{bmatrix} = \begin{bmatrix} T_{11} & \cdots & T_{16} & T_{17} & \cdots & T_{1-11} \\ \vdots & \ddots & \vdots & \vdots & \ddots & \vdots \\ T_{61} & \cdots & T_{66} & T_{67} & \cdots & T_{6-11} \\ T_{71} & \cdots & T_{76} & T_{77} & \cdots & T_{7-11} \\ \vdots & \ddots & \vdots & \vdots & \ddots & \vdots \\ T_{11-1} & \cdots & T_{11-6} & T_{11-7} & \cdots & T_{11-11} \end{bmatrix} \bullet \begin{bmatrix} \Delta \delta_1 \\ \vdots \\ \Delta \delta_6 \\ \Delta \delta_7 \\ \vdots \\ \Delta \delta_{11} \end{bmatrix} \quad (5.27)$$

Each off-diagonal term in the coefficient matrix, T_{ij} , is technically a transmission stiffness coefficient [4] as an incremental change in power from the i th bus toward the j th bus for a given change in angle at the j th bus. Each of these terms takes on the same

form mathematically as a synchronizing power coefficient. However the physical meaning of a stiffness coefficient is subtly different as each bus does not necessarily have mass connected to it and thus synchronizing does not necessarily take place. The off-diagonal terms may be expressed as

$$T_{ij} = -E_i E_j [B_{ij} \cos \delta_{ij_0} - G_{ij} \sin \delta_{ij_0}] \quad (5.28)$$

Diagonal terms take on the form

$$T_{ii} = \sum_{\substack{j=1 \\ j \neq i}}^n E_i E_j [B_{ij} \cos \delta_{ij_0} - G_{ij} \sin \delta_{ij_0}] \quad (5.29)$$

The conductance and susceptance terms in (5.26) and (5.27) are terms that must come from the 11 x 11 admittance matrix that is the result of the original 23 x 23 matrix reduced to an 11 x 11 system. This procedure is a Kron reduction as was done to reduce the system to a 6 x 6 in the analyses done previously. This matrix must be the post-fault matrix of the system.

The first six terms in the power and angle vectors of equation (5.27) must be understood as power flows and angles associated with the six machines on the power system. The last six terms are associated with the physical buses where frequencies are being monitored. These frequency measurements are considered to be output quantities in the power system's state model.

In order to manipulate (5.25) to yield a relationship that associates machine speeds with frequency measurements, the partitions are written in compact form as follows

$$\begin{bmatrix} \Delta \mathbf{P}_s \\ \Delta \mathbf{P}_m \end{bmatrix} = \begin{bmatrix} \mathbf{T}_{11} & \mathbf{T}_{12} \\ \mathbf{T}_{21} & \mathbf{T}_{22} \end{bmatrix} \bullet \begin{bmatrix} \Delta \boldsymbol{\delta}_s \\ \Delta \boldsymbol{\delta}_m \end{bmatrix} \quad (5.30)$$

Recognizing that $\Delta \mathbf{P}_m$ is identically equal to a zero vector in \mathbf{R}^5 as the loads are accounted for in the admittance matrix, the bottom-row equation partition may be expressed as

$$\mathbf{0} = \mathbf{T}_{21} \Delta \boldsymbol{\delta}_s + \mathbf{T}_{22} \Delta \boldsymbol{\delta}_m \quad (5.31)$$

From equation (5.31) the measurement angles may be expressed as

$$\Delta \boldsymbol{\delta}_m = -\mathbf{T}_{22}^{-1} \mathbf{T}_{21} \Delta \boldsymbol{\delta}_s \quad (5.32)$$

and taking the derivative of both sides of (5.30) with respect to time yields

$$\Delta \boldsymbol{\omega}_m(t) = -\mathbf{T}_{22}^{-1} \mathbf{T}_{21} \Delta \boldsymbol{\omega}_s(t) \quad (5.33)$$

Careful examination of (5.31) shows conformable vector-matrix multiplication. Further, examination of the terms of the matrix \mathbf{T}_{22} reveals that it is always invertible for a well-conditioned system – it will be a strictly diagonally dominant matrix if all of the T_{ij} terms are negative. In the case of a lossless system \mathbf{T}_{22} will invert as long as at least two off-diagonal terms per row are non-zero. In the case when the diagonal elements are zero, the system's load-flow Jacobian matrix will not invert and the proposed system state is not even in a valid.

The system's output matrix will be designated as \mathbf{C}

$$\mathbf{C} = -\mathbf{T}_{22}^{-1} \mathbf{T}_{21} \quad (5.34)$$

and the complete linear state equation for the electromechanical system is

$$\begin{bmatrix} \dot{\Delta \boldsymbol{\delta}}(t) \\ \dot{\Delta \boldsymbol{\omega}}(t) \\ \dot{\Delta \mathbf{P}}_m(t) \end{bmatrix} = \begin{bmatrix} \mathbf{0} & \mathbf{I} & \mathbf{0} \\ \mathbf{S}_p & \mathbf{D} & \mathbf{H}^{-1} \\ \mathbf{0} & \mathbf{R}^{-1} & \boldsymbol{\Lambda} \end{bmatrix} \bullet \begin{bmatrix} \Delta \boldsymbol{\delta}(t) \\ \Delta \boldsymbol{\omega}(t) \\ \Delta \mathbf{P}_m(t) \end{bmatrix} \quad (5.35)$$

$$\Delta \mathbf{y}(t) = \mathbf{C} \Delta \boldsymbol{\omega}(t)$$

where it is understood that the output vector $\Delta \mathbf{y}(t)$ is a vector of frequency deviations at the selected buses.

Notice from equations (5.28) and (5.29) that for each disturbance that is to be analyzed the output matrix must be reformulated just as the plant matrix must be reformulated. This is because of two reasons: 1) the system's post-fault admittance matrix is generally different for each disturbance; and 2) the post-fault q-point angles will generally be different for each disturbance. Since each term in the output matrix depends on both the q-point angles and terms from the admittance matrix, it must be completely recalculated for each disturbance.

The effectiveness of this technique will be demonstrated for all four of the disturbances analyzed in sections 5.3.1 through 5.3.4. Matrix pencil results from the simulation for machine speeds in each mode will be used as input quantities – machine speed residues (magnitude and phase for each machine in each oscillatory mode) will be assembled into an input vector, $\Delta \boldsymbol{\omega}_s$, which will be acted upon by the output matrix. Since each component of the $\Delta \boldsymbol{\omega}_s$ vector is a residue, and thus a phasor, both the component's magnitude and phase must be entered into the vector. A phasor analysis is able to be performed for each mode separately due to the superposition of the modes. The results of this transformation will be compared with the simulation results for the frequency quantities measured.

Results are shown in tables 5.22 through 5.25. All of the lowest frequency modes show decent accuracy with errors typically below five percent indicating both a correct magnitude and correct direction in the output vector space for the calculated value. Other modes have moderate to very low accuracy in the calculated values. Reasons for these

inaccuracies may be multiple. Due to the consistent accuracy demonstrated in the mode shape and oscillation frequency calculations in previous parts of section 5.3 it may be assumed that, although the machine speed calculations determined by the simulator are accurate, that the frequency measurements may be inaccurate. The exact algorithm that the simulator uses to calculate frequency is not known and should be considered suspect at this point. Further, signal processor, Matrix Pencil, appears to be accurate as the simulation-produced signals and the reproduced signals appear to be very close to each other.

As a review of what the modal analysis theory assumes throughout this work, frequency measurements are assumed to be the first time derivative of the angle. This assumption is considered true whether the voltage in question is an internal machine

Table 5.22: frequency residues: calculated vs. simulated-measured, 151-152 outage

151-152 Outage			
1.9328Hz mode			
Bus	calculated $\times 10^{-4}$	measured $\times 10^{-4}$	error
151	0.0344	0.0327	0.0494
201	0.0718	0.0646	0.1003
205	0.2281	0.2115	0.0728
3008	0.0701	0.0577	0.1769
3001	0.0267	0	1.0000
1.7875Hz mode			
Bus	calculated $\times 10^{-4}$	measured $\times 10^{-4}$	error
151	0.0498	0.0377	0.2430
201	0.1263	0.1086	0.1401
205	0.4380	0.4084	0.0676
3008	0.4444	0.4148	0.0666
3001	0.0163	0	1.0000
1.4752Hz mode			
Bus	calculated $\times 10^{-4}$	measured $\times 10^{-4}$	error
151	0.3084	0.2953	0.0425
201	0.1883	0.1904	-0.0112
205	0.0923	0.0934	-0.0119
3008	0.0563	0.0578	-0.0266
3001	0.0155	0.0178	-0.1484
1.2881Hz mode			
Bus	calculated $\times 10^{-3}$	measured $\times 10^{-3}$	error
151	0.0536	0.0518	0.0336
201	0.0324	0.0308	0.0494
205	0.0221	0.0226	-0.0226
3008	0.0539	0.054	-0.0019
3001	0.1746	0.1743	0.0017

Table 5.23: frequency residues: calculated vs. simulated-measured, 201-204 outage

201-204 Outage			
1.9078Hz mode			
Bus	calculated $\times 10^{-4}$	measured $\times 10^{-4}$	error
151	0.0684	0.0485	0.2909
201	0.0993	0.0765	0.2296
205	0.5650	0.5128	0.0924
3008	0.0893	0.0514	0.4244
3001	0.0612	0.0283	0.5376
1.7469Hz mode			
Bus	calculated $\times 10^{-3}$	measured $\times 10^{-3}$	error
151	0.0140	0.0079	0.4357
201	0.0264	0.0195	0.2614
205	0.1725	0.1599	0.0730
3008	0.1463	0.1343	0.0820
3001	0.0031	0.0058	-0.8710
1.4958Hz mode			
Bus	calculated $\times 10^{-4}$	measured $\times 10^{-4}$	error
151	0.1709	0.1697	0.0070
201	0.0676	0.0632	0.0651
205	0.0295	0.0287	0.0271
3008	0.0167	0.0189	-0.1317
3001	0.0536	0.0519	0.0317
1.2988Hz mode			
Bus	calculated $\times 10^{-3}$	measured $\times 10^{-3}$	error
151	0.0477	0.0461	0.0335
201	0.0493	0.0476	0.0345
205	0.0393	0.0388	0.0127
3008	0.0646	0.0639	0.0108
3001	0.1867	0.1859	0.0043

Table 5.24: frequency residues: calculated vs. simulated-measured, 3003-3005 outage

3003-3005 Outage			
1.9611Hz mode			
Bus	calculated $\times 10^{-4}$	measured $\times 10^{-4}$	error
151	0.0292	0.0196	0.3288
201	0.0518	0.0408	0.2124
205	0.1583	0.1415	0.1061
3008	0.0568	0.0419	0.2623
3001	0.0346	0.0000	1.0000
1.8120Hz mode			
Bus	calculated $\times 10^{-4}$	measured $\times 10^{-4}$	error
151	0.0700	0.0482	0.3114
201	0.1569	0.1319	0.1593
205	0.5495	0.5111	0.0699
3008	0.5912	0.5527	0.0651
3001	0.0363	0.0000	1.0000
1.5133Hz mode			
Bus	calculated $\times 10^{-5}$	measured $\times 10^{-5}$	error
151	0.2882	0.2562	0.1110
201	0.0915	0.1190	-0.3005
205	0.0174	0.0000	1.0000
3008	0.0377	0.0000	1.0000
3001	0.0336	0.0000	1.0000
1.2762Hz mode			
Bus	calculated $\times 10^{-3}$	measured $\times 10^{-3}$	error
151	0.0935	0.0896	0.0417
201	0.0825	0.0786	0.0473
205	0.0163	0.0136	0.1656
3008	0.0325	0.0344	-0.0585
3001	0.3101	0.3111	-0.0032

Table 5.25: frequency residues: calculated vs. simulated-measured, 3005-3006 outage

3005-3006 Outage			
1.9611Hz mode			
Bus	calculated $\times 10^{-5}$	measured $\times 10^{-5}$	error
151	0.0226	0.0154	0.3186
201	0.0417	0.0332	0.2038
205	0.1306	0.1175	0.1003
3008	0.0387	0.0287	0.2584
3001	0.0141	0.0000	1.0000
1.8120Hz mode			
Bus	calculated $\times 10^{-6}$	measured $\times 10^{-6}$	error
151	0.1137	0.0704	0.3808
201	0.2471	0.1949	0.2113
205	0.8567	0.7787	0.0910
3008	0.9031	0.8239	0.0877
3001	0.0422	0.0000	1.0000
1.5133Hz mode			
Bus	calculated $\times 10^{-5}$	measured $\times 10^{-5}$	error
151	0.2900	0.0000	1.0000
201	0.1113	0.0000	1.0000
205	0.0124	0.0000	1.0000
3008	0.0276	0.0000	1.0000
3001	0.0287	0.0000	1.0000
1.2762Hz mode			
Bus	calculated $\times 10^{-3}$	measured $\times 10^{-3}$	error
151	0.1606	0.1571	0.0218
201	0.1349	0.1312	0.0274
205	0.0095	0.0104	-0.0947
3008	0.1490	0.1485	0.0034
3001	0.5785	0.5759	0.0045

voltage or a bus voltage. It could be the case that PSS/E, the simulation engine, uses a different algorithm to determine frequency at various buses and that oscillation frequencies have some effect on the amplitude of the frequency. Further, many of the residues drop below $\times 10^{-5}$ per unit corresponding to an amplitude of around $\frac{1}{2}$ mHz. Accuracy should be expected to drop as amplitudes approach zero.

Chapter 6 Final Remarks

6.1 *Conclusions*

Basic frequency characteristics associated with oscillatory activity are described and analytically developed. Analytical development is via axioms of a synchronous machine electromechanical model – specifically the swing equation coupled with power-angle equations. These characteristics lend themselves to a theory which states that frequency measurements on any bus of an electric power system may be used to determine what dynamic modes a power system is operating in following a disturbance. The modes referred to here are modes associated with the natural response of a system. In this work the model used to predict these modes is state-space and it 1) predicts machine speed modes and 2) expresses frequency measurements as linear combinations of all of the machine speeds on the system. The model must be linearized as non-linear power flow equations make up terms in machine acceleration power. Non-idealized aspects of power system modeling are incorporated into the electromechanical model such as transmission line losses, shunt susceptances and speed governors. The state model developed in this work is based on P.M. Anderson's model [19]. In addition to the non-idealizations mentioned above, this work refines the former state model by more accurately determining the system's post-fault q-point. The inroad to this refinement comes primarily through assuming that the initial point and the post-fault q-point must not be identical points in the state-space as was assumed in [19]. In addition to refinements in the model, a new use of electromechanical state-space models is presented in this work as previous models were not used in conjunction with wide-area frequency monitoring systems. The previous models were used exclusively for stability calculations.

M.Baldwin

The model of the physical system and the q-point determination are adequately verified for determining system natural response: mode shapes, damping ratios, natural frequencies. The model demonstrates that natural response manifests itself in oscillations in frequency measurements and that with detailed modeling of the system, the oscillation frequencies can be determined to within 0.5 percent accuracy – accuracy that is sufficient for distinguishing disturbances. It is also verified that the linearized model provides very accurate results for substantially severe disturbances. It has been formerly understood that a linearized model will not provide good accuracy when the applied disturbance is greater than about 1 percent of system demand – the present model is verified for disturbances that are over 10 percent of demand for the test system used. An explanation for this accuracy is that any system that *is* stable will invariably approach some q-point. As the system state approaches the q-point, small-signal behavior dominates the system. Thus as the system approaches the q-point, the model becomes more and more accurate regardless of any initial nonlinear behavior.

Simulation results for the test system used in chapter five indicate that small-signal behavior dominates the system's activity for most, if not all, of the simulation time. I draw this conclusion based on the fact that the matrix pencil results do not yield eigenvalues that are linear multiples (or any other multiples) of the predicted state activity results (from the eigenanalysis). If system activity were large-signal, oscillatory modes, other than those that were predicted, should show up in the simulation results. This was not the case with any of the disturbances that were analyzed except for a double-frequency mode that showed up in measurements for the 3003-3005 outage. As mentioned before, this was more likely a signal processing problem than an actual

nonlinear activity as the double-frequency mode did not show up on the states – it was only in the measurements. Based on this explanation, any disturbance that does not result in instability could be analyzed using a linearized model.

During the verification process this work has revealed some system characteristics that provide counter-perceptions to conventional thought in power system oscillations and linear system theory in general – primarily that transmission losses and loads do not affect electromechanical damping. It was also shown that losses have a slight tendency to stiffen electromechanical coupling. Speed governors are shown to have a substantial effect on system damping. Factors that affect oscillation frequencies are revealed throughout the theoretical development and verification.

6.2 Contributions

The main contribution of this work should be considered model development: 1) electromechanical model refinement and application. Model refinement comes mainly from a more accurate determination of system q-point thus, yielding a more accurate linearized model. This improvement in accuracy has the potential to enhance stability calculations. An example would be in cases where a dynamic simulation execution may not be feasible such as in real-time contingency analysis, a process that a power system operator must continually carry out in order maintain system security. Pole motion could be tracked each time a security analysis is ran and thus a trend of electromechanical stability could be tracked 2) development of a model that has potential for use with wide-area phasor measurements in addition to frequency measurements. The model was used to determine the affect of system parameters on oscillation frequency and damping. The potential of this model for use in formulating damping solutions is evident as was

shown in chapter 4. As interarea oscillation damping becomes more and more of a concern in modern power systems, the model should provide promising applications. Non-oscillatory behavior is also characterized by the theory developed.

A secondary contribution is in developing an understanding of machine speed oscillations and their relationship to frequency as measured at any point on a power system. The theory developed in chapter two provides rigorously developed relationships with no small-signal approximations. These relationships are based solely on principles of simple AC circuit analysis and very simple partial differential equations. The notion of non-observable oscillatory modes was presented in chapter two and verified using simulation for both two-machine and three-machine systems. This notion of observability should prove useful in both wide-area frequency and phasor measurement applications especially in measurement unit placement problems. The output matrix developed in section 5.3.6 has potential for use in both frequency and phasor measurement unit applications such as disturbance identification.

A third contribution related to model development is in the fact that this model, which is used to describe oscillatory activity, is a lumped parameter model. The model gives an alternate viewpoint of electromechanical oscillation from the models that view an electric power system as a distributed-parameter system. A distributed-parameter system is normally used to analyze such phenomena as time-delays, wave reflections and transmissions, and propagation speeds. A DP model is not conventionally used to determine characteristics such as mode shape and oscillation damping factors.

6.3 Potential Future Research

As with all modeling, potential future developments can include more detailed modeling. Machine saliency's effect on damping should be explored further. I would propose using the damping coefficient for a machine's associated swing equation developed in [27]. It should be mentioned here that all machines, whether salient-pole or round rotor, exhibit strong saliency effects when the machine speed is dynamic. Excitation modeling needs to be included in future models as synchronizing power coefficients are linearly proportional to internal voltages. I propose that exciters in small-signal environments may have smaller-than-expected contributions to electromechanical behavior, as we may expect that generator bus voltages to not oscillate with high amplitudes in small-signal. However, this may certainly not always be the case and thus the inclusion of excitation systems in the electromechanical model should be explored. All of the speed governor models used in this work are intended to be accurate models for coal units. Much more elaborate models need to be developed for gas units as gas units may be expected to have speed governors and an increasing proportion of all generators on a modern electric power system are gas units.

Further future research may include more investigations of signal processing, further investigation of PSS/E's method of frequency measurement determination, test of the output matrix using different simulators.

Super-severe disturbances such as loss of synchronism or tie line loss possibly should be investigated further due to the fact that, though loss of synchronism should push the system far into its nonlinear region, the system should settle to some q-point

and thus approach dynamic operation that may be closely approximated by a linear model.

References

1. Miller, R.H. and J.H. Malinowski, *Power System Operation*. 3rd ed. 1994, New York: McGraw-Hill. xiii, 271 p.
2. Fitzgerald, A.E., C. Kingsley, and S.D. Umans, *Electric Machinery*. 4th ed. McGraw-Hill series in electrical engineering. Power and energy. 1983, New York: McGraw-Hill. xii, 571 p.
3. *Area Control Error (ACE) and Frequency Real Time Monitoring System; Completion Summary Report of Program Software*. 2002, Electric Power Group, LLC.
4. Kundur, P., N.J. Balu, and M.G. Lauby, *Power System Stability and Control*. EPRI power system engineering series. 1994, New York: McGraw-Hill. xxiii, 1176 p.
5. Jaleeli, N., et al., *Understanding Automatic Generation Control*. Power Systems, IEEE Transactions on, 1992. **7**(3): p. 1106-1122.
6. Zhian, Z., et al., *Power System Frequency Monitoring Network (FNET) Implementation*. Power Systems, IEEE Transactions on, 2005. **20**(4): p. 1914-1921.
7. Horowitz, S.H. and A.G. Phadke, *Power System Relaying*. 2nd ed. 1995, Taunton, Somerset, England New York: Research Studies Press; Wiley. xiv, 319 p.
8. *IEEE Standard General Requirements for Liquid-Immersed Distribution, Power, and Regulating Transformers*. IEEE Std C57.12.00-2000, 2000: p. i-53.
9. *NEMA Standards Publication MG-1-2006, Motors and Generators*. ANSI/NEMA Standard MG-1, 2006.
10. *IEEE Guide for Identification, Testing, and Evaluation of the Dynamic Performance of Excitation Control Systems*. IEEE Std 421.2-1990, 1990.
11. Taylor, C.W. and S. Lefebvre, *HVDC Controls for System Dynamic Performance*. Power Systems, IEEE Transactions on, 1991. **6**(2): p. 743-752.
12. Hingorani, N.G., et al., *Understanding FACTS : Concepts and Technology of Flexible AC Transmission Systems*. 2000, New York: IEEE Press. xix, 432 p.
13. Gardner, R.M., *Conditioning of FNET Data and Triangulation of Generator Trips in the Eastern Interconnected System*, in *Electrical and Computer Engineering*. 2005, Virginia Tech: Blacksburg, VA. p. 120.
14. Gardner, R.M., et al., *Non-Parametric Power System Event Location Using Wide-Area Measurements*, in *IEEE Power Systems Conference and Exposition*. 2006, IEEE: Atlanta, GA.
15. NERC, *Understand and Calculate Frequency Response*, T.R.W. Group, Editor. 2003. p. 28.
16. Wang, J.K., R.M. Gardner, and Y. Liu, *Analysis of System Oscillations Using Wide-Area Measurements*, in *IEEE PES General Meeting*. 2006: Montreal.
17. Phadke, A.G., *Synchronized Phasor Measurements - A Historical Overview*, in *Transmission and Distribution Conference and Exhibition 2002*. 2002, IEEE.
18. Stevenson, W.D., *Elements of Power System Analysis*. 4th ed. McGraw-Hill series in electrical engineering. Power and energy. 1982, New York: McGraw-Hill. xii, 436 p.

19. Anderson, P.M. and A.A. Fouad, *Power System Control and Stability*. 1st ed. 1977, Ames: Iowa State University Press. v.
20. Kamen, E.W., *Introduction to signals and systems*. 2nd ed. 1990, New York London: Macmillan; Collier Macmillan. xiv, 706.
21. Rugh, W.J., *Linear System Theory*. 2nd ed. Prentice-Hall information and system sciences series. 1996, Upper Saddle River, N.J.: Prentice Hall. xv, 581.
22. Shultz, R.D. and R.A. Smith, *Introduction to Electric Power Engineering*. 1985, New York: Harper & Row. viii, 264 p.
23. Ross, S.L. and S.L. Ross, *Introduction to Ordinary Differential Equations*. 4th ed. 1989, New York: Wiley. xi, 609 p.
24. Wood, A.J. and B.F. Wollenberg, *Power Generation, Operation, and Control*. 2nd ed. 1996, New York: J. Wiley & Sons. xv, 569 p.
25. Pereira, T.K.S.a.O., *Using the Matrix Pencil Method to Estimate the Parameters of a Sum of Complex Exponentials*. IEEE Antennas and Propagation Magazine, 1995. **37**(1): p. 48-55.
26. Concordia, C., *Effect of Steam-Turbine Reheat on Speed-Governor Performance*. ASME Journal of Engineering for Power, 1959. **81**: p. 6.
27. Machowski, J., J.W. Bialek, and J.R. Bumby, *Power system dynamics and stability*. 1997, Chichester ; New York: John Wiley. xxii, 461 p.

Appendix I Proof of Equation 3.9

$$\mathbf{x}(t) = \langle \boldsymbol{\Psi}_1, \mathbf{x}(t_0) \rangle \cdot \boldsymbol{\Phi}_1 \cdot e^{\lambda_1 t} + \dots + \langle \boldsymbol{\Psi}_n, \mathbf{x}(t_0) \rangle \cdot \boldsymbol{\Phi}_n \cdot e^{\lambda_n t} \quad (\text{A.1})$$

According to the conventional definition of a matrix exponential, $e^{\mathbf{A}t}$ may be expressed as an infinite power series

$$e^{\mathbf{A}t} = \sum_{n=0}^{\infty} \frac{(\mathbf{A}t)^n}{n!} = I + \mathbf{A}t + \frac{(\mathbf{A}t)^2}{2} + \frac{(\mathbf{A}t)^3}{6} + \dots \quad (\text{A.2})$$

Assuming conventional differentiation rules for matrix exponentials

$\frac{d}{dt} [e^{\mathbf{A}t}] = \mathbf{A}e^{\mathbf{A}t}$, $\mathbf{x}(t) = e^{\mathbf{A}t} \cdot \mathbf{x}_0$ may be substituted into $\dot{\mathbf{x}}(t) = \mathbf{A}\mathbf{x}(t)$ to yield

$\frac{d}{dt} [e^{\mathbf{A}t} \cdot \mathbf{x}_0] = \mathbf{A}e^{\mathbf{A}t} \cdot \mathbf{x}_0 = \mathbf{A}\mathbf{x}(t)$ and so this expression for the solution, $\mathbf{x}(t)$ is not only a

solution, but is the only solution associated with the initial condition \mathbf{x}_0 .

Since it is assumed that \mathbf{A} is a diagonalizable matrix via the right and left eigenvector modal matrices, equation (2.23) is repeated here

$$\mathbf{A} = \mathbf{P}\mathbf{\Lambda}\mathbf{P}^{-1} = \boldsymbol{\Phi} \begin{bmatrix} \lambda_1 & 0 & 0 \\ 0 & \ddots & 0 \\ 0 & 0 & \lambda_n \end{bmatrix} \boldsymbol{\Psi} \quad (\text{A.3})$$

where $\boldsymbol{\Phi} = [\boldsymbol{\Phi}_1 \quad \dots \quad \boldsymbol{\Phi}_n]$ and $\boldsymbol{\Psi} = [\boldsymbol{\Psi}_1^t \quad \dots \quad \boldsymbol{\Psi}_n^t]^t$

then the solution $\mathbf{x}(t)$ may be expressed as

$$\mathbf{x}(t) = e^{\mathbf{P}\mathbf{\Lambda}\mathbf{P}^{-1}t} \cdot \mathbf{x}_0 \quad (\text{A.4})$$

The proof of the following identity follows in the next section of the appendix

$$e^{\mathbf{P}\mathbf{\Lambda}\mathbf{P}^{-1}t} = \mathbf{P}e^{\mathbf{\Lambda}t}\mathbf{P}^{-1} \quad \text{and so} \quad (\text{A.5})$$

$$\mathbf{x}(t) = \mathbf{P}e^{\mathbf{\Lambda}t}\mathbf{P}^{-1} \cdot \mathbf{x}_0 = \boldsymbol{\Phi}e^{\mathbf{\Lambda}t}\boldsymbol{\Psi} \cdot \mathbf{x}_0 \quad (\text{A.6})$$

now $\Psi \cdot x_0$ may be expressed as

$$\Psi \mathbf{x}_0 = [\psi_1^t \quad \cdots \quad \psi_n^t]^t \mathbf{x}_0 = \begin{bmatrix} \psi_1 \\ \vdots \\ \psi_n \end{bmatrix} \mathbf{x}_0 = \begin{bmatrix} \langle \psi_1, \mathbf{x}_0 \rangle \\ \vdots \\ \langle \psi_n, \mathbf{x}_0 \rangle \end{bmatrix} \quad (\text{A.7})$$

and so

$$\mathbf{x}(t) = \Phi e^{\Lambda t} \begin{bmatrix} \langle \psi_1, \mathbf{x}_0 \rangle \\ \vdots \\ \langle \psi_n, \mathbf{x}_0 \rangle \end{bmatrix} \quad (\text{A.8})$$

and since $e^{\Lambda t}$ is a diagonal matrix that may be expressed as

$$e^{\Lambda t} = \begin{bmatrix} e^{\lambda_1 t} & 0 & 0 \\ 0 & \ddots & 0 \\ 0 & 0 & e^{\lambda_n t} \end{bmatrix} \quad (\text{A.9})$$

then $\mathbf{x}(t)$ may be expressed as

$$\mathbf{x}(t) = \Phi e^{\Lambda t} \begin{bmatrix} \langle \psi_1, \mathbf{x}_0 \rangle \\ \vdots \\ \langle \psi_n, \mathbf{x}_0 \rangle \end{bmatrix} = \Phi \begin{bmatrix} e^{\lambda_1 t} \langle \psi_1, \mathbf{x}_0 \rangle \\ \vdots \\ e^{\lambda_n t} \langle \psi_n, \mathbf{x}_0 \rangle \end{bmatrix} = [\phi_1 \quad \cdots \quad \phi_n] \begin{bmatrix} e^{\lambda_1 t} \langle \psi_1, \mathbf{x}_0 \rangle \\ \vdots \\ e^{\lambda_n t} \langle \psi_n, \mathbf{x}_0 \rangle \end{bmatrix} \quad (\text{A.10})$$

which finally reduces to

$$\mathbf{x}(t) = \langle \psi_1, \mathbf{x}(t_0) \rangle \cdot \phi_1 \cdot e^{\lambda_1 t} + \cdots + \langle \psi_n, \mathbf{x}(t_0) \rangle \cdot \phi_n \cdot e^{\lambda_n t} \quad (\text{A.11})$$

Appendix II Sample Plant Matrix Formulation

Generator 1 Trip

From pre-event and post-event load flows the following values were obtained:

$$E_2 = 1.0341 \quad (\text{Machine 2 internal voltage})$$

$$E_3 = 1.0541 \quad (\text{Machine 3 internal voltage})$$

$$\delta_{2q} = 0.6892 \quad (\text{Machine 2 quiescent point internal voltage angle})$$

$$\delta_{3q} = 0.6966 \quad (\text{Machine 3 quiescent point internal voltage angle})$$

The post-event \mathbf{Y}_{bus} is formed directly from the one-line diagram of figure 3.4 as follows:

$$\mathbf{Y}_{bus} = \begin{bmatrix} -j20.0 & 0 & 0 & j20.0 & 0 & 0 \\ 0 & -j4.831 & 0 & 0 & j4.831 & 0 \\ 0 & 0 & -j5.650 & 0 & 0 & j5.650 \\ \hline j20.0 & 0 & 0 & -j27.703 & j2.703 & j5.0 \\ 0 & j4.831 & 0 & j2.703 & -j11.534 & j4.0 \\ 0 & 0 & j5.650 & j5.0 & j4.0 & -j14.650 \end{bmatrix} \quad (\text{A.12})$$

Since machine 1 is offline for the above matrix, it should be noted that machine's 2 and 3 internal voltages are accounted as buses 2 and 3 respectively and the infinite bus is designated as bus 1. Since machine 1 is offline it's reactance and the series branch that connects it to the transmission ring is not included in the matrix. See figure 3A.1 below. Buses 4, 5, and 6 are the interconnection points on the transmission ring for machines 1, 2, and 3 respectively. In the next step, the above \mathbf{Y}_{bus} matrix will be reduced so that the entire transmission system may be analyzed as a three-port linear system. In doing this, buses 4, 5, and 6 are eliminated from the system and their corresponding admittances are absorbed into the reduced \mathbf{Y}_{bus} matrix, \mathbf{Y}_{bus}^r . This reduction is performed using a Kron reduction [17]. In the above 6 x 6 matrix, the upper left partition is designated the \mathbf{K} matrix, the upper right \mathbf{L} , the lower left \mathbf{L}^t , and the lower right \mathbf{M} . The reduced \mathbf{Y}_{bus} matrix is computed as

$$\mathbf{Y}_{bus}^r = \mathbf{K} - \mathbf{LM}^{-1}\mathbf{L}^t \quad (\text{A.13})$$

$$\mathbf{Y}_{bus}^r = \begin{bmatrix} -j3.614 & j1.542 & j2.072 \\ j1.542 & -j2.451 & j0.909 \\ j2.072 & j0.909 & -j2.981 \end{bmatrix} \quad (\text{A.14})$$

The following equation must be set up for $i = 2$ and 3 ; and $n = 3$

$$\frac{d^2 \Delta \delta_i(t)}{dt^2} = -\frac{\omega_s}{2H_i} \sum_{j=1}^n P_{Sij} [\Delta \delta_i(t) - \Delta \delta_j(t)] \quad (\text{A.15})$$

where

$$P_{Sij} = E_i E_j B_{ij} \cos(\delta_{i0} - \delta_{j0}) \quad \text{and} \quad \omega_s = 377 \quad \text{for a 60Hz system.}$$

Using the following values, each of the P_{Sij} terms may be computed

$$H_2 = 8 \text{ seconds}$$

$$H_3 = 12 \text{ seconds}$$

$$B_{12} = B_{21} = 1.542$$

$$B_{23} = B_{32} = 0.909$$

$$B_{31} = B_{13} = 2.072$$

$$\begin{aligned} P_{S12} &= (1.0)(1.0341)(1.542) \cos(39.486) = 1.254 \\ &= P_{S21} \end{aligned} \quad (\text{A.16})$$

$$\begin{aligned} P_{S13} &= (1.0)(1.0541)(2.072) \cos(-39.913) = 1.673 \\ &= P_{S31} \end{aligned} \quad (\text{A.17})$$

$$\begin{aligned} P_{S23} &= (1.0341)(1.0541)(1.542) \cos(39.486) = 1.008 \\ &= P_{S32} \end{aligned} \quad (\text{A.18})$$

since

$$\frac{d^2 \Delta \delta_i(t)}{dt^2} = \frac{d \Delta \omega_i(t)}{dt} \quad (\text{A.19})$$

then

$$\frac{d \Delta \omega_2(t)}{dt} = -53.279 \Delta \delta_2(t) + 23.740 \Delta \delta_3(t) \quad (\text{A.20})$$

and

$$\frac{d \Delta \omega_3(t)}{dt} = 15.827 \Delta \delta_2(t) - 42.108 \Delta \delta_3(t) \quad (\text{A.21})$$

and so the final state equation takes on the form

$$\frac{d}{dt} \begin{bmatrix} \Delta\delta_2 \\ \Delta\delta_3 \\ \Delta\omega_2 \\ \Delta\omega_2 \end{bmatrix} = \begin{bmatrix} 0 & 0 & 1 & 0 \\ 0 & 0 & 0 & 1 \\ -53.279 & 23.740 & 0 & 0 \\ 15.827 & -42.108 & 0 & 0 \end{bmatrix} \begin{bmatrix} \Delta\delta_2 \\ \Delta\delta_3 \\ \Delta\omega_2 \\ \Delta\omega_2 \end{bmatrix} \quad (\text{A.22})$$

The eigenvalues of the plant matrix are $\sigma(\mathbf{A}) = \{\pm j8.238, \pm j5.246\}$ which correspond to natural frequencies of 1.31Hz and 0.83Hz.

The normalized right eigenvectors of A are the columns of the matrix

$$\Phi = \begin{bmatrix} -j0.103 & j0.103 & -j0.1269 & j0.1269 \\ j0.063 & -j0.063 & -j0.1377 & j0.1377 \\ 0.8458 & 0.8458 & 0.6657 & 0.6657 \\ -0.5197 & -0.5197 & 0.7223 & 0.7223 \end{bmatrix} \quad (\text{A.23})$$

Appendix III Sample Output Matrix Formulation

Figure 3A.1 shows the circuit that must be used to formulate the \mathbf{B} matrix which is the first step in output matrix formulation. This circuit diagram shows all circuit elements converted to admittances, lumping together series elements where possible. Generator number 1 is the machine taken offline and so the machine 1 branch has been removed from the circuit. The infinite bus is taken as bus number 1. Not all of the elements of the \mathbf{B} matrix need to be determined as the final output matrix is a function of only the last four rows of the \mathbf{B} matrix. Thus, only \mathbf{B}_{4i} , \mathbf{B}_{5i} , \mathbf{B}_{6i} , and \mathbf{B}_{7i} for $i = 1$ to 7 need to be calculated. Notice that the diagonal elements of B are equal to the negative of the susceptance totals connected to each node. This procedure is in contrast to the one used to calculate a \mathbf{Y} matrix where the total admittance connected to each node is used instead of the negative. Else the procedure is exactly the same, save the fact that all elements of the B matrix are pure real numbers.

From figure 3A.1 the \mathbf{B}_{21} and \mathbf{B}_{22} matrices may be determined to be

$$\mathbf{B}_{21} = \begin{bmatrix} 0 & 0 & 0 \\ 0 & -4.83 & 0 \\ 0 & 0 & -6.37 \\ -20 & 0 & 0 \end{bmatrix} \text{ and } \mathbf{B}_{22} = \begin{bmatrix} 10.88 & -5.88 & 0 & -5.0 \\ -5.88 & 14.71 & -4.0 & 0 \\ 0 & -4.0 & 15.37 & -5.0 \\ -5.0 & 0 & -5.0 & 30.0 \end{bmatrix} \quad (\text{A.24})$$

and from \mathbf{B}_{21} and \mathbf{B}_{22} the output matrix may be determined to be

$$\mathbf{C} = -\mathbf{B}_{22}^{-1}\mathbf{B}_{21} = \begin{bmatrix} 0.54 & 0.30 & 0.16 \\ 0.31 & 0.49 & 0.20 \\ 0.35 & 0.15 & 0.50 \\ 0.81 & 0.08 & 0.11 \end{bmatrix} \quad (\text{A.25})$$

Since bus 1 is the reference bus and has an angle of zero for all time (and thus a frequency deviation of zero for all time), the first column of the C matrix may be removed.

$$\mathbf{C}^r = \begin{bmatrix} 0.30 & 0.16 \\ 0.49 & 0.20 \\ 0.15 & 0.50 \\ 0.08 & 0.11 \end{bmatrix} \quad (\text{A.26})$$

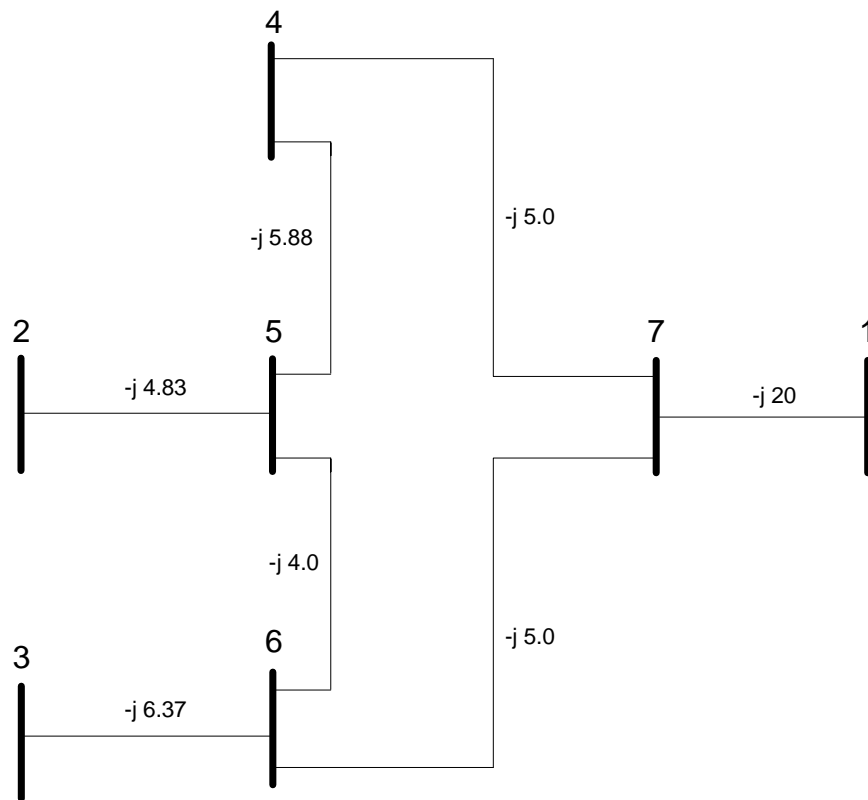


Figure AIII.1: system diagram for output matrix formulation

Appendix IV Test System Static and Dynamic Parameter Files for PSS/E

Static File:

```

0, 100.00 / PSS/E-29.3 TUE, OCT 16 2007 12:13
PSS/E PROGRAM APPLICATION GUIDE EXAMPLE
BASE CASE INCLUDING SEQUENCE DATA
 101,'NUC-A ', 21.6000,2, 0.000, 0.000, 1, 77,1.02000,
-0.9767, 11
 102,'NUC-B ', 21.6000,2, 0.000, 0.000, 1, 77,1.02000,
-0.9767, 11
 151,'NUCPANT ', 500.0000,1, 0.000, -600.000, 1, 1,1.02074,
-4.5342, 1
 152,'MID500 ', 500.0000,1, 0.000, 0.000, 1, 1,1.04468, -
12.1340, 1
 153,'MID230 ', 230.0000,1, 0.000, 0.000, 1, 1,1.02018, -
13.6676, 1
 154,'DOWNTN ', 230.0000,1, 0.000, 300.000, 1, 1,0.99012, -
16.8111, 1
 201,'HYDRO ', 500.0000,1, 0.000, 0.000, 2, 2,1.04213,
-7.3779, 22
 202,'EAST500 ', 500.0000,1, 0.000, 0.000, 2, 2,1.03693, -
12.2725, 2
 203,'EAST230 ', 230.0000,1, 0.000, 50.000, 2, 2,1.00396, -
15.7991, 2
 204,'SUB500 ', 500.0000,1, 0.000, 0.000, 2, 2,1.01314, -
13.2672, 2
 205,'SUB230 ', 230.0000,1, 0.000, 100.000, 2, 2,0.98818, -
16.3761, 2
 206,'URBGEN ', 18.0000,2, 0.000, 0.000, 2, 2,1.00000, -
11.7490, 22
 211,'HYDRO_G ', 20.0000,2, 0.000, 0.000, 2, 2,1.04000,
-2.8768, 22
 3001,'MINE ', 230.0000,1, 0.000, 0.000, 5, 5,1.03747,
-4.0416, 55
 3002,'E. MINE ', 500.0000,1, 0.000, 0.000, 5, 5,1.05448,
-5.8443, 5
 3003,'S. MINE ', 230.0000,1, 0.000, 0.000, 5, 5,1.03036,
-6.3281, 5
 3004,'WEST ', 500.0000,1, 0.000, 0.000, 5, 5,1.04225, -
12.2092, 5
 3005,'WEST ', 230.0000,1, 0.000, 0.000, 5, 5,1.00056, -
14.2014, 5
 3006,'UPTOWN ', 230.0000,1, 0.000, 0.000, 5, 5,1.01507, -
13.8274, 5
 3007,'RURAL ', 230.0000,1, 0.000, 0.000, 5, 5,0.96692, -
18.3218, 5
 3008,'CATDOG ', 230.0000,1, 0.000, 0.000, 5, 5,0.98598, -
16.7499, 55
 3011,'MINE_G ', 13.8000,3, 0.000, 0.000, 5, 5,1.04000,
0.0000, 55
 3018,'CATDOG_G', 13.8000,2, 0.000, 0.000, 5, 5,1.02000, -
11.9069, 55
0 / END OF BUS DATA, BEGIN LOAD DATA

```

```

153,'1 ','1, 1, 1, 300.000, 150.000, 0.000, 0.000,
0.000, 0.000, 1
154,'1 ','1, 2, 1, 300.000, 200.000, 0.000, 0.000,
0.000, 0.000, 1
154,'2 ','1, 2, 1, 200.000, 150.000, 0.000, 0.000,
0.000, 0.000, 100
203,'1 ','1, 2, 2, 300.000, 150.000, 0.000, 0.000,
0.000, 0.000, 2
205,'1 ','1, 2, 2, 800.000, 450.000, 0.000, 0.000,
0.000, 0.000, 2
3005,'1 ','1, 5, 5, 400.000, 200.000, 0.000, 0.000,
0.000, 0.000, 5
3007,'1 ','1, 5, 5, 400.000, 150.000, 0.000, 0.000,
0.000, 0.000, 5
3008,'1 ','1, 5, 5, 75.000, 30.000, 0.000, 0.000,
0.000, 0.000, 5
0 / END OF LOAD DATA, BEGIN GENERATOR DATA
101,'1 ', 475.000, -1.248, 600.000, -100.000,1.02000, 0,
900.000, 0.00000, 0.30000, 0.00000, 0.00000,1.00000,1, 100.0,
810.000, 0.000, 11,0.6667, 1,0.3333
102,'1 ', 475.000, -1.248, 600.000, -100.000,1.02000, 0,
900.000, 0.00000, 0.30000, 0.00000, 0.00000,1.00000,1, 100.0,
810.000, 0.000, 11,0.6667, 1,0.3333
206,'1 ', 600.000, 101.094, 600.000, 0.000,1.00000, 0,
1000.000, 0.00000, 0.25000, 0.00000, 0.00000,1.00000,1, 100.0,
900.000, 0.000, 2,0.4000, 22,0.6000
211,'1 ', 400.000, -7.863, 400.000, -100.000,1.04000, 0,
725.000, 0.00000, 0.26000, 0.00000, 0.00000,1.00000,1, 100.0,
616.250, 0.000, 2,0.4000, 22,0.6000
3011,'1 ', 761.227, 37.929, 600.000, -100.000,1.04000, 0,
1000.000, 0.00000, 0.35000, 0.00000, 0.00000,1.00000,1, 100.0,
900.000, 0.000, 55,0.3846, 5,0.3077, 22,0.2308, 11,0.0769
3018,'1 ', 100.000, 44.795, 80.000, 0.000,1.02000, 0,
130.000, 0.00000, 0.35000, 0.00000, 0.00000,1.00000,1, 100.0,
117.000, 0.000, 55,0.5556, 5,0.4444
0 / END OF GENERATOR DATA, BEGIN BRANCH DATA
151, 152,'1 ', 0.00260, 0.04600, 3.50000, 1200.00, 1300.00,
1.00, 0.00000, 0.00000, 0.00000, 0.00000,1, 0.00, 1,1.0000
151, 152,'2 ', 0.00260, 0.04600, 3.50000, 1200.00, 1300.00,
1.00, 0.00000, 0.00000, 0.00000, 0.00000,1, 0.00, 1,1.0000
151, 201,'1 ', 0.00100, 0.01500, 1.20000, 1200.00, 1300.00,
1.00, 0.00000, 0.00000, 0.00000, 0.00000,1, 0.00, 1,1.0000
152, -202,'1 ', 0.00080, 0.01000, 0.95000, 1200.00, 1300.00,
1.00, 0.00000, 0.00000, 0.00000, 0.00000,1, 0.00, 1,1.0000
152, 3004,'1 ', 0.00300, 0.03000, 2.50000, 0.00, 0.00,
1.00, 0.00000, 0.00000, 0.00000, 0.00000,1, 0.00, 1,1.0000
153, 154,'1 ', 0.00500, 0.04500, 0.10000, 300.00, 350.00,
1.00, 0.00000, 0.00000, 0.00000, 0.00000,1, 0.00, 1,0.7500,
100,0.2500
153, 154,'2 ', 0.00600, 0.05400, 0.15000, 300.00, 350.00,
1.00, 0.00000, 0.00000, 0.00000, 0.00000,1, 0.00, 1,1.0000
153, 3006,'1 ', 0.00100, 0.01200, 0.03000, 0.00, 0.00,
1.00, 0.00000, 0.00000, 0.00000, 0.00000,1, 0.00, 1,1.0000
154, 203,'1 ', 0.00400, 0.04000, 0.10000, 200.00, 250.00,
1.00, 0.00000, 0.00000, 0.00000, 0.00000,1, 0.00, 1,1.0000
154, 205,'1 ', 0.00033, 0.00333, 0.09000, 600.00, 660.00,
1.00, 0.00000, 0.00000, 0.00000, 0.00000,1, 0.00, 1,1.0000

```



```

154, 3008,'1 ', 0.00270, 0.02200, 0.30000, 400.00, 440.00,
1.00, 0.00000, 0.00000, 0.00000, 0.00000,1, 0.00, 1,1.0000
201, 202,'1 ', 0.00200, 0.02500, 2.00000, 1200.00, 1300.00,
1.00, 0.00000, 0.00000, 0.00000, 0.00000,1, 0.00, 22,1.0000
201, 204,'1 ', 0.00300, 0.03000, 2.50000, 1200.00, 1300.00,
1.00, 0.00000, 0.00000, 0.00000, 0.00000,1, 0.00, 22,1.0000
203, -205,'1 ', 0.00500, 0.04500, 0.08000, 200.00, 250.00,
1.00, 0.00000, 0.00000, 0.00000, 0.00000,1, 0.00, 2,1.0000
203, -205,'2 ', 0.00500, 0.04500, 0.08000, 200.00, 250.00,
1.00, 0.00000, 0.00000, 0.00000, 0.00000,1, 0.00, 2,1.0000
3001, 3003,'1 ', 0.00000, 0.00800, 0.00000, 0.00, 0.00,
1.00, 0.00000, 0.00000, 0.00000, 0.00000,1, 0.00, 55,1.0000
3002, 3004,'1 ', 0.00600, 0.05400, 2.50000, 0.00, 0.00,
1.00, 0.00000, 0.00000, 0.00000, 0.00000,1, 0.00, 5,1.0000
3003, 3005,'1 ', 0.00600, 0.05400, 0.09000, 0.00, 0.00,
1.00, 0.00000, 0.00000, 0.00000, 0.00000,1, 0.00, 5,1.0000
3003, 3005,'2 ', 0.00600, 0.05400, 0.09000, 0.00, 0.00,
1.00, 0.00000, 0.00000, 0.00000, 0.00000,1, 0.00, 5,1.0000
3005, 3006,'1 ', 0.00350, 0.03000, 0.07000, 0.00, 0.00,
1.00, 0.00000, 0.00000, 0.00000, 0.00000,1, 0.00, 5,1.0000
3005, 3007,'1 ', 0.00300, 0.02500, 0.06000, 0.00, 0.00,
1.00, 0.00000, 0.00000, 0.00000, 0.00000,1, 0.00, 5,1.0000
3005, 3008,'1 ', 0.00600, 0.05000, 0.12000, 0.00, 0.00,
1.00, 0.00000, 0.00000, 0.00000, 0.00000,1, 0.00, 5,1.0000
3007, 3008,'1 ', 0.00300, 0.02500, 0.06000, 0.00, 0.00,
1.00, 0.00000, 0.00000, 0.00000, 0.00000,1, 0.00, 5,1.0000
0 / END OF BRANCH DATA, BEGIN TRANSFORMER DATA
151, 101, 0,'1 ',1,1,1, 0.00000, 0.00000,2,' ',1,
1,1.0000
0.00030, 0.01360, 100.00
1.00000, 0.000, 0.000, 1250.00, 1350.00, 1750.00, 0, 0,
1.10000, 0.90000, 1.10000, 0.90000, 5, 0, 0.00000, 0.00000
1.00000, 0.000
151, 102, 0,'1 ',1,1,1, 0.00000, 0.00000,2,' ',1,
1,1.0000
0.00030, 0.01360, 100.00
1.00000, 0.000, 0.000, 1250.00, 1350.00, 1750.00, 0, 0,
1.10000, 0.90000, 1.10000, 0.90000, 5, 0, 0.00000, 0.00000
1.00000, 0.000
152, 153, 0,'1 ',1,1,1, 0.00000, 0.00000,2,' ',1,
1,1.0000
0.00000, 0.00500, 100.00
1.01000, 0.000, 0.000, 2500.00, 3000.00, 3500.00, 1, 154,
1.05000, 0.95000, 1.00000, 0.98000, 33, 0, 0.00000, 0.00000
1.00000, 0.000
201, 211, 0,'1 ',1,1,1, 0.00000, 0.00000,2,' ',1,
22,1.0000
0.00070, 0.02125, 100.00
1.00000, 0.000, 0.000, 800.00, 1000.00, 1120.00, 0, -201,
1.10000, 0.90000, 1.05000, 0.95000, 5, 0, 0.00000, 0.00000
1.00000, 0.000
202, 203, 0,'1 ',1,1,1, 0.00000, 0.00000,2,' ',1,
2,1.0000
0.00040, 0.01625, 100.00
1.00000, 0.000, 0.000, 800.00, 1040.00, 1200.00, 3,
0,30.00000,-30.00000,555.00000,545.00000, 33, 0, 0.00000, 0.00000
1.00000, 0.000

```

```

204, 205, 0,'1 ',1,1,1, 0.00000, 0.00000,2,' ',1,
2,1.0000
0.00030, 0.01500, 100.00
1.00000, 0.000, 0.000, 800.00, 1040.00, 1200.00, 1, 205,
1.05000, 0.95000, 1.00000, 0.98000, 33, 0, 0.00000, 0.00000
1.00000, 0.000
205, 206, 0,'1 ',1,1,1, 0.00000, 0.00000,2,' ',1,
2,1.0000
0.00026, 0.01333, 100.00
1.00000, 0.000, 0.000, 900.00, 1080.00, 1350.00, 0, 0,
1.10000, 0.90000, 1.10000, 0.90000, 5, 0, 0.00000, 0.00000
1.00000, 0.000
3001, 3002, 0,'1 ',1,1,1, 0.00000, 0.00000,1,' ',1,
55,1.0000
0.00030, 0.01500, 100.00
1.00000, 0.000, 0.000, 800.00, 1040.00, 1200.00, 0, 0,
1.10000, 0.90000, 1.05000, 0.95000, 33, 0, 0.00000, 0.00000
1.00000, 0.000
3001, 3011, 0,'1 ',1,1,1, 0.00000, 0.00000,2,' ',1,
55,1.0000
0.00020, 0.01000, 100.00
1.00000, 0.000, 0.000, 1300.00, 1560.00, 1820.00, 0, 0,
1.10000, 0.90000, 1.05000, 0.95000, 5, 0, 0.00000, 0.00000
1.00000, 0.000
3004, 3005, 0,'1 ',1,1,1, 0.00000, 0.00000,1,' ',1,
5,1.0000
0.00040, 0.01625, 100.00
1.00000, 0.000, 0.000, 800.00, 1040.00, 1200.00, 0, 0,
1.10000, 0.90000, 1.05000, 0.95000, 33, 0, 0.00000, 0.00000
1.00000, 0.000
3008, 3018, 0,'1 ',1,1,1, 0.00000, 0.00000,2,' ',1,
55,1.0000
0.00021, 0.08500, 100.00
1.00000, 0.000, 0.000, 150.00, 200.00, 250.00, 0, 0,
1.10000, 0.90000, 1.05000, 0.95000, 5, 0, 0.00000, 0.00000
1.00000, 0.000
0 / END OF TRANSFORMER DATA, BEGIN AREA DATA
0 / END OF AREA DATA, BEGIN TWO-TERMINAL DC DATA
0 / END OF TWO-TERMINAL DC DATA, BEGIN VSC DC LINE DATA
0 / END OF VSC DC LINE DATA, BEGIN SWITCHED SHUNT DATA
0 / END OF SWITCHED SHUNT DATA, BEGIN IMPEDANCE CORRECTION DATA
0 / END OF IMPEDANCE CORRECTION DATA, BEGIN MULTI-TERMINAL DC DATA
0 / END OF MULTI-TERMINAL DC DATA, BEGIN MULTI-SECTION LINE DATA
0 / END OF MULTI-SECTION LINE DATA, BEGIN ZONE DATA
1,'FIRST '
2,'SECOND '
5,'FIFTH '
77,'PLANT '
0 / END OF ZONE DATA, BEGIN INTER-AREA TRANSFER DATA
0 / END OF INTER-AREA TRANSFER DATA, BEGIN OWNER DATA
1,'TRAN 1 '
2,'TRAN 2 '
5,'TRAN 5 '
11,'GEN 1 '
22,'GEN 2 '
55,'GEN 5 '
100,'NO BUSES'

```

0 / END OF OWNER DATA, BEGIN FACTS DEVICE DATA
 0 / **END OF FACTS DEVICE DATA**

Dynamics File:

101	'GENCLS'	1	4.0000	0.0000	/	
101	'TGOV1'	1	0.0500	0.50000	1.0500	0.07000
			1.0000	1.0000	0.0000	/
102	'GENCLS'	1	4.0000	0.0000	/	
102	'TGOV1'	1	0.0500	0.50000	1.0500	0.07000
			1.0000	1.0000	0.0000	/
206	'GENCLS'	1	2.5000	0.0000	/	
206	'TGOV1'	1	0.0500	0.50000	1.0500	0.07000
			1.0000	1.0000	0.0000	/
211	'GENCLS'	1	5.0000	0.0000	/	
3011	'GENCLS'	1	3.0000	0.0000	/	
3018	'GENCLS'	1	3.0000	0.0000	/	

Appendix V MATLAB Codes Used to Generate Plant Matrix and Output Matrix

Instruction Manual for MATLAB Codes

To run the eigenanalysis and the output matrix calculators, you must run the programs in the order listed below from a) to d).

a) *PaRcalc.m* - this program is used to set the mechanical powers on each machine – the $\Delta\omega$ quantity is used to set the mechanical powers. $\Delta\omega$ is a guess of the frequency deviation; and load flow is ran. change the frequency deviation until the swing bus power is equal to the pre-fault swing bus power.

b) *sixbusLF_iter.m* - run this program in conjunction with *PaRcalc* to determine the q-point angles; the topology must be set by the user in this program.

Both programs above, a) and b), must be run to load into memory the susceptance, conductance and q-point angles that are required to run both the eigenanalysis and the output matrix program.

c) *PlantMatrix.m* - this program determines the entries in the plant matrix and does the eigenanalysis on it.

d) *OutputMatrix.m* - this program determines the elements of the output matrix.
Programs

a) and b) above must be ran before running this one. *OutputMatrix.m* needs the q-point angles, voltages, and admittance quantities to be loaded into memory for it to work.

These other two programs, a) and b), will load this data into memory.

PaRcalc.m

```
% Defining the mechanical powers by selecting frequency deviation
```

```
deltaohm = 0.0000796  
R1 = 1/180  
R2 = 1/180  
R4 = 0.005  
deltaPm1 = deltaohm/R1  
deltaPm2 = deltaohm/R2  
deltaPm4 = deltaohm/R4
```

```
Pm1 = 4.75 - deltaPm1  
Pm2 = 4.75 - deltaPm2  
Pm3 = 4.00  
Pm4 = 6.00 - deltaPm4
```

M.Baldwin

```
Pm5 = 1.00
Pm6 = 7.6123
```

```
%Loading inertias into memeory
```

```
H1 = 36.0
H2 = 36.0
H3 = 36.25
H4 = 25.0
H5 = 3.9
H6 = 30.0
```

```
% Setting electrical powers and loading them into memory for LF analysis
```

```
Pse1 = Pm1
Pse2 = Pm2
Pse3 = Pm3
Pse4 = Pm4
Pse5 = Pm5
```

```
Pmtot = Pm1 + Pm2 + Pm3 + Pm4 + Pm5 + Pm6
deltaPm = deltaPm1 + deltaPm2 + deltaPm4
```

SixbusLF_iter.m

```
iter_index=1;
epsilon=1e-6;
d1 = 8.2796 / 360 * 2 * pi
d2 = 8.2796 / 360 * 2 * pi
d3 = 5.6469 / 360 * 2 * pi
d4 = -5.4753 / 360 * 2 * pi
d5 = 0.7934 / 360 * 2 * pi
d6 = 13.680 / 360 * 2 * pi % this number is fixed - not variable
D(:,iter_index)=[d1*180/pi; d2*180/pi; d3*180/pi; d4*180/pi; d5*180/pi];
```

```
while true
```

```
% List Bus to Bus Branches and Line Shunts
```

```
z01_10 = 0.0003 + j*0.0469; % GSU
y01_10 = 1 / z01_10
y10_01 = y01_10
```

```
z02_10 = 0.0003 + j*0.0469; % GSU
y02_10 = 1 / z02_10
y10_02 = y02_10
```

```
z03_11 = 0.0007 + j*0.0572; % GSU
y03_11 = 1 / z03_11
y11_03 = y03_11
```

```
z04_23 = 0.00026 + j*0.0383; % GSU
y04_23 = 1 / z04_23
y23_04 = y04_23
```

```
z05_20 = 0.00021 + j*0.3542; % GSU
y05_20 = 1 / z05_20
y20_05 = y05_20
```

```
z06_08 = 0.0002 + j*0.0450; % GSU
y06_08 = 1 / z06_08
y08_06 = y06_08
```

```
z07_08 = 0.0003 + j*0.0150; % Transformer Branch
y07_08 = 1 / z07_08
y08_07 = y07_08
```

```

z07_09 = 0.0060 + j*0.0540;
y07_09 = 1 / z07_09
y09_07 = y07_09
y07_09LS = j*1.25
y09_07LS = y07_09LS

z08_12 = 0.0000 + j*0.0080;
y08_12 = 1 / z08_12
y12_08 = y08_12
y08_12LS = 0
y12_08LS = y08_12LS

z09_13 = 0.0030 + j*0.0300;
y09_13 = 1 / z09_13
y13_09 = y09_13
y09_13LS = j*1.25
y13_09LS = y09_13LS

z09_15 = 0.0004 + j*0.0163; % Transformer Branch
y09_15 = 1 / z09_15
y15_09 = y09_15

z10_13 = 0.0026 + j*0.0460; % This impedance represents one of the two branches that connect 10 and 13
y10_13 = 2 * (1/z10_13) % Duplicate Parallel Circuits - change the "2 *"s to "1 *"s to trip one of the circuits
y13_10 = y10_13
y10_13LS = j* 2 * 1.75
y13_10LS = y10_13LS

z10_11 = 0.0010 + j*0.0150;
y10_11 = 1/z10_11
y11_10 = y10_11
y10_11LS = j*0.6
y11_10LS = y10_11LS

z11_14 = 0.0020 + j*0.0250;
y11_14 = 1/z11_14
y14_11 = y11_14
y11_14LS = j*1.0
y14_11LS = y11_14LS

z11_21 = 0.0030 + j*0.0300;
y11_21 = 1/z11_21
y21_11 = y11_21
y11_21LS = j*1.25
y21_11LS = y11_21LS

z12_15 = 0.0060 + j*0.0540; % This impedance represents one of the two branches that connect 12 and 15
y12_15 = 2 * (1 / z12_15) % Duplicate Parallel Circuits - change the "2 *" 's to "1 *" 's to trip one of the circuits
y15_12 = y12_15
y12_15LS = j * 2 * 0.045
y15_12LS = y12_15LS

z13_14 = 0.0008 + j*0.0100;
y13_14 = 1 / z13_14
y14_13 = y13_14
y13_14LS = j*0.475
y14_13LS = y13_14LS

z13_17 = 0.0000 + j*0.0050; % Transformer Branch
y13_17 = 1 / z13_17
y17_13 = y13_17

z14_18 = 0.0004 + j*0.01625; % Transformer Branch

```

y14_18 = 1 / z14_18
y18_14 = y14_18

z15_16 = 0.0030 + j*0.0250;
y15_16 = 1 / z15_16
y16_15 = y15_16
y15_16LS = j*0.03
y16_15LS = y15_16LS

z15_19 = 0.0035 + j*0.0300;
y15_19 = 1 / z15_19
y19_15 = y15_19
y15_19LS = j*0.035
y19_15LS = y15_19LS

z15_20 = 0.0060 + j*0.0500;
y15_20 = 1 / z15_20
y20_15 = y15_20
y15_20LS = j*0.06
y20_15LS = y15_20LS

z16_20 = 0.0030 + j*0.0250;
y16_20 = 1 / z16_20
y20_16 = y16_20
y16_20LS = j*0.03
y20_16LS = y16_20LS

z17_19 = 0.0010 + j*0.0120;
y17_19 = 1 / z17_19
y19_17 = y17_19
y17_19LS = j*0.015
y19_17LS = y17_19LS

z17_22_1=0.0050+j*0.0450;%%
y17_22_1 = 1 / z17_22_1 %
y22_17_1 = y17_22_1 %
y17_22_1LS = j*0.05 % These two branches are non-duplicate parallel branches %
y22_17_1LS = y17_22_1LS % between buses 17 and 22 %
z17_22_2 = 0.0060 + j*0.0540; %
y17_22_2 = 1 / z17_22_2 %
y22_17_2 = y17_22_2 %
y17_22_2LS = j*0.075 %
y22_17_2LS=y17_22_2LS%%
%%

z18_22 = 0.0040 + j*0.0400;
y18_22 = 1 / z18_22
y22_18 = y18_22
y18_22LS = j*0.05
y22_18LS = y18_22LS

z18_23 = 0.0050 + j*0.0450; % This impedance represents one of the two branches that connect 18 and 23
y18_23 = 2 * (1 / z18_23) % Duplicate Parallel Circuits - change the "2 *" to "1 *" to trip one of the circuits
y23_18 = y18_23
y18_23LS = j*2 * (0.04)
y23_18LS = y18_23LS

z20_22 = 0.0027 + j*0.0220;
y20_22 = 1 / z20_22

```

y22_20 = y20_22
y20_22LS = j*0.15
y22_20LS = y20_22LS

```

```

z21_23 = 0.0003 + j*0.0150;    % Transformer Branch
y21_23 = 1 / z21_23
y23_21 = y21_23

```

```

z22_23 = 0.00033 + j*0.00333;
y22_23 = 1 / z22_23
y23_22 = y22_23
y22_23LS = j*0.045
y23_22LS = y22_23LS

```

```
% Finish Bus to Bus Branches and Line Shunts
```

```
% List Load and Compensation Shunt Branches
```

```

y10COMP = -j*6.0
y15LOAD = 3.9955 - j*1.9978
y16LOAD = 4.2784 - j*1.6044
y17LOAD = 2.8825 - j*1.4412
y18LOAD = 2.9764 - j*1.4882
y18COMP = j*0.5
y20LOAD = 0.7715 - j*0.3086
y22LOAD = 5.1003 - j*3.5702
y22COMP = j*3.0
y23LOAD = 8.1925 - j*4.6083
y23COMP = j*1.0

```

```
% Finish Load and Compensation Shunt Branches
```

```
Y=0
```

```
% Calculating Self Admittances
```

```

Y(01,01) = y01_10
Y(02,02) = y02_10
Y(03,03) = y03_11
Y(04,04) = y04_23
Y(05,05) = y05_20
Y(06,06) = y06_08
Y(07,07) = y07_08 + y07_09 + y07_09LS
Y(08,08) = y08_06 + y08_07 + y08_12
Y(09,09) = y09_07 + y09_13 + y09_15 + y09_07LS + y09_13LS
Y(10,10) = y10_01 + y10_02 + y10_11 + y10_13 + y10_11LS + y10_13LS + y10COMP
Y(11,11) = y11_03 + y11_10 + y11_14 + y11_21 + y11_10LS + y11_14LS + y11_21LS
Y(12,12) = y12_08 + y12_15 + y12_15LS
Y(13,13) = y13_09 + y13_10 + y13_14 + y13_17 + y13_09LS + y13_10LS + y13_14LS
Y(14,14) = y14_11 + y14_13 + y14_18 + y14_11LS + y14_13LS
Y(15,15) = y15_09 + y15_12 + y15_16 + y15_19 + y15_20 + y15_12LS + y15_16LS + y15_19LS + y15_20LS + y15LOAD
Y(16,16) = y16_15 + y16_20 + y16_15LS + y16_20LS + y16LOAD
Y(17,17) = y17_13 + y17_19 + y17_22_1 + y17_22_2 + y17_19LS + y17_22_1LS + y17_22_2LS + y17LOAD
Y(18,18) = y18_14 + y18_22 + y18_23 + y18_22LS + y18_23LS + y18LOAD + y18COMP
Y(19,19) = y19_15 + y19_17 + y19_15LS + y19_17LS
Y(20,20) = y20_05 + y20_15 + y20_16 + y20_22 + y20_15LS + y20_16LS + y20_22LS + y20LOAD
Y(21,21) = y21_11 + y21_23 + y21_11LS
Y(22,22) = y22_17_1 + y22_17_2 + y22_18 + y22_20 + y22_23 + y22_17_1LS + y22_17_2LS + y22_18LS + y22_20LS +
y22_23LS + y22LOAD + y22COMP
Y(23,23) = y23_04 + y23_18 + y23_21 + y23_22 + y23_18LS + y23_22LS + y23LOAD + y23COMP

```

```
% End Calculating Self Admittances
```

```
% Calculating Transfer Admittances
```


$$Y(01,10) = - (y01_{10})$$

$$Y(10,01) = Y(01,10)$$

$$Y(02,10) = - (y02_{10})$$

$$Y(10,02) = Y(02,10)$$

$$Y(03,11) = - (y03_{11})$$

$$Y(11,03) = Y(03,11)$$

$$Y(04,23) = - (y04_{23})$$

$$Y(23,04) = Y(04,23)$$

$$Y(05,20) = - (y05_{20})$$

$$Y(20,05) = Y(05,20)$$

$$Y(06,08) = - (y06_{08})$$

$$Y(08,06) = Y(06,08)$$

$$Y(07,08) = - (y07_{08})$$

$$Y(08,07) = Y(07,08)$$

$$Y(07,09) = - (y07_{09})$$

$$Y(09,07) = Y(07,09)$$

$$Y(08,12) = - (y08_{12})$$

$$Y(12,08) = Y(08,12)$$

$$Y(09,13) = - (y09_{13})$$

$$Y(13,09) = Y(09,13)$$

$$Y(09,15) = - (y09_{15})$$

$$Y(15,09) = Y(09,15)$$

$$Y(10,11) = - (y10_{11})$$

$$Y(11,10) = Y(10,11)$$

$$Y(10,13) = - (y10_{13})$$

$$Y(13,10) = Y(10,13)$$

$$Y(11,14) = - (y11_{14})$$

$$Y(14,11) = Y(11,14)$$

$$Y(11,21) = - (y11_{21})$$

$$Y(21,11) = Y(11,21)$$

$$Y(12,15) = - (y12_{15})$$

$$Y(15,12) = Y(12,15)$$

$$Y(13,14) = - (y13_{14})$$

$$Y(14,13) = Y(13,14)$$

$$Y(13,17) = - (y13_{17})$$

$$Y(17,13) = Y(13,17)$$

$$Y(14,18) = - (y14_{18})$$

$$Y(18,14) = Y(14,18)$$

$$Y(15,16) = - (y15_{16})$$

$$Y(16,15) = Y(15,16)$$

$$Y(15,19) = - (y15_{19})$$

$$Y(19,15) = Y(15,19)$$

$$Y(15,20) = - (y15_{20})$$

$$Y(20,15) = Y(15,20)$$

$$Y(16,20) = - (y16_{20})$$

$$Y(20,16) = Y(16,20)$$

$$Y(17,19) = - (y17_{19})$$

```

Y(19,17) = Y(17,19)

Y(17,22) = -(y17_22_1 + y17_22_2)
Y(22,17) = Y(17,22)

Y(18,22) = -(y18_22)
Y(22,18) = Y(18,22)

Y(18,23) = -(y18_23)
Y(23,18) = Y(18,23)

Y(20,22) = -(y20_22)
Y(22,20) = Y(20,22)

Y(21,23) = -(y21_23)
Y(23,21) = Y(21,23)

Y(22,23) = -(y22_23)
Y(23,22) = Y(22,23)

% End Calculating Transfer Admittances

% Begin decomposing matrix for Kron reduction where Ybus = K - L * inv(M) * L'

% Begin extracting top-left matrix designated K
K1=0
K1(6,17) = 0
PK = [eye(6) K1]
K = PK * Y * PK'
% End Extracting top-left matrix designated K

% Begin Extracting Bottom-Right Matrix Designated M
M1=0
M1(17,6) = 0
PM = [M1 eye(17)]
M = PM * Y * PM'
% End Extracting Bottom-Right Matrix Designated M

% Begin Extracting Top-Right Matrix Designated L
L1=0
L1(6,17) = 0
PL1 = [eye(6) L1]
PL2 = [L1; eye(17)]
L = PL1 * Y * PL2
% End Extracting Top-Right Matrix Designated L

% Finally Reduce the Y matrix

Ybus = K - L * inv(M) * L'

% Beginning 6-bus load flow calculations

%%%%%%%%%%%%%%%%%%%%%%%%%%%%%%%%%%%%%%%%%%%%%%%%%%%%%%%%%%%%%%%%%%%%%%%%

% Defining preVoltages - these voltages do not change
V1 = 1.0313
V2 = 1.0313
V3 = 1.0464
V4 = 1.0362
V5 = 1.1684
V6 = 1.0835

% Defining values for angles

d12 = d1-d2
d21 = d2-d1
d13 = d1-d3

```

d31 = d3-d1
d14 = d1-d4
d41 = d4-d1
d15 = d1-d5
d51 = d5-d1
d16 = d1-d6
d61 = d6-d1

d23 = d2-d3
d32 = d3-d2
d24 = d2-d4
d42 = d4-d2
d25 = d2-d5
d52 = d5-d2
d26 = d2-d6
d62 = d6-d2

d34 = d3-d4
d43 = d4-d3
d35 = d3-d5
d53 = d5-d3
d36 = d3-d6
d63 = d6-d3

d45 = d4-d5
d54 = d5-d4
d46 = d4-d6
d64 = d6-d4

d56 = d5-d6
d65 = d6-d5

%%%%%%%%%

% Defining Self and Mutual Susceptances and Conductances

G11 = real(Ybus(1,1))
B11 = imag(Ybus(1,1))
G22 = real(Ybus(2,2))
B22 = imag(Ybus(2,2))
G33 = real(Ybus(3,3))
B33 = imag(Ybus(3,3))
G44 = real(Ybus(4,4))
B44 = imag(Ybus(4,4))
G55 = real(Ybus(5,5))
B55 = imag(Ybus(5,5))
G66 = real(Ybus(6,6))
B66 = imag(Ybus(6,6))

G12 = real(Ybus(1,2))
G21 = G12
G13 = real(Ybus(1,3))
G31 = G13
G14 = real(Ybus(1,4))
G41 = G14
G15 = real(Ybus(1,5))
G51 = G15
G16 = real(Ybus(1,6))
G61 = G16

G23 = real(Ybus(2,3))
G32 = G23
G24 = real(Ybus(2,4))
G42 = G24
G25 = real(Ybus(2,5))
G52 = G25
G26 = real(Ybus(2,6))
G62 = G26

G34 = real(Ybus(3,4))
G43 = G34

G35 = real(Ybus(3,5))
 G53 = G35
 G36 = real(Ybus(3,6))
 G63 = G36

G45 = real(Ybus(4,5))
 G54 = G45
 G46 = real(Ybus(4,6))
 G64 = G46

G56 = real(Ybus(5,6))
 G65 = G56

B12 = imag(Ybus(1,2))
 B21 = B12
 B13 = imag(Ybus(1,3))
 B31 = B13
 B14 = imag(Ybus(1,4))
 B41 = B14
 B15 = imag(Ybus(1,5))
 B51 = B15
 B16 = imag(Ybus(1,6))
 B61 = B16

B23 = imag(Ybus(2,3))
 B32 = B23
 B24 = imag(Ybus(2,4))
 B42 = B24
 B25 = imag(Ybus(2,5))
 B52 = B25
 B26 = imag(Ybus(2,6))
 B62 = B26

B34 = imag(Ybus(3,4))
 B43 = B34
 B35 = imag(Ybus(3,5))
 B53 = B35
 B36 = imag(Ybus(3,6))
 B63 = B36

B45 = imag(Ybus(4,5))
 B54 = B45
 B46 = imag(Ybus(4,6))
 B64 = B46

B56 = imag(Ybus(5,6))
 B65 = B56

% Calculating Electrical Powers for each machine

$$Pe1 = V1^2 * G11 + V1 * V2 * [B12 * \sin(d12) + G12 * \cos(d12)] + V1 * V3 * [B13 * \sin(d13) + G13 * \cos(d13)] + V1 * V4 * [B14 * \sin(d14) + G14 * \cos(d14)] + V1 * V5 * [B15 * \sin(d15) + G15 * \cos(d15)] + V1 * V6 * [B16 * \sin(d16) + G16 * \cos(d16)]$$

$$Pe2 = V2^2 * G22 + V2 * V1 * [B21 * \sin(d21) + G21 * \cos(d21)] + V2 * V3 * [B23 * \sin(d23) + G23 * \cos(d23)] + V2 * V4 * [B24 * \sin(d24) + G24 * \cos(d24)] + V2 * V5 * [B25 * \sin(d25) + G25 * \cos(d25)] + V2 * V6 * [B26 * \sin(d26) + G26 * \cos(d26)]$$

$$Pe3 = V3^2 * G33 + V3 * V1 * [B31 * \sin(d31) + G31 * \cos(d31)] + V3 * V2 * [B32 * \sin(d32) + G32 * \cos(d32)] + V3 * V4 * [B34 * \sin(d34) + G34 * \cos(d34)] + V3 * V5 * [B35 * \sin(d35) + G35 * \cos(d35)] + V3 * V6 * [B36 * \sin(d36) + G36 * \cos(d36)]$$

$$Pe4 = V4^2 * G44 + V4 * V1 * [B41 * \sin(d41) + G41 * \cos(d41)] + V4 * V2 * [B42 * \sin(d42) + G42 * \cos(d42)] + V4 * V3 * [B43 * \sin(d43) + G43 * \cos(d43)] + V4 * V5 * [B45 * \sin(d45) + G45 * \cos(d45)] + V4 * V6 * [B46 * \sin(d46) + G46 * \cos(d46)]$$

$$Pe5 = V5^2 * G55 + V5 * V1 * [B51 * \sin(d51) + G51 * \cos(d51)] + V5 * V2 * [B52 * \sin(d52) + G52 * \cos(d52)] + V5 * V3 * [B53 * \sin(d53) + G53 * \cos(d53)] + V5 * V4 * [B54 * \sin(d54) + G54 * \cos(d54)] + V5 * V6 * [B56 * \sin(d56) + G56 * \cos(d56)]$$

$$Pe6 = V6^2 * G66 + V6 * V1 * [B61 * \sin(d61) + G61 * \cos(d61)] + V6 * V2 * [B62 * \sin(d62) + G62 * \cos(d62)] + V6 * V3 * [B63 * \sin(d63) + G63 * \cos(d63)] + V6 * V4 * [B64 * \sin(d64) + G64 * \cos(d64)] + V6 * V5 * [B65 * \sin(d65) + G65 * \cos(d65)]$$

% Defining Instantaneous Initial Power Mismatches

Pa1 = Pm1 - Pe1
 Pa2 = Pm2 - Pe2
 Pa3 = Pm3 - Pe3
 Pa4 = Pm4 - Pe4
 Pa5 = Pm5 - Pe5
 Pa6 = Pm6 - Pe6
 Patot = Pa1 + Pa2 + Pa3 + Pa4 + Pa5 + Pa6
 Pmtot = Pm1 + Pm2 + Pm3 + Pm4 + Pm5 + Pm6

% Calculating Acceleration Power Ratio for each machine

PaR1 = (Pm1 - Pe1)/36.0 * 100;
 PaR2 = (Pm2 - Pe2)/36.0 * 100;
 PaR3 = (Pm3 - Pe3)/18.125 * 100;
 PaR4 = (Pm4 - Pe4)/25.0 * 100;
 PaR5 = (Pm5 - Pe5)/ 3.9 * 100;
 PaR6 = (Pm6 - Pe6)/30.0 * 100;

%% Calculating Jacobian
 %%% Elements

% Calculating Jacobian Diagonals

dP1dD1=V1*V2*[B12*cos(d12)-G12*sin(d12)]+V1*V3*[B13*cos(d13)-G13*sin(d13)]+V1*V4*[B14*cos(d14)-G14*sin(d14)]+
 V1*V5*[B15*cos(d15)-G15*sin(d15)]+V1*V6*[B16*cos(d16)-G16*sin(d16)];

dP2dD2=V2*V1*[B21*cos(d21)-G21*sin(d21)]+V2*V3*[B23*cos(d23)-G23*sin(d23)]+V2*V4*[B24*cos(d24)-G24*sin(d24)]+
 V2*V5*[B25*cos(d25)-G25*sin(d25)]+V2*V6*[B26*cos(d26)-G26*sin(d26)];

dP3dD3=V3*V1*[B31*cos(d31)-G31*sin(d31)]+V3*V2*[B32*cos(d32)-G32*sin(d32)]+V3*V4*[B34*cos(d34)-G34*sin(d34)]+
 V3*V5*[B35*cos(d35)-G35*sin(d35)]+V3*V6*[B36*cos(d36)-G36*sin(d36)];

dP4dD4=V4*V1*[B41*cos(d41)-G41*sin(d41)]+V4*V2*[B42*cos(d42)-G42*sin(d42)]+V4*V3*[B43*cos(d43)-G43*sin(d43)]+
 V4*V5*[B45*cos(d45)-G45*sin(d45)]+V4*V6*[B46*cos(d46)-G46*sin(d46)];

dP5dD5=V5*V1*[B51*cos(d51)-G51*sin(d51)]+V5*V2*[B52*cos(d52)-G52*sin(d52)]+V5*V3*[B53*cos(d53)-G53*sin(d53)]+
 V5*V4*[B54*cos(d54)-G54*sin(d54)]+V5*V6*[B56*cos(d56)-G56*sin(d56)];

J=0

J(1,1) = dP1dD1;
 J(2,2) = dP2dD2;
 J(3,3) = dP3dD3;
 J(4,4) = dP4dD4;
 J(5,5) = dP5dD5;

dP1dD2 = V1*V2*[G12*sin(d12) - B12*cos(d12)];
 dP1dD3 = V1*V3*[G13*sin(d13) - B13*cos(d13)];
 dP1dD4 = V1*V4*[G14*sin(d14) - B14*cos(d14)];
 dP1dD5 = V1*V5*[G15*sin(d15) - B15*cos(d15)];

dP2dD1 = V2*V1*[G21*sin(d21) - B21*cos(d21)];
 dP2dD3 = V2*V3*[G23*sin(d23) - B23*cos(d23)];
 dP2dD4 = V2*V4*[G24*sin(d24) - B24*cos(d24)];
 dP2dD5 = V2*V5*[G25*sin(d25) - B25*cos(d25)];

dP3dD1 = V3*V1*[G31*sin(d31) - B31*cos(d31)];
 dP3dD2 = V3*V2*[G32*sin(d32) - B32*cos(d32)];
 dP3dD4 = V3*V4*[G34*sin(d34) - B34*cos(d34)];
 dP3dD5 = V3*V5*[G35*sin(d35) - B35*cos(d35)];

dP4dD1 = V4*V1*[G41*sin(d41) - B41*cos(d41)];
 dP4dD2 = V4*V2*[G42*sin(d42) - B42*cos(d42)];
 dP4dD3 = V4*V3*[G43*sin(d43) - B43*cos(d43)];
 dP4dD5 = V4*V5*[G45*sin(d45) - B45*cos(d45)];

```

dP5dD1 = V5*V1*[G51*sin(d51) - B51*cos(d51)];
dP5dD2 = V5*V2*[G52*sin(d52) - B52*cos(d52)];
dP5dD3 = V5*V3*[G53*sin(d53) - B53*cos(d53)];
dP5dD4 = V5*V4*[G54*sin(d54) - B54*cos(d54)];

J(1,2) = dP1dD2;
J(1,3) = dP1dD3;
J(1,4) = dP1dD4;
J(1,5) = dP1dD5;

J(2,1) = dP2dD1;
J(2,3) = dP2dD3;
J(2,4) = dP2dD4;
J(2,5) = dP2dD5;

J(3,1) = dP3dD1;
J(3,2) = dP3dD2;
J(3,4) = dP3dD4;
J(3,5) = dP3dD5;

J(4,1) = dP4dD1;
J(4,2) = dP4dD2;
J(4,3) = dP4dD3;
J(4,5) = dP4dD5;
%J(4,6) = dP4dD6;

J(5,1) = dP5dD1;
J(5,2) = dP5dD2;
J(5,3) = dP5dD3;
J(5,4) = dP5dD4;

deltaP = [Pse1 - Pe1; Pse2 - Pe2; Pse3 - Pe3; Pse4 - Pe4; Pse5 - Pe5];

deltaD = inv(J) * deltaP;

PaR6 = (Pm6 - Pe6)/H6

d1 = (d1 + deltaD(1,1));
d2 = (d2 + deltaD(2,1));
d3 = (d3 + deltaD(3,1));
d4 = (d4 + deltaD(4,1));
d5 = (d5 + deltaD(5,1));

%Store d's for review after execution
D(:,iter_index+1)=[d1*180/pi; d2*180/pi; d3*180/pi; d4*180/pi; d5*180/pi];

%Check solution, break loop if below tolerance
if max(abs(deltaD)<epsilon)
    break
elseif iter_index>100
    disp('Maximum number of iterations exceeded. Loop terminated. ');
    break
end

iter_index=iter_index+1;
end

PaInterc = Pa1+Pa2+Pa3+Pa4+Pa5+Pa6;
deltaw = PaInterc/(180+180+200);
deltaf = deltax*60;

Pe6

angle1 = d1 * (180/pi)
angle2 = d2 * (180/pi)
angle3 = d3 * (180/pi)
angle4 = d4 * (180/pi)
angle5 = d5 * (180/pi)
angle6 = d6 * (180/pi)

```

PlantMatrix.m

```

%%%%%%%%%%%%%%%%%%%%%%%%%%%%%%%%%%%%%%%%%%%%%%%%%%%%%%%%%%%%%%%%%%%%%%%%
%   Calculating Elements of the Synchronizing Power Coefficients

Sp(1,2) = V1 * V2 * [B12*cos(d12) - G12*sin(d12)] * (60*2*pi)/(2*H1);
Sp(1,3) = V1 * V3 * [B13*cos(d13) - G13*sin(d13)] * (60*2*pi)/(2*H1);
Sp(1,4) = V1 * V4 * [B14*cos(d14) - G14*sin(d14)] * (60*2*pi)/(2*H1);
Sp(1,5) = V1 * V5 * [B15*cos(d15) - G15*sin(d15)] * (60*2*pi)/(2*H1);
Sp(1,6) = V1 * V6 * [B16*cos(d16) - G16*sin(d16)] * (60*2*pi)/(2*H1);

Sp(2,1) = V2 * V1 * [B21*cos(d21) - G21*sin(d21)] * (60*2*pi)/(2*H2);
Sp(2,3) = V2 * V3 * [B23*cos(d23) - G23*sin(d23)] * (60*2*pi)/(2*H2);
Sp(2,4) = V2 * V4 * [B24*cos(d24) - G24*sin(d24)] * (60*2*pi)/(2*H2);
Sp(2,5) = V2 * V5 * [B25*cos(d25) - G25*sin(d25)] * (60*2*pi)/(2*H2);
Sp(2,6) = V2 * V6 * [B26*cos(d26) - G26*sin(d26)] * (60*2*pi)/(2*H2);

Sp(3,1) = V3 * V1 * [B31*cos(d31) - G31*sin(d31)] * (60*2*pi)/(2*H3);
Sp(3,2) = V3 * V2 * [B32*cos(d32) - G32*sin(d32)] * (60*2*pi)/(2*H3);
Sp(3,4) = V3 * V4 * [B34*cos(d34) - G34*sin(d34)] * (60*2*pi)/(2*H3);
Sp(3,5) = V3 * V5 * [B35*cos(d35) - G35*sin(d35)] * (60*2*pi)/(2*H3);
Sp(3,6) = V3 * V6 * [B36*cos(d36) - G36*sin(d36)] * (60*2*pi)/(2*H3);

Sp(4,1) = V4 * V1 * [B41*cos(d41) - G41*sin(d41)] * (60*2*pi)/(2*H4);
Sp(4,2) = V4 * V2 * [B42*cos(d42) - G42*sin(d42)] * (60*2*pi)/(2*H4);
Sp(4,3) = V4 * V3 * [B43*cos(d43) - G43*sin(d43)] * (60*2*pi)/(2*H4);
Sp(4,5) = V4 * V5 * [B45*cos(d45) - G45*sin(d45)] * (60*2*pi)/(2*H4);
Sp(4,6) = V4 * V6 * [B46*cos(d46) - G46*sin(d46)] * (60*2*pi)/(2*H4);

Sp(5,1) = V5 * V1 * [B51*cos(d51) - G51*sin(d51)] * (60*2*pi)/(2*H5);
Sp(5,2) = V5 * V2 * [B52*cos(d52) - G52*sin(d52)] * (60*2*pi)/(2*H5);
Sp(5,3) = V5 * V3 * [B53*cos(d53) - G53*sin(d53)] * (60*2*pi)/(2*H5);
Sp(5,4) = V5 * V4 * [B54*cos(d54) - G54*sin(d54)] * (60*2*pi)/(2*H5);
Sp(5,6) = V5 * V6 * [B56*cos(d56) - G56*sin(d56)] * (60*2*pi)/(2*H5);

Sp(6,1) = V6 * V1 * [B61*cos(d61) - G61*sin(d61)] * (60*2*pi)/(2*H6);
Sp(6,2) = V6 * V2 * [B62*cos(d62) - G62*sin(d62)] * (60*2*pi)/(2*H6);
Sp(6,3) = V6 * V3 * [B63*cos(d63) - G63*sin(d63)] * (60*2*pi)/(2*H6);
Sp(6,4) = V6 * V4 * [B64*cos(d64) - G64*sin(d64)] * (60*2*pi)/(2*H6);
Sp(6,5) = V6 * V5 * [B65*cos(d65) - G65*sin(d65)] * (60*2*pi)/(2*H6);

Sp(1,1) = - (      Sp(1,2) + Sp(1,3) + Sp(1,4) + Sp(1,5) + Sp(1,6));
Sp(2,2) = - (Sp(2,1) +      Sp(2,3) + Sp(2,4) + Sp(2,5) + Sp(2,6));
Sp(3,3) = - (Sp(3,1) + Sp(3,2) +      Sp(3,4) + Sp(3,5) + Sp(3,6));
Sp(4,4) = - (Sp(4,1) + Sp(4,2) + Sp(4,3) +      Sp(4,5) + Sp(4,6));
Sp(5,5) = - (Sp(5,1) + Sp(5,2) + Sp(5,3) + Sp(5,4) +      Sp(5,6));
Sp(6,6) = - (Sp(6,1) + Sp(6,2) + Sp(6,3) + Sp(6,4) + Sp(6,5)      );

%%%%%%%%%%%%%%%%%%%%%%%%%%%%%%%%%%%%%%%%%%%%%%%%%%%%%%%%%%%%%%%%%%%%%%%%
%   Calculating Elements of the "M" Matrix
%   These elements represent the proportionality constant between
%   each machine's speed rate function (ohmegadot) and its mechanical
%   power.

Mass(1,1) = (60*2*pi) / (2*H1);
Mass(2,2) = (60*2*pi) / (2*H2);
Mass(4,3) = (60*2*pi) / (2*H4);
Mass(6,3) = 0;

%%%%%%%%%%%%%%%%%%%%%%%%%%%%%%%%%%%%%%%%%%%%%%%%%%%%%%%%%%%%%%%%%%%%%%%%
%   Calculating Elements of the "Rinv" Matrix
%   Each of these elements represents the proportionality constant
%   from mechanical power ratefunction and machine speed

T1 = 0.5;
T2 = 0.5;
T4 = 0.5;

Rinv(1,1) = -1 / ((60*2*pi) * R1 * T1);
Rinv(2,2) = -1 / ((60*2*pi) * R2 * T2);
Rinv(3,4) = -1 / ((60*2*pi) * R4 * T4);
Rinv(3,6) = 0;

%%%%%%%%%%%%%%%%%%%%%%%%%%%%%%%%%%%%%%%%%%%%%%%%%%%%%%%%%%%%%%%%%%%%%%%%

```

```

% Calculating Elements of the "Lambda" Matrix
% Each of these elements represents the proportionality constant
% from mechanical power ratefunction to mechanical power

Lambda(1,1) = -1/T1;
Lambda(2,2) = -1/T2;
Lambda(3,3) = -1/T4;

%%%%%%%%%%%%%%%%%%%%%%%%%%%%%%%%%%%%%%%%%%%%%%%%%%%%%%%%%%%%%%%%%%%%%%%%
% Calculating Zero Partitions of the Plant Matrix
% define all of the zero matrices: Z11, Z13, Z31
Z11(6,6) = 0;
Z22(6,6) = 0;
Z13(6,3) = 0;
Z31(3,6) = 0;
% Assemble the partitions
A = [Z11 eye(6) Z13; Sp Z22 Mass; Z31 Rinv Lambda];

[V,D] = eig(A)

```

OutputMatrix.m

```

% Creating 23-bus impedance matrix from 23 bus Y matrix that was created
% in the sixbusLF_iter.m routine
Zf = inv(Y)

% Begin extracting top-left matrix out of the 23-bus Z matrix
K2=0;
K2(6,17) = 0;
PK2 = [eye(6) K2];
Z = PK2 * Zf * PK2';
Z6 = Z
% End Extracting top-left matrix

% Defining diagonal elements of the 11 x 11 Zbus, Z. The first 6
% diagonal elements are already defined in previous step
Z(07,07) = Zf(10,10);
Z(08,08) = Zf(11,11);
Z(09,09) = Zf(23,23);
Z(10,10) = Zf(20,20);
Z(11,11) = Zf(08,08);
% Finished defining diagonal elements of the 11 x 11 Zbus, Z

% Defining upper-right 6 x 5 matrix of the 11 x 11 Zbus, Z

Z(01,07) = Zf(01,10);
Z(01,08) = Zf(01,11);
Z(01,09) = Zf(01,23);
Z(01,10) = Zf(01,20);
Z(01,11) = Zf(01,08);

Z(02,07) = Zf(02,10);
Z(02,08) = Zf(02,11);
Z(02,09) = Zf(02,23);
Z(02,10) = Zf(02,20);
Z(02,11) = Zf(02,08);

Z(03,07) = Zf(03,10);
Z(03,08) = Zf(03,11);
Z(03,09) = Zf(03,23);
Z(03,10) = Zf(03,20);
Z(03,11) = Zf(03,08);

Z(04,07) = Zf(04,10);
Z(04,08) = Zf(04,11);
Z(04,09) = Zf(04,23);
Z(04,10) = Zf(04,20);
Z(04,11) = Zf(04,08);

Z(05,07) = Zf(05,10);

```



```

Z(05,08) = Zf(05,11);
Z(05,09) = Zf(05,23);
Z(05,10) = Zf(05,20);
Z(05,11) = Zf(05,08);

Z(06,07) = Zf(06,10);
Z(06,08) = Zf(06,11);
Z(06,09) = Zf(06,23);
Z(06,10) = Zf(06,20);
Z(06,11) = Zf(06,08);

% Finished Defining upper-right 6 x 5 matrix of the 11 x 11 Zbus, Z
% Defining lower-left 5 x 6 matrix of the 11 x 11 Zbus, Z

Z(07,01)=Z(01,07);
Z(07,02)=Z(02,07);
Z(07,03)=Z(03,07);
Z(07,04)=Z(04,07);
Z(07,05)=Z(05,07);
Z(07,06)=Z(06,07);

Z(08,01)=Z(01,08);
Z(08,02)=Z(02,08);
Z(08,03)=Z(03,08);
Z(08,04)=Z(04,08);
Z(08,05)=Z(05,08);
Z(08,06)=Z(06,08);

Z(09,01)=Z(01,09);
Z(09,02)=Z(02,09);
Z(09,03)=Z(03,09);
Z(09,04)=Z(04,09);
Z(09,05)=Z(05,09);
Z(09,06)=Z(06,09);

Z(10,01)=Z(01,10);
Z(10,02)=Z(02,10);
Z(10,03)=Z(03,10);
Z(10,04)=Z(04,10);
Z(10,05)=Z(05,10);
Z(10,06)=Z(06,10);

Z(11,01)=Z(01,11);
Z(11,02)=Z(02,11);
Z(11,03)=Z(03,11);
Z(11,04)=Z(04,11);
Z(11,05)=Z(05,11);
Z(11,06)=Z(06,11);

% Finished defining lower-left 5 x 6 matrix of the 11 x 11 Zbus, Z
% Defining off-diagonals of lower-right 5 x 5 matrix

Z(07,08) = Zf(10,11);
Z(07,09) = Zf(10,23);
Z(07,10) = Zf(10,20);
Z(07,11) = Zf(10,08);

Z(08,09) = Zf(11,23);
Z(08,10) = Zf(11,20);
Z(08,11) = Zf(11,08);

Z(09,10) = Zf(23,20);
Z(09,11) = Zf(23,08);

Z(10,11) = Zf(20,08);

Z(11,10) = Z(10,11);

Z(11,09) = Z(09,11);
Z(10,09) = Z(09,10);

Z(11,08) = Z(08,11);
Z(10,08) = Z(08,10);
Z(09,08) = Z(08,09);

Z(08,07) = Z(07,08);
Z(09,07) = Z(07,09);
Z(10,07) = Z(07,10);

```

```

Z(11,07) = Z(07,11);
% Finished defining off-diagonals of lower-right 5 x 5 matrix

% Calculating injected currents from the six machines
%%%%%%%%%%%%%%%%%%%%%%%%%%%%%%%%%%%%%%%%%%%%%%%%%%%%%%%%%%%%%%%%%%%%%%%%

% Reestablishing 6-bus matrices and determining injected currents at
% each machine, then determining the q-point voltages on the measurement
% buses

Y6 = inv(Z6);
Vsix = [V1*exp(i*d1); V2*exp(i*d2); V3*exp(i*d3); V4*exp(i*d4); V5*exp(i*d5);
        V6*exp(i*d6)];

I6 = Y6*Vsix;
I11 = [I6 ;0 ;0 ;0 ;0 ;0];
veleven = Z * I11;

% Finished reestablishing the 6-bus system
% Using the magnitude of the voltages in the V11 vector, the q-point
% voltages for the measurement (or output) buses have been determined

% Begin extracting magnitudes and phase angles of all elements of the V11
% vector

V7 = abs(veleven(7));
V8 = abs(veleven(8));
V9 = abs(veleven(9));
V10 = abs(veleven(10));
V11 = abs(veleven(11));

d7 = angle(veleven(7));
d8 = angle(veleven(8));
d9 = angle(veleven(9));
d10 = angle(veleven(10));
d11 = angle(veleven(11));

% Finished extracting magnitudes and phase angles of all elements of the V11
% vector

% Defining angle differences
%%%%%%%%%%%%%%%%%%%%%%%%%%%%%%%%%%%%%%%%%%%%%%%%%%%%%%%%%%%%%%%%%%%%%%%%
d7_1 = d7-d1;
d7_2 = d7-d2;
d7_3 = d7-d3;
d7_4 = d7-d4;
d7_5 = d7-d5;
d7_6 = d7-d6;

d7_8 = d7-d8;
d7_9 = d7-d9;
d7_10 = d7-d10;
d7_11 = d7-d11;

d1_7 = -d7_1;
d2_7 = -d7_2;
d3_7 = -d7_3;
d4_7 = -d7_4;
d5_7 = -d7_5;
d6_7 = -d7_6;

d8_7 = -d7_8;
d9_7 = -d7_9;
d10_7 = -d7_10;
d11_7 = -d7_11;
%%%%%%%%%%%%%%%%%%%%%%%%%%%%%%%%%%%%%%%%%%%%%%%%%%%%%%%%%%%%%%%%%%%%%%%%

%%%%%%%%%%%%%%%%%%%%%%%%%%%%%%%%%%%%%%%%%%%%%%%%%%%%%%%%%%%%%%%%%%%%%%%%
d8_1 = d8-d1;
d8_2 = d8-d2;
d8_3 = d8-d3;
d8_4 = d8-d4;
d8_5 = d8-d5;

```



```

C22(09,09) = v9*v1*[B9_1*cos(d9_1) - G9_1*sin(d9_1)] +
            v9*v2*[B9_2*cos(d9_2) - G9_2*sin(d9_2)] +
            v9*v3*[B9_3*cos(d9_3) - G9_3*sin(d9_3)] +
            v9*v4*[B9_4*cos(d9_4) - G9_4*sin(d9_4)] +
            v9*v5*[B9_5*cos(d9_5) - G9_5*sin(d9_5)] +
            v9*v6*[B9_6*cos(d9_6) - G9_6*sin(d9_6)] +
            v9*v7*[B9_7*cos(d9_7) - G9_7*sin(d9_7)] +
            v9*v8*[B9_8*cos(d9_8) - G9_8*sin(d9_8)] +
            v9*v10*[B9_10*cos(d9_10) - G9_10*sin(d9_10)] +
            v9*v11*[B9_11*cos(d9_11) - G9_11*sin(d9_11)];
C22(10,10) = v10*v1*[B10_1*cos(d10_1) - G10_1*sin(d10_1)] +
            v10*v2*[B10_2*cos(d10_2) - G10_2*sin(d10_2)] +
            v10*v3*[B10_3*cos(d10_3) - G10_3*sin(d10_3)] +
            v10*v4*[B10_4*cos(d10_4) - G10_4*sin(d10_4)] +
            v10*v5*[B10_5*cos(d10_5) - G10_5*sin(d10_5)] +
            v10*v6*[B10_6*cos(d10_6) - G10_6*sin(d10_6)] +
            v10*v7*[B10_7*cos(d10_7) - G10_7*sin(d10_7)] +
            v10*v8*[B10_8*cos(d10_8) - G10_8*sin(d10_8)] +
            v10*v9*[B10_9*cos(d10_9) - G10_9*sin(d10_9)] +
            v10*v11*[B10_11*cos(d10_11) - G10_11*sin(d10_11)];
C22(11,11) = v11*v1*[B11_1*cos(d11_1) - G11_1*sin(d11_1)] +
            v11*v2*[B11_2*cos(d11_2) - G11_2*sin(d11_2)] +
            v11*v3*[B11_3*cos(d11_3) - G11_3*sin(d11_3)] +
            v11*v4*[B11_4*cos(d11_4) - G11_4*sin(d11_4)] +
            v11*v5*[B11_5*cos(d11_5) - G11_5*sin(d11_5)] +
            v11*v6*[B11_6*cos(d11_6) - G11_6*sin(d11_6)] +
            v11*v7*[B11_7*cos(d11_7) - G11_7*sin(d11_7)] +
            v11*v8*[B11_8*cos(d11_8) - G11_8*sin(d11_8)] +
            v11*v9*[B11_9*cos(d11_9) - G11_9*sin(d11_9)] +
            v11*v10*[B11_10*cos(d11_10) - G11_10*sin(d11_10)]
;
;

```

```
% Finished forming diagonals of output matrix before reduction
```

```
% Begin forming off-diagonals of output matrix C22
```

```

C22(07,08) = -v7*v8*[B7_8*cos(d7_8) - G7_8*sin(d7_8)];
C22(07,09) = -v7*v9*[B7_9*cos(d7_9) - G7_9*sin(d7_9)];
C22(07,10) = -v7*v10*[B7_10*cos(d7_10) - G7_10*sin(d7_10)];
C22(07,11) = -v7*v11*[B7_11*cos(d7_11) - G7_11*sin(d7_11)];

C22(08,07) = -v8*v7*[B8_7*cos(d8_7) - G8_7*sin(d8_7)];
C22(08,09) = -v8*v9*[B8_9*cos(d8_9) - G8_9*sin(d8_9)];
C22(08,10) = -v8*v10*[B8_10*cos(d8_10) - G8_10*sin(d8_10)];
C22(08,11) = -v8*v11*[B8_11*cos(d8_11) - G8_11*sin(d8_11)];

C22(09,07) = -v9*v7*[B9_7*cos(d9_7) - G9_7*sin(d9_7)];
C22(09,08) = -v9*v8*[B9_8*cos(d9_8) - G9_8*sin(d9_8)];
C22(09,10) = -v9*v10*[B9_10*cos(d9_10) - G9_10*sin(d9_10)];
C22(09,11) = -v9*v11*[B9_11*cos(d9_11) - G9_11*sin(d9_11)];

C22(10,07) = -v10*v7*[B10_7*cos(d10_7) - G10_7*sin(d10_7)];
C22(10,08) = -v10*v8*[B10_8*cos(d10_8) - G10_8*sin(d10_8)];
C22(10,09) = -v10*v9*[B10_9*cos(d10_9) - G10_9*sin(d10_9)];
C22(10,11) = -v10*v11*[B10_11*cos(d10_11) - G10_11*sin(d10_11)];

C22(11,07) = -v11*v7*[B11_7*cos(d11_7) - G11_7*sin(d11_7)];
C22(11,08) = -v11*v8*[B11_8*cos(d11_8) - G11_8*sin(d11_8)];
C22(11,09) = -v11*v9*[B11_9*cos(d11_9) - G11_9*sin(d11_9)];
C22(11,10) = -v11*v10*[B11_10*cos(d11_10) - G11_10*sin(d11_10)];

```

```
% End forming off-diagonals of output matrix C22
```

```
% Begin forming elements of output matrix C21
```

```

C22(07,01) = -v7*v1*[B7_1*cos(d7_1) - G7_1*sin(d7_1)];
C22(07,02) = -v7*v2*[B7_2*cos(d7_2) - G7_2*sin(d7_2)];
C22(07,03) = -v7*v3*[B7_3*cos(d7_3) - G7_3*sin(d7_3)];
C22(07,04) = -v7*v4*[B7_4*cos(d7_4) - G7_4*sin(d7_4)];
C22(07,05) = -v7*v5*[B7_5*cos(d7_5) - G7_5*sin(d7_5)];
C22(07,06) = -v7*v6*[B7_6*cos(d7_6) - G7_6*sin(d7_6)];

C22(08,01) = -v8*v1*[B8_1*cos(d8_1) - G8_1*sin(d8_1)];
C22(08,02) = -v8*v2*[B8_2*cos(d8_2) - G8_2*sin(d8_2)];
C22(08,03) = -v8*v3*[B8_3*cos(d8_3) - G8_3*sin(d8_3)];
C22(08,04) = -v8*v4*[B8_4*cos(d8_4) - G8_4*sin(d8_4)];
C22(08,05) = -v8*v5*[B8_5*cos(d8_5) - G8_5*sin(d8_5)];
C22(08,06) = -v8*v6*[B8_6*cos(d8_6) - G8_6*sin(d8_6)];

C22(09,01) = -v9*v1*[B9_1*cos(d9_1) - G9_1*sin(d9_1)];
C22(09,02) = -v9*v2*[B9_2*cos(d9_2) - G9_2*sin(d9_2)];
C22(09,03) = -v9*v3*[B9_3*cos(d9_3) - G9_3*sin(d9_3)];
C22(09,04) = -v9*v4*[B9_4*cos(d9_4) - G9_4*sin(d9_4)];

```

```

C22(09,05) = -v9*v5*[B9_5*cos(d9_5) - G9_5*sin(d9_5)];
C22(09,06) = -v9*v6*[B9_6*cos(d9_6) - G9_6*sin(d9_6)];

C22(10,01) = -v10*v1*[B10_1*cos(d10_1) - G10_1*sin(d10_1)];
C22(10,02) = -v10*v2*[B10_2*cos(d10_2) - G10_2*sin(d10_2)];
C22(10,03) = -v10*v3*[B10_3*cos(d10_3) - G10_3*sin(d10_3)];
C22(10,04) = -v10*v4*[B10_4*cos(d10_4) - G10_4*sin(d10_4)];
C22(10,05) = -v10*v5*[B10_5*cos(d10_5) - G10_5*sin(d10_5)];
C22(10,06) = -v10*v6*[B10_6*cos(d10_6) - G10_6*sin(d10_6)];

C22(11,01) = -v11*v1*[B11_1*cos(d11_1) - G11_1*sin(d11_1)];
C22(11,02) = -v11*v2*[B11_2*cos(d11_2) - G11_2*sin(d11_2)];
C22(11,03) = -v11*v3*[B11_3*cos(d11_3) - G11_3*sin(d11_3)];
C22(11,04) = -v11*v4*[B11_4*cos(d11_4) - G11_4*sin(d11_4)];
C22(11,05) = -v11*v5*[B11_5*cos(d11_5) - G11_5*sin(d11_5)];
C22(11,06) = -v11*v6*[B11_6*cos(d11_6) - G11_6*sin(d11_6)];

K3=0;
K3(5,6) = 0;
PK3 = [K3 eye(5)];
PK3P = [eye(6); K3];
C21 = PK3*C22*PK3P

K4=0;
K4(5,6) = 0;
PK4 = [K4 eye(5)];
C22 = PK4*C22*PK4

C = -C22^-1 * C21

```